Applications of Thiele's Ester Derivatives from Biological to Material

by

Jun Chen
B.Sc., East China University of Science and Technology, 2011
M.Phil., Queen's University Belfast, 2013

A Dissertation Submitted in Partial Fulfillment
of the Requirements for the Degree of

DOCTOR OF PHILOSOPHY

in the Department of Chemistry

Supervisory Committee

Applications of Thiele's Ester Derivatives from Biological to Material

by

Jun Chen
B.Sc., East China University of Science and Technology, 2011
M.Phil., Queen's University Belfast, 2012

Supervisory Committee

Dr. Jeremy E. Wulff, Department of Chemistry
Supervisor

Dr. Natia L. Frank, Department of Chemistry
Departmental Member

Dr. David J. Berg, Department of Chemistry
Departmental Member

Dr. Alisdair B. Boraston, Department of Biochemistry and Microbiology
Outside Member

Abstract

Supervisory Committee
Dr. Jeremy E. Wulff, Department of Chemistry
Supervisor
Dr. Natia L. Frank, Department of Chemistry
Departmental Member
Dr. David J. Berg, Department of Chemistry
Departmental Member
Dr. Alisdair B. Boraston, Department of Biochemistry and Microbiology
Outside Member

Building upon existing synthetic methods, we have optimized the synthesis of Thiele's methyl ester to an efficient and scalable methodology. As part of a study of chemo- and regioselective transformations within the Thiele's ester scaffold, we designed and synthesized a new suite of molecular scaffolds incorporating a broad range (from 123° to 176°) of cleft angles.

In addition to this, we compared two competing conceptual models for their ability to rationalize the selective formation of Thiele's ester and two minor regioisomers which arise during the formation of the target product. We found that radical stabilization arguments (based on Deslongchamps' seminal work) outperformed the classic frontier molecular orbital theory model in predicting the regioselectivity of Thiele's ester dimerization. When this method was combined with simple steric arguments, we arrived at a general algorithm to rationalize Thiele type dimerization, including all the known homo- and heterodimerizations in the literature as well as a novel phosphine oxide-containing Thiele acid analogue discovered as part of this thesis work.

In order to stimulate the use of Thiele's ester chemistry in a diverse range of applications, we took advantage of our Thiele's ester methodology to achieve a mono ester-substituted dicyclopentadiene (colloquially referred to as a "half" Thiele's ester), and used this as the precursor of a novel functionalized polydicyclopentadiene (*f*PDCPD) ROMP polymer. The resulting *f*PDCPD has the highest glass-transition temperature reported for any polydicyclopentadiene material and allows for the facile manipulation of the surface chemistry through alteration of the embedded functional group.

A long-term goal in the Wulff lab is to use Thiele's ester as a scaffold for the generation of conformationally restricted ("peramivir-like") neuraminidase inhibitors. Setting the groundwork for this, we explored the selectivity of various peramivir derivatives toward group-1 vs. group-2 neuraminidase enzymes. To this end, we coupled a wide range of alkyl chains and aromatic rings with different length and size parameters onto the primary amine of peramivir. We found that our de-guanidinylated peramivir analogues showed a rare target selectivity against group-2 neuraminidases instead of group-1 neuraminidases, which might due to the ring geometry of peramivir as well as the reduced electrostatic interaction between the amino group from our analogues and the Asp147-His150 residues from the enzyme. This suggested that it is possible for

group-2 neuraminidases to have a more open 150-cavity state than group-1 neuraminidases. Additionally, the respectable IC_{50} values for these compounds, together with their significantly reduced polarity (relative to peramivir itself) may prove advantageous from a bioavailability standpoint.

Table of Contents

List of Tables

List of Figures

List of Schemes

List of Charts

Acknowledgments

Firstly, I would like to thank Dr. Jeremy Wulff for all the help, guidance, advice and support during last four years. Thank you for giving me encouragement when encountering challenging problems, enriching my knowledge in chemistry and research experience, and cultivating me as an independent chemist. Secondly, I would like to give my thanks to Dr. Mike Brant, who trained me and shared his wisdom (highly contaminated by nicotine and sulfone) with me. My thanks also go to Ronan Hanley, who accompanied me for this four years journey at UVic, inspired me with his amazing talents, entertained me with his dark humor and occasionally put out "unexpected" fires for me. Thirdly, I would like to thank all the past and current Wulff group members (Dr. Natasha O'Rourke, Dr. Jason Davy, Dr. Tyler Cuthbert, Dr. Lok-hang Yan, Tom Doerksen, Andy Un, Tong Li, Jon Sader, Derek Blevins) for bringing a positive atmosphere to the lab. In addition to these fine individuals, I would like to thank all of the undergraduate students with whom I have worked closely over the years: Rosa Zhang, Brenden Kilpatrick, XuXin Sun, Ivica Bratanovic, Deepak Jaswal, Cameron Zheng, and LingXiao Lu.

I would like to thank all of my committee members for their support during this four years: Dr. Natia Frank, Dr. David Berg and Dr. Alisdair Boraston. Of course, my work and thesis presented within would have been impossible without the help of all the collaborators and UVic staff: Dr. Matthew Moffitt, Dr. Allen Oliver, Chris Barr, Dr. Ori Granot and many others.

Furthermore, to the "dream team" members (Natasha, Alok and Ronan), thank you for adding so much joy and happiness to my spare time as well as for encouraging and helping me to face all the obstacles in my life. I'm beyond blessed to have friends like you guys!

Finally, I would like to thank my parents and family for understanding and supporting me during this whole four years.

List of Abbreviations

γ_{sv}	overall surface tension
γ_{sv}^{d}	dispersion surface tension
γ_{sv}^{p}	polar surface tension
^{13}C NMR	carbon nuclear magnetic resonance
^{1}H NMR	proton nuclear magnetic resonance
^{o}C	degrees Celsius
Å	Angstrom
AFM	atomic force microscopy
Ala	alanine
aq.	aqueous
Arg	arginine
Bn	benzyl
Boc	*tert*-butyloxycarbonyl
br	broad
calcd	calculated
cm^{-1}	wavenumbers
COSY	^{1}H – ^{1}H correlation spectroscopy
CP	cyclopentadiene
d	doublet
d.r.	diastereomeric ratio
DBU	1,8-diazabicyclo[5.4.0]undec-7-ene
DCM	dichloromethane
DCPD	dicyclopentadiene
dd	doublet of doublets
ddd	doublet of doublet of doublets
DFT	density functional theory
DMAP	*N*,*N*-(dimethylamino)pyridine
DMF	dimethylformamide
DMSO	dimethyl sulfoxide
dn/dc	refractive index increment
dq	doublet of quartets
dt	doublet of triplets
e.g.	for example
eq.	equivalents
Et	ethyl
FDA	Food and Drug Administration
*f*PDCPD	functionalized polydicyclopentadiene
FT-IR	Fourier transform infrared
g	grams
Glu	glutamic acid
GPC	gel permeation chromatography
HA	hemagglutinin
HOMO	highest occupied molecular orbital

HRMS	high resolution mass spectrometry
HSQC	heteronuclear single-quantum correlation spectroscopy
Hz	hertz, s^{-1}
i	iso
IC50	maximal inhibitory concentration
Ilu	isoleucine
IR	infrared spectroscopy
J	coupling constant
Kd	dissociation rate constant
kDa	kiloDalton
Ki	inhibition constant
L	litre
LC-MS	liquid chromatography-mass spectrometry
LUMO	lowest unoccupied molecular orbital
M	molar
m	multiplet (or multiple overlapping resonances)
Me	methyl
mg	milligrams
MHz	megahertz
mM	millimolar
mmol	millimoles
M*n*	number average molecular weight
mN	milliNewton
MOFs	metal-organic frameworks
mol	moles
mp	melting point
MS	mass spectrometry
M*w*	weight average molecular weight
M*n*	number average molecular weight
NA	neuraminidase
nM	nanomolar
NMO	*N*-methylmorpholine-*N*-oxide
NMR	nuclear magnetic resonance spectroscopy
NOE	nuclear Overhauser effect
NOESY	nuclear Overhauser effect spectroscopy
Nu	nucleophile
OWRK	Owens, Wendt, Rabel, and Kaelble
p	*para*
PDCPD	polydicyclopentadiene
PDI	polydispersity index
Ph	phenyl
psi	pounds per square inch
q	quartet
R_a	surface roughness
RNA	ribonucleic acid
RT	room temperature

s	singlet
t	triplet
t or *tert*	tertiary
T_g	glass transition temperature
TGA	thermogravimetric analysis
THF	tetrahydrofuran
TLC	thin layer chromatography
TOCSY	total correlation spectroscopy
Trp	tryptophan
Tyr	tyrosine
WHO	World Health Organization
δ	chemical shift
μM	micromolar

Dedication

Dedicated to the memory of my grandfather, Xiaoqian Chen (1928-2009).

Chapter One: Introduction

1.0.0. Overview

The origin of Thiele's acid and ester can be traced back over 100 years. In 1901, Thiele first reported that a dimeric product was achieved with the molecular formula of $C_{12}H_{12}O_4$ by treating cyclopentadiene with potassium and carbon dioxide.[1] This diacid compound **2** and its corresponding ester **3** are thus known as Thiele's acid and ester respectively. Their unique conformational properties make them attractive as molecular scaffolds for supramolecular, materials or biological applications. This thesis describes the optimization of a direct synthesis of Thiele's esters, the development of a predictive algorithm accounting for Thiele's ester's unusual regiochemistry, and several applications of Thiele's ester derivatives.

The first goal of this project was to investigate the fundamental chemistry of Thiele's ester – optimization of its synthesis, chemo- and regioselective transformations that can be carried out upon it, and the systematic prediction of the Diels-Alder dimerization leading to Thiele's ester and its analogues. Based on this foundation, more Thiele's esters and derivatives were designed and synthesized towards different applications such as beta-hairpin mimic scaffolds, ring opening metathesis polymers and rigid polycyclic synthetic building blocks.

One of our potential interests involves using derivatives of Thiele's ester as scaffolds for the creation of conformationally constrained neuraminidase inhibitors that will mimic the enzyme-bound conformation of peramivir (one of the most potent commercially available viral neuraminidase inhibitors). The use of a conformationally restricted scaffold could not only increase the potency, but also improve the selectivity of an inhibitor against a desired enzyme target such as human neuraminidase. However, little is known about the selectivity of peramivir analogues toward different subtypes of viral or human neuraminidases. In order to efficiently design how to project functional groups out from a Thiele's ester scaffold, we synthesized several novel analogues of peramivir, and tested these against different neuraminidase enzymes.

1.1.0. Synthesis of Thiele's ester and acid

The synthesis of Thiele's ester can be essentially divided into two approaches: 1) the "acid first" approach, and 2) the "ester first" approach.

1.1.1. The "acid first" approach

The "acid first" approach, typified by Thiele's original synthesis, is the most commonly used way to produce Thiele's acid and ester. The carboxylated cyclopentadiene **1** can be prepared by deprotonation of cyclopentadiene using strong bases such as potassium metal[1], sodium metal[2], lithium metal[3] or a Grignard reagent,[4] and then quenching with carbon dioxide (**Scheme 1**). The resulting intermediates **1a-c** (which rapidly interconvert *via* [1,5] hydride-shifts) dimerize through a Diels-Alder reaction pathway even at room temperature to give Thiele's acid **2** as the major product. The subsequent acid-catalyzed esterification can convert this diacid **2** to Thiele's ester **3**, albeit with a certain level of by-products (*vide infra*)**.**

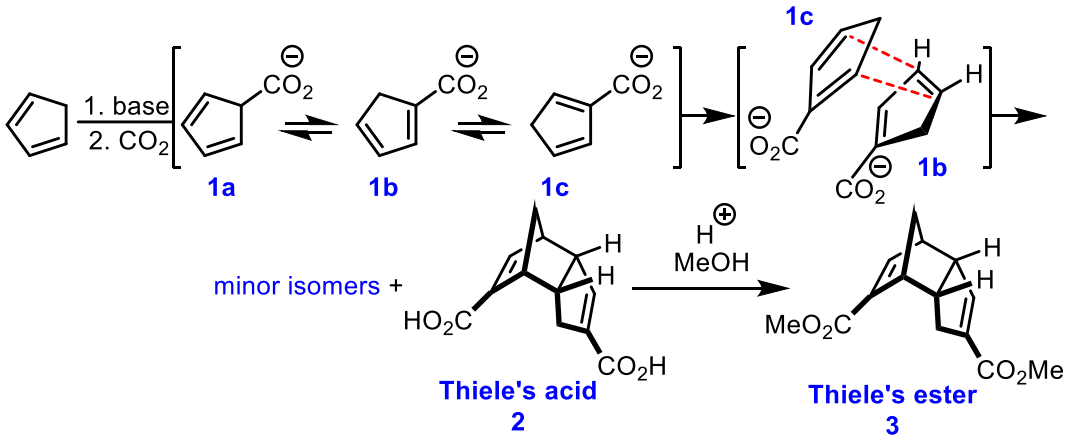

Scheme 1: Thiele's 1901 synthesis of Thiele's acid and ester.

Despite its ubiquity, there are two principal disadvantages to this synthesis. Firstly, the purity of the resulting Thiele's ester is unsatisfying. Owing to the nature of the Diels-Alder reaction and to the poor solubility of Thiele's acid, Thiele's original preparation suffered from a low yield and the product was contaminated with other regioisomers. Multiple recrystallizations were required to obtain **2** in pure form[1]. Although Marchand and Watson modified the procedure and improved the crude yield up to 80%, the resulting product still contained unwanted regioisomers even after recrystallization[5]. In cases where regioisomeric mixtures are inconsequential for the intended application, crude Thiele's acid or ester is typically used without any further purification. The poor quality of the NMR spectra of **3** in the literature highlights this purification challenge[6]. In addition to this, the esterification of Thiele's acid to ester is not as trivial as it might seem. This simple transformation was found to be accompanied by conjugate addition onto the strained norbornene alkene[7] (**Scheme 2**).

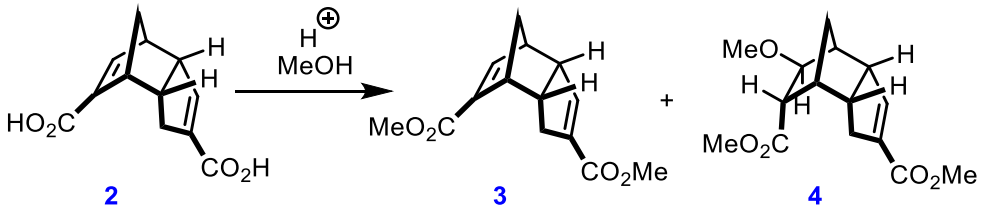

Scheme 2: Esterification of Thiele' acid and the accompanying unwanted byproduct.

One way to avoid handling the insoluble Thiele's acid would be to perform the esterification prior to the dimerization. In 1959, Peters and coworkers reported their efforts to investigate this alternative route. Despite the fact that the dimerization of the monomeric ester **5** did give Thiele's ester, this route suffered from an even lower overall yield which is likely due to the stability and volatility of **5** itself. The difficulty in accessing **5** directly is also highlighted by the fact that Peters actually generated this compound by depolymerization of **3**[8] (**Scheme 3**)!

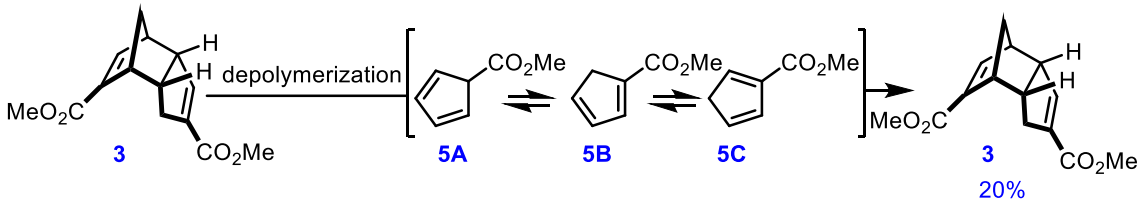

Scheme 3: Peters' dimerization of monomeric ester.

In an unusual approach, norbornadiene has also been used in place of cyclopentadiene as a starting material for Thiele's acid[6] (**Scheme 4**). Nonetheless, cyclopentadienylide is still generated *in situ* from the degradation of norbornadiene in this method. Considering the fact that cyclopentadiene (at least in dimeric form) is already a cheap and abundant chemical, this does not represent a substantial improvement.

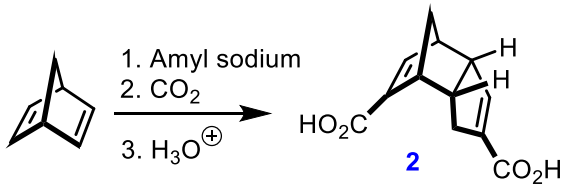

Scheme 4: Synthesis of Thiele's acid from norbornadiene.

1.1.2. The "ester first" approach

Recently, Dive and coworkers published a direct route to Thiele's ester that does not require passing through the acid intermediate **2**[9]. By generating a stable metal salt intermediate **6** from dimethyl carbonate and sodium cyclopentadienylide, they strategically avoided handling the problematic neutral species **5**. After acidifying the salt **6** back to its neutral form *in situ*, the dimerization was trigged to afford Thiele's ester with two minor regioisomers **7** and **8** in an overall yield of 53% (**Scheme 5**). Since the solubility of the diester is significantly better than that of the diacid, the resulting mixture could be further purified by column chromatography to achieve regioisomerically pure Thiele's ester. Although Dive's method was limited by its relatively low yield, and his assignments for the structures of his minor regioisomers turned out to be incorrect, this result nonetheless opens a new window to efficiently allow access to regioisomerically pure Thiele's ester. For this reason, we used this method as a starting point for our own synthetic studies (in Chapter 2).

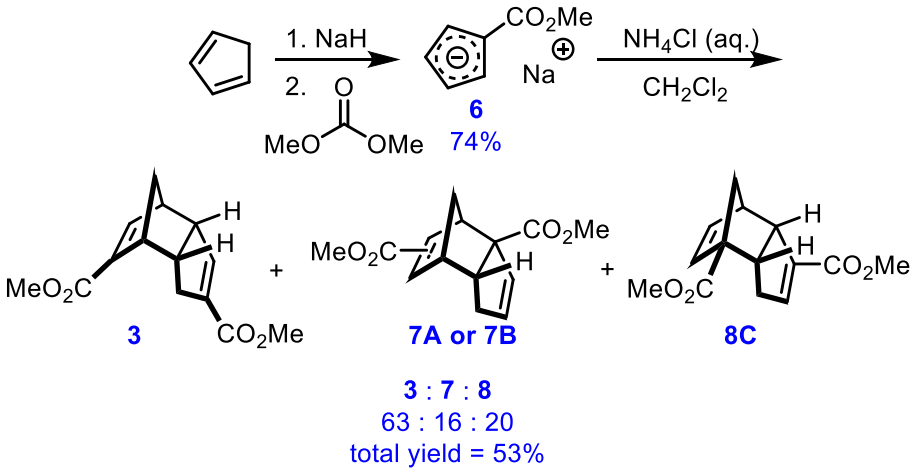

Scheme 5: Dive's direct synthesis of Thiele's ester.

1.2.0. Structure of Thiele's ester and its regioisomers

The structural characterization of Thiele's acid and ester posed a significant challenge for a long while. The rapid interconversion between three possible monomeric substituted cyclopentadienes **5** *via* [1,5] hydride shifts dramatically amplifies the complexity of this Diels-Alder reaction. In fact, theoretically, there are actually 72 possible products that could be envisioned for the reaction (36 *endo* adducts and 36 *exo* adducts) as shown in **Chart 1**.

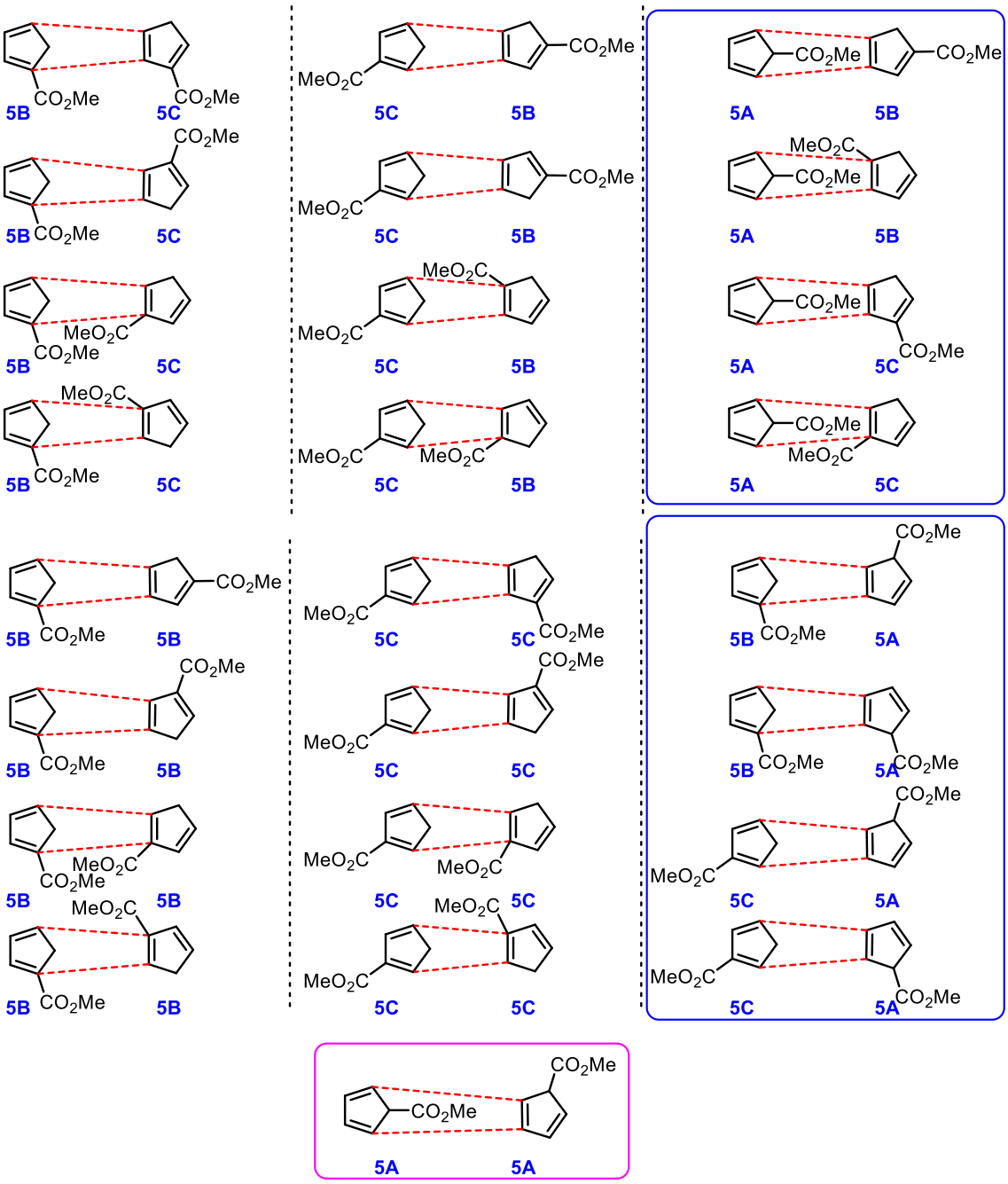

Chart 1: 72 possible pathways of Thiele's dimerization (36 *endo* adducts and 36 *exo* adducts). The blue box indicates pairings for which two additional sets of diastereomers would be produced from each reaction pathway. The pink box indicates pairings for which four additional sets of diastereomers would be produced from each reaction pathway.

1.2.1. Structure of Thiele's ester

The structural details of Thiele's ester were first revealed by Peters in 1959. He reported UV spectroscopic studies on the ester and drew the conclusion that both carboxylate groups are conjugated to the two double bonds[8]. Subsequently, this result was confirmed by NMR spectral data from another group[6]. However, none of these investigations were sufficient to determine the exact regiochemistry. This structural puzzle was eventually solved by Dunn and Donohue in 1968[10]. The fact that Thiele's ester could be cyclized photochemically proves that Thiele's ester bears an *endo* configuration. The IR data for the subsequent anhydride formation further confirmed the position of both carboxylate groups (**Scheme 6**).

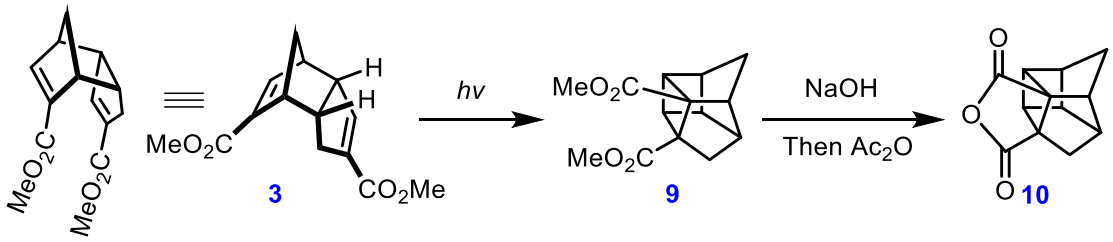

Scheme 6: Dunn and Donohue's structural assignment *via* photochemical cyclization and subsequent anhydride formation.

1.2.2. Structures of minor regioisomers

As discussed above, the Diels-Alder reaction that leads to Thiele's acid or ester also results in the formation of minor regioisomers. However, while the synthetic community has been in broad agreement about the structure of Thiele's ester ever since Dunn and Donohue's pioneering work, there is actually a substantial disagreement regarding the assignment of the exact structures of the two minor regioisomers that are formed alongside **3**. Even the number of minor regioisomers is still ambiguous in the literature (**Figure 1**).

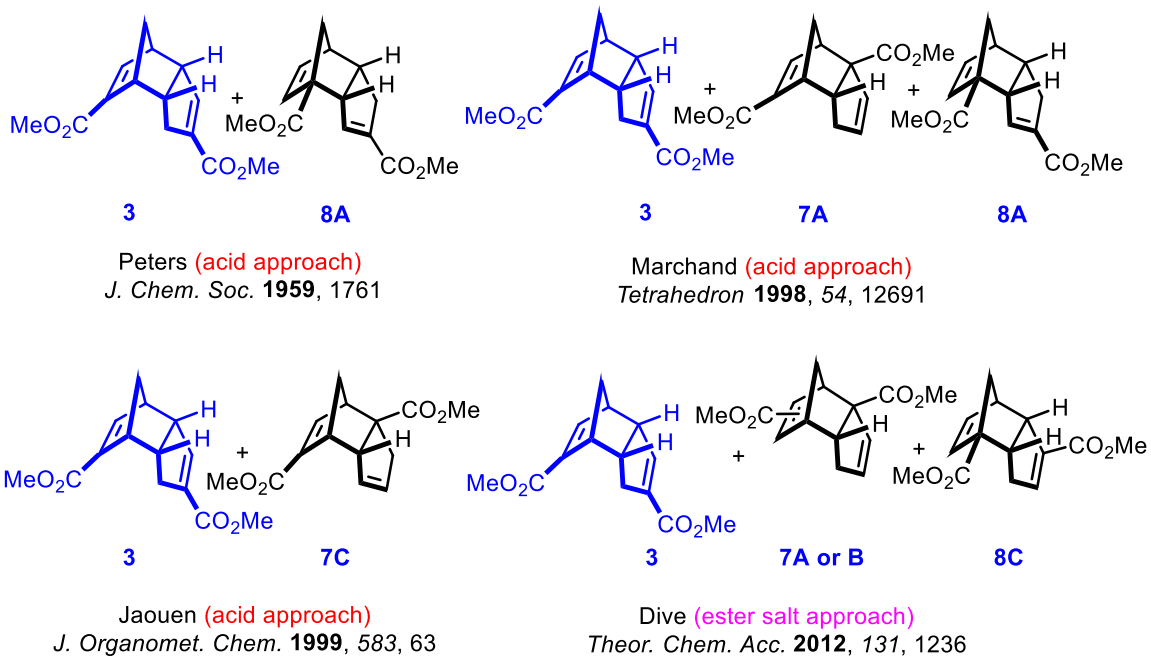

Figure 1: Conflicting structures of Thiele's ester's minor regioisomers, reported from various research groups. "Acid approach" indicates that the isomers were reported following dimerization of cyclopentadienecarboxylates 1a–c, or protonated forms thereof. "Ester salt approach" indicates that the isomers were reported following dimerization of the corresponding esters, 5a–c, obtained *via in situ* acidification of salt 6.

In 1959, Peters first contributed a UV spectroscopic study to this field. By determining that one of the methyl ester groups was conjugated to the alkene on the cyclopentene ring, and that the other methyl ester group was not conjugated to the alkene on the norbornene moiety, Peters and coworkers tentatively assigned the structure of the only minor regioisomer that they isolated as **8A**[8]. Later, in 1998, inspired by Dunn and Donohue's early work on the characterization of Thiele's ester, Marchand used the same photochemical method coupled with more advanced NMR analysis to conclude the structures of both minor regioisomers as **7A** and **8A**, respectively[5]. In contrast, Jaouen reported that Thiele's acid was isolated along with only one regioisomer **7C** in an approximately 1:1 ratio. In the most recent literature (as discussed above), Dive reported that two isolable minor regioisomers arose from their novel ester-first approach. Dive assigned one of the minor regioisomers as another new structure **8C**, but indicated that the position of the methyl ester group on the norbornene moiety of the second regioisomer was still not clear to them even with the help of modern 2D NMR[9].

Knowing the structures of the two minor regioisomers would obviously help one understand the mechanistic origin of this unusual Diels-Alder reaction. More importantly, the fact that Dive's

assignment of the minor regioisomers was totally different from any other existing literature makes one question whether the original “acid first approach” and Dive’s direct ester approach afford the same regiochemical outcome. This is an important question, since it speaks to the tunability of the underlying cycloaddition.

1.3.0. Mechanism for the formation of Thiele’s ester

The Diels-Alder reaction is considered to be one of the most powerful synthetic reactions for constructing a wide range of complex cyclic and heterocyclic ring systems[11]. One of the biggest challenges in Diels-Alder reactions is how to mechanistically predict the regiochemical outcome of these transformations. The formation of Thiele’s ester has long been recognized as a useful test for the predictive power of mechanistic models used to forecast the outcome of cycloaddition reactions[12].

1.3.1. Woodward-Hoffmann rules

Since the Diels-Alder reactions is a pericyclic reaction, the Woodward Hoffmann rules were first used to describe these two-component [4+2] cycloadditions by using orbital symmetry considerations. Preservation of orbital symmetry requires the transformation of the molecular orbital of reactants into those of products to proceed continuously. Thus, the Woodward Hoffmann rules only apply to concerted pericyclic reactions. Based on the observations for cycloaddition reactions of π-systems, the Woodward-Hoffmann rules for cycloaddition reactions can be summarized in terms of the number of electron pairs involved in the cyclization. In the case of the [4n+2] system, the suprafacial-suprafacial addition is thermally allowed and the suprafacial-antarafacial addition is photochemically allowed. Although it doesn’t not necessary explain the *endo/exo* selectivity nor the regioselective, it does establish the foundation for the frontier molecular orbital theory which was reported by Fukui in 1952[13].

1.3.2. Frontier molecular orbital model theory

The most common and well-known predictive tool for the Diels-Alder reaction is the classic frontier molecular orbital theory which was popularized by Fleming[12a] (following Fukui[14], Houk[15] and others[16]). Notably, in Fleming’s classic text on applying frontier orbital theory to organic reactions, a long paragraph was used to explain the formation of Thiele’s ester[12a]. Basically, Fleming argued that among the three interconverting cyclopentadiene species, **5A** has the highest HOMO, **5B** has the lowest LUMO and **5C** is in between. However, **5A** has a low presence in solution, since it is somewhat higher in energy than its more conjugated cousins. Thus, the smallest energy gap among species likely to encounter one another is between the HOMO of **5C** and the LUMO of **5B,** making this the preferred combination. And indeed, Thiele’s ester **3** does form from a dimerization between **5C** and **5B** (**Figure 2**). After approximating the orbital coefficients by conceptually mixing the orbitals of butadiene with the orbitals of allyl cation (to account for the electron-withdrawing

ester group), Fleming aligned the largest orbital coefficients together and showed that his methods are successful in predicting the correct regiochemical outcome in the formation of Thiele's ester.

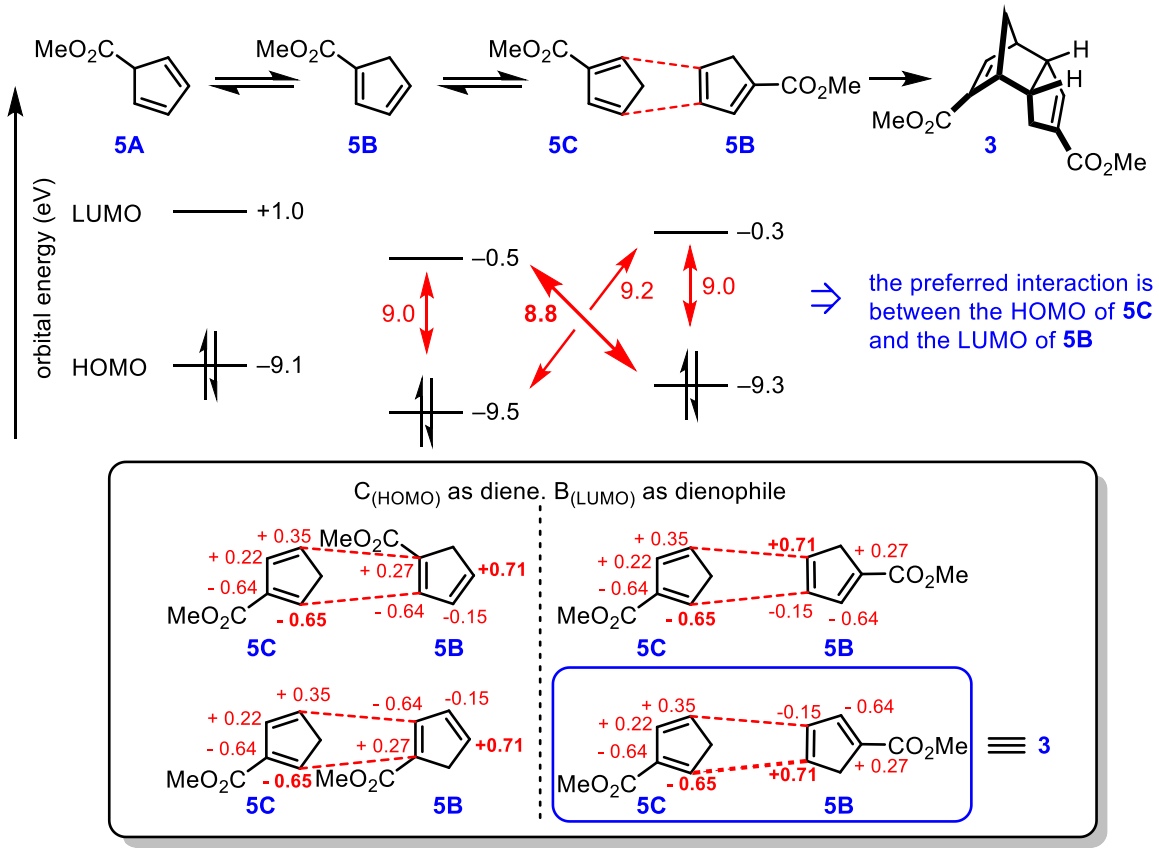

Figure 2: Fleming's standard frontier molecular orbital explanation for Thiele's ester formation. Blue box indicates the predicted combination.

Although this seems at first glance to be a useful validation of Fleming's frontier orbital arguments, the method described above only predicts the correct product if Fleming's rather ad hoc estimates for the orbital coefficients are used. The use orbital coefficients that were calculated by DFT or other modern methods (see Chapter 3) leads to incorrect predictions. This provides an impetus to look beyond simple frontier orbital arguments in rationalizing the outcome of complex Diels-Alder reactions like the Thiele dimerization.

1.3.3. Radical stabilization

Rather than rely upon the closed-shell system, which is used by both the frontier molecular orbital theory and the Woodward-Hoffmann rules, to predict the regiochemistry of Diels–Alder reactions, Deslongchamps and Deslongchamps argue that both the diene and dienophile should be viewed as their corresponding *s-cis* open-shell singlet diradical resonance structures (a consequence from bent bond theory)[12b,17]. In contrast to the closed-shell system in which molecular orbitals are doubly occupied, the open-shell system describes one or more orbitals that contain one or more unpaired

electrons. Singlet states can exist in closed-shell or open -shell configurations, in which the open-shell species (e.g. radicals) are often more reactive.

Unlike the frontier molecular orbital theory which describes the Diels-Alder reaction as a concerted pericyclic reaction, Deslongchamps and Deslongchamps suggest that the reaction goes through a concerted but asynchronous reaction mechanism, where the formation of the first bond, involving the least stable radical center on both diene and dienophile, is somewhat faster than the formation of the second bond. This model is akin to proposing that the transition state goes through an open shell singlet rather than closed shell singlet. After ruling out any obviously sterically hindered combinations, one should then be able to predict the favoured regioisomeric outcome based on simple rules opf radiacl stablity[12b].

In considering the heterodimerization of **5B** and **5C** to afford Thiele's ester, Deslongchamps and Deslongchamps first assigned the cross-conjugated **5C** as the better diene (less electron poor and less steric hindrance at the diene termini) and linear-conjugated **5B** as the better dienophile (more electron poor and containing a less-substituted olefin). Regardless of the fact that the role of diene and dienophile is theoretically switchable in this Diels-Alder reaction (the existence of two minor regioisomers **7** and **8** is a strong indication of this), this radical stabilization method does indeed predict the correct regiochemical outcome for the parent Thiele dimerization. The least stable radical of each diradical resonance structure **5C-r** and **5B-r** can be assigned as indicated with the blue coloring in **Figure 3**. After the formation of the first bond between two least stable radicals, it appears that there are two possible transition states **TSA** and **TSB** which could lead to products **3** and **11** respectively. **TSB** is rejected on the basis of steric effects (**11** has two adjacent quaternary centers), which leaves compound **3** (Thiele's ester) as the most likely product.

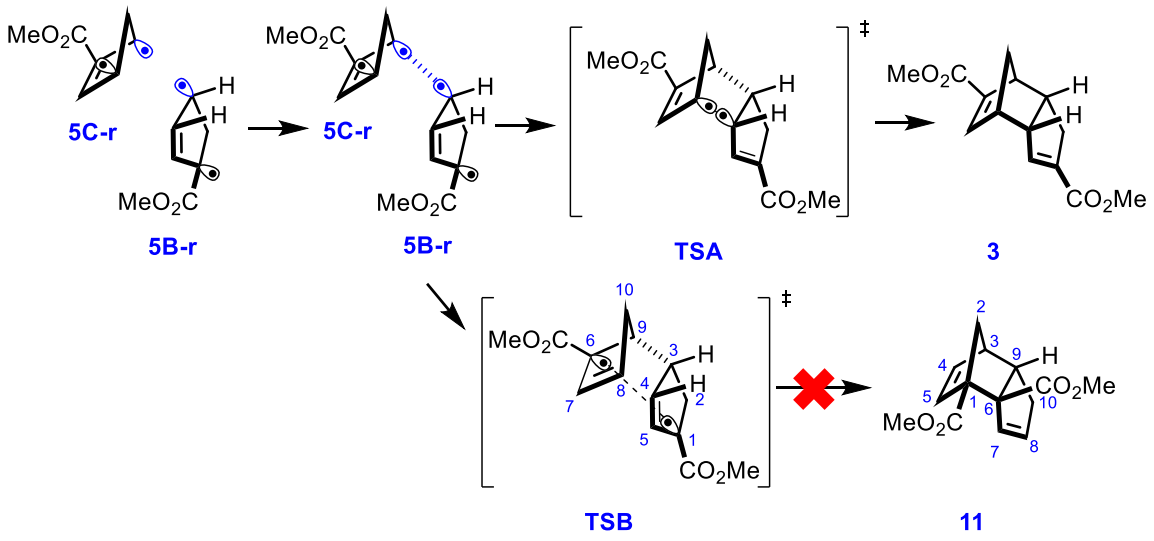

Figure 3: Predication of Thiele's ester regiochemistry by Deslongchamps' radical stabilization method (blue dot indicates the least stable radical).

1.3.4. Subdominant orbital interactions

In the previous two models, both authors claimed that the low concentration of **5A** or **1A** in the solution is the main reason why it was not considered as a coupling candidate in the formation of Thiele's ester or acid. It is true that the observable components of monomeric carboxylated cyclopentadienes (**5** or **1**) have been shown to be the cross-conjugated and linear-conjugated compounds (**5B/C** or **1B/C**) by both chemical trapping methods[18] and NMR spectral data[3]. But one could still argue that the low concentration of **5A** or **1A** does not imply their mechanistic irrelevance. On the contrary, the higher energy intermediate often dictates the principal reaction pathway. In 1998, Spino invoked the concept of subdominant orbital interactions to explain the apparently anomalous Diels-Alder reactivity of cross-conjugated dienes like **5C** and **1C**[12d], in a way that did not require the pre-exclusion of the unconjugated diene **5A** or **1A**.

In cases where a single molecular orbital interaction (*e.g.* between the HOMO of the diene and the LUMO of the dienophile) acts as the "dominant" interaction in a cycloaddition, traditional frontier molecular orbital theory serves as a powerful predictive tool. However, when dienes that have a conjugating substituent at the C2 or C3 positions are involved, the reactions' regioselectivity and reactivity do not appear to obey standard reactivity patterns predicted by frontier molecular orbital theory[12d,19]. For instance, in Thiele's ester formation, diene **5A** should be a much better diene (based on the FMOs calculations in **Figure 2**), but it does not contribute to any isolatable products (to the best of our knowledge). Instead, **5C** which has a conjugating substituent at C2 position acts as a more reactive diene in the formation of Thiele's ester (**Figure 2**). This phenomenon can be rationalized by the "subdominant" orbital interactions. Spino argued that using the energetic state of the starting materials for predictive argument is at least partially invalid. The calculated typical C2-C3 bond length of the diene in its reaction transition state is about 1.39 Å (compared with 1.47 Å in the starting material) which is closer to a double bond (**Figure 4**). If the diene has a substituent that can conjugate to this well-developed C2-C3 π bond, this extra conjugation would decrease the overall energy of the transition state[12d]. This "subdominant" interaction ($HOMO_{dienophile}$-$LUMO_{diene}$ intereaction) would have an even bigger influence than the original "dominant" interaction ($HOMO_{diene}$-$LUMO_{dienophile}$).

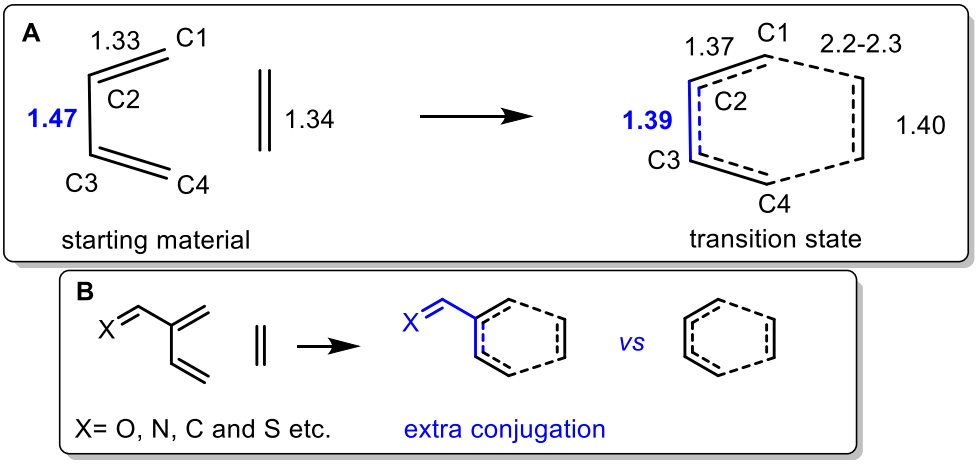

Figure 4: A: Calculated typical bond lengths in the Diels-Alder transition state, for a reaction between butadiene and ethylene. All bond lengths are shown in Å. B: Extra conjugation in orbitals of dienes that have a conjugating substituent at C2 or C3 positions.

1.3.5. Paralocalization energy and diradicaloid character in the transition state of cycloaddition reactions

It has been argued for some time now that Diels-Alder reactions may involve diradical or diradicaloid character in the transition states. Unlike Deslongchamps' explanation which is based around bent bond theory, Brown (and later Spino) suggested that paralocalization energy has a huge influence in terms of the reactivity of cycloadditions such as the Diels-Alder reaction[19b,20]. In a Diels-Alder reaction, the paralocalization energy of diene and dienophile represent the energy that required to reorganize the π-bonds. Energetically, they propose an early reorganisation of the π-electrons in the Diels-Alder reaction, such that both the diene and dienophile coupling partners should be viewed as the corresponding diradicals. The diene that has lower paralocalization energy would generally exhibit better reactivity in cycloadditions. Although this method does not explicitly explain the regioselectivity observed in the formation of Thiele's ester, it does justify the unusual reactivity of electron-poor 2-methoxycarbonylbutadiene **12** (structurally similar to **5C** in Thiele's ester dimerization) and its derivatives with electron-rich dienes, which cannot be predicted by traditional frontier molecular orbital considerations (**Figure 5**).

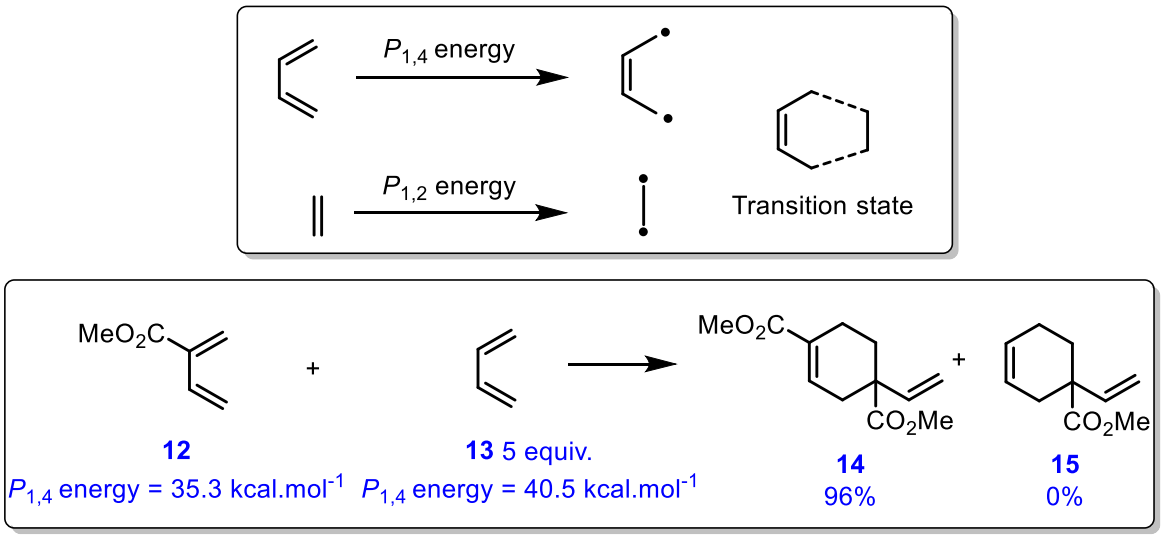

Figure 5: Paralocalization energy and Spino's proposed transition state for the Diels-Alder reaction; paralocalization energy explains the unusual reactivity of electron-poor 2-methoxycarbonylbuta-1,3-diene.

Further support for the idea of diradical character in the transition states of Diels-Alder reactions came from Dewar and co-workers, who calculated the reactions of 1,3-butadiene with ethylene, acrylonitrile, maleonitrile, fumaronitrile, and 1,1-dicyanoethylene, and reported that these reactions cannot be explained on the basis of a synchronous mechanism. The calculated lengths of the forming C-C bonds supported the existence of unsymmetrical transition states which were very close to the reactants' corresponding diradical structures[21]. Dewar further argued that the regioselectivity and reactivity of a Diels-Alder reaction can be predicted by invoking diradical structures.

1.4.0. Structural properties

Thiele's acid has a chiral, rigid and chemically inert backbone that projects functionality outward from its tricyclic core at a fixed angle. This V-shaped geometry means that it can be viewed as a chiral molecular cleft. Compounds which have similar structural properties (such as Thiele's acid's "basic brother" Tröger's base) have already demonstrated a broad range of applications in the areas of supramolecular, organometallic, biological and materials chemistry[22]. While a variety of functionalized Tröger's base analogues have been developed for different applications, such as hydrogen bonding receptors[23], receptors for bisammonium salts[24], chiral receptors for small organic molecules[25], Tröger's base amino acid building blocks[26], molecular torsion balances for studying weak molecular recognition forces[27], chiral ligands for asymmetric synthesis[28], DNA binding probes[29] etc. (**Figure 7**), surprisingly much less research has been focused on the corresponding applications of Thiele's acid. From a structural perspective, Thiele's acid bears a smaller cleft angle

than Tröger's base (**Figure 6**) which makes it an interesting choice for applications that requires narrower projection vectors.

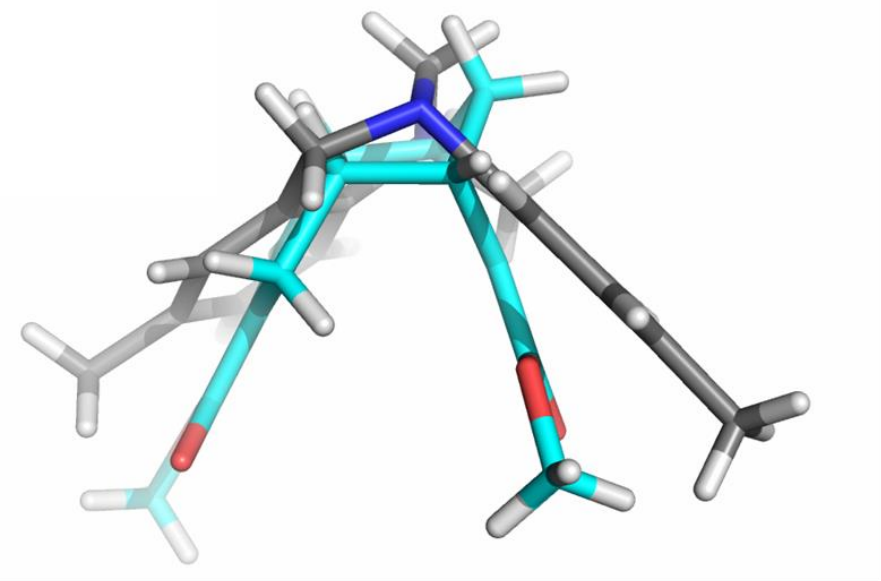

Figure 6: Comparison of the cleft angle between Tröger's base (gray) and Thiele's acid methyl ester (cyan).

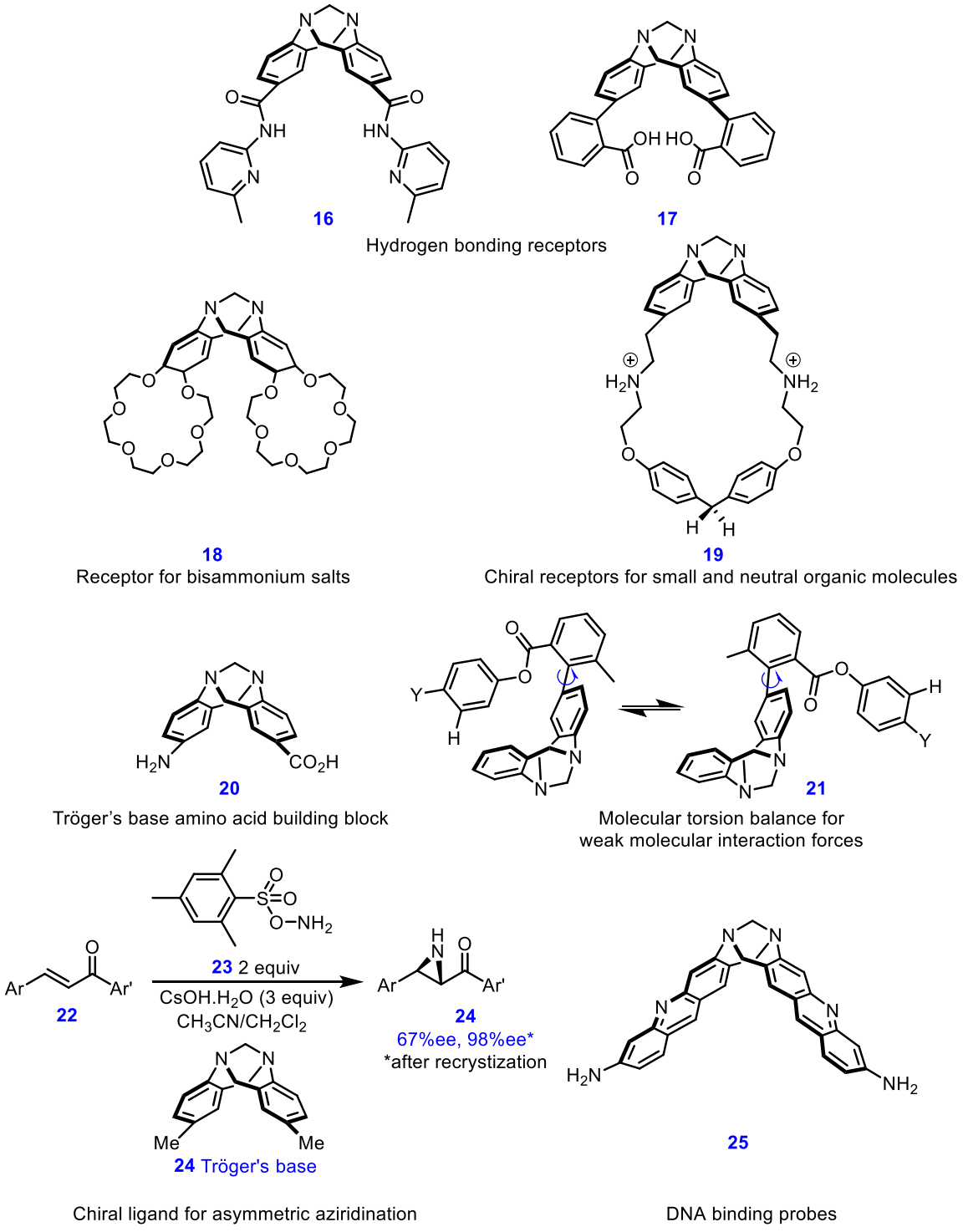

Figure 7: Selected applications of Tröger's base and its analogues.

1.5.0. Existing applications of Thiele's acid and ester

Since Thiele's first paper describing the synthesis of **2** and **3**[1], over a century has passed. Despite all this time, relatively few applications of Thiele-type compounds have emerged in the literature, and these can generally be grouped into three research directions.

1.5.1. Precursor to bioactive metal complexes

Many metallic elements play important roles in living systems. However, the area of enzyme inhibitors has been dominated by small organic molecules which have a combination of specific weak interactions with target proteins (such as electrostatic interactions, hydrogen bonding and van der Waals interactions etc.). Over the past three decades, organometallic pharmaceuticals have been recognized as an important direction for drug development. In such organometallic complexes, the metal serves as the core of the complex that organizes the organic ligands in three-dimensional space. As a result, organometallic complexes can potentially allow one to explore chemical space in ways that would not be possible with traditional organic drug molecules. Cyclopentadiene as a small and chemically tunable ligand has long been known for its ability to mimic arene rings in drug development[30]. One of the primary applications of Thiele's ester is as the ligand precursor for bioactive organometallic complexes of substituted cyclopentadienes. Jaouen first reported a synthetic pathway to an interesting radiopharmaceutical nucleotide (η^5-$C_5H_4COOH)Re(CO)_3$ by using Thiele's acid as the precursor of the ligand[3]. Following the initial metal coordination, retro Diels-Alder reaction occurred rapidly at low temperature (relative to typical thermal retro Diels-Alder) to afford the monomeric complex (**Scheme 7**). Since then, a wide range of novel organometallic complexes bearing a bioactive cyclopentadiene ligand have been developed in the same manner[31].

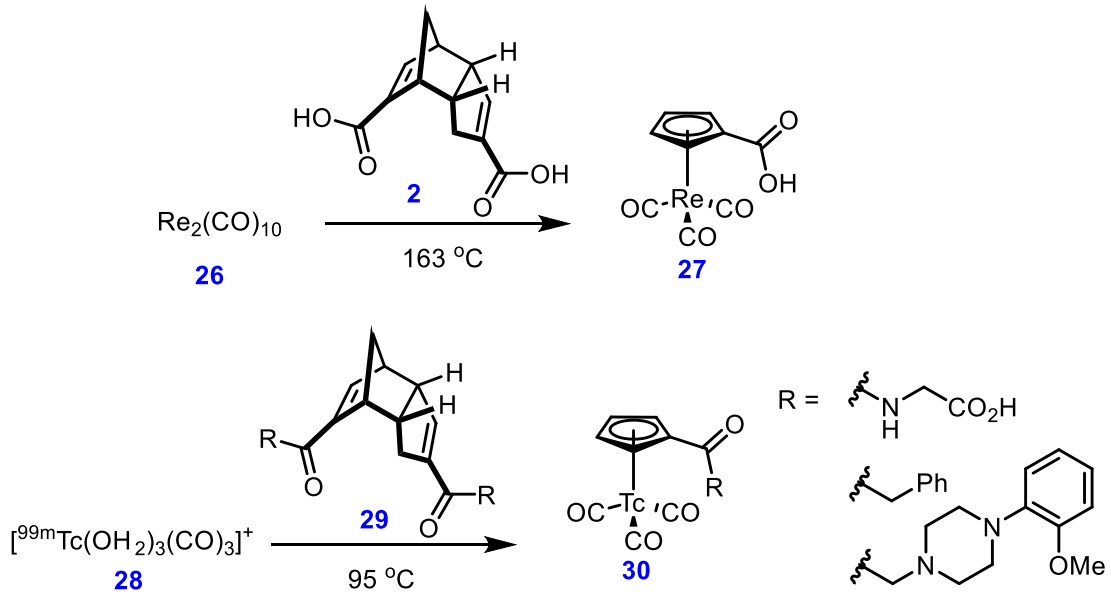

Scheme 7: Preparation of radiopharmaceuticals from Thiele's acid and derivatives thereof.

1.5.1.1. Organometallic analogues of Tamoxifen

Tamoxifen is an antagonist of the estrogen receptor and is widely used for the treatment of breast cancer[32]. Owing to the fact that Tamoxifen's ferrocenyl analogues **32** have already demonstrated a better cytotoxic effect than the Tamoxifen itself[30], Joauen and co-workers developed a new rhenium based analogue **33** with additional radiopharmaceutical potential. The similar bioactivity between **33**, **32** and Tamoxifen opened more possibilities for organometallic complexes in the area of drug discovery[33] (**Figure 8**).

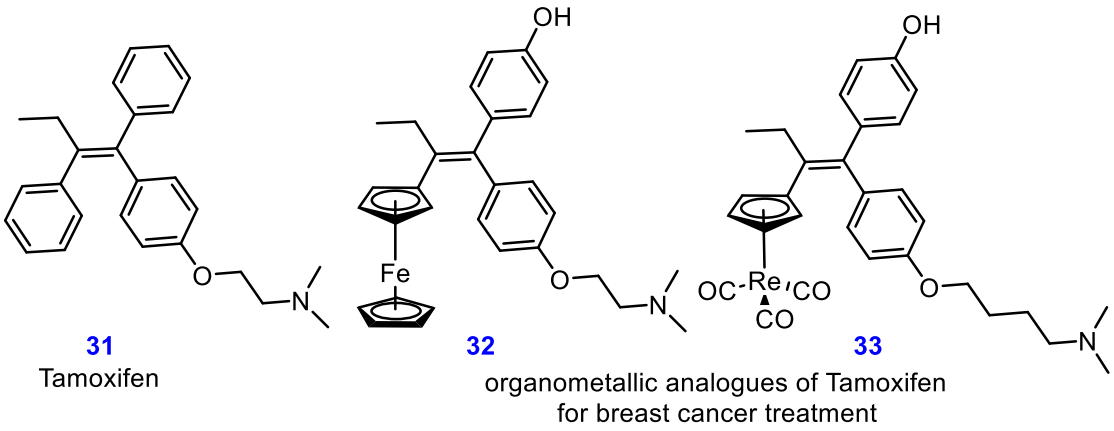

Figure 8: Tamoxifen and its organometallic analogues.

1.5.1.2. Carbonic anhydrase inhibitors

Due to the early success of these organometallic Tamoxifen analogues, more and more attention has been spent on bioactive organometallic complexes. In 2012, Alberto and coworkers described

a synthesis of a series of Re complexes and their ^{99m}Tc homologues by using functionalized Thiele's acid as their ligand precursor[34] (**Scheme 8**). While the Re complexes displayed nanomolar affinities against human carbonic anhydrase and superior selectivity towards two pharmaceutically relevant isoenzymes hCA IX and hCA XII, the ^{99m}Tc homologues (exhibiting identical bioactivity) can also serve as imaging agents in single photon emission computed tomography.

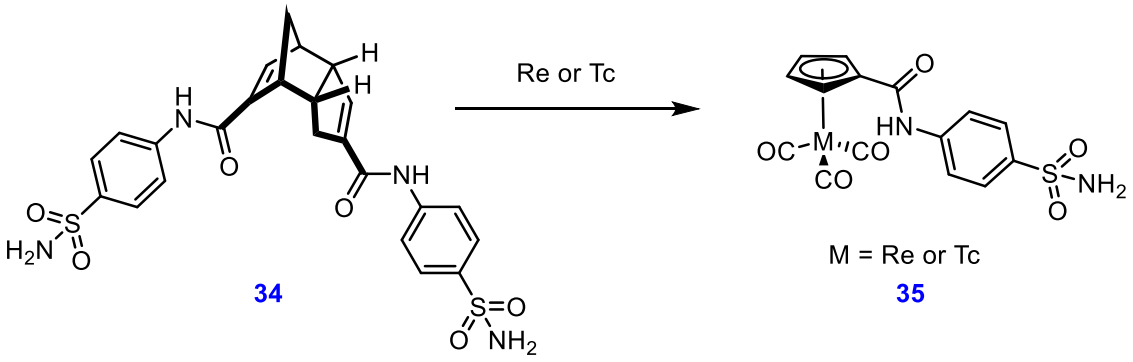

Scheme 8: Synthesis of carbonic anhydrase inhibitors from functionalized Thiele's acid.

1.5.1.3. Inhibitor of the human repair enzyme 8-oxo-dGTPase

The other pioneer who explored this biologically relevant chemical space with organometallic complexes is Eric Meggers. A class of novel ruthenium half-sandwich complex was discovered by his group as selective inhibitors of human repair enzyme 7,8-dihydro-8-oxoguanosine triphosphatase (8-oxo-dGTPase, NUDT1, MTH1)[35]. Among all of the Ru complexes, thanks to the combination of additional hydrogen-bonding interactions and rigid conformation, **38** and **39** which both have a functionalized CP ligand exhibited dramatically enhanced affinity and specificity. These complexes could be useful tools for exploring the biological function of MTH1 as a valuable drug target for anticancer therapy (**Figure 9**).

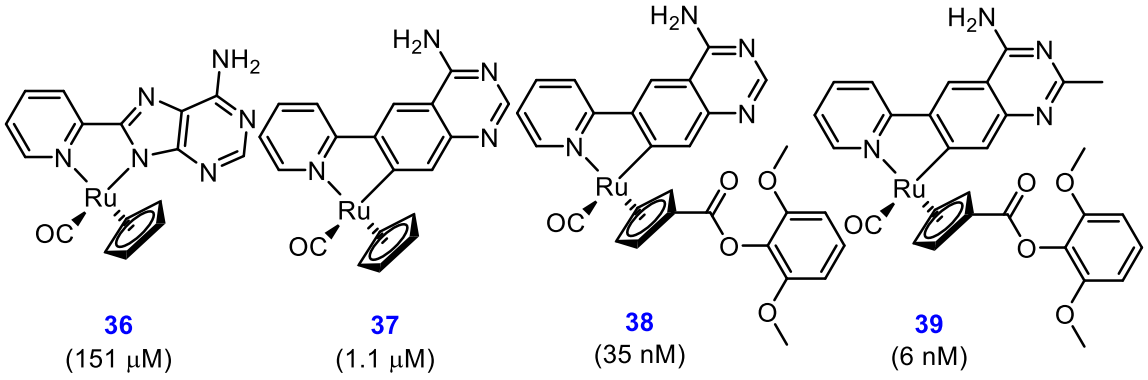

Figure 9: Ruthenium complexes as MTH1 inhibitors. Determined IC_{50} values are given in brackets.

1.5.1.4. Cyclopentadienyl-based organometallic amino acid

There is no need to emphasize the importance of amino acids in biological systems. The demand for different types of unnatural amino acids has never faltered. In 2012, Alberto and co-workers described the synthesis and biological behaviors of a new class of organometallic amino acid analogues, as shown in **Scheme 9** (M = Mn, Re and ^{99m}Tc).[36] These compounds can be recognized by the L-type amino acid transporter 1 (LAT1) which has been reported to be overexpressed in many tumor cell lines. The ^{99m}Tc homologue that can be prepared from Thiele's acid derivatives became a useful molecular imaging agent for visualizing rapidly growing cells such as in cancer.

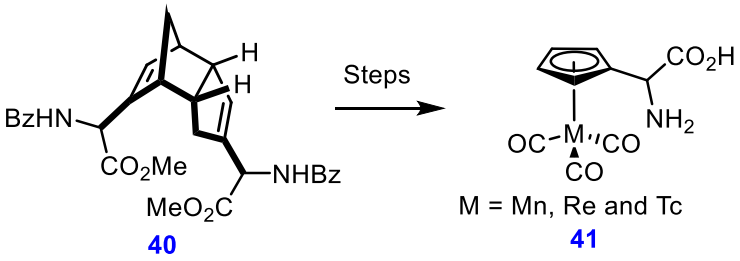

Scheme 9: Synthesis of a cyclopentadienyl organometallic amino acid.

1.5.2. Polymer backbone

Highly crosslinked polymers are useful in the field of structural materials due to their superior mechanical properties such as high durability, high fracture strength, and solvent resistance[37].

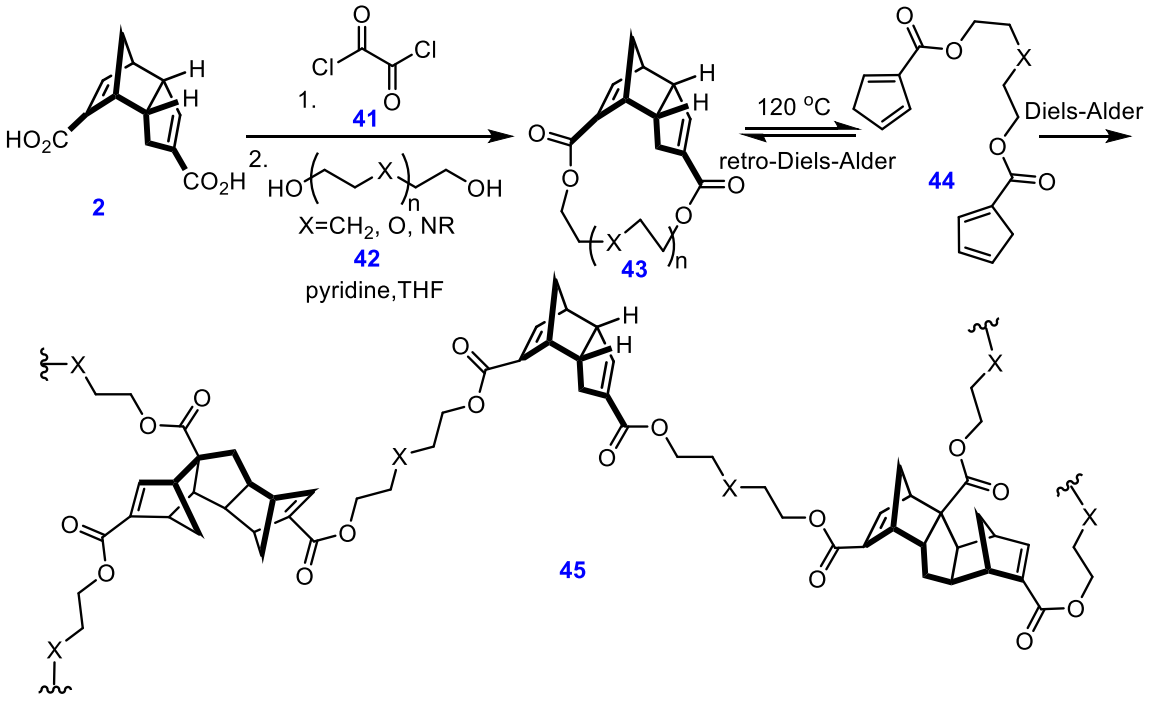

Scheme 10: Self-healing polymer with Thiele's acid as backbone.

Unfortunately, many crosslinked materials are prone to the formation of microcracks under high stress, which results in catastrophic failure. One strategy to avoid this problem is to take advantage of a thermally reversible reaction such as the Diels-Alder reaction to create a self-healing material[37]. Based on this concept, Wudl and co-workers first prepared monomer **43** from lactonization of the two carboxylic acid groups within Thiele's acid, using variable diols. This premonomer could undergo a thermally reversible Diels-Alder reaction to reveal two reactive cyclopentadienes. These units could be polymerized by Diels-Alder reaction between the cyclopentadiene motifs. In addition to this, it's also possible that a second Diels-Alder reaction between a third cyclopentadiene and freshly formed Thiele's ester units could lead to the formation of cyclopentadiene trimers. These covalent crosslinking polymer networks showed great healing efficiency under thermal treatment conditions.

1.5.3. Synthetic building blocks

Thiele's ester has a rigid *endo* tricyclic dicyclopentadiene core that projects two ester functions from both alkenes at a well-controlled angle. Its unique structure and easily predictable molecular shape makes Thiele's ester an interesting choice as the starting material for the synthesis of novel cage structures and other polycyclic systems.

1.5.3.1. Synthesis of triquinacene and its derivatives

Deslongchamps and coworkers first reported their synthetic route towards triquinacene and its derivatives by using Thiele's acid as starting material[38]. In this paper, they demonstrated that Thiele's acid can be transformed into a tricyclic diketone **47** following Curtis rearrangement. Following Baeyer-Villiger oxidation and DIBAL-H reduction to open the lactone, the resulting structure **49** inherited relative stereochemistry from Thiele's acid, which allowed it to cyclize under acidic condition to yield the tricyclic core of triquinacene (**Scheme 11**).

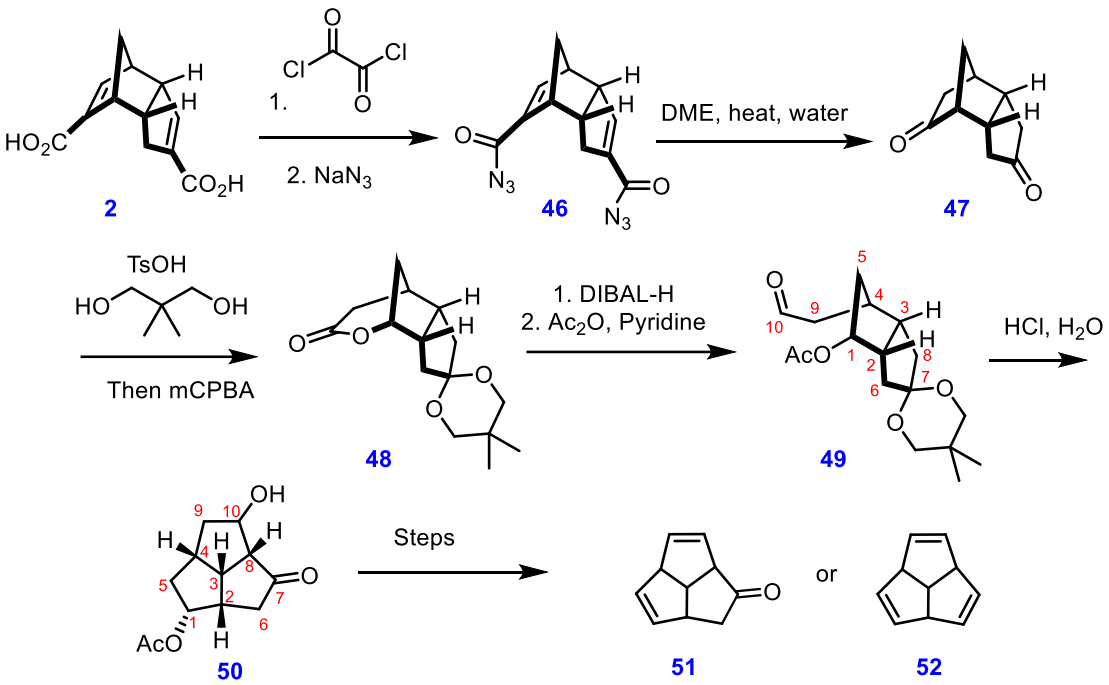

Scheme 11: Deslongchamps' synthetic route towards triquinacene and its derivatives.

1.5.3.2. Synthesis of Thiele's acid based molecular cages

[2+2] photocyclization between the two alkenes of Thiele's acid (or ester) has been known since Dunn's early work in the 1960s. The resulting product (**9** in the case of the methyl ester) can be viewed as a cage-like molecule (**Scheme 12**) and can therefore function as a useful precursor to other molecular cages. Marchand and co-workers first constructed a novel polycyclic ring system from this cyclized product **9**. A Na/K promoted reduction of **9** can break the strained carbon-carbon bond between two esters. The resulting compound **53** can be cyclized by Dieckmann condensation, followed by Wolff-Kishner reduction to afford a mixture of two isomeric cage compounds (**55**).

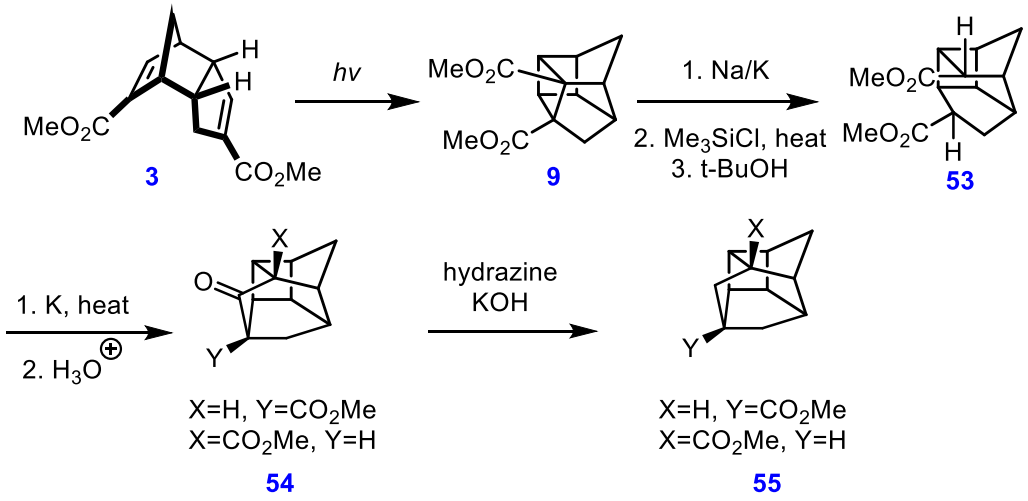

Scheme 12: Synthesis of cage structures from Thiele's ester.

1.6.0. Potential applications of Thiele's acid and ester

Other than the three types of applications mentioned above, there has essentially been no further attention paid to Thiele's acid or ester. Given that structurally reminiscent compounds like Tröger's base have found a wide range of uses in multiple areas (**Figure 7**), we envision that the potential applications of Thiele's ester could likewise be expanded to more diverse fields.

1.6.1. Supramolecular building blocks

Non-covalent interactions define the field of supramolecular chemistry. These weak interactions include hydrogen bonding, π-π interactions, ion-ion interactions and hydrophobic effects.[39] Exploiting such interactions in a systematic way to design new host–guest systems, molecular sensors, etc. has led to a great deal of interest in rigid, functionalized cleft molecules like Tröger's base. Just as Tröger's base can be readily functionalized at the *para*-positions of the two aromatic rings, Thiele's acid or esters can in principle be derivatized through reaction at the two carbonyl groups and associated alkenes. This could drastically amplify the potential utilities of Thiele's ester derivatives. Furthermore, the fact that Thiele's ester is inherently chiral (and at least in principle, resolvable) could facilitate sensing capability for chiral analyte detection, especially in biological applications. Last but not least, by manipulating the functional groups on the alkenes (or by changing the hybridization state of these carbon atoms), a wide range of cleft angles could be obtained. Such flexibility in host frameworks has been very important for molecular recognition in such applications as drug-receptor complexes[40] (**Figure 10**).

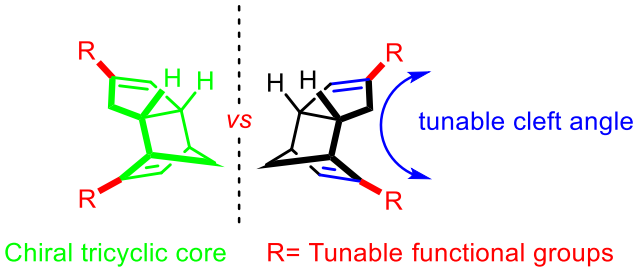

Figure 10: Features of Thiele's acid towards supramolecular chemistry.

1.6.2. Molecular motors

Molecular motors are molecular machines that can be used to transport cargo at the nano-scale[41]. In 1999, the very first light-driven rotary molecular motor was produced by Ben Feringa[42] who recently shared the 2016 Nobel prize due to his work in this area[43]. Based upon this work, in 2011, the well-known molecular four-wheeled nanocar was developed by the same group, which enriched the field of molecular motors to a sophisticated molecular engineering level (**Figure 11**).

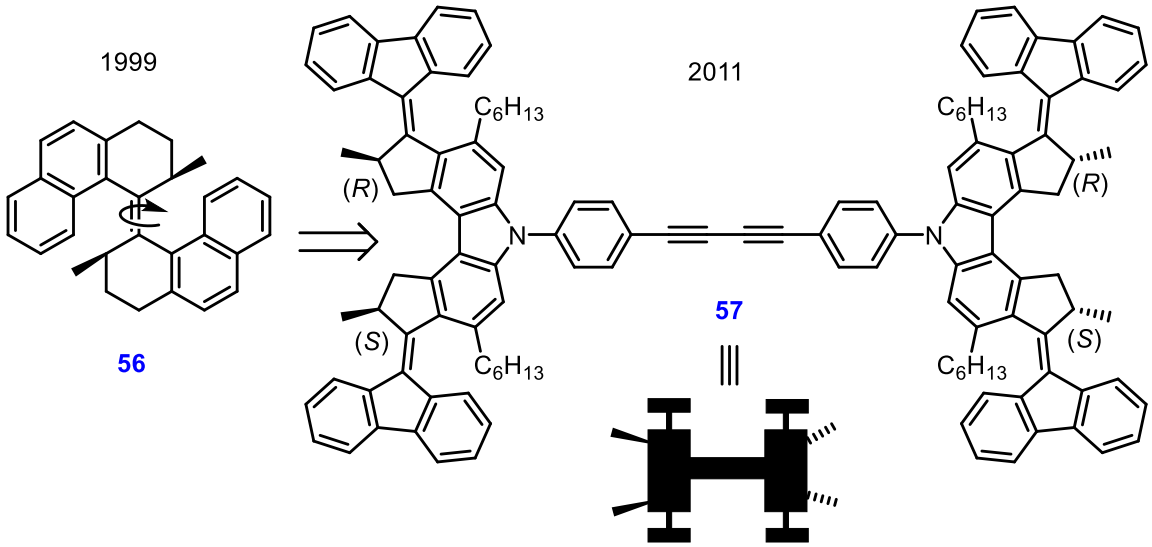

Figure 11: The first light-driven monodirectional rotary molecular motor, and application in a four-wheeled nanocar.

While more and more research has been focused on this rotary-motion type of molecular motor, there has been less development of molecular motors with a tweezers-like (or piston-like) motion. The known photochemically reactive alkenes on Thiele's ester make it possible to design a new class of photo-thermal controllable tweezers-like molecular machines, which might play some interesting roles in molecular-scale delivery (**Scheme 13**).

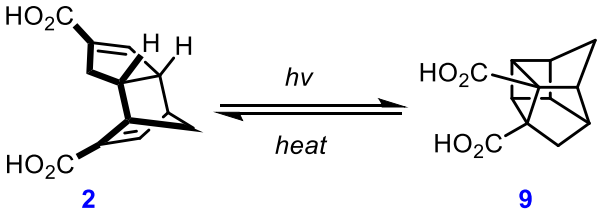

Scheme 13: Photo-thermal controllable tweezers-like molecular machine.

1.6.3. Ligands

Thiele's ester is basically a bis-ester functionalized dicyclopentadiene. The two electron rich alkenes on dicyclopentadiene itself make it a good candidate for use as a diene ligand. Indeed, dicyclopentadiene-transition metal complexes have found applications in various kinds of chemical transformations. For instance, a [(*N,O*-ligand)Rh^{I}(dicyclopentadiene)] complex was reported by Bruin and coworkers as a powerful catalyst to polymerize ethyl diazoacetate to high-molecular weight and highly stereoregular functionalized polymethylenes[44]. Other metals such as Ru, Ir, Pd, Os, and Pt have also showed abilities to use dicyclopentadiene as a ligand[45].

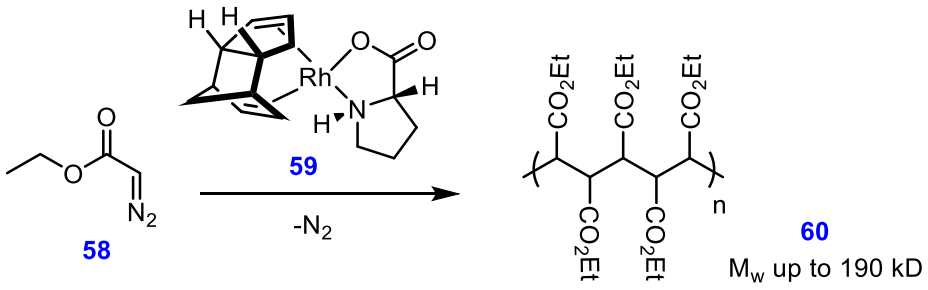

Scheme 14: Rh-Mediated polymerization of carbenes.

The chiral and functionalizable dicyclopentadiene Thiele's ester not only allows one to tune the electronic and steric effects on the ligand, but also opens a new path to develop a novel class of diene ligands for asymmetric synthesis.

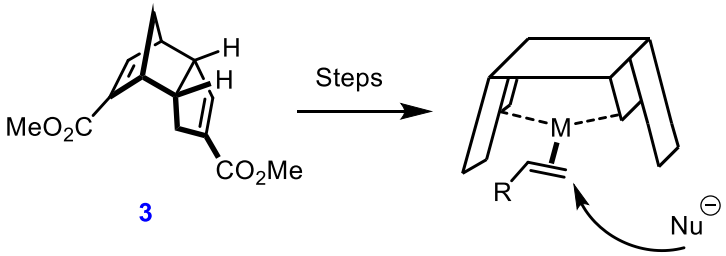

Scheme 15: Potential application of Thiele's ester in asymmetric synthesis.

1.6.4. Metal-organic frameworks

Metal-organic frameworks (MOFs) are a class of material that consists of coordinate bonds between organic ligand linkers and transition metals. MOFs are well known for their porous structures, which allow them to be used for gas storage, purifications and separations as well as for catalysis and sensing[46]. However, most commonly used organic linkers for MOFs are aromatic based carboxylate molecules[47]. Surprisingly, although the structure of MOFs is highly reliant on the shape of both acceptors and donors (**Figure 12**), there are actually relatively very few choices available in terms of both donor-shapes and acceptor-shapes[48]. The use of Thiele's acid analogues as organic linkers could bring a greater structural diversity to MOF chemistry. Although the parent Thiele acid might suffer from unwanted retro Diels-Alder reactions under typical MOFs preparation, both of its alkenes can be selectively functionalized to strategically enhance the stability as an organic linker. More importantly, the tweezers-like shape of Thiele's acid has its own distinct internal angle which could provide additional spacing for organometallic carbon−metal bond formation[49]. This, coupled with its chemical tunability (affording different cleft angles and therefore potentially different MOF structures) could result in a novel series of structurally unique MOFs. And unlike most other alkyl based organic linkers[50], the structural rigidity of Thiele's acid based linkers would also reduce unwanted aggregation and distortion of their local structural features[50a].

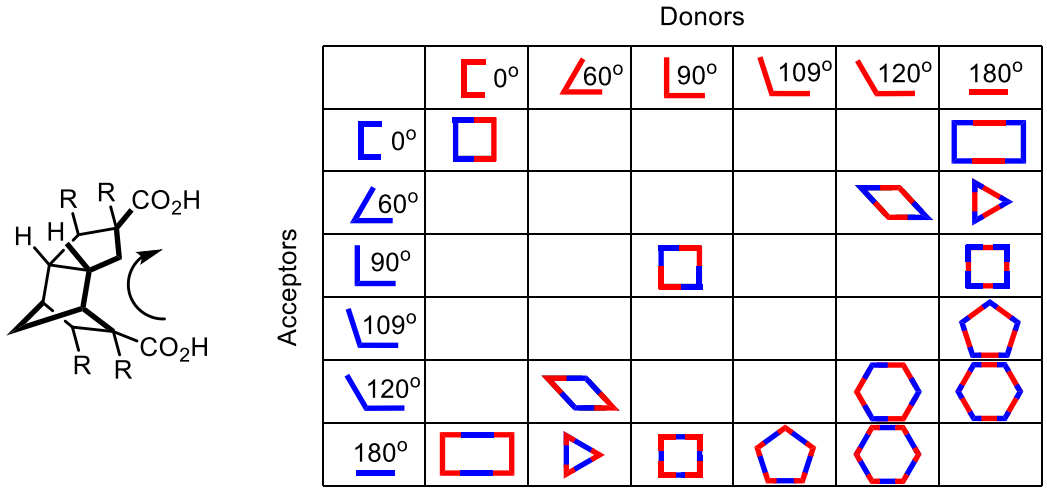

Figure 12: Internal angle of Thiele's acid analogues and the use of ditopic building blocks for the generation of 2D MOF scaffolds *via* self-assembly.

1.6.5. Functional polymers

Ring-opening metathesis polymerization of dicyclopentadiene is known to produce a tough, extensively crosslinked polymer (polydicyclopentadiene, PDCPD). This polymer is widely used in the automotive industry,[51] but its properties are not particularly tunable. As has already been mentioned, Thiele's ester represents an attractive functionalized analogue of dicyclopentadiene, and so one could imagine that polymerization of Thiele's ester would give rise to a useful, functionalized form of PDCPD. Of course, introduction of an ester group onto the norbornene ring of dicyclopentadiene would be expected to restrict the olefin metathesis reaction that underpins polymerization. This could perhaps be remedied by using the so-called "half" Thiele's ester **61** as the monomer instead (**Scheme 16**).

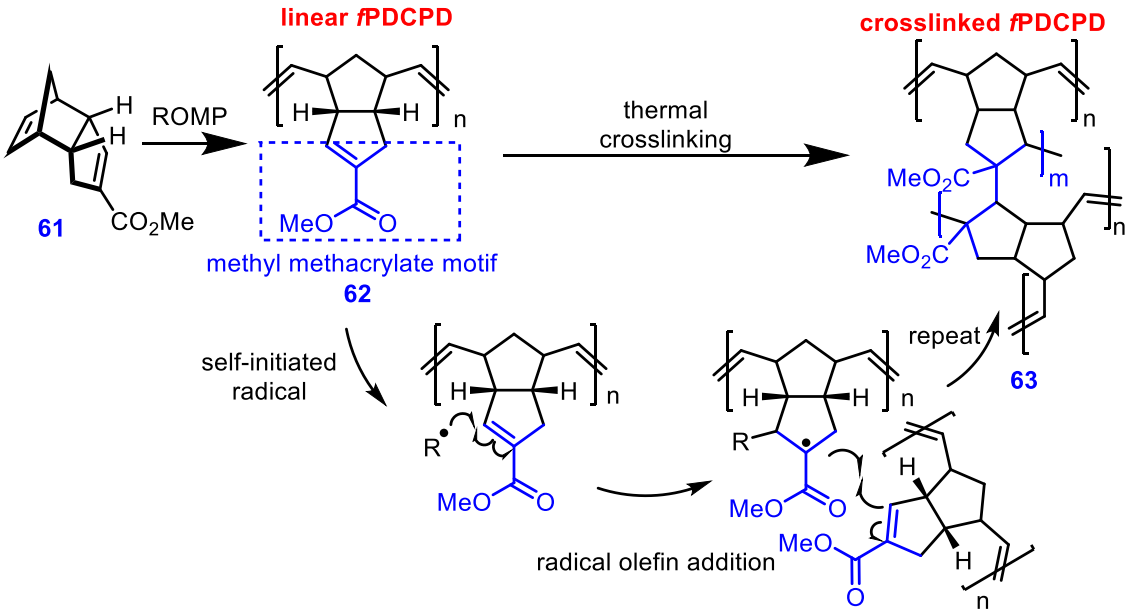

Scheme 16: Proposed synthesis of crosslinked functionalized polydicyclopentadiene *f*PDCPD *via* controllable thermal radical cyclization.

Just like dicyclopentadiene itself, the monoester-substituted monomer **61** contains a reactive norbornene-type alkene that should be susceptible to polymerization. The resulting linear polymer could then undergo thermal (radical) cyclization to yield a highly crosslinked material. The presence of the additional methyl ester group (relative to the parent PDCPD) would provide opportunities for tuning the chemical and physical properties of the material. Another limitation of polydicyclopentadiene is its lack of recyclability. With this additional ester group, different crosslinking and decrosslinking strategies (such as retro-Michael additions) could be applied, which opens the potential of designing a recyclable form of PDCPD.

1.6.6. Constrained enzyme inhibitor scaffolds

In designing active-site enzyme inhibitors, the native conformation of their core scaffold is extremely important to ensure that they can project functional groups to the appropriate subpockets of the enzyme's active site. Previously, in the Wulff group, a sulfone-based bicyclic scaffold has already shown that its rigidified bicyclic core could provide some benefits towards inhibiting viral neuraminidase by mimicking the enzyme-bound conformation of peramivir (the most potent compound among the three commercial influenza neuraminidase inhibitors)[52]. We envision that the unique conformational control of Thiele's ester could also be harnessed for the development of neuraminidase inhibitors (**Figure 13D**). The rigidity of its polycyclic core could not only reduce entropy of binding, but also enhance target selectivity between different isoforms of viral and human neuraminidases (see more detailed explanation in Chapter 5).

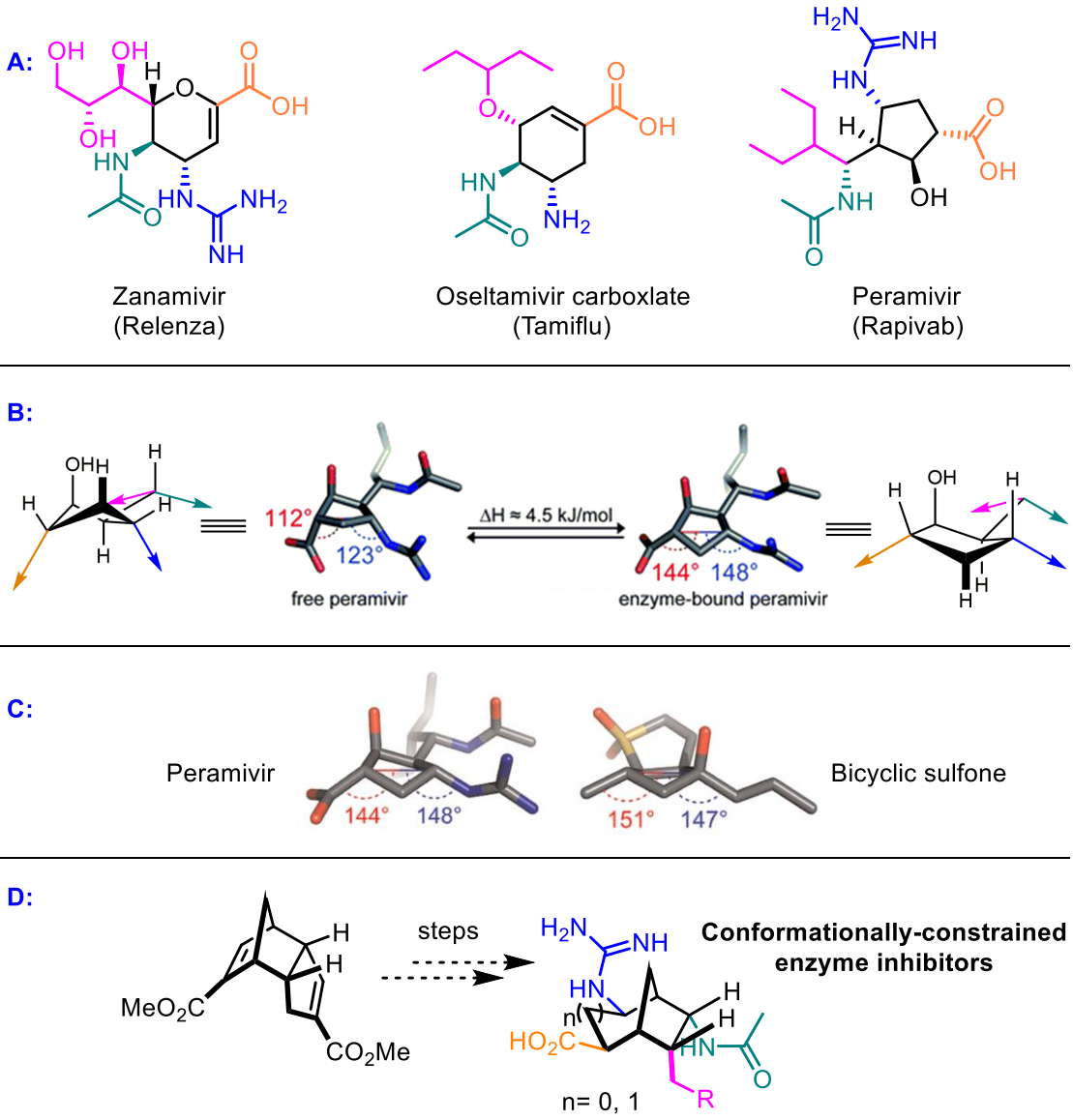

Figure 13: A: Three commercially available viral neuraminidase inhibitors; B: Difference between free and enzyme-bound peramivir; C: Conformational comparison of peramivir and bicyclic sulfone; D: Proposal to utilize Thiele's ester as the starting material for the production of new neuraminidase inhibitors.

Chapter Two: Exploration of the fundamental chemistry of Thiele's ester

The material in this chapter was adapted from: "Expansion of Thiele's Acid Chemistry in Pursuit of a Suite of Conformationally Constrained Scaffolds" **J. Chen**, B. Kilpatrick, A. G. Oliver and J. E. Wulff*, *J. Org. Chem.* **2015**, *80,* 8979-8989[53]; "Resolution of Thiele's Acid" **J. Chen**, X. Sun, A. G. Oliver, and J. E. Wulff*, *Can. J. Chem.*, **2016**, *95* (3), 234-238[54].

The optimization of Thiele's ester formation, the synthesis of **67** and **69**, and the attempts of the synthesis of **71**, **73**, **77**, **79** and **81** were accomplished by Brenden Kilpatrick under JC's supervision. The chiral amine screening for the resolution of Thiele's acid was conducted by Xuxin Sun under JC's supervision. The rest of synthesis, analysis and characterization of data were performed by JC. All X-ray structures were solved by Dr. Allen G. Oliver (University of Notre Dame). Dr. Ori Granot collected the HRMS data. All the DFT calculations were conducted by Dr. Jeremy E. Wulff.

2.0.0. Overview

Despite the fact that Thiele's ester has been known for over a century, its potential applications have not been fully recognized by the chemistry community. It is true that Thiele's ester has already achieved some attention from the fields of organic synthesis (as a rigid starting material)[38c], organometallic synthesis (as a ligand precursors)[3] and polymeric materials (as a backbone for self-healing polymeric networks)[37,55]. There are still many other interesting applications of Thiele's ester that are worth investigating. Thus, exploring the fundamental chemistry of Thiele's ester is worthwhile. In this chapter, an optimization of an efficient synthetic route to achieve regioisomerically pure Thiele's ester and its analogues is described. A quick survey of the reactivity of both alkenes and esters on Thiele's ester was performed to investigate the chemo- and regioselectivity of Thiele's ester. We were also able to acquire a series of Thiele's ester-based molecular clefts with a wide range of cleft angles[53]. Last but not least, a resolution of Thiele's acid was conducted to obtain both enantiomerically enriched Thiele's acids which could extend its applications in the fields of supramolecular and biological chemistry[54].

2.1.0. Optimization of the direct Thiele's ester synthesis

The "acid first" approach, which is typified by Thiele's original synthesis, is still the most commonly used way to produce Thiele's ester. By treating cyclopentadiene with base and CO_2, three intermediates which rapidly interconvert *via* [1,5] hydride shifts are achieved. Finally, Thiele's ester will be produced following Diels-Alder dimerization and esterification. However, due to the difficult purification of Thiele's acid and the formation of byproducts resulting from unwanted conjugate addition during the esterification step, neither the yield nor the purity is satisfactory.

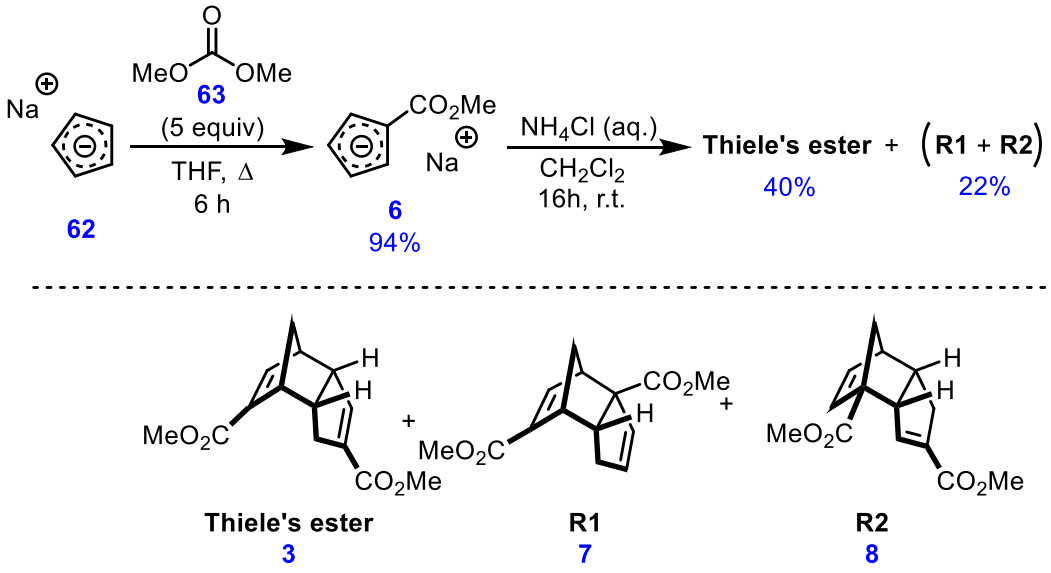

Scheme 17: First attempt to employ Dive's reaction conditions.

Recently, Dive and coworkers reported a modified synthetic route to Thiele's ester. By forming a stable metal salt intermediate **6** first, they avoided handling the problematic neutral compound **5.** The resulting salt can be reprotonated by aqueous ammonium chloride to give Thiele's ester as the major product in 34% yield. Dive's synthetic method was therefore envisioned as a starting point for our optimization. We noticed that the reported yield of salt intermediate **6** in Dive's work is only about 74% (in Chapter 1 **Scheme 5**). By simply increasing the amount of dimethyl carbonate to 5 equivalents, the salt intermediate **6** could be isolated by vacuum filtration to give a satisfying 94% yield. Although this resulting salt **6** can be isolated in its pure form, it does exhibit a slow degradation in the air. We then quickly treated **6** under Dive's conditions (aqueous NH_4Cl, dichloromethane, room temperature and overnight), and a slightly improved 40% yield of Thiele's ester was achieved after column chromatography, along with an additional 22% of an approximately 1:1 mixture of two regioisomers **7** and **8**. As the time, **7** and **8** were not structurally characterized; refer to chapter three for detailed structural analysis of these regioisomers. Since the solvent, temperature, reaction time and acid source would have a certain amount of influence over the reaction, we started working on each aspect to optimize the yield of Thiele's ester (**Table 1**).

Elevating the temperature from room temperature to 50 °C first modestly improved the isolated yield of Thiele's ester (*e.g.,* compare entry 1 with entry 2 or entry 4 with entry 5 in **Table 1**). Unfortunately, a serious decomposition was observed when more harsh temperature (110 °C in toluene) was applied (*e.g*., entry 8). Thus, a moderate temperature (50 °C) was selected for the rest of the conditions screened. Different reaction times (compare entry 6 with entry 5) and acid sources (*e.g*. entry 1, 3 and 4) were also explored. While AcOH and H_2SO_4 revealed themselves as better acid sources than aqueous NH_4Cl, there was no significant improvement of the yield by increasing the reaction time. However, the solvent effects did have a significant impact on both yield and product distribution, which suggests that this reaction may go through a polar reaction mechanism. This actually shed light on the mechanism of the formation of Thiele's ester and encouraged us to apply the radical stabilization logic to rationalize the formation of Thiele's ester (in Chapter 3). While extreme polar solvent (DMSO entry 9), acetic acid (entry 11) and neat condition (entry 10) all gave relatively poor yields (lower than 40%), aprotic solvents (toluene entry 7, THF entry 12, ether entry 13, DCM entry 14 and EtOAc entry 15) provided a slightly higher yield (all better than 40%). Polar protic solvents such as alcohols were found to offer the best results (MeOH entry 6, *i*PrOH entry 16 and 2-pentanol entry 17) with a clear trend that bulky solvents benefit the reaction yield. Although 2-pentanol gave a slightly better result than isopropanol (60% *vs.* 56%, respectively), the significant cost difference between two solvents led us to compromise with isopropanol as our solvent choice.

A quick screening of acid promoter was conducted again using isopropanol as the solvent. No distinguishable difference was found between acetic acid (entry 18) and sulfuric acid (entry 16) (both 56%). By contrast, the addition of *p*-toluenesulfonic acid reduced the yield to 48% (entry 19).

We eventually determined the most effective condition to be a combination of sulfuric acid and isopropanol at 50 °C overnight. These conditions provided consistent yields across different scales (1.76 g, 5 g and 10 g) with a slightly boosted yield of around 64% (entry 21, 22 and 23).

Table 1: Optimization of Thiele's ester formation.

	solvent	scale[a] (mg)	Acid	temp (°C)	crude ratio **3 : 7 : 8**	isolated yield of **3**
1	MeCN	500	AcOH[j]	r.t.[h]	100 : 21 : 22	39%[b]
2	MeCN	250	AcOH[j]	50[g]	100 : 24 : 21	53%
3	MeOH	250	NH_4Cl[j]	r.t.[i]	100 : 18 : 13	27%[b]
4	MeOH	250	H_2SO_4[k]	r.t.[i]	100 : 17 : 14	38%[b]
5	MeOH	250	H_2SO_4[k]	50[g]	100 : 15 : 13	48%
6	MeOH	250	H_2SO_4[k]	50[i]	n.d.	46%
7	toluene	250	AcOH[j]	50[g]	100 : 31 : 36	42%
8	toluene	250	AcOH[j]	110[c,g]	n.d.	0%[e]
9	DMSO	250	AcOH[j]	50[g]	100 : 26 : 36	28%
10	–[d]	250	AcOH[j]	50[i]	100 : 50 : 19	33%
11	AcOH	250	AcOH[j]	50[g]	n.d.	38%
12	THF	250	AcOH[j]	50[g]	n.d.	41%
13	Et_2O	250	AcOH[j]	r.t.[i]	100 : 32 : 42	41%[b]
14	CH_2Cl_2	250	AcOH[j]	40[c,h]	100 : 33 : 38	49%
15	EtOAc	250	AcOH[j]	50[g]	100 : 35 : 44	52%
16	**iPrOH**	**250**	**H_2SO_4[k]**	**50[g]**	**100: 19 : 18**	**56%**
17	2-pentanol	250	H_2SO_4[k]	50[g]	100 : 23 : 21	60%
18	iPrOH	500	AcOH[j]	50[g]	100 : 22 : 24	56%
19	iPrOH	500	*p*-TsOH[j]	50[g]	100 : 24 : 27	48%
20	iPrOH	500	H_2SO_4[k]	83[c,g]	100 : 13 : 9	< 58%[f]
21	**iPrOH**	**1750**	**H_2SO_4[k]**	**50[g]**	**n.d.**	**63%**
22	**iPrOH**	**5000**	**H_2SO_4[k]**	**50[g]**	**n.d.**	**64%**
23	**iPrOH**	**10000**	**H_2SO_4[k]**	**50[g]**	**n.d.**	**64%**

[a] Mass of **6** used. [b] Calculated yield, accounting for minor impurities in the isolated product. [c] Reflux temperature for the solvent. [d] This reaction was conducted in the absence of additional solvent. [e] Extensive decomposition precluded the isolation of any pure compound. [f] This product contained an unidentified impurity. [g] The reaction was run for 16 h. [h] The reaction was run for 48 h. [i] The reaction was run for 72 h. [j] 1.05 equiv of the acid source was used. [k] 0.55 equiv of the acid source was used.

2.2.0. Synthesis of Thiele's ester analogues

The possible applications of Thiele's ester are heavily dependent on the functional group handles that project outwards from the central core. The capability of our methodology in terms of derivatizing Thiele's ester to more interesting analogues was verified by applying a variety of electrophiles to the standard reaction conditions in **Table 2**.

Table 2: Electrophile screening for different Thiele's ester analogues.

electrophile	product	electrophile	product
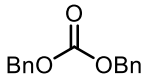 **64** **1.5 equiv** **Method B**	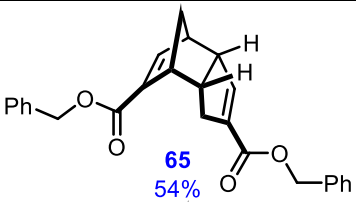 **65** 54%	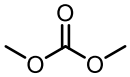 **63** **5 equiv** **Method A**	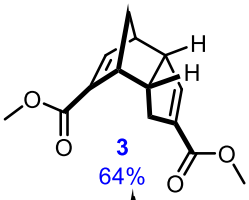 **3** 64%
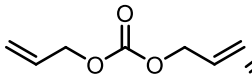 **66** **1 equiv** **Method A**	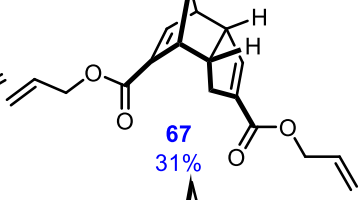 **67** 31%	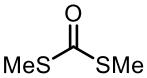 **74** **1.1 equiv** **Method B**	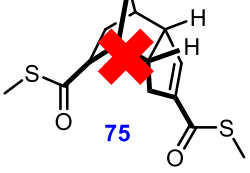 **75**
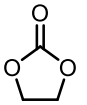 **68** **1 equiv** **Method A**	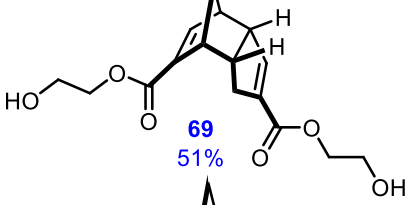 **69** 51%	CS_2 **76** **1.1 equiv** **Method B**	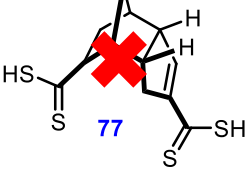 **77**
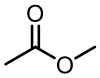 **70** **3 equiv** **Method B**	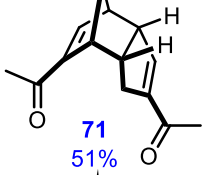 **71** 51%	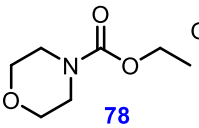 **78** **1 equiv** **Method B**	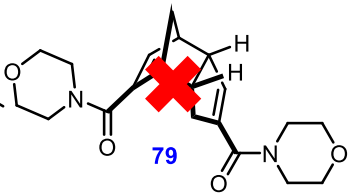 **79**
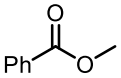 **72** **3 equiv** **Method B**	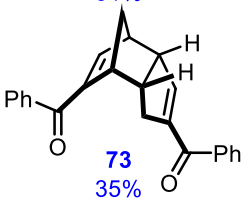 **73** 35%	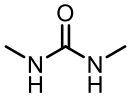 **80** **3 equiv** **Method B**	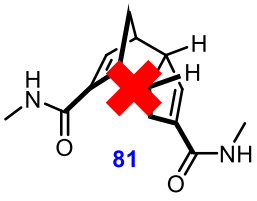 **81**

Method A: the intermediate salt was isolated by vacuum filtration, washed with ether, and dried prior to acidification in 2-propanol. Method B: the intermediate salt was used directly in the acidification step, without any purification.

Knowing that disubstituted carbonate works well under our conditions, a dibenzyl carbonate **64** was first tested. However, the resulting intermediate is somewhat more air sensitive than the methyl ester salt **6**. Thus, we modified our procedure to one in which the intermediate salt was directly acidified to trigger the desired Diels−Alder dimerization. This direct acidification protocol, referred

to as ‘Method B’ in **Table 2** was found to improve the yields of several related species. Due to the cost of electrophile **64**, we also reduced its usage from 5 to 1.5 equivalents. Despite this modification to the procedure, dibenzyl Thiele’s ester **65** was still achieved in a respectable 54% isolated yield. In order to access compounds containing functional group handles for subsequent derivatization, both diallyl carbonate **66** and ethylene carbonate **68** were employed as electrophiles to provide **67** (containing terminal olefins for subsequent cross-metathesis reactions) and **69** (containing primary alcohols for subsequent esterification reactions). Other types of electrophiles such as esters also proved themselves as suitable reaction partners under our conditions. We were able to access two ketone analogues (**71** and **73**) in serviceable yields (51% and 35%, respectively). Unfortunately, our attempts to use other heteroatom-containing electrophiles (such as dithiocarbonate, carbamate, carbon disulfide and urea) were not successful.

2.3.0. Chemo- and regioselective derivatization of Thiele’s ester in pursuit of molecular clefts with tunable cleft angles

With our optimized scalable methodology to Thiele’s ester and its analogues, we then directed our attention to exploring the fundamental chemistry of Thiele’s ester. One of our primary goals in this research was to identify chemo- and regioselective transformations that allow us to selectively modify the individual alkenes and individual carbonyl groups of Thiele’s ester.

2.3.1. Tunable molecular cleft

Thiele’s acid can be viewed as a molecular cleft. These kinds of structures (but not yet Thiele’s acid itself) have been widely used in the field of supramolecular chemistry[56]. We designed three alkene functionalized Thiele’s acids (mono-cyclopropane **82**, bis-cyclopropane **83** and bis-acetonide **84**) as our synthetic targets. By changing the hybridization states of the terminal carbons in this way, we hoped this would allow us to get access to a series of tunable molecular clefts as templates for the preparation of ß-hairpin peptidomimetics and other scaffolds. The preliminary DFT computational simulation (by Spartan’14 using B3LYP functionals with a 6-31G* basis set) also illustrated that our target molecular clefts together with Thiele’s acid itself would cover a broad range of cleft angle from approximately 120° to 190° (**Figure 14**).

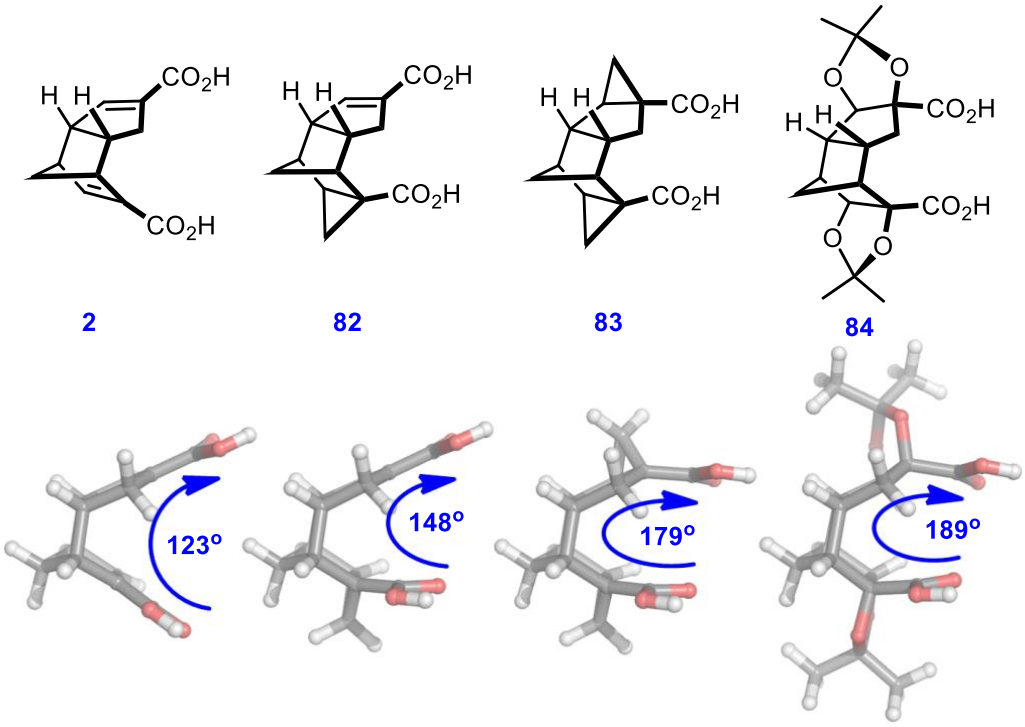

Figure 14: Computational prediction of cleft angles for synthetic Thiele's ester molecular clefts. Refer to Table 3 for an explanation of cleft angle determination.

With these computational results in mind, a nucleophilic cyclopropanation method—a Corey-Chaykovsky reaction—was performed on Thiele's ester. This reaction exhibited exclusive regioselectivity toward the more strained C5-C6 alkene to afford compound **85** as a single regioisomer and single diastereomer. The subsequent saponification selectively removed the methyl group at the C2' carboxyl group to give **86** as the desired target compound which allows us to couple peptides on the backbone for ß-hairpin mimics (**Scheme 18**).

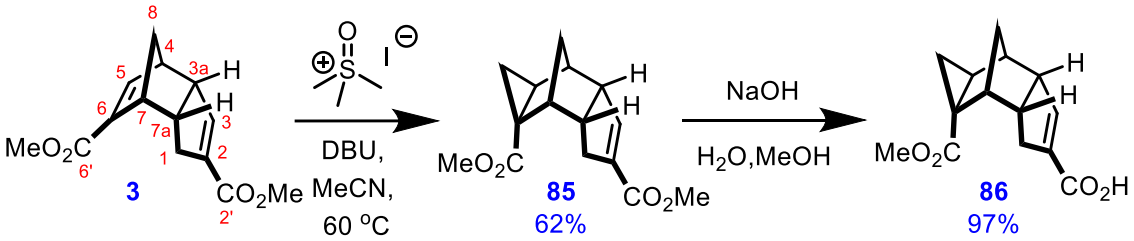

Scheme 18: Synthesis of mono-cyclopropyl Thiele's acid.

For the synthesis of our next target bis-acetonide **84**, we used osmium tetraoxide-mediated dihydroxylation to convert **3** to tetraol **87** with perfect diastereoselectivity at both sides of alkenes.

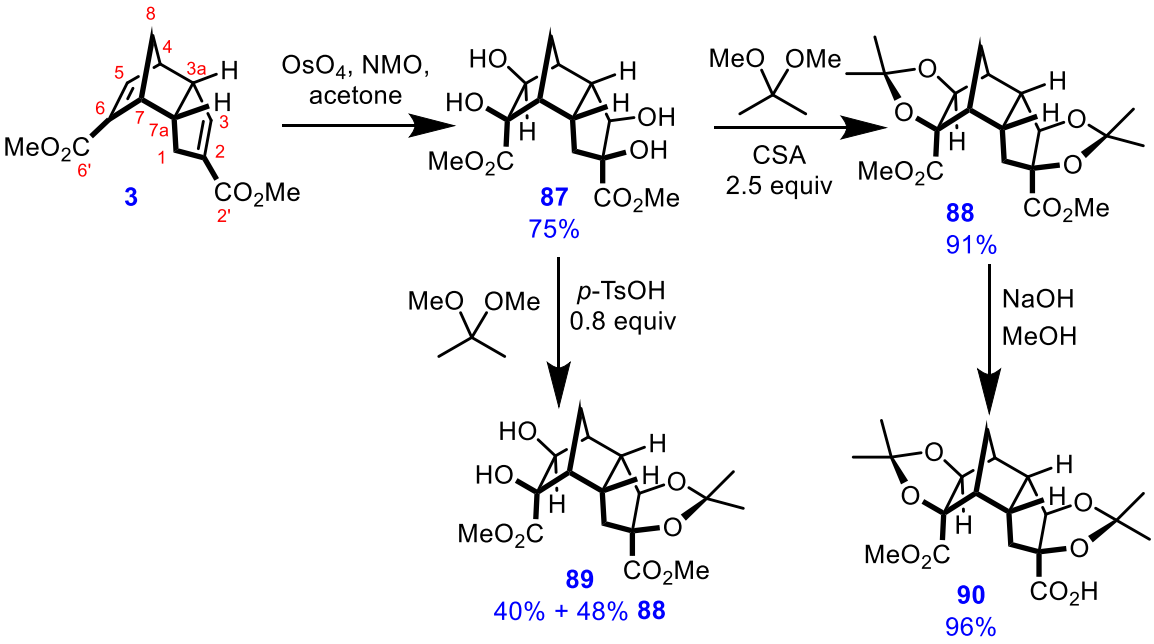

Scheme 19: Synthesis of bis-acetonide Thiele's acid.

Once again, a good level of regioselectivity was obtained during the diol protection. The C2-C3 diol reacted more rapidly than the C6-C5 diol. Under different acid catalyzed conditions, both fully protected compound **88** (obtained using a superstoichiometric amount of camphorsulfonic acid) and partially protected compound **89** (obtained using 0.8 equivalents of *p*-toluenesulfonic acid) can be achieved in 91% and 40% yield, respectively. A similar level of selectivity at the C2' position (as had been observed earlier in the conversion of **85** to **86**) was found during the subsequent hydrolysis of **88**. An excellent 96% yield of mono-hydrolyzed compound **90** was obtained, completing the synthesis of our second synthetic target.

The last target turned out to be a bit more challenging to us since the second cyclopropanation would not occur under Corey-Chaykovsky cyclopropanation conditions even with elevated temperature (possibly due to the unique geometry of the 5-membered ring). In order to complete our synthetic plan, we strategically reduced both esters on **85** to diol **91** to make the C3-C2 alkene more electron rich. The electrophilic Simmons-Smith cyclopropanation then successfully installed the second cyclopropane ring on **91** to provide **92** in an almost quantitative 97% yield. The subsequent Ru-catalyzed oxidation of the two primary alcohols allowed us eventually acquire the last diacid target **83**.

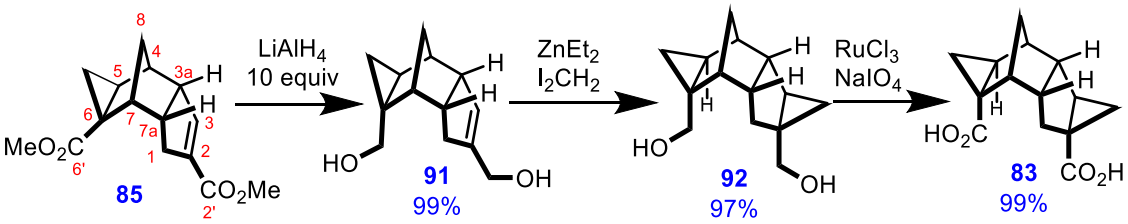

Scheme 20: Synthesis of bis-cyclopropyl Thiele's acid.

Fortunately, we managed to grow X-ray diffraction grade single crystals of both **86** and **90**. Together with the known crystal structure of **3** itself (CCDC 704728)[49], we were pleased to find that our DFT calculations of the cleft angles for the target diacid compounds were relatively close to the X-ray crystallography results. The cleft angle is defined by us as (360°-(α+β)) in **Table 3**. By defining the angle in this way, it allows us to define a U-turn shape as 180° and a right-angle shape as 90°.

The crystal structure of diester **3** possesses a slightly narrower cleft angle (133°) than the DFT calculated result for diacid **2** (123°). On the other hand, the solid-state structure of mono-acid **90** reveals a slightly broader cleft angle (176°) than calculated diacid **84** (189°). The difference between X-ray data of mono-acid **86** (149°) and the DFT calculation for diacid **83** (148°) was negligible. Although there is up to ±10° disagreement between the experimental and our computational stimulations in the case of **2** and **84** (which might be caused by a variety of factors. *e.g.*, our DFT calculation is a gas-phase simulation; diacids were calculated as targets; crystal packing effects, etc.), it does give us a rough idea that this bis-cyclopropyl diacid compound **83** should carry a cleft angle in the midway between **82** and **84**. Despite the fact we did not have X-ray data of **83**, based on our early DFT calculation (**Figure 14**), the cleft angle of can **83** still be assumed to be approximately 179°.

Table 3: Comparison between X-ray data and DFT calculations.

Cleft angle = $(360^{o}-(\alpha+\beta))$

X-ray data	DFT calculations
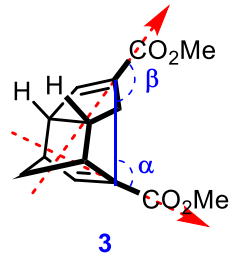 **3** 133°*	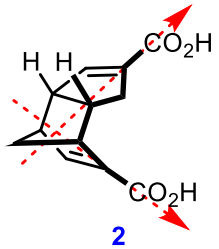 **2** 123°
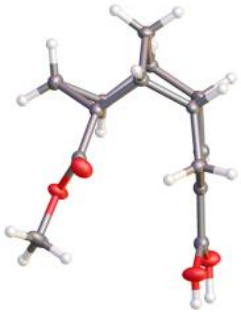 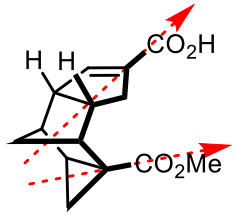 **86** 149°	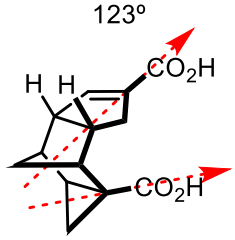 **82** 148°
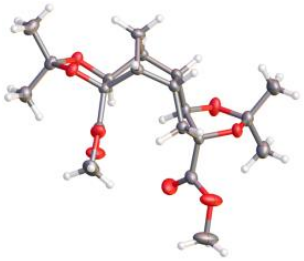 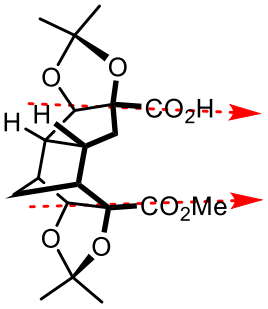 **90** 176°	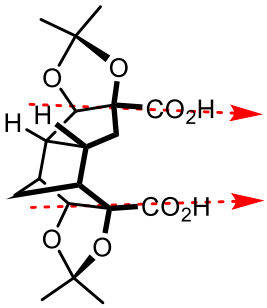 **84** 189°

* Crystal structure was obained from CCDC 704728

2.3.2 Synthesis of diacid analogue of mono-cyclopropyl Thiele's acid

Despite the fact that the hydrolysis of **88** and **86** took place with impressive regioselectivity which introduces the potential to make a new series of conformationally tunable Thiele's amino acids via Curtis rearrangement, we still wanted to address the limitation to directly afford diacid compounds. Since a hydrogenolysis pathway might exhibit different reactivity from hydrolysis, dibenzyl Thiele's ester **65** was chosen as the starting material instead of methyl Thiele's ester. Similar regioselectivity as described above was obtained following Corey-Chaykovsky cyclopropanation of **65**. The resulting diester **93** was reacted under standard hydrogenolysis conditions to convert the diester to

the corresponding diacid **94**. However, this was accompanied by additional reduction on the remaining C2-C3 olefin, to afford **94** in quantitative yield.

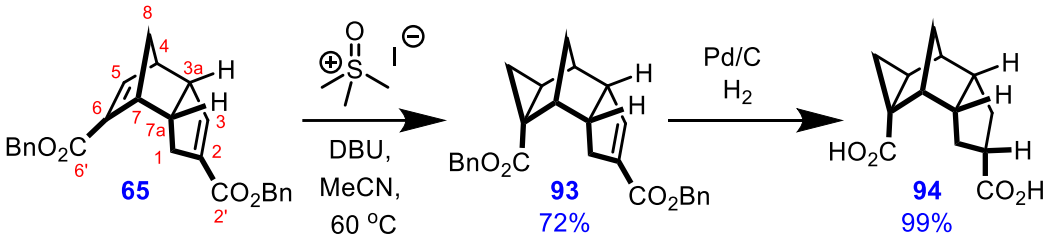

Scheme 21: Synthesis of diacid homologue of mono-cyclopropyl Thiele's acid.

2.3.3. Additional regioselective transformations from mono-cyclopropyl Thiele's acid

The interesting regioselectivity leading to mono-cyclopropyl Thiele's acid **86** encouraged us to undertake further investigation around this structure. Two more reactions were tested to probe the general reactivity of two esters on **85**. Grignard addition resulted in exclusive attack at the C2' ester to give **96** in 70% yield (even with 4 equivalents of methyl Grignard reagent). In the case of $LiAlH_4$ reduction (with a reduced amount of $LiAlH_4$), although the C2' ester is more reactive than the C6' ester, the reaction still gave a mixture of **95** and **91** in 50% and 39% yield, respectively. This selectivity presumably can be enhanced by more careful control of the amount of reducing reagent.

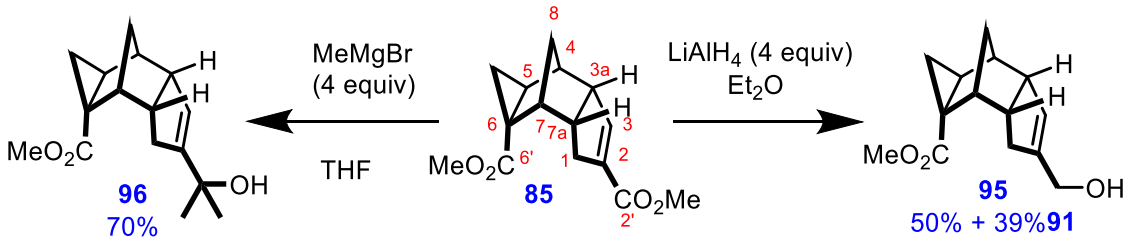

Scheme 22: Exploring additional regioselective of mono-cyclopropyl Thiele's acid.

2.3.4. Optimized hydrolysis of Thiele's ester

It is known that Fisher esterification of Thiele's acid suffers from unwanted conjugate addition from the reaction solvent[7]. The same competing reaction was found in the hydrolysis of Thiele's ester as well[57]. In order to improve the yield and the purity of Thiele's acid, we conducted this hydrolysis reaction with a bulky solvent (isopropanol). A 92% yield was achieved and the resulting Thiele's acid was isolated in pure form, without any observation of the unwanted conjugate addition product.

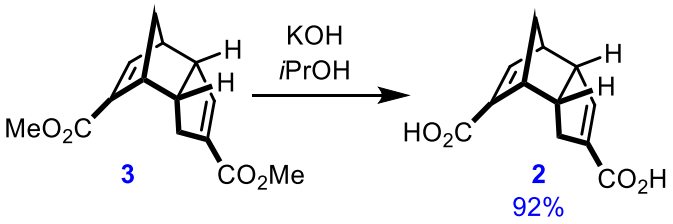

Scheme 23: Optimized hydrolysis of Thiele's ester.

2.3.5. Preliminary results in pursuit of a conformationally constrained neuraminidase inhibitor

One of our long-term interests in this research is utilizing Thiele's ester as the bicyclic core of a conformationally constrained neuraminidase inhibitor. During our Thiele's ester-based molecular cleft study, the regio- and chemoselectivity that Thiele's ester demonstrated with respect to both the alkenes and the esters encouraged us to do some preliminary tests to explore the possibility of pursuing the synthesis of a Thiele's ester based neuraminidase inhibitor. The binding sites of a neuraminidase inhibitor can be generally divided into four subsites. The S1 subsite is a pocket made up of an Arg 118, Arg 292, Arg 371, Tyr 347 and Tyr 409. The arginine triad residues, which are highly conserved across the neuraminidase family, provide a positively charged electrostatic and hydrogen-bonding environment for anionic substituents on inhibitors, such as carboxylates or phosphonates[58]. The S2 subsite is a region consisting of three negatively charged residues Glu 119, Glu 227, Asp 151 and the backbone carbonyl of Trp 178.[59] Typically, the amino and guanidino groups of potent inhibitors show a strong electrostatic interaction to these acid residues. The S3 subsite is a lipophilic pocket made up of Trp 178, Ile 222 and Arg 152. Commonly, the acetamide group also constitutes a recognition element. The methyl group on the acetamide has a favourable interaction with a small hydrophobic pocket comprised of elements from Trp 178 and Ile 222, while the carbonyl group can also form a hydrogen bond with Arg 152. The S4 subsite consists of an extended hydrophobic surface including Ala 246, Ile 222, Arg 224 and the carboxylate of Glu 276 in its *trans* conformation[59b]. When Glu 276 exists in an alternative conformation with its carboxylate binding to Arg 224, its methylene group along with other hydrophobic surfaces (from Ala 246, Ile 222 and Arg 224) will provide a hydrophobic pocket[59b]. Both the lipophilic 3-pentyl group (in oseltamivir and peramivir) and more polar triol group (in zanamivir) have been applied in this pocket. Unfortunately, these pockets also limit the clinical utility of peramivir and oseltamivir. A point mutation wherein histidine 274 is replaced with a bulkier tyrosine residue prohibits glutamic acid 276 from rotating out of the active site[60].

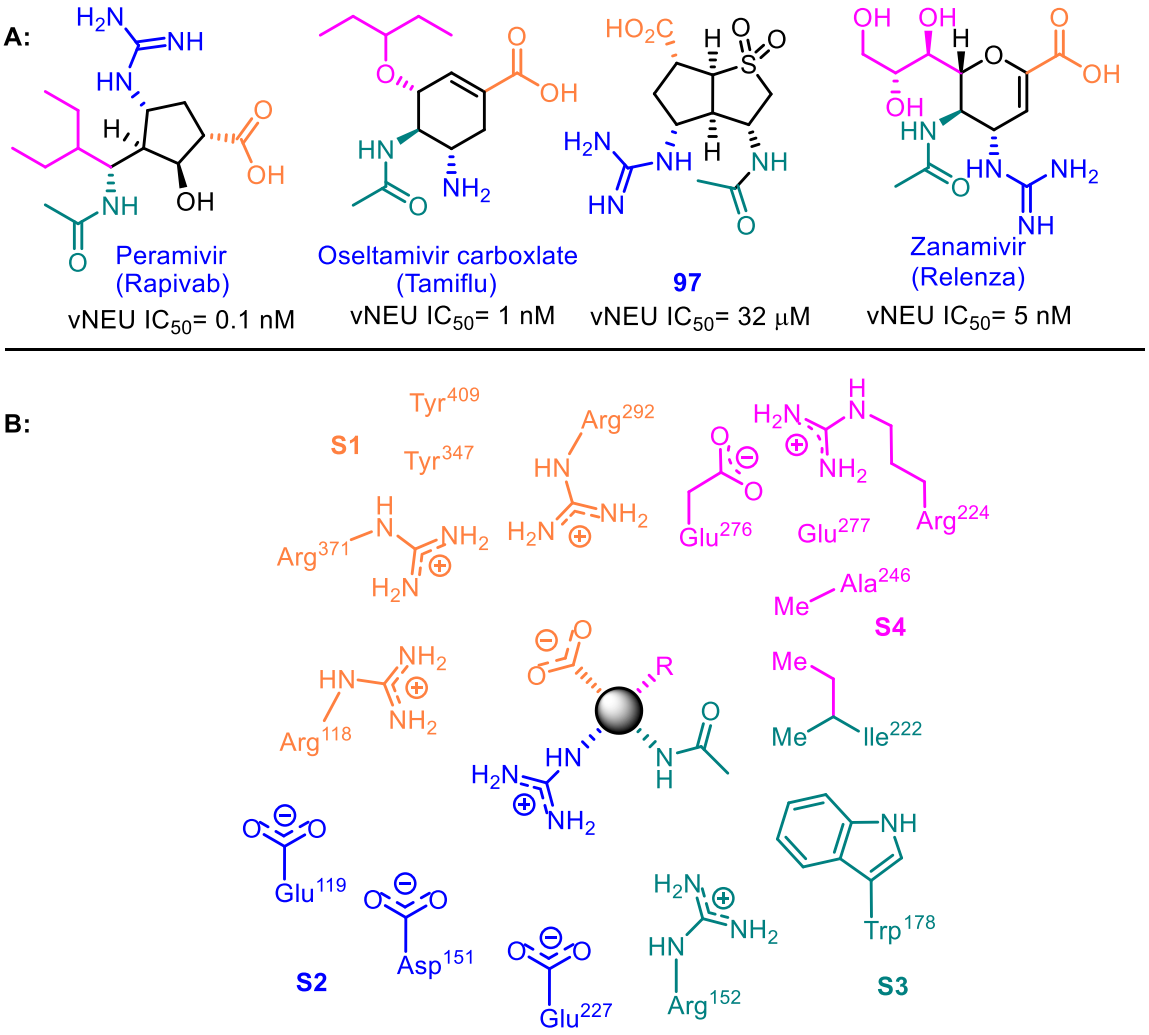

Figure 15: A: Structures of three commercially available viral neuraminidase inhibitors (peramivir, oseltamivir carboxylate, zanamivir) and a bicyclic sulfone-based viral neuraminidase inhibitor; B: Important interacting residues present in the sialic acid binding domain of neuraminidase.

Thiele's ester already has two ester groups which could be converted to carboxylic acids in order to provide interaction with the S1 pocket. According to our reigo- and chemoselectivity study of Thiele's ester, the conjugated C5-C6 alkene is a much better Michael acceptor than the C2-C3 alkene. In order to install amine or guanidine group on the ring to bind the S2 pocket, benzyl amine was chosen as a convenient, nucleophilic masked ammonia surrogate. This reaction gave a mixture of two diastereomers **98** (53%) and **99** (19%). Exposure of **98** to more DBU and higher temperature facilitated isomerization to the more stable **99**, although some elimination of benzylamine was also observed under these conditions. The remaining C2-C3 alkene could then be oxidized to **100** in a 52% yield. This resulting diol **100** could allow us to install the crucial

acetamide for compatibility for the S3 pocket (oxidative cleavage of the diol followed by Curtis rearrangement) and polar/nonpolar side chains for S4 pockets.

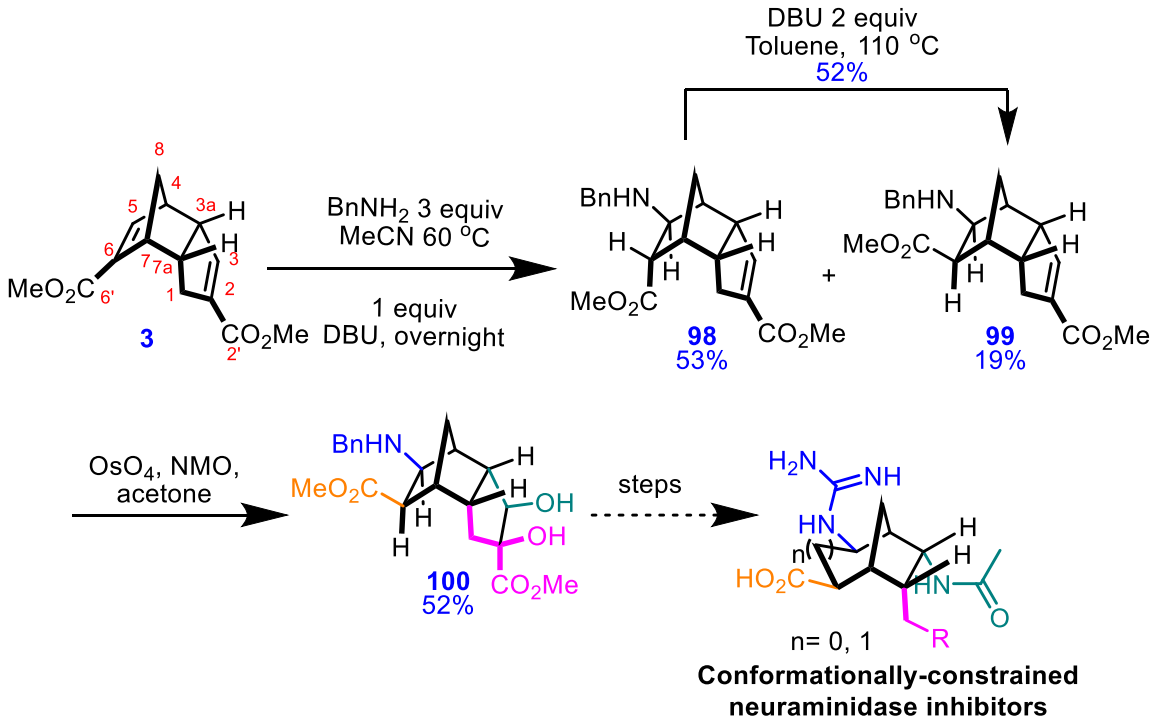

.

Scheme 24: Preliminary attempt towards a Thiele's ester-based bicyclic neuraminidase inhibitor.

2.4.0. Resolution of Thiele's acid

Molecular clefts such as Tröger's base have found a wide range of applications, as mentioned in Chapter 1. A significant amount of those applications required an enantiomerically pure material. While the well-developed Tröger's base has several different ways to produce both enantiomers[61], the resolution of Thiele's acid has not yet been reported in the literature. Thus, we contributed our efforts to developing the first resolution of Thiele's acid.

2.4.1. Screening of chiral amines

Owning to the fact that Thiele's acid is a chiral diacid compound, we hypothesized that a combination of chiral amines and Thiele's acid would lead to the formation of a diastereomerically enriched crystalline salt. Ideally, one enantiomer would be easier to crystalize with the "right" amine which eventually allows us to achieve enantiomerically pure compound after aqueous workup. As illustrated in **Table 4**, a variety of chiral amines were screened including (*S*)-(–)-methylbenzylamine **101**, L-tryptophan ethyl ester **102**, L-tyrosine hydrazide **103**, and (–)-cinchonidine **104**. None of

them showed any selectivity even in a broad range of crystallization solvents (EtOH, acetone, water, EtOAc, *i*PrOH and MeOH).

Table 4: Screening of chiral amine and the diastereoselectivity ratio of bis-brucine-Thiele's acid salt.

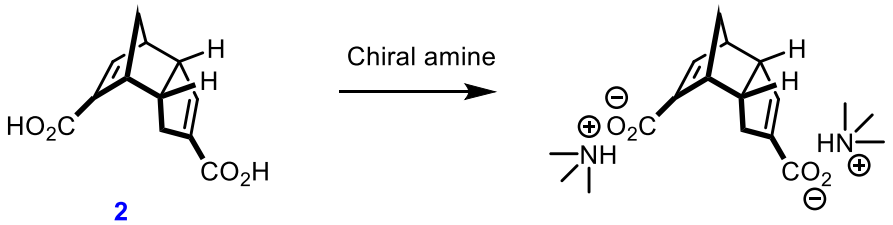

2
Thiele's acid

Diastereomer salt

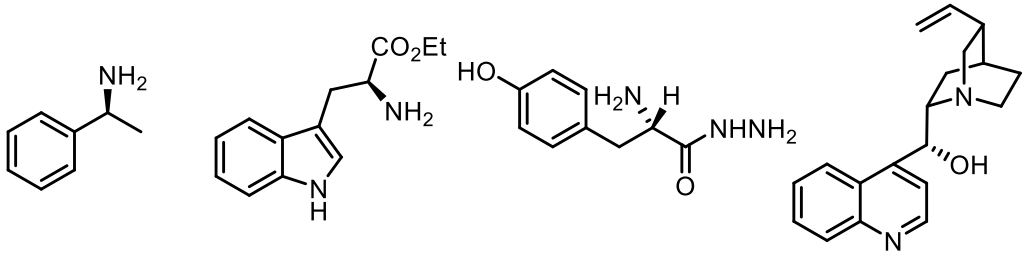

101 **102** **103** **104**

No selectivity in a wide range of solvents:
EtOH, acetone, water, EtOAc, iPrOH, MeOH

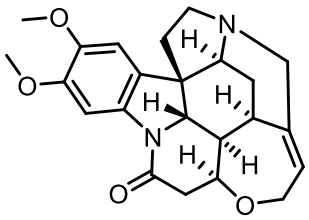

brucine **105**

crystalization solvent	d.r.[a]
ethanol	no crystal
isopropanol	1.5 : 1
methanol	3.6 : 1
methanol[b]	> 18 : 1

a. Diastereoselectivity ratio (d.r.) is measured by NMR in a mixture solvent (8.3: 1 = benzene-d_6: $CDCl_3$); b. After three recrystallizations from methanol.

Fortunately, brucine **105** and Thiele's ester in alcoholic solvents provided at least partially enriched salt crystal. Methanol provided a better ratio of diastereomers (3.6:1) than ethanol or isopropanol. Using the same conditions, with the help of two further recrystallizations from methanol, the d.r. eventually was enhanced up to 18:1, as assessed by NMR (**Figure 16**).

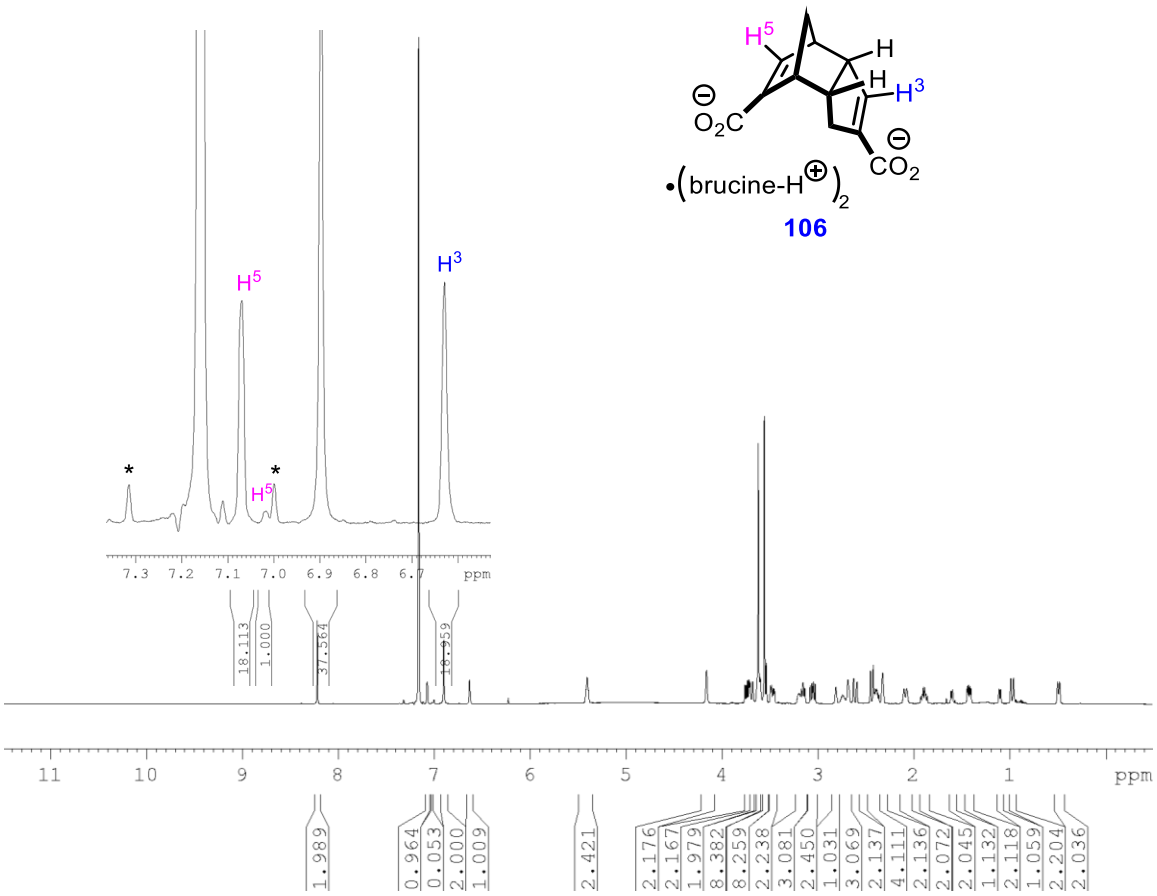

Figure 16: ^{1}H NMR spectrum of the bis-brucine salt of Thiele's acid 106 after the third recrystallization from methanol, recorded in 8.3:1 C_6D_6–$CDCl_3$. Signals corresponding to the two vinyl C–H protons are labeled. The peaks indicated by the single asterisks correspond to a ^{13}C satellite from benzene.

2.4.2. Preparative Resolution

This recrystallization method can be scaled up to 1.1 g of starting Thiele's acid. A respectable 1.9 g (37% yield) of diastereomerically enriched salt **106** was obtained. The purified salt was acidified to remove the brucine, and the desired diacid was extracted into ethyl acetate. The organic solution was dried and evaporated, affording a near-quantitative recovery of **(–)-2** (determined by optical rotation $[a]_D^{28.6}$ = – 228°). The overall yield of **(–)-2** from the initial racemic mixture was 72%. The recovered mother liquor can undergo the same procedure (acidification then extraction with ethyl acetate) to yield the other enantiomer **(+)-2** (**Scheme 25**).

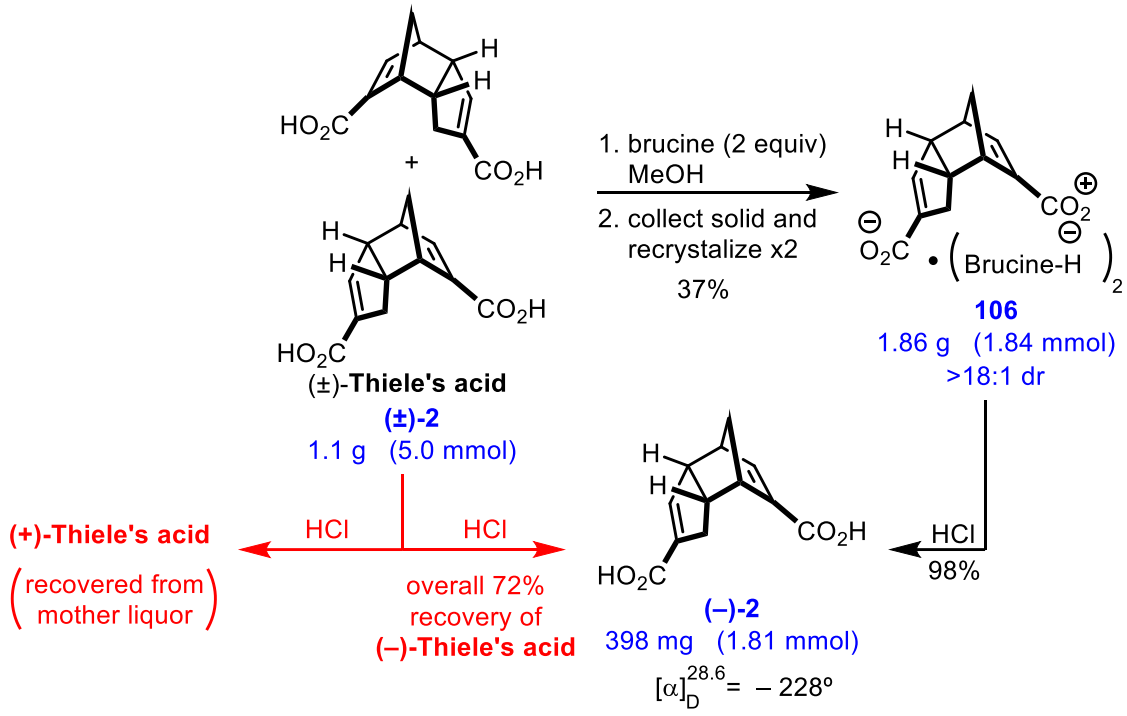

Scheme 25: Resolution of Thiele's acid.

2.4.3. Determination of absolute configuration

In order to figure out the absolute configuration of isolated pure enantiomers, both X-ray diffraction (XRD) and vibrational/electronic circular dichroism (VCD/ECD) could be useful methods. Unfortunately, due to the difficulty of crystallization and the poor solubility of Thiele's acid, neither of these two methods can be used in the present case for diacid **2**. However, the X-ray structure of the racemic methyl ester derivative was reported in the literature[3]. Thus, we converted both **(–)-2** and **(+)-2** to their corresponding dimethyl ester derivatives via carbodiimide-promoted esterification reactions. The spectra for **(–)-3** and **(+)-3** were identical, and the magnitudes of their optical rotations were equal within experimental error ($[a]_D^{25}$ = – 216° *vs* $[a]_D^{24}$ = + 269°). Gratifyingly, crystals produced from **(–)-3** diffracted well, and high-quality X-ray diffraction data were obtained. A copper microfocus source was used to reliably determine the absolute stereochemistry despite the absence of heavy atoms in the crystal. These data ultimately allowed us to assign the absolute configuration of **(–)-2** and **(–)-2** as 3a*R*,4*R*,7*S*,7a*R*.

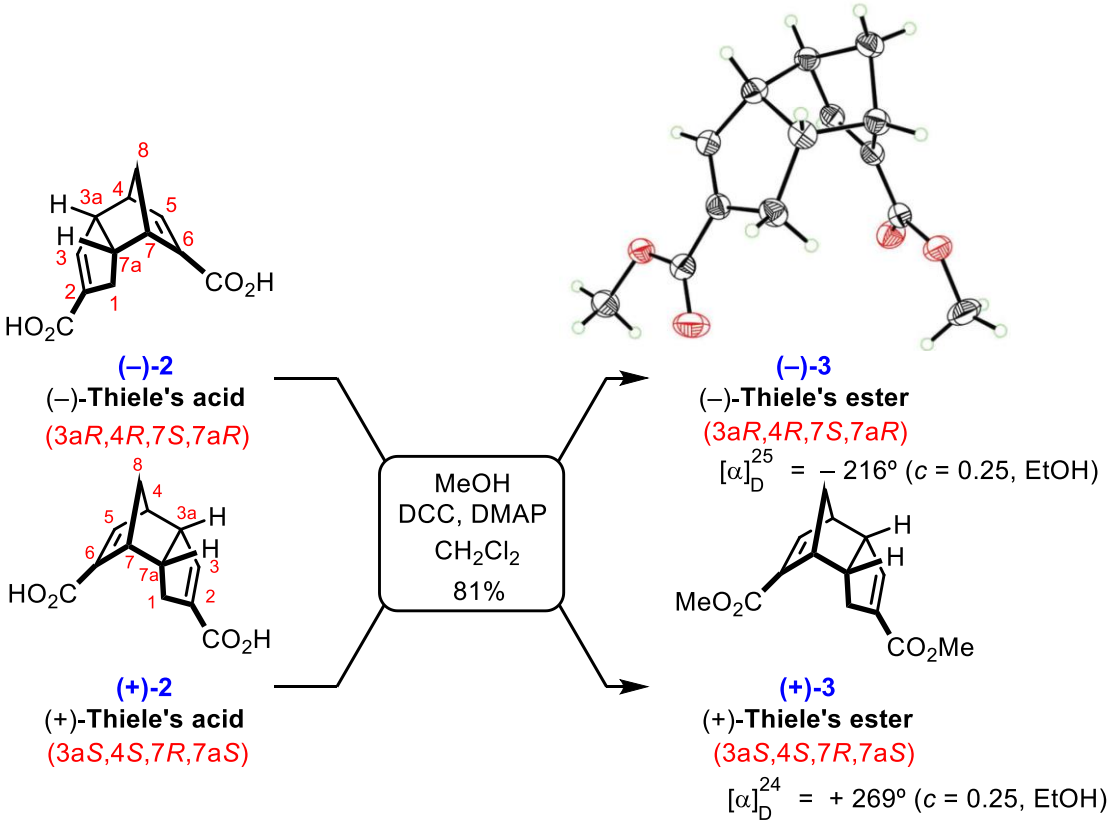

Scheme 26: Esterification of resolved Thiele's acids and X-ray structure for (–)-Thiele's ester.

2.5.0. Concluding remarks

We have successfully optimized the synthesis of Thiele's methyl ester to an efficient and scalable methodology. Five additional Thiele's esters and ketones were prepared in the same manner. During our study of chemo- and regioselectivity in Thiele's ester chemistry, we found that its C5-C6 alkene is more reactive under nucleophilic condition and its C2-C3 alkene exhibits a preference for reactivity under electrophilic condition. Conversely, in the case of mono cyclopropyl or acetonide functionalized (at the C5-C6 alkene) Thiele's ester, the C2' esters are more reactive than the C6' esters under a board range of reactions ($LiAlH_4$ reduction, hydrolysis, Grignard addition). Taking advantage of these selectivities, we prepared a series of Thiele's ester based molecular clefts with a range of cleft angle from 123° to 176°. In addition to these, a preliminary attempt towards a Thiele's ester based bicyclic neuraminidase inhibitor was undertaken. The positive results do encourage us to keep pursuing this as a potential direction. Finally, a resolution of Thiele's acid to both of its pure enantiomers can be obtained by using a chiral amine (brucine). This work encourages the future supramolecular and biological applications of Thiele's acid.

Chapter Three: Determination of the structures of two minor regioisomers and utilizing a radical stabilization algorithm to predict the regioisomeric outcomes of Thiele's type dimerizations

The material in this chapter was adapted from: "Expansion of Thiele's Acid Chemistry in Pursuit of a Suite of Conformationally Constrained Scaffolds" **J. Chen**, B. Kilpatrick, A. G. Oliver and J. E. Wulff*, *J. Org. Chem.* **2015**, *80,* 8979-8989[53]; "Revisiting the Mechanistic Origins of Thiele's Ester Dimerization: Probing the Reliability of Predictive Models for Cycloadditions" **J. Chen**, and J. E. Wulff *, *Org. Biomol. Chem*., **2016**, 14, 10170-10173[62]; "Radical Stabilization Algorithm as a Predictive Tool for Novel and Reported Noncanonical Thiele's Acid Analogues" **J. Chen**, L. Lu, and J. E. Wulff*, *Synlett,* **ASAP**[63].

All the synthesis, analysis and characterization of data were performed by JC with the exception of ^{1}H-NMR data of **109a** which was obtained from Lingxiao Lu. All X-ray structures were solved by Dr. Allen G. Oliver (University of Notre Dame). Dr. Ori Granot collected the HRMS data. All the DFT calculations were conducted by Dr. Jeremy E. Wulff.

3.0.0. Overview

As described in Chapter 1, the minor regioisomers produced alongside Thiele's ester have been assigned very ambiguously by other groups. Not only did the previous structural assignments not agree with one another, different authors have even differed in their reports of the number of regioisomers produced in the reaction (**Figure 1** in Chapter 1)[3,5,8-9]. There are a few reasons why we are eager to know this unrevealed information. First, the ambiguity with respect to the minor regioisomers makes one question whether the traditional "acid first" and our "ester first" approach give the same regioisomeric outcome. Second, from a mechanistic perspective, knowing the exact structure of each regioisomer would be a crucial piece of information if one tries to systematically study the regioselectivity of this complicated Diels-Alder reaction. In addition to this, the predictive power of mechanistic methods (discussed in Chapter 1) can also be further verified by forecasting the precise regioselectivity of each minor regioisomer, along with the major compound Thiele's ester itself. In this chapter, we describe our contribution to the structural elucidation of two isolatable minor regioisomers through an extensive 1D- and 2D-NMR study (^{1}H, ^{13}C, COSY, NOESY, HSQC, HMBC, TOCSY). With the correct structures in hand, we found that orbital energy levels are sufficient to describe gross reactivity for the system, but that orbital coefficient arguments (and frontier molecular orbital theory in general) do not reliably predict the regioisomeric outcome for the reaction. However, Deslongchamps' radical stabilization arguments (which extend from the bent bond model of reactivity) not only precisely predicted the formation of Thiele's ester and its two associated minor regioisomers, but also successfully rationalized the regioselectivity of all the existing Thiele's ester analogues, once steric factors are taken into account.

3.1.0. NMR study of two minor regioisomers

The multigram-scale synthesis of Thiele's ester provided us sufficient amounts of both minor regioisomers to conduct our NMR study. We quickly noticed that not only were both minor regioisomers spectroscopically identical to those isolated by Dive (the first direct ester approach) and Marchand (the traditional "acid first" approach), but also that the elution sequences of these minor regioisomers from the chromatography column were exactly the same as what Marchand described in his *Tetrahedron* paper. Regardless of the exact structures of the two minor regioisomers, these crucial data at least solved the first puzzle by suggesting that both the traditional "acid first" and our "ester first" approach result in the identical regiochemical outcome, albeit with somewhat variable product ratios (ratio of compound **3**:**7**:**8** in Dive's approach= 64:20:16; ratio of compound **3**:**7**:**8** in Marchand's approach=81:2:17). Due to all of the reasons that described above, our priority then became to unambiguously solve the structures of both isolated minor regioisomers. 1D- and 2D nuclear magnetic resonance (NMR) spectroscopy is arguably one of the most powerful analytic techniques in terms of resolving small molecule structural information (X-ray crystal diffraction could be even stronger than NMR when high quality single crystals of the

desired compound are available, but that was not achievable in this instance). Thus, we started our study by acquiring NMR spectroscopic data for the two purified regioisomers.

3.1.1. Minor regioisomer #1

From the ^{1}H-NMR spectrum of minor regioisomer **7** (the compound eluting from the chromatography column first after Thiele's ester), we found that the two set of peaks at approximately 5.5 ppm have very similar chemical shifts to the unstrained dicyclopentadiene alkene protons at C2-C3. A doublets of doublets was also observed at 6.8 ppm which is more downfield than the strained C5-C6 alkene protons on the parent structure.

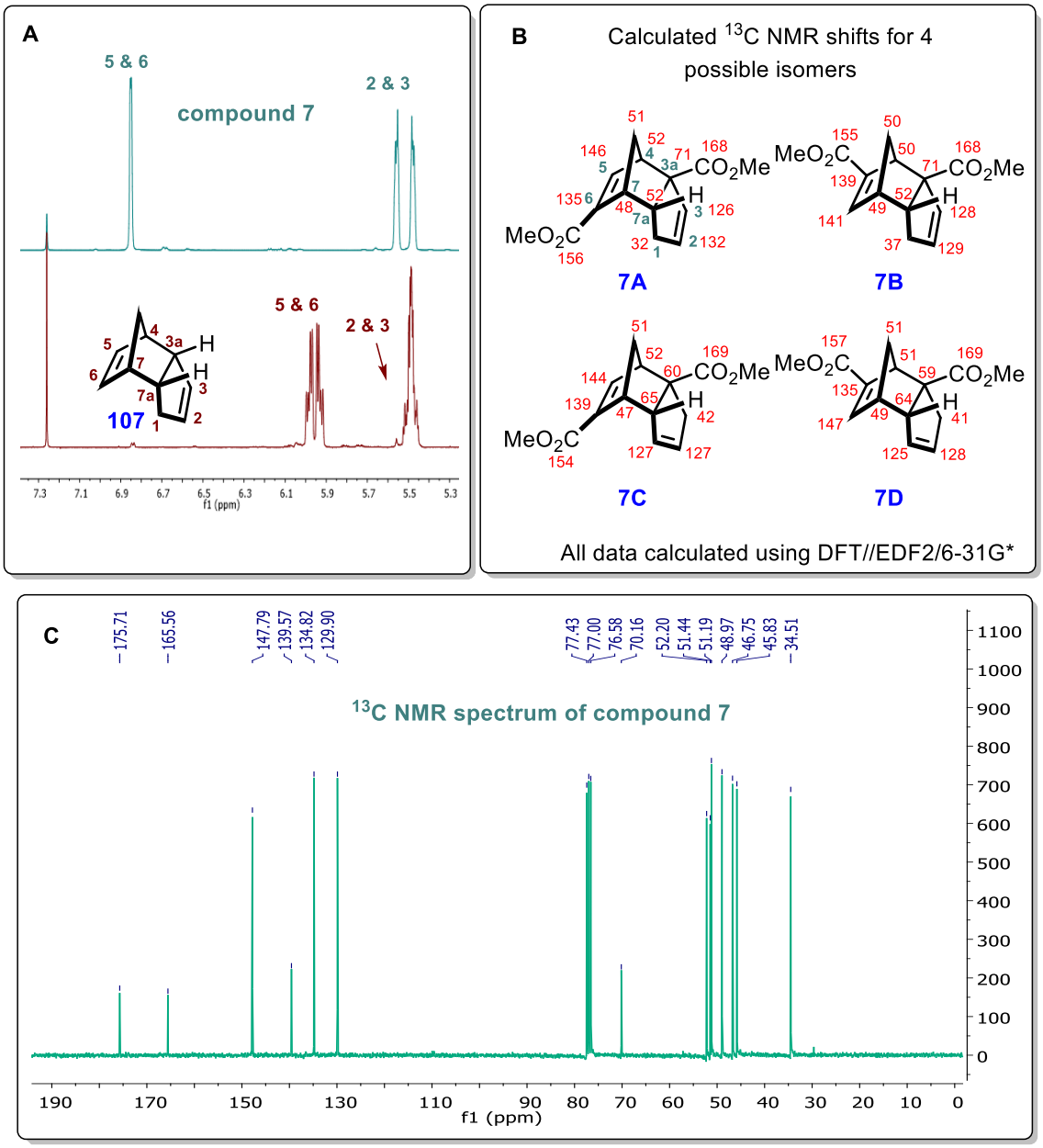

Figure 17: A: A comparison of ^{1}H NMR spectra for dicyclopentadiene and compound 7; B: DFT calculation of ^{13}C NMR shifts of 7 A-D; C: ^{13}C NMR spectrum of 7 in $CDCl_3$.

These observations indicate that the C2-C3 positions are unsubstituted in structure **7**. By contrast, one of the two methyl ester groups should be attached on either C5 or C6, causing the chemical shift of the adjacent vinyl proton to move more downfield. Meanwhile, DEPT NMR confirmed the presence of two methylene groups (CH_2), and a quaternary alkyl carbon. This allowed us to place the remaining methyl ester group at either one of the ring-fusion positions (i.e. C3a or C7a). With these data in mind, four possible structures for **7** were proposed by us (Figure 17B). These are the only possible structures which fit the above criteria.

After narrowing down **7** to four candidates, more sophisticated 2D NMR techniques (COSY, NOESY, HSQC, HMBC and TOCSY) were needed to complete the structure determination. However, the first challenge that we ran into was the overlap of certain protons.

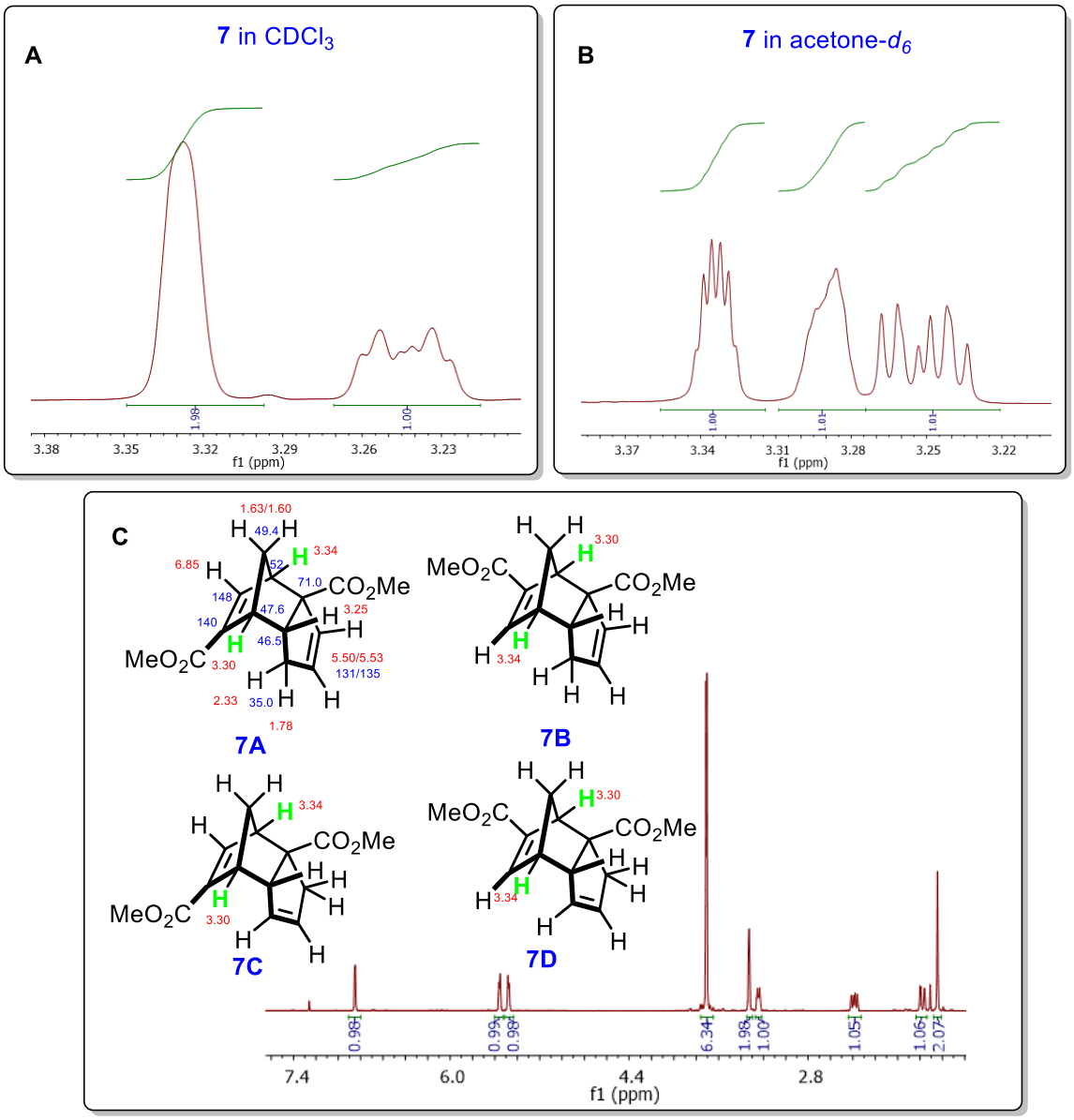

Figure 18: A: ^{1}H NMR spectrum of 7 in $CDCl_3$ (from 3.20 to 3.40 ppm); B: ^{1}H NMR spectrum of 7 in acetone-d_6 (from 3.20 to 3.40 ppm); C: possible positions of two merged protons (at 3.25 ppm) in each candidate and overall ^{1}H NMR spectrum of 7 in $CDCl_3$.

More specifically, the two protons (most likely would be two bridgehead protons) around 3.33 ppm are completely overlapped in $CDCl_3$. Both of these two protons are at the central area of the tricyclic scaffold. In order to take advantage of 2D-NMR to determine the structure of **7**, it is absolutely essential to have the two protons separated. Fortunately, after a screening of different deuterated solvents, we found that acetone-d_6 provided sufficient separation between the two peaks.

With a good quality spectrum (in acetone-d_6) in hand, both COSY and TOCSY experiments were performed on **7**. However, due to the congested cyclic nature of this compound, all the distinguishable proton-proton correlations fit to every single candidate structure.

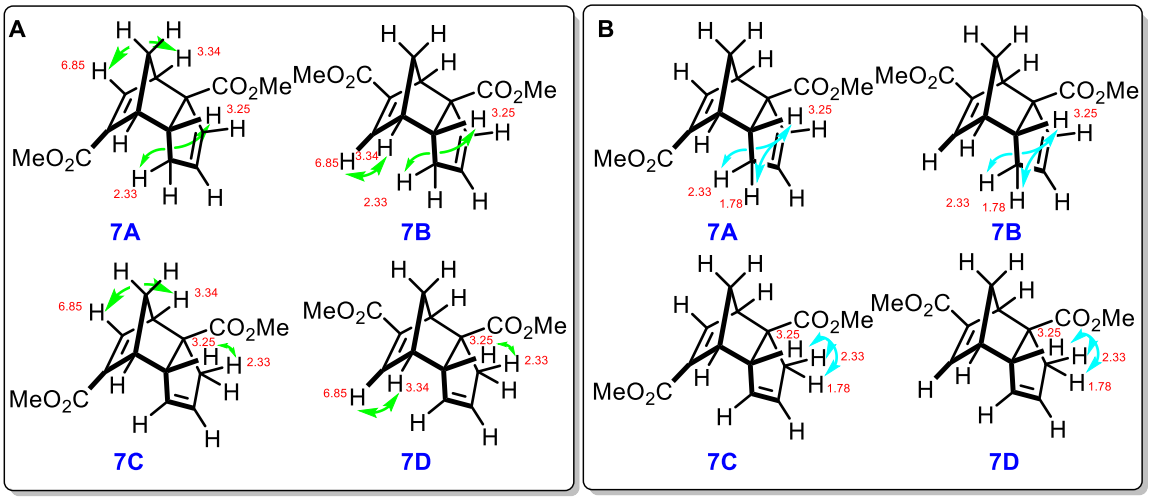

Figure 19: A: COSY (green) correlations in each proposed compound of 7; B: TOCSY (cyan) correlations in each possible structure for 7.

Although the rigidity of the molecule brought up more challenges due to the number of long-range couplings in the HMBC (particularly the 4^J couplings), we nonetheless managed to determine the identity of **7** by HMBC. The two key carbon-proton correlations (carbon at 140 ppm to proton at 3.25 ppm and carbon at 47.6 ppm to both protons at 2.33 and 1.78 ppm) that we observed in the HMBC spectrum provided us sufficient evidence to rule out three of our four candidates (**Figure 20**). In the case of **7B**, **7C** and **7D**, we would need to invoke one or two structurally unreasonable 4^J couplings in order to rationalize the observed cross peaks. Although we still observed that there is a 4^J coupling in **7A** (from carbon at 176 ppm to proton at 1.78 ppm), that one can be explained by long-range W coupling (in dashed pink). In addition to this, **7C** and **3D** could be further eliminated on the basis of comparison to the calculated ^{13}C chemical shift data (**Figure 17B**), wherein the expected shifts for C3a and C7a were >10 ppm away from the observed signals (see **Figure 17B** for atom numbering). Our structural assignment of **7A** as the first isolated regioisomer was further proved by the collection of X-ray data for a single crystal. While this structure is of low quality due to internal disorder, it is nonetheless sufficient to confirm that the two ester functions exist on opposite faces of the molecule. The X-ray data also confirmed the *endo* conformation of the molecule.

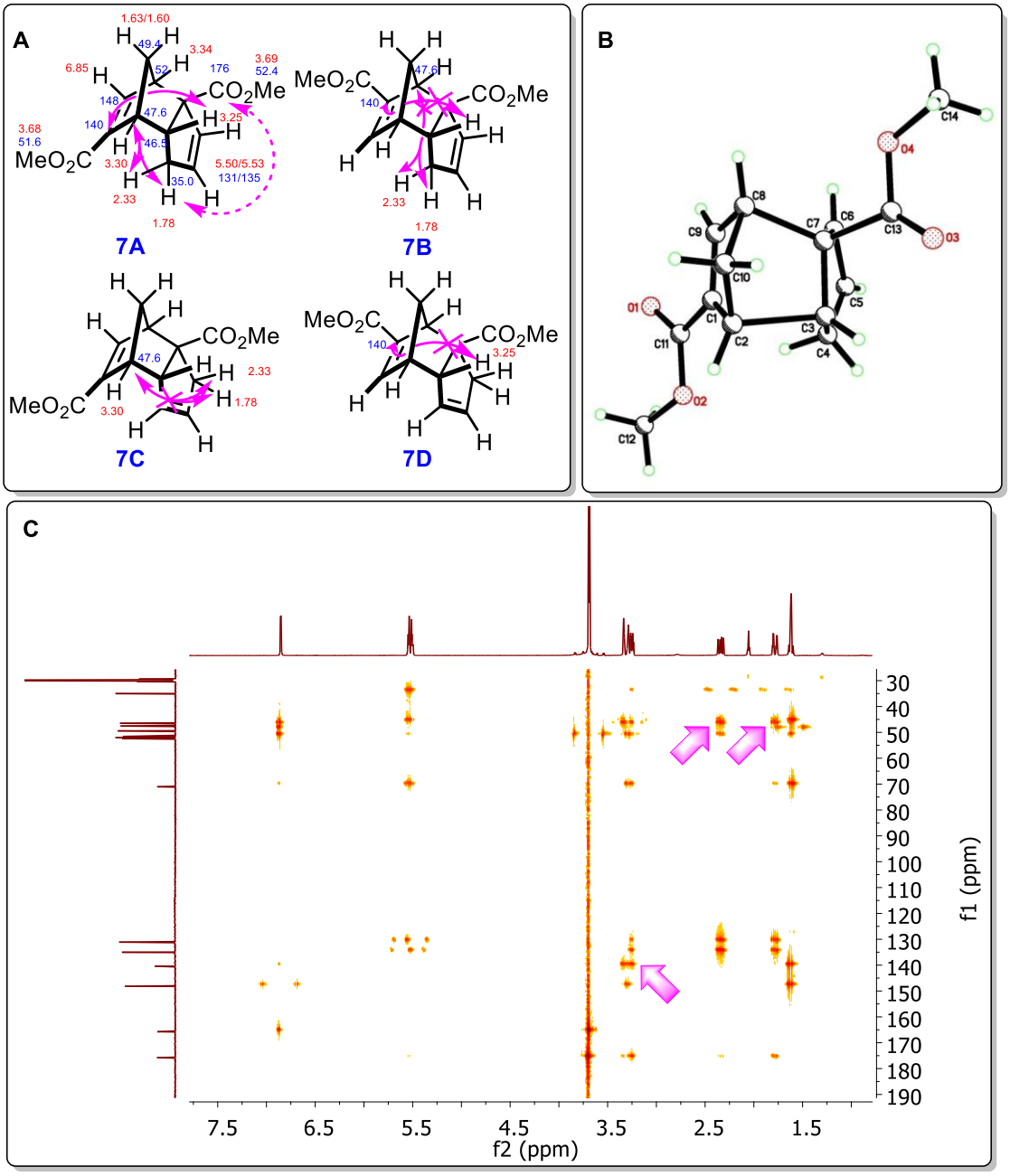

Figure 20: A: Structural assignment for 7 as 7A: blue, ^{13}C chemical shifts; red, ^{1}H chemical shifts; solid pink, 3^{J} HMBC correlations: dashed pink, 4^{J} HMBC correlations. Only the most significant correlations are shown from each data set. Crosses indicate data that would be incompatible with the proposed structures; B: X-ray structure for 7; C: HMBC spectrum of 7 with pink arrows which indicate the most significant correlations.

3.1.2. Minor regioisomer #2

Regarding the characterization of the second minor regioisomer, compound **8** (which eluted out of the chromatography column second after Thiele's ester), we found that the chemical shift, peak shape and coupling constant for the proton at 6.60 ppm was very similar to the C3 proton of Thiele's ester (**Figure 21A**). The remaining two alkene signals (at ~6.10 ppm) were more upfield than the C5 proton of Thiele's ester, but more downfield than the C5-C6 protons of dicyclopentadiene.

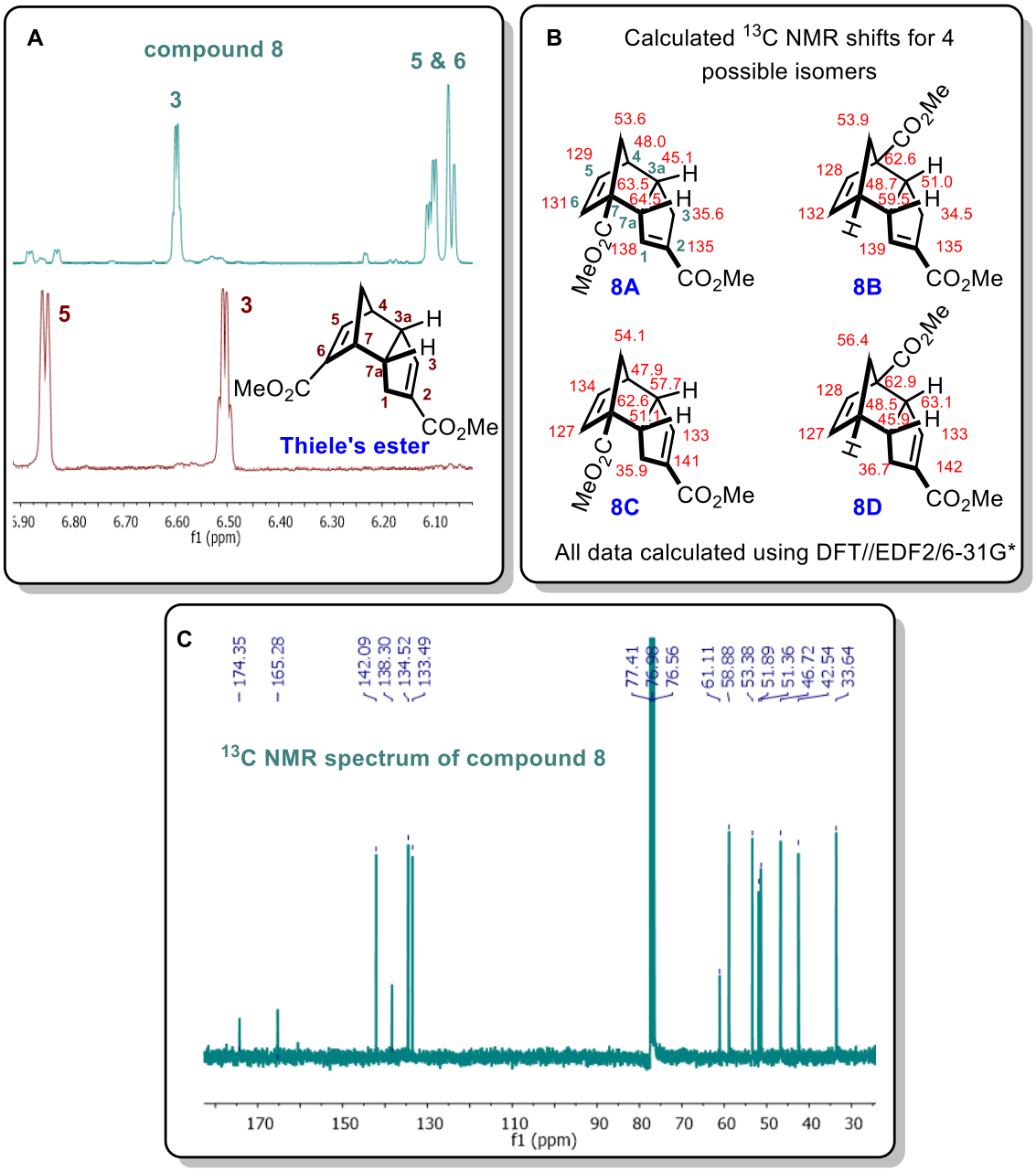

Figure 21: A: A comparison of ^{1}H NMR spectra between Thiele's ester and 8; B: DFT calculation of ^{13}C NMR shifts of 8 A-D; C: ^{13}C NMR spectrum of 8 in $CDCl_3$.

These data indicate that compound **8** might share a similar structure as the eastern portion of Thiele's ester. With regards to the western portion of the molecule, it clearly retains the unsubstituted strained alkene of dicyclopentadiene. However, due to the fact that the chemical shifts of these two alkenes were found between the C5 proton of Thiele's ester and the C5-C6 protons of dicyclopentadiene, there might be an ester group adjacent to this C5-C6 double bond. This was confirmed by DEPT analysis which once again revealed two methylene signals and a quaternary alkyl carbon, allowing us to place the remaining ester substituent at one of the two bridgehead carbons. As was the case with the first minor regioisomer, based on the ^{1}H NMR and ^{13}C NMR data as well as our calculated ^{13}C NMR shifts for **8**, we narrowed down the possible structures of **8** to **8A-D** (shown in **Figure 21B**).

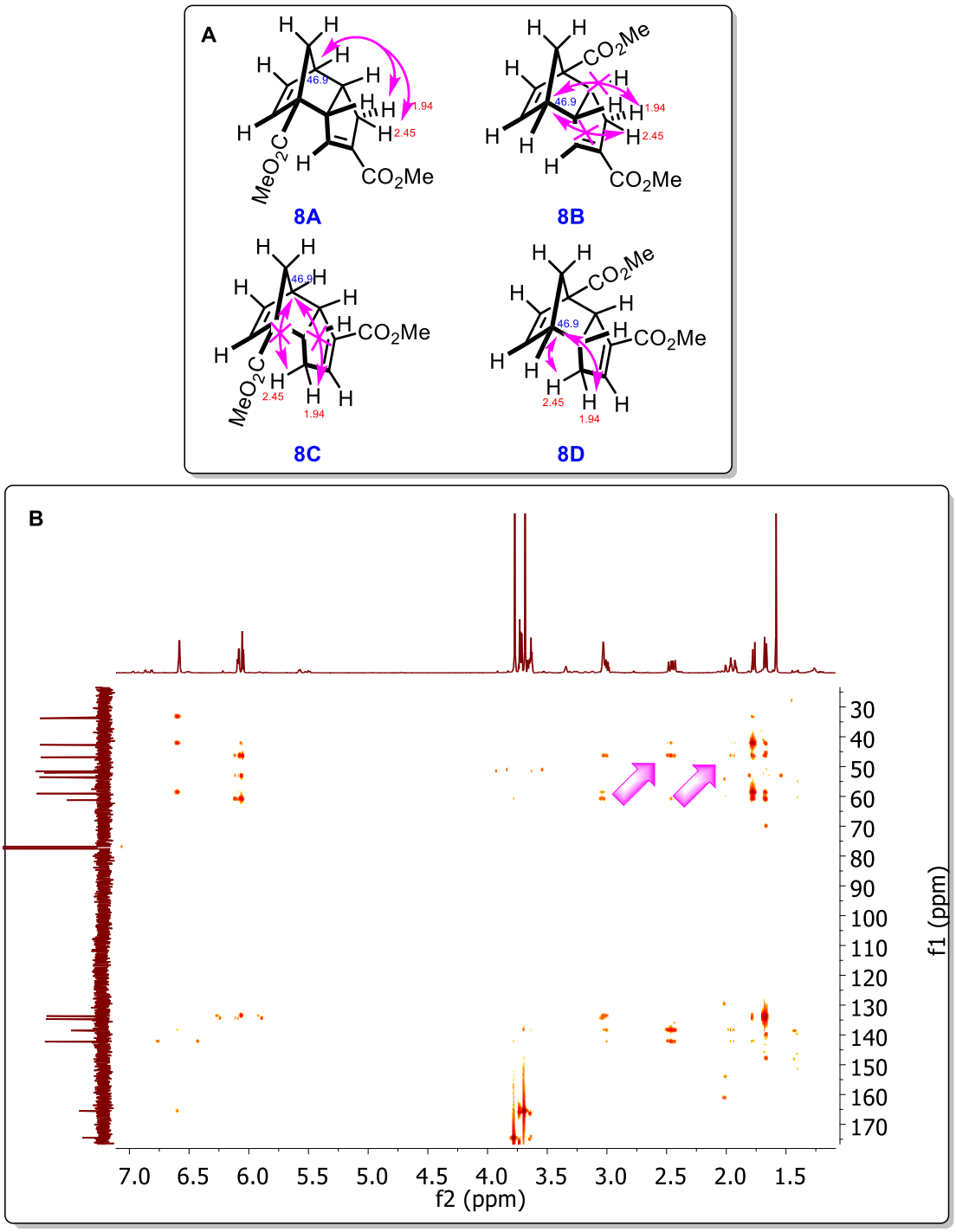

Figure 22: A: HMBC (pink) correlations in each proposed structure for 8; B: HMBC spectrum of 8 with pink arrows which indicate the most significant correlations.

Our next step was to undertake all the same 2D NMR experiments for **8** that we earlier used to assign **7**. While the COSY did not offer to much help for structural assignment, HMBC again provided us extremely valuable information. Both **8B** and **8C** could be eliminated, on the basis of

what would be unreasonable 4^J couplings in the HMBC. This left us **8A** and **8D** which were more challenging to differentiate by 2D NMR. Ultimately, **8D** was ruled out on the basis of the peak shape and coupling constant for the vinyl proton at 6.58 ppm in the ^{1}H NMR spectrum (green in **Figure 23**). This signal appears as an approximate quartet with a ~2 Hz coupling. Such a coupling pattern is inconsistent with the calculated geometry-optimized structure for **8D**, where at least one larger coupling (>5 Hz) would be expected for the proton attached to the conjugated olefin. Although we were unable to obtain a high quality single crystal of **8** for X-ray analysis, an NOE interaction between the methylene proton at 1.94 ppm and the alkene proton at 6.09 ppm confirmed that this structure was also an *endo* adduct.

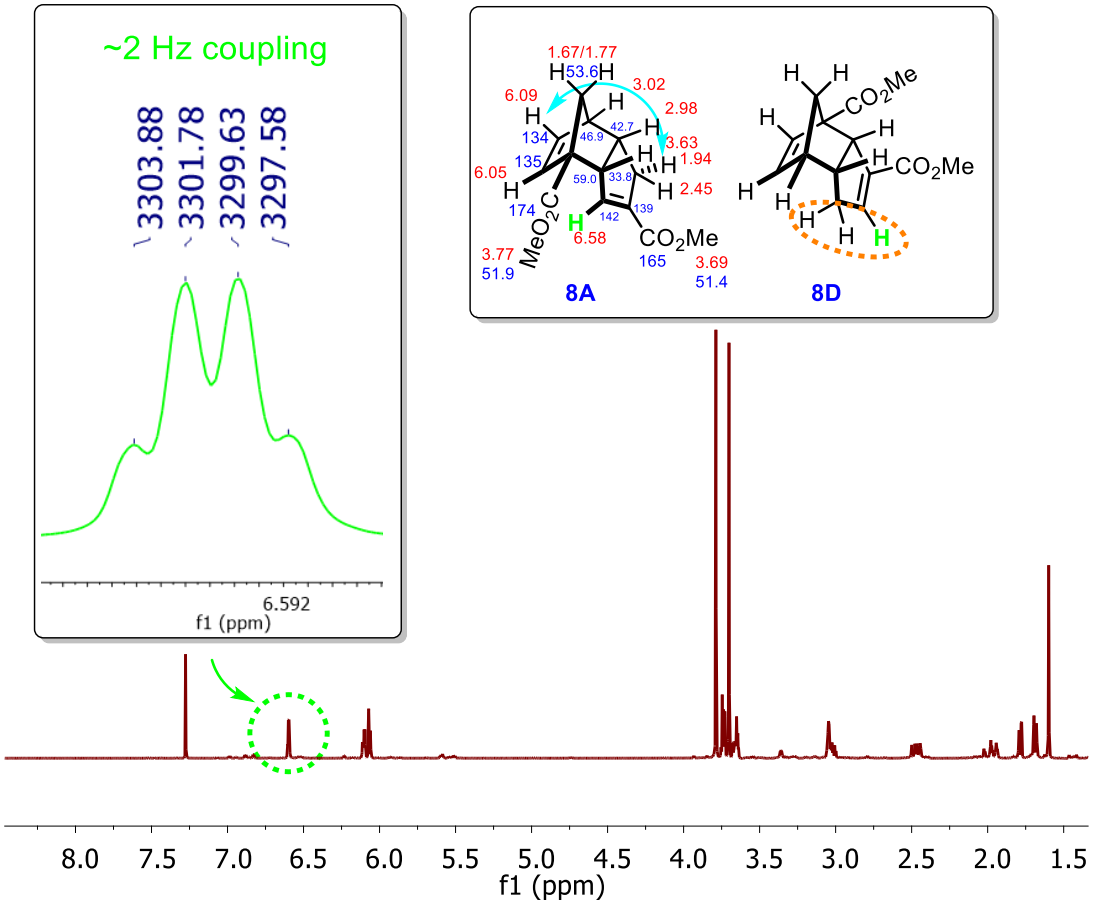

Figure 23: ^{1}H NMR spectrum of 8 in $CDCl_3$, expansion of vinyl proton at 6.58 ppm, comparison of 8A and 8D (regions circled in orange would be expected to contribute to couplings and peak shapes *different* from those observed in the ^{1}H NMR spectrum, a key 1D-NOE (cyan) interaction in 8, and structural assignment for compound 8 as 8A.

These analyses served to unambiguously determine the structures of the two minor regioisomers **8** and **7** that accompany the production of Thiele's ester**.** Our data also reveal for the first time that

the “ester first” approach (Dive’s work and our own) and the “acid first” approach (Marchand) in fact lead to the same three regioisomers, albeit in somewhat different amounts.

3.2.0. Mechanistic considerations in the synthesis of Thiele’s ester

After we fully understood each structure for the three compounds that arise from the Thiele’s ester synthesis, we started asking ourselves how we could rationalize the regioselectivity of this Diels–Alder reaction. In the literature, both Fleming and Deslongchamps successfully explained the formation of the major compound—Thiele’s ester—by invoking very different mechanistic hypotheses (frontier molecular orbital theory and radical stabilization effects, respectively). However, the structures of the minor products were not considered in either analysis. Now, following our efforts to characterize these regioisomers, we hoped to incorporate those structures into the existing mechanistic frameworks. We envision that this exercise provides a unique opportunity to evaluate the strengths and weaknesses of the two competing models, while also perhaps shedding light on the underlying mechanism of this unusual Diels–Alder reaction.

3.2.1. Prediction of Thiele’s ester regioselectivity by frontier molecular orbital theory

As described in chapter one, frontier molecular orbital theory is one of the most powerful predictive methods to forecast the regioselectivity of Diels-Alder reactions. Thiele’s ester formation was even discussed in Fleming’s well-known book, Frontier Orbitals and Organic Chemical Reactions[64]. By calculating the HOMO and LUMO energies of three isomeric dienes **5**, **5A** is shown to be the most reactive nucleophile due to its highest-energy HOMO, **5B** is the best electrophile with the lowest LUMO and **5C** is in the middle in terms of reactivity. But **5A** is known to have a very low concentration in solution, which evidently makes it a neglectable source of products.

We began this work by calculating the relative heats of formation for the three interconverting cyclopentadienes **5A–C**. The calculated results in **Chart 1** qualitatively agree with the relative distributions observed within the ^{1}H-NMR spectrum for the mixture of compounds **5** (**Figure 24**). An equilibrating mixture of these three species would be expected to contain mostly **5B** along with a smaller amount of **5C**, and this is exactly what we see in the NMR spectrum. No detectable **5A** signal was observed.

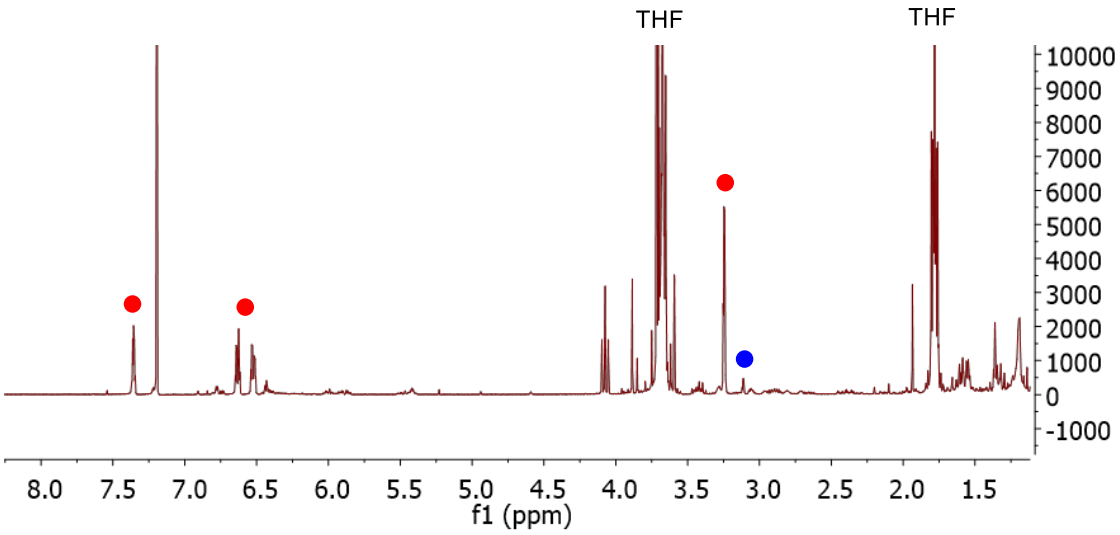

Figure 24: ^{1}H NMR spectrum of crude 5 in THF solution in $CDCl_3$. Peaks that correspond to 5B are labeled in Red spots. The most diagnostic peak for 5C (methylene) is labeled in Blue spot. The most diagnostic peak for 5A (methine) is supposed to be around 3.7 ppm as a triplet.

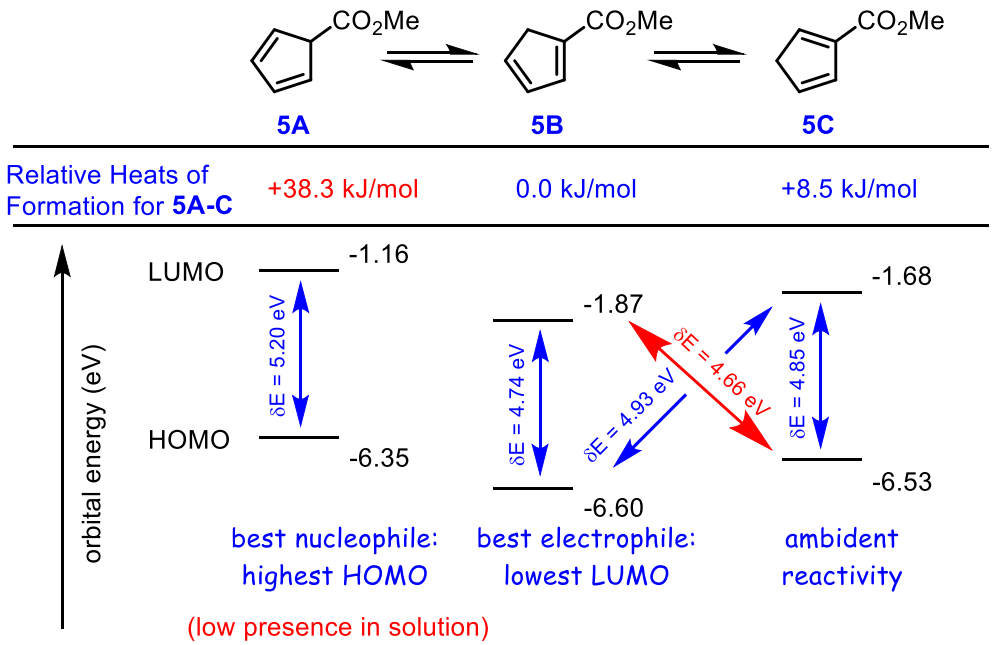

Chart 2: Relative heats of formation for 5A–C and orbital energy levels for reacting species 5A–C. Numerical values are from DFT calculations using a B3LYP functional and cc-pVTZ basis set.

Although our calculated orbital energies for **5A–C** (**Chart 2**) are not identical to Fleming's estimates (shown in **Chart 3**), they nonetheless supported Fleming's conclusion about the predictive power of the HOMO–LUMO energy gap in predicting the gross reactivity of reagents.

As shown in **Charts 2** and **3**, in both the methyl ester and carboxylic acid cases, the energy gap between the HOMO of **5C** or **108C** and LUMO of **5B** or **108B** is the smallest among the various orbital combinations. This implies that heterodimerization between these two species should be most favoured. The only exception is carboxylate anion **1**. However, it's unlikely that these species react as naked anions anyway, since such an interaction would suffer from significant repulsive effects in the Diels–Alder transition state.

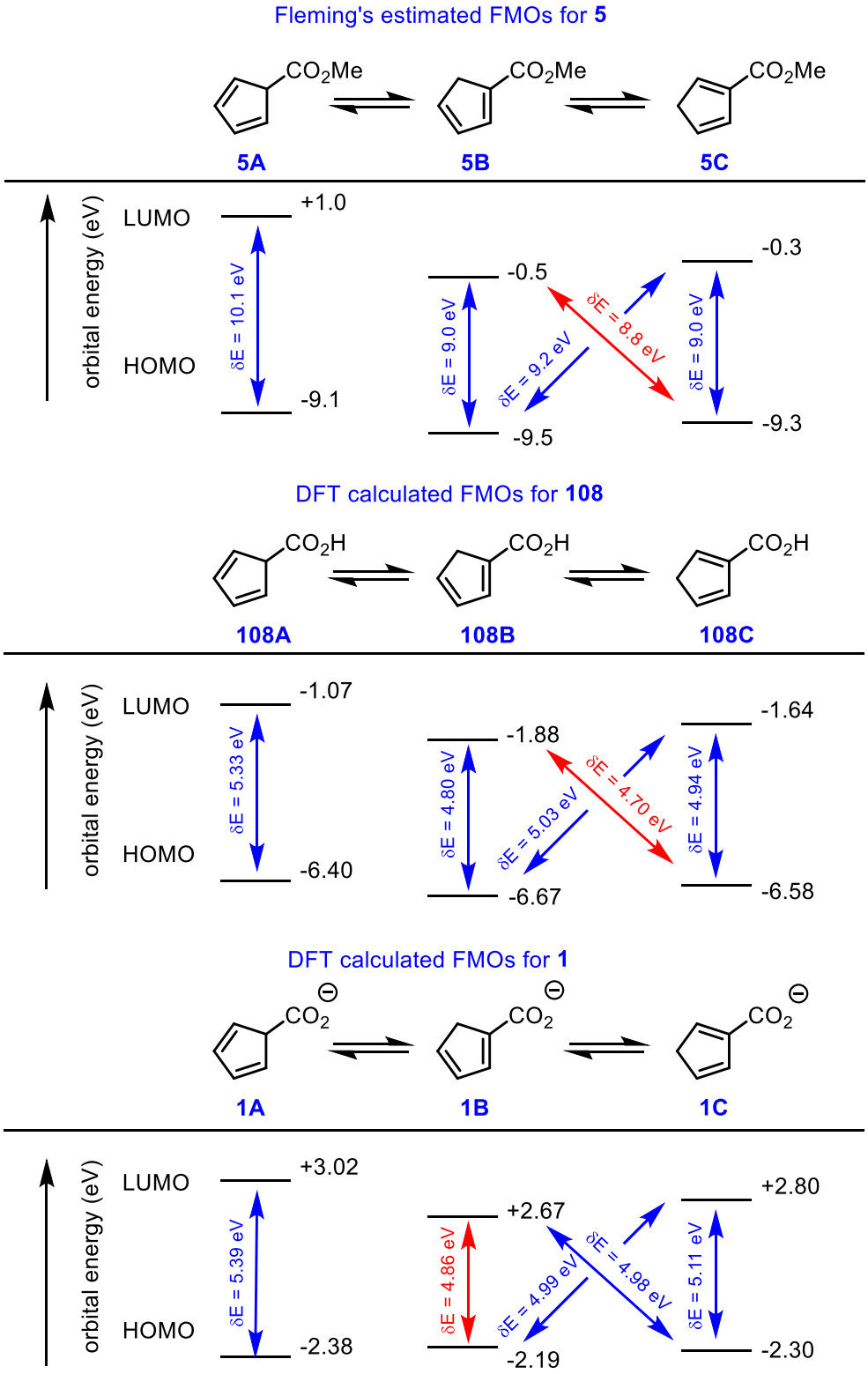

Calculated values are from DFT calculations using a B3LYP functional and cc-PVTZ basis set

Chart 3: Graphical illustration of orbital energy levels for substituted cyclopentadiene intermediates. The red arrows indicate the smallest orbital energy gap in each case.

While this simple orbital energy analysis perhaps explains why the major product arises from heterodimerization of **5B** and **5C** (since this pairing provides the smallest HOMO–LUMO energy gap), it does not explain which of the 8 possible **5B**+**5C** products should predominate. In order to account for the regioselectivity of these products, we then started focusing on the calculation of orbital coefficients. In Fleming's book chapter, he claimed that his methods are successful in predicting the correct regiochemical outcome of Thiele's ester (in **Figure 2** Chapter 1). However, this is only true using the coefficients estimated from the orbital-hybrid method which he described in his book[64]. While Fleming does not provide a percentage of the alkene and cation orbitals used to generate his hybrids, the 1:1 ratios employed in **Table 5** generate values that are consistent with the graphical representations provided in his book. However, when we applied modern DFT stimulation to calculate the orbital coefficients of different electron-withdrawing groups (anionic carboxylate, neutral carboxylic acid, methyl ester) on the parent cyclopentadiene, completely different results were obtained that contrasted Fleming's estimates in **Table 5**. A variety of additional computation methods (DFT/B3LYP/cc-PVTZ, HF/STO-3G, and simple Hückel approximation**)** were also explored (the results are reported in **Table 6**). All of these gave fairly consistent results, and none matched to Fleming's early estimates.

Table 5: Effect of the substituent on the calculated coefficients.

structure		$Z = CO_2H$ [(b)] **108** HOMO	LUMO		$Z = CO_2Me$ [(b)] **5** HOMO	LUMO		Fleming's estimates [(c)] **5** HOMO	LUMO
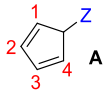	C1	+0.58	+0.58	C1	+0.58	+0.58	C1	+0.60	+0.60
	C2	+0.41	-0.40	C2	+0.41	-0.40	C2	+0.37	-0.37
	C3	-0.41	-0.40	C3	-0.41	-0.40	C3	-0.37	-0.37
	C4	-0.58	+0.58	C4	-0.58	+0.58	C4	-0.60	+0.60
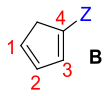	C1	-0.58	**+0.58**	C1	-0.587	**+0.58**	C1	**+0.63**[(d)]	**+0.71**[(e)]
	C2	-0.42	-0.24	C2	-0.41	-0.24	C2	+0.45[(d)]	-0.15[(e)]
	C3	+0.36	-0.57	C3	+0.36	-0.57	C3	-0.26[(d)]	-0.64[(e)]
	C4	**+0.60**	+0.53	C4	**+0.593**	+0.53	C4	-0.57[(d)]	+0.27[(e)]
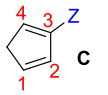	C1	**+0.60**	+0.39	C1	**+0.60**	+0.39	C1	+0.35[(f)]	+0.39[(g)]
	C2	+0.42	-0.18	C2	+0.43	-0.17	C2	+0.22[(f)]	-0.24[(g)]
	C3	-0.38	-0.47	C3	-0.37	-0.47	C3	-0.64[(f)]	-0.24[(g)]
	C4	-0.56	**+0.77**	C4	-0.56	**+0.77**	C4	**-0.65**[(f)]	**+0.85**[(g)]

[(a)] For comparative purposes, all sets of coefficients were normalized such that $\Sigma c^2=1.00$ across the four numbered atoms of the diene system.

[(b)] DFT calculations were performed using a B3LYP functional and a cc-pVTZ basis set.

[(c)] Calculated from the orbital-hybrid method described by Fleming (see notes d–g for details). The 1:1 ratios employed here generate values that are consistent with the graphical representations provided in Fleming's book chapter.

[(d)] Determined by summing the coefficients from the HOMO of hexatriene and the HOMO of the pentadienyl cation, then normalizing as above.

[(e)] Determined by summing the coefficients from the LUMO of hexatriene and the LUMO of the pentadienyl cation, then normalizing as above.

[(f)] Determined by summing the coefficients from the HOMO of butadiene and the HOMO of the allyl cation, then normalizing as above.

[g] Determined by summing the coefficients from the LUMO of butadiene and the LUMO of the allyl cation, then normalizing as above.

Table 6: Normalized coefficients for ester-substituted cyclopentadiene intermediates and comparison of calculation methods. [a]

structure	DFT/B3LYP/cc-PVTZ HOMO	DFT/B3LYP/cc-PVTZ LUMO	DFT/B3LYP/6-31G* HOMO	DFT/B3LYP/6-31G* LUMO	HF/STO-3G HOMO	HF/STO-3G LUMO	simple Hückel approx [b] HOMO	simple Hückel approx [b] LUMO
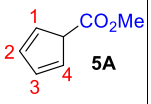 **5A**	C1 +0.58	+0.58	C1 +0.58	+0.58	C1 +0.57	+0.57	C1 +0.60	+0.60
	C2 +0.41	-0.40	C2 +0.41	-0.41	C2 +0.42	-0.42	C2 +0.37	-0.37
	C3 -0.41	-0.40	C3 -0.41	-0.41	C3 -0.42	-0.42	C3 -0.37	-0.37
	C4 -0.58	+0.58	C4 -0.58	+0.58	C4 -0.57	+0.57	C4 -0.60	+0.60
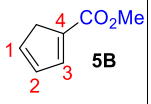 **5B**	C1 -0.587	**+0.58**	C1 -0.59	-0.58	C1 -0.56	-0.55	C1 +0.59	**-0.68**
	C2 -0.41	-0.24	C2 -0.41	+0.24	C2 -0.41	+0.29	C2 +0.42	+0.18
	C3 +0.36	-0.57	C3 +0.36	**+0.59**	C3 +0.42	**+0.58**	C3 -0.31	+0.63
	C4 **+0.593**	+0.53	C4 **+0.60**	-0.51	C4 **+0.59**	-0.53	C4 **-0.62**	-0.34
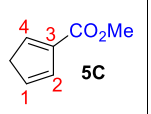 **5C**	C1 **+0.60**	+0.39	C1 **+0.60**	+0.39	C1 -0.57	+0.43	C1 **-0.63**	+0.36
	C2 +0.43	-0.17	C2 +0.43	-0.18	C2 -0.42	-0.25	C2 -0.41	-0.13
	C3 -0.37	-0.47	C3 -0.36	-0.47	C3 +0.43	-0.46	C3 +0.37	-0.31
	C4 -0.56	**+0.77**	C4 -0.56	**+0.78**	C4 +0.57	**+0.73**	C4 +0.55	**+0.87**

[a] In cases where double or triple zeta methods were used, coefficients were taken as the sum of (PZ+PZ') or else (PZ+PZ'+PZ"). Raw coefficient values were normalized such that $\Sigma c^2=1.00$ across the four numbered atoms of the diene system. Values in bold indicate the largest coefficient in each set. In all cases the simple Hückel approximation data agree qualitatively with the DFT results.

[b] Calculations were performed using the Interactive Simple Hückel Molecular Orbital Calculator (SHMO) from Arvi Rauk and Rich Cannings: http://www.ucalgary.ca/rauk/shmo.

When we attempted to use the coefficients calculated above to predict the outcome of the Diels-Alder reaction of **5B** with **5C**, we found that this method did not correctly identify the right pairing among the 8 possible **5B·C** heterodimerizations. Likewise, incorrect outcomes were identified for heterodimerizations of **5B** and **5C**, respectively (see **Chart 4**).

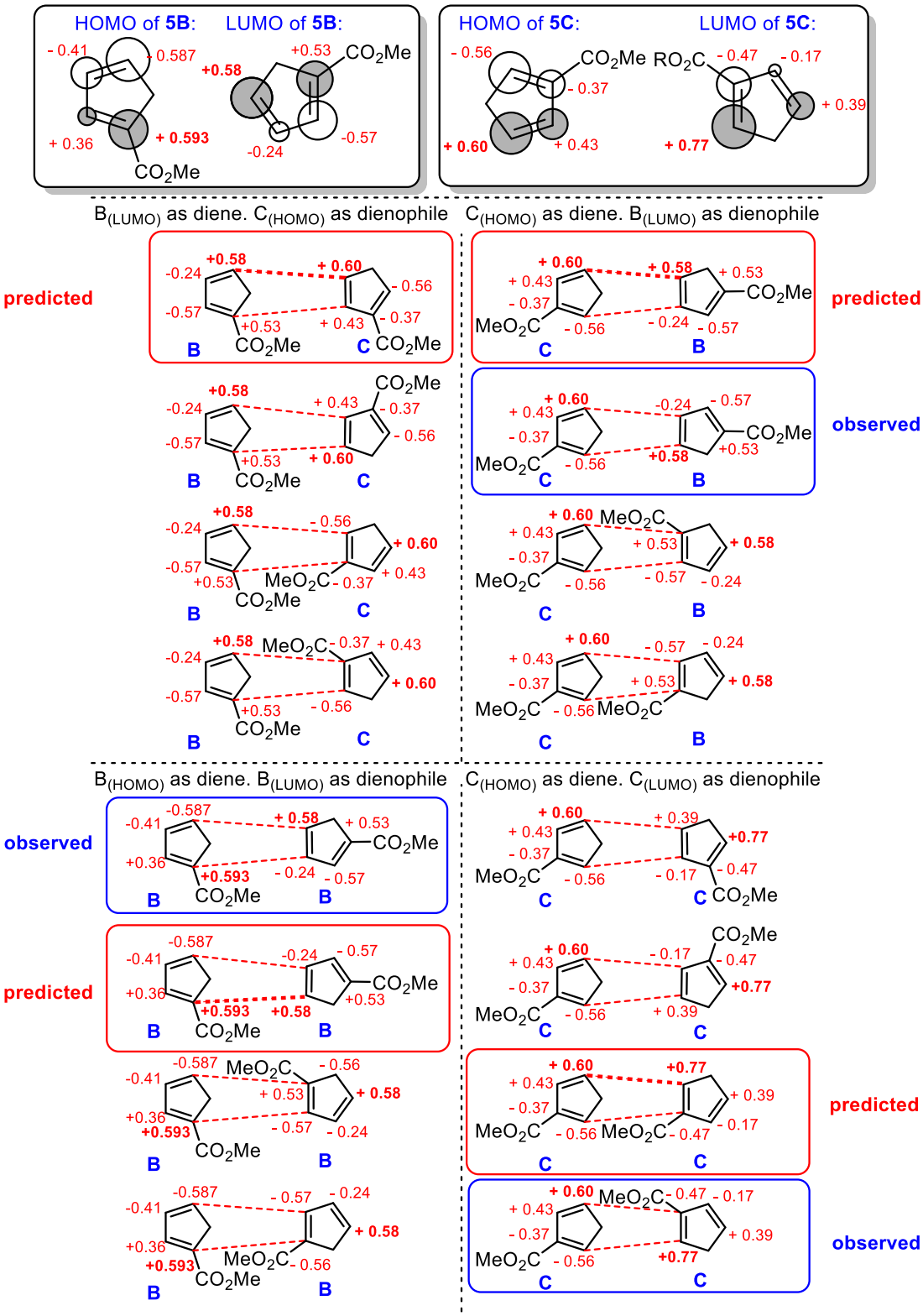

Chart 4: Application of normalized orbital coefficients to possible B·C pairings, B·B pairings and C·C pairings. Values are from DFT calculations using a B3LYP functional and cc-pVTZ basis set.

3.2.2. Radical stabilization algorithm as a predictive tool for Thiele's ester formation

While the classic frontier molecular orbital theory did not help us to understand the observed compounds that arise from the Thiele's ester dimerization, Deslongchamps' radical stabilization argument (a consequence of bend bond theory) does correctly predict the formation of the major product Thiele's ester. Deslongchamps argues that both the diene and dienophile should be viewed as their corresponding singlet diradical resonance structures (a *trans*-disposed 1,4-diradical in the case of the diene)[12b]. By aligning the two least stabilized radical centres on each of the reaction coupling partners, one should be able to predict the regioselectivity of a cycloaddition.

Because of the negligible concentration of **5A** among the three carboxylated cyclopentadiene intermediates, only **5B** and **5C** would be available to participate in Diels-Alder dimerizations. Thus, we first assigned the least stable radical centres on both **5B** and **5C** in **Figure 25**.

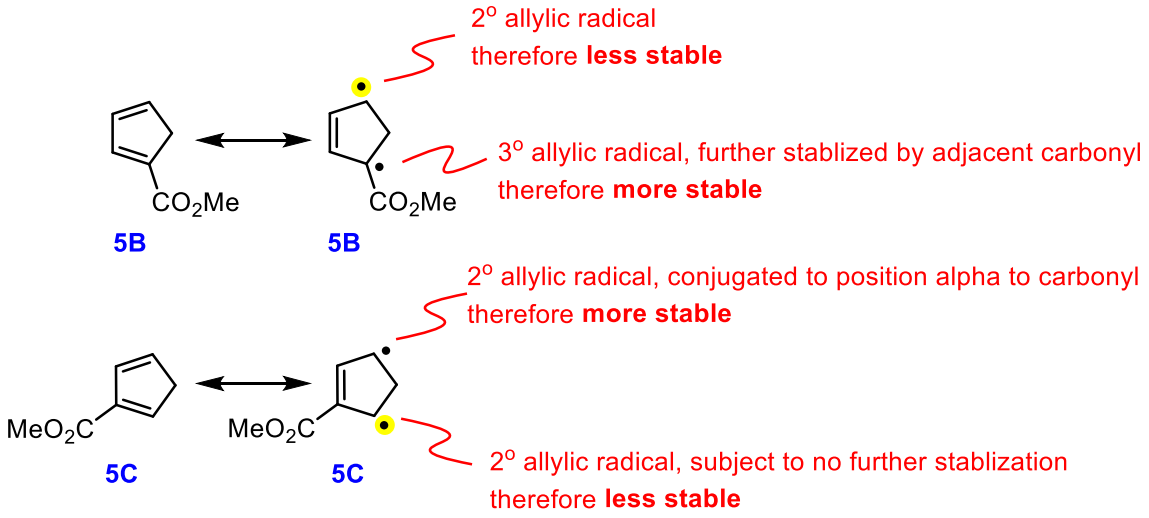

Figure 25: Assignment of the least stable radical centre in 5B and 5C.

In Deslongchamps' discussion of Thiele's ester formation in his original paper, he considered that cross conjugated **5C** is a better diene (less electron-withdrawing and lesser steric hindrance at diene termini) and **5B** is a better dienophile (more electron-withdrawing)[12b]. This argument does not hold true when one considers the existence of the two minor regioisomers, however. Compounds **7** and **8** resulted from the homodimerization of **5B** and **5C**, which proved that both **5B** and **5C** can act as either diene or dienophile. (Of course, the structures of the minor regioisomers would not have been known to Deslongchamps.)

Thus, when we extended Deslongchamps' model (**Chart 5**), structures **5B** and **5C** were considered as both diene and dienophile in this Diels-Alder reaction. The resulting 8 possible combinations can be further refined by the alignment of the least stabilized radical for each monomer. By doing so, two candidate couplings (in coloured boxes in **Chart 5**) stood out among the 8 combinations. The pairing in the red box would generate two adjacent quaternary centres in the resulting product, and

so this combination was rejected on steric grounds. This leaves only a single combination (shown in the blue box). Indeed, this one and only predicted regioisomeric outcome for dimerization of **5B** and **5C** matched with the observed major compound Thiele's ester!

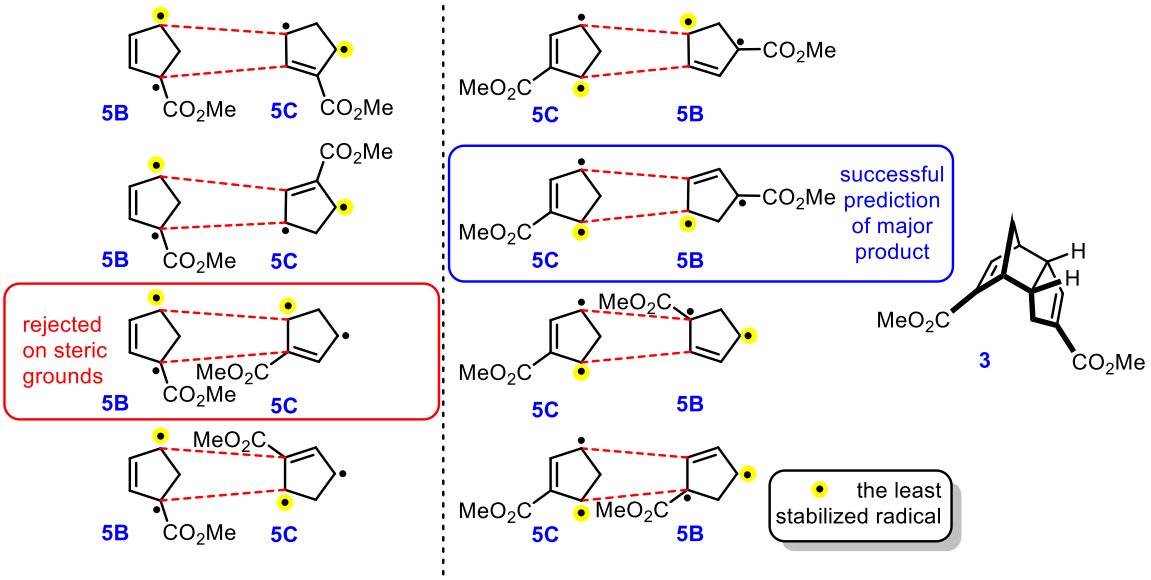

Chart 5: Application of radical stabilization algorithm to possible B·C pairings. Yellow highlighting indicates the least stabilized radical for each structure.

Regarding the two minor regioisomers that Deslongchamps did not consider in his own work, we found that both minor regioisomers which arise from the homodimerizations of **5B** or **5C** could be precisely predicted by this method as well, as shown in **Chart 6**.

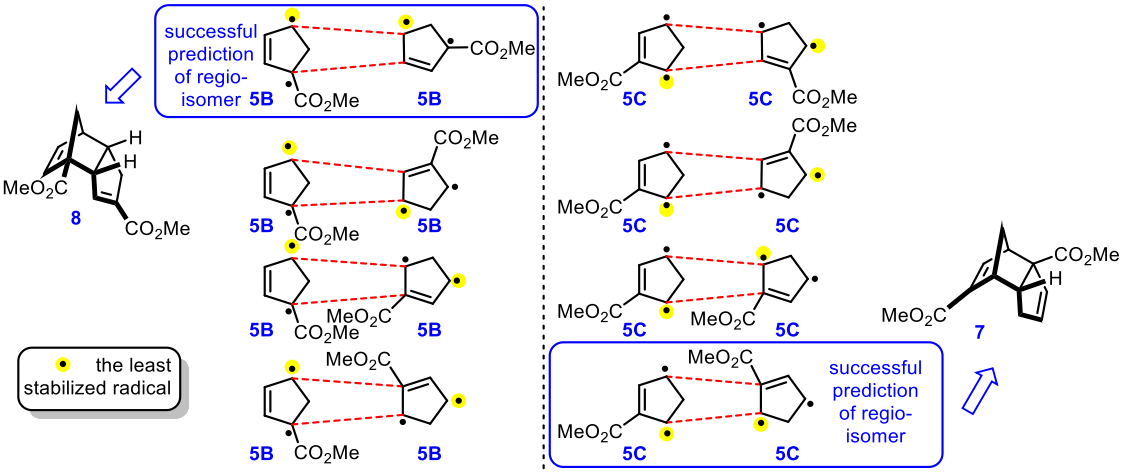

Chart 6: Application of radical stabilization algorithm to possible B·B pairings and C·C pairings. Yellow highlighting indicates the least stabilized radical for each structure.

To the best of our knowledge, this is the first time that the radical stabilization model (which does not require any intensive computational work) has outperformed the traditional frontier orbital approach in describing the regionchemical outcome of such a complicated Diels–Alder reaction. Together with Deslongchamps' report highlighting the ability for radical stabilization arguments to

correctly predict the regiochemistry (and even stereochemistry) of more traditional Diels–Alder reactions, we expect that this study will stimulate the use of this predictive algorithm in broader contexts.

3.3.0. Synthesis of non-canonical Thiele's ester analogues and the prediction of their regiochemical outcome

The success of radical stabilization arguments in predicting the regiochemical outcome of the Thiele's ester dimerization encouraged us to keep investigating the predictive power of this method with non-canonical Thiele-type dimerizations. Thus, novel phosphine oxide-containing Thiele dimers were proposed as our synthetic targets.

3.3.1. Thiele Phosphine oxide analogues

The spectra of the cyclopentadiene-phosphine oxides **109** (^{1}H, ^{31}P and P-HMBC) illustrated a similar distribution between three interconvertible intermediates. Linear conjugated **109B** once again appeared as the dominated species, along with a visible amount of cross conjugated **109C**. No existence of **109A** could be observed in NMR data.

The dimerization could be triggered by heating the neat mixture of **109** at 50 °C. However, this time only one single compound **110a** which clearly had a different substitution pattern from Thiele's ester was isolated in 60% yield. An extensive collection of NMR data (^{1}H, ^{13}C, COSY, HMQC, ^{31}P-HMBC, 1D-NOE) was acquired. With the help of the phosphorus atom as an additional NMR handle, ^{31}P-HMBC became extremely useful for the structural assignment of **110a**.

Two long-range couplings from the phosphorous at 23.6 ppm to the alkene proton at 5.38 ppm as well as to the methylene protons at 2.50 and 1.89 ppm helped us to assign the substitution pattern of the Eastern hemisphere of the product **110a**. Similarly, long-range couplings from the phosphorus at 29.9 ppm (to both bridge protons at 1.68 and 1.85 ppm, to the downfield methine proton at 3.95 ppm, and to the alkene proton at 6.20 ppm) eventually confirmed the structure of the norbornene moiety. 1D NOE data (correlation from the bridge methylene proton at 1.68 ppm to both methine protons at 3.95 ppm and 3.00 ppm) confirmed the *endo* ring architecture.

Notably this compound **110a** is analogous to one of the two minor regioisomers **8** in Thiele's acid or ester dimerization. A slightly less hindered phosphine oxide electrophile **111b** was then used in place of diphenylphosphinic chloride to see whether this would impact the regiochemical outcome. In the event, the same excusive regiochemistry was obtained to give **110b** in 65% yield. Clearly then, the presence of the phosphine oxide functional group is exerting a significant control over the reaction outcome.

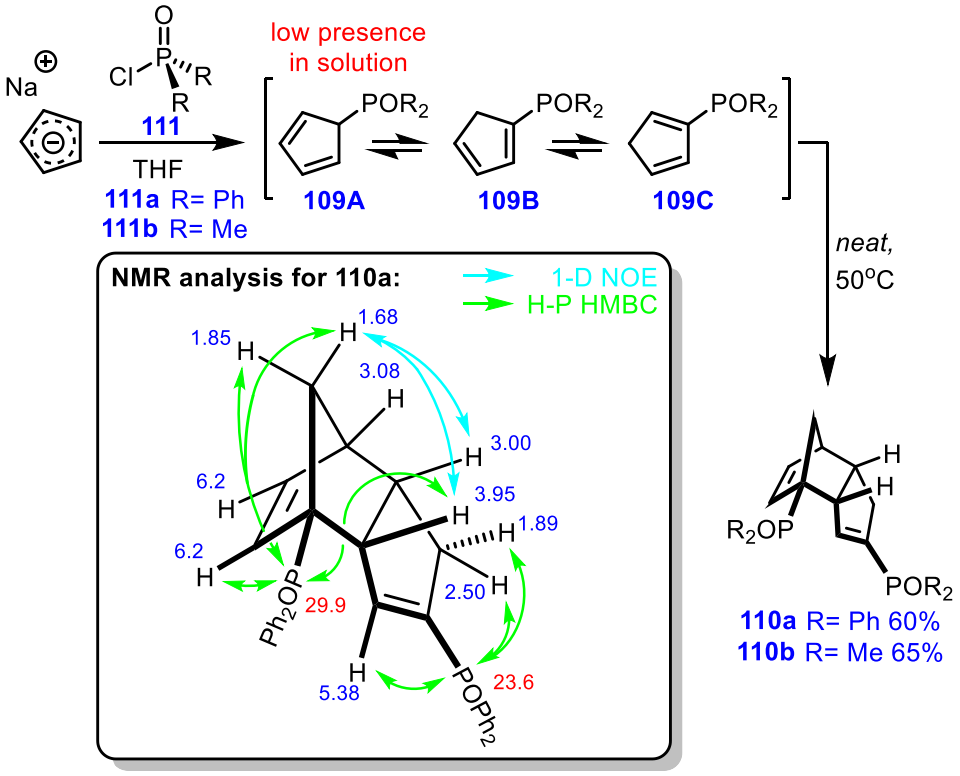

Scheme 27: Synthesis of non-canonical Thiele's acid analogues incorporating phosphine oxide groups, and selected NMR data for product 110a. Values in blue indicate ^{1}H NMR shifts. Values in red indicate ^{31}P NMR shifts.

In order to study this irregular regiochemical outcome, we listed all possible combinations between **109B** and **109C** (couplings involving **109A** were discounted in view of the apparent absence of this species from the reaction mixture).

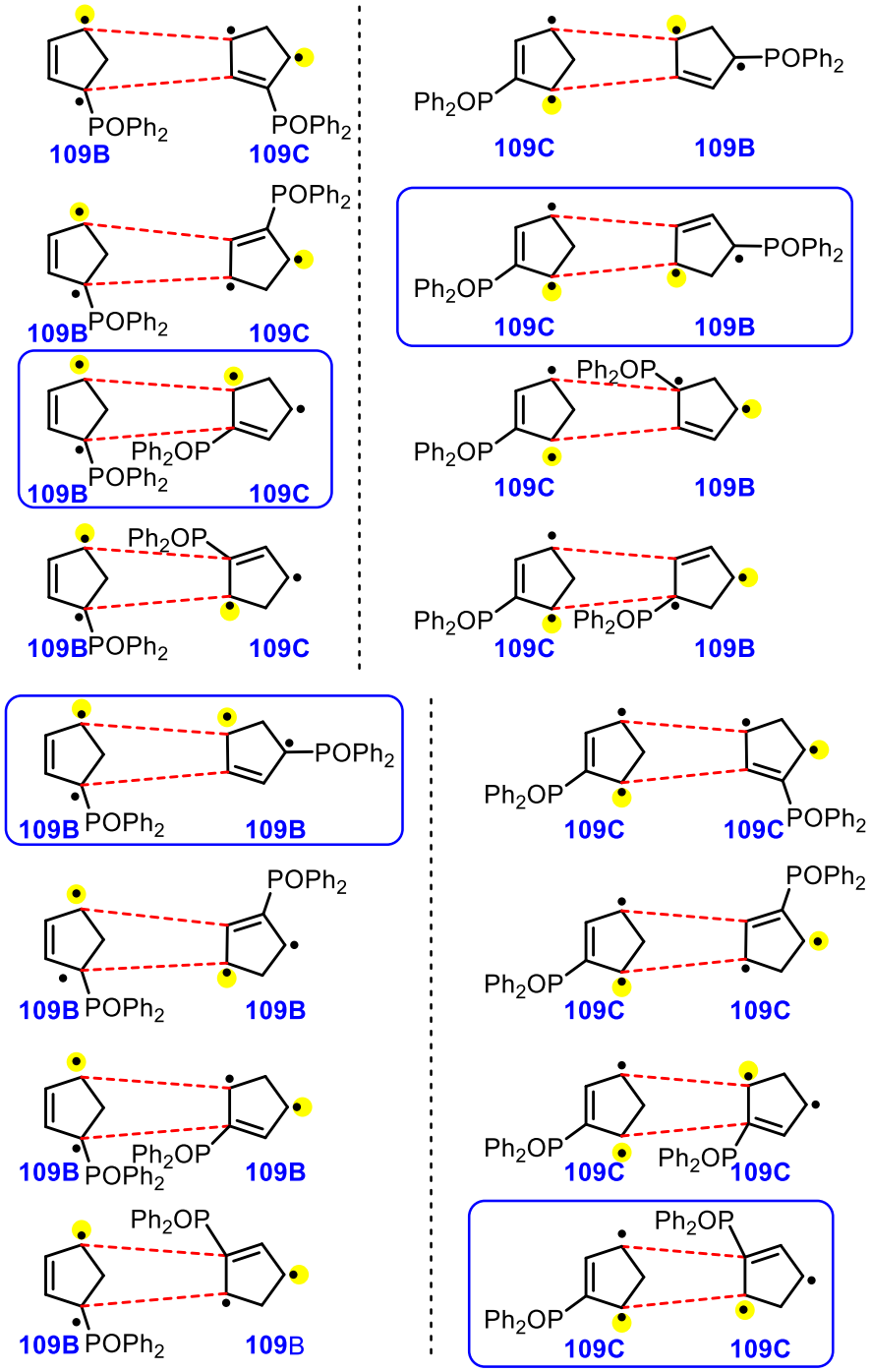

Chart 7: Application of radical stabilization logic to possible combination of 109B and 109C. (Electronically favoured combinations are in blue boxes)

Of the 16 possible pairings considered in **Chart 7**, only 4 possible products (in blue box) would result from alignment of the least stabilized radicals from each coupling partner. These were therefore considered further (**Figure 26**).

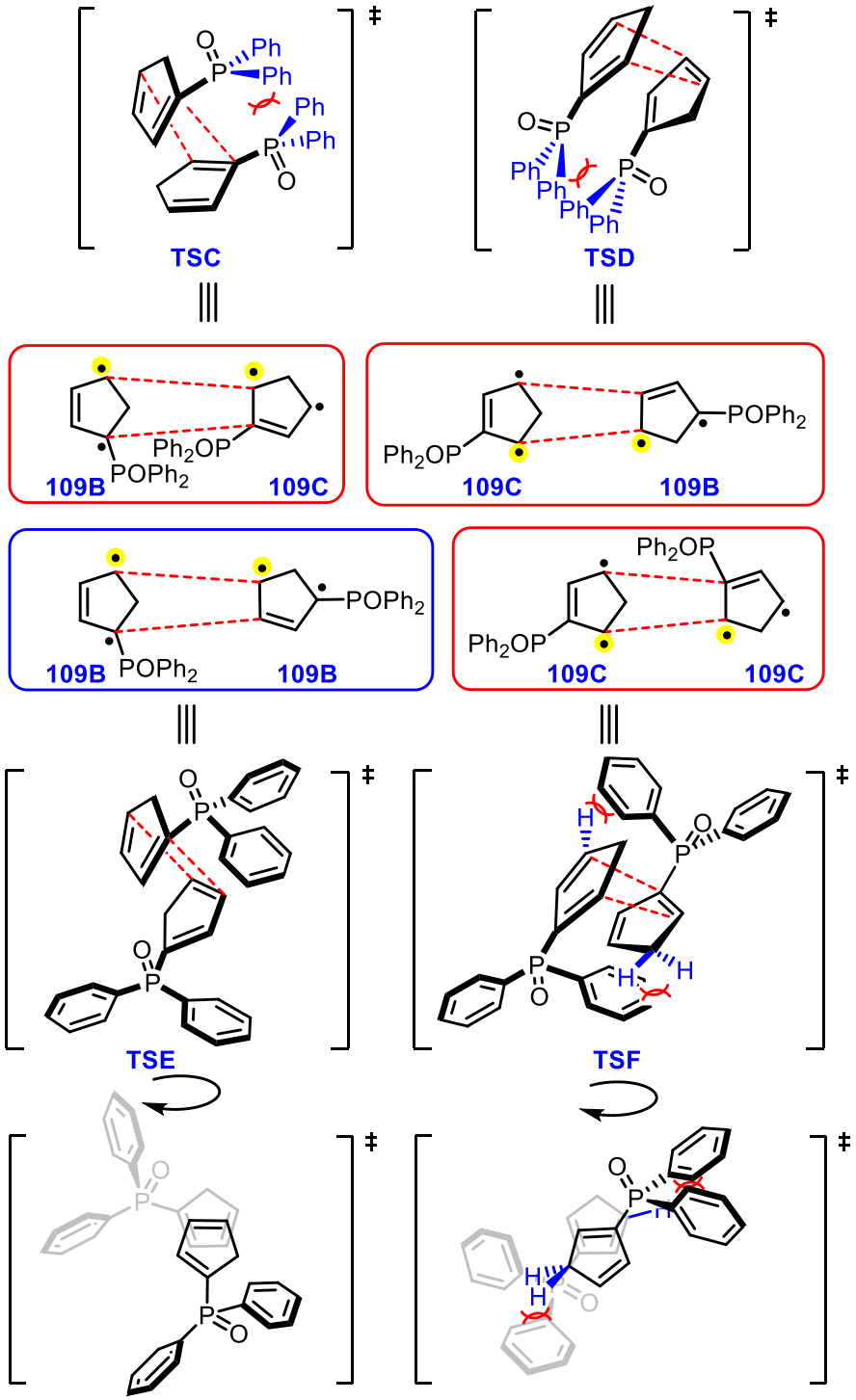

Figure 26: Electronically favoured combinations for the formation of possible phosphine oxide dimers, and their transition states. Yellow highlighting indicates the least stabilized radical for each structure. Transition states were approximated through observations of plastic models.

The phosphine oxide function is much more bulky than the ester group introduced previously, since it is approximately tetrahedral in geometry and bears two alkyl (or aryl) substituents on the phosphorus centre. As such, we were fully aware that steric effects in the Diels–Alder transition state may play an important role in determining the outcome of this non-canonical Thiele type dimerization. Thus, the transition states of each electronically viable combination were approximated through observations of plastic models.

TSC would clearly be rejected on steric grounds, owing to the formation of two adjacent quaternary centres. **TSD**—which is analogous to the combination that leads to Thiele's ester—would suffer from substantial steric hindrance from four phenyl rings being brought into proximity with one another in the transition state.

Between **TSE** and **TSF**, it is less obvious which one would be favoured. However, rotation of the transition states reveals that **TSF** suffers from steric repulsion between the phenyl substituents and the protons on the cyclopentadiene ring (blue in **Figure 26**). This leaves **TSE** as the least sterically hindered combination among all of the four electronically favoured candidates. Impressively, this one and only prediction once again matched to the observed product **110a** out of 25 possible combinations (16 possible outcomes if the participation of **109A** is discounted at the outset).

3.3.2. Thiele Sulfone analogues

In order to test the reliability of this combined predictive method, we dived more deeply into the literature and found that there are two sulfonyl Thiele products which were published by two separate groups[65].

The first one was reported by Bridges and Fisher for the dimerization of sulfonylated cyclopentadienes **112** to afford the bis-sulfone **113** in 55% yield as a single isolatable product (**Scheme 28**). Owning to the nature of the tetrahedral geometry of the sulfonyl group, a similar transition state argument as for the phosphine oxide Thiele product **110** could be applied to this reaction. **TSG** which is geometrically identical to **TSE** becomes the favoured combination in this case. Once again, the predicted transition state **TSG** perfectly matched to the observed regiochemical outcome.

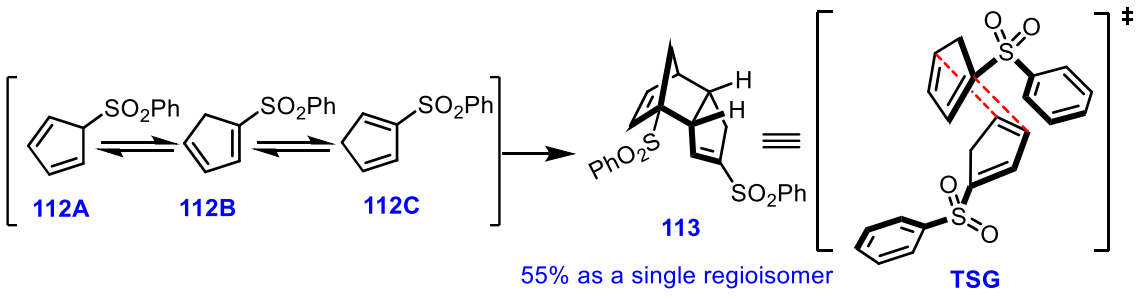

Scheme 28: Bridges' synthesis of bis-sulfonylated dicyclopentadiene.

The second example turned out to be more complicated. In 1986, Kämpchen and co-workers reported a dimerization of bis-sulfonylated cyclopentadienes **114** to afford the tetrakis-sulfonylated dicyclopentadiene **115** in 72% yield (**Scheme 29**).[65a]

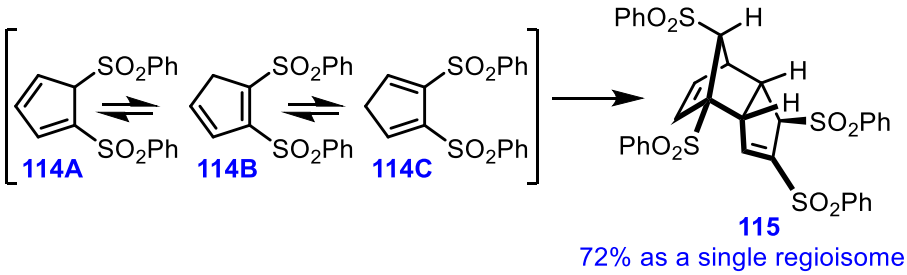

Scheme 29: Kämpchen's synthesis of tetrasulfonylated dicyclopentadiene.

In this case, however, there were no available NMR data to reveal the distribution of the three interconvertible cyclopentadiene monomers **114A-C**. Thus, we just considered all 25 possible pairings (**Chart 8**).

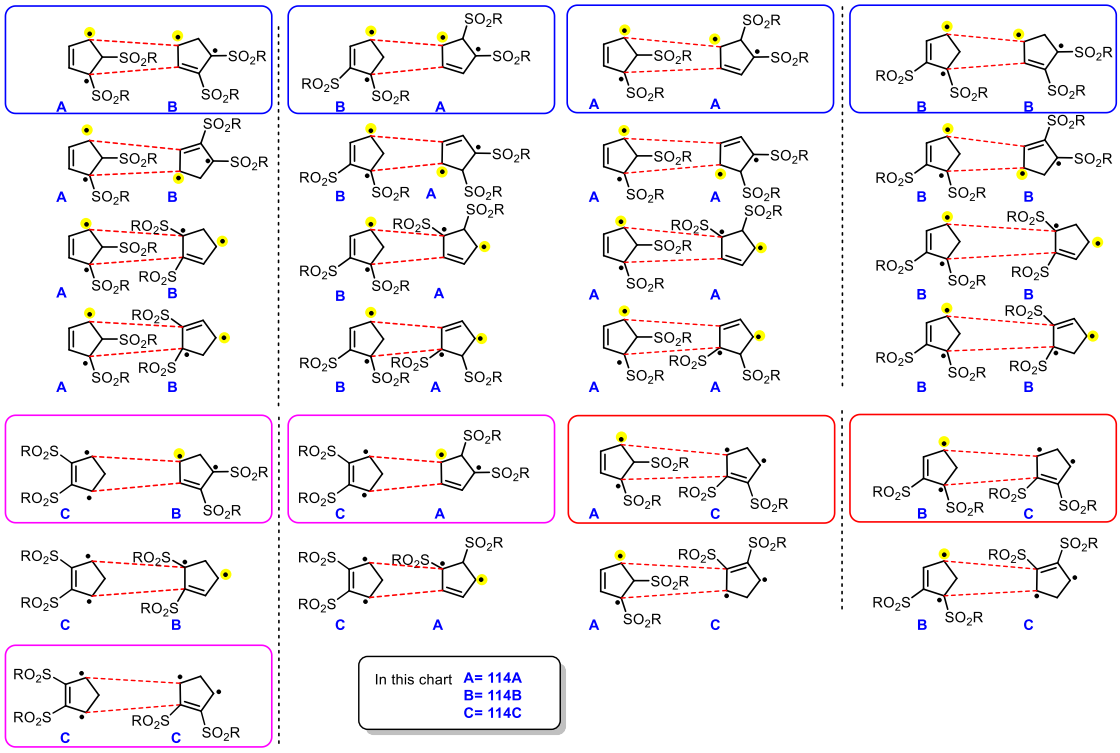

Chart 8: Application of radical stabilization logic to all possible combinations of 114A, 114B and 114C (R = Ph). (Electronically favoured combinations are in boxes. Pairings in blue boxes are discussed below. Red boxes indicate that resulting products will have two adjacent quaternary centres. Pink boxes indicate that resulting products will suffer from obvious steric clashes in their transition states which showed in Figure 27)

After matching the least stable radical centre from each monomer, up to 9 pairings are considered as electronically favoured (in boxes in **Chart 8**). Among these 9 combinations, pairings in red boxes

will have two adjacent quaternary centres in their corresponding products, and pairings in pink boxes will suffer from obvious steric clashes in their transition states **(TS3.6**, **TS3.7** and **TS3.8)** which are illustrated in **Figure 27**. Thus, we were left with four reasonable trajectories for the reaction (highlighted in blue boxes).

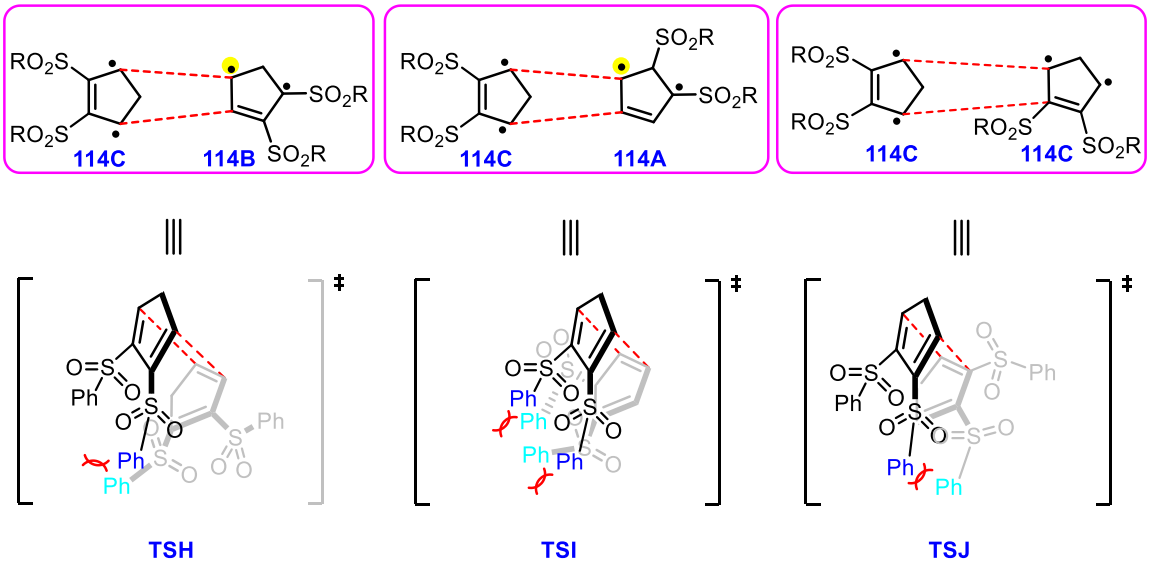

Figure 27: Transition states and steric clashes for pairings $114C_{DIENE}$ + $114B_{DIENOPHILE}$, $114C_{DIENE}$ + $114A_{DIENOPHILE}$ and $114C_{DIENE}$ + $114C_{DIENOPHILE}$ (R = Ph).

The transition states of each combination in blue boxes in **Chart 8** were considered with the aid of plastic models. While **TSK**, **TSL** and **TSN** each have at least one pair of phenyl rings which would repel one another, **TSM** suffers comparatively less steric hindrance. This makes **TSM** the most likely reaction pathway. Remarkably, this simple procedure correctly identifies the regiochemical outcome observed in the isolated compound **115**! It also means that the radical stabilization algorithm managed to successfully forecast the outcome of all known canonical and non-canonical Thiele type homo dimerization products. This is a much better rate of success than that observed for classic frontier molecular orbital theory approaches.

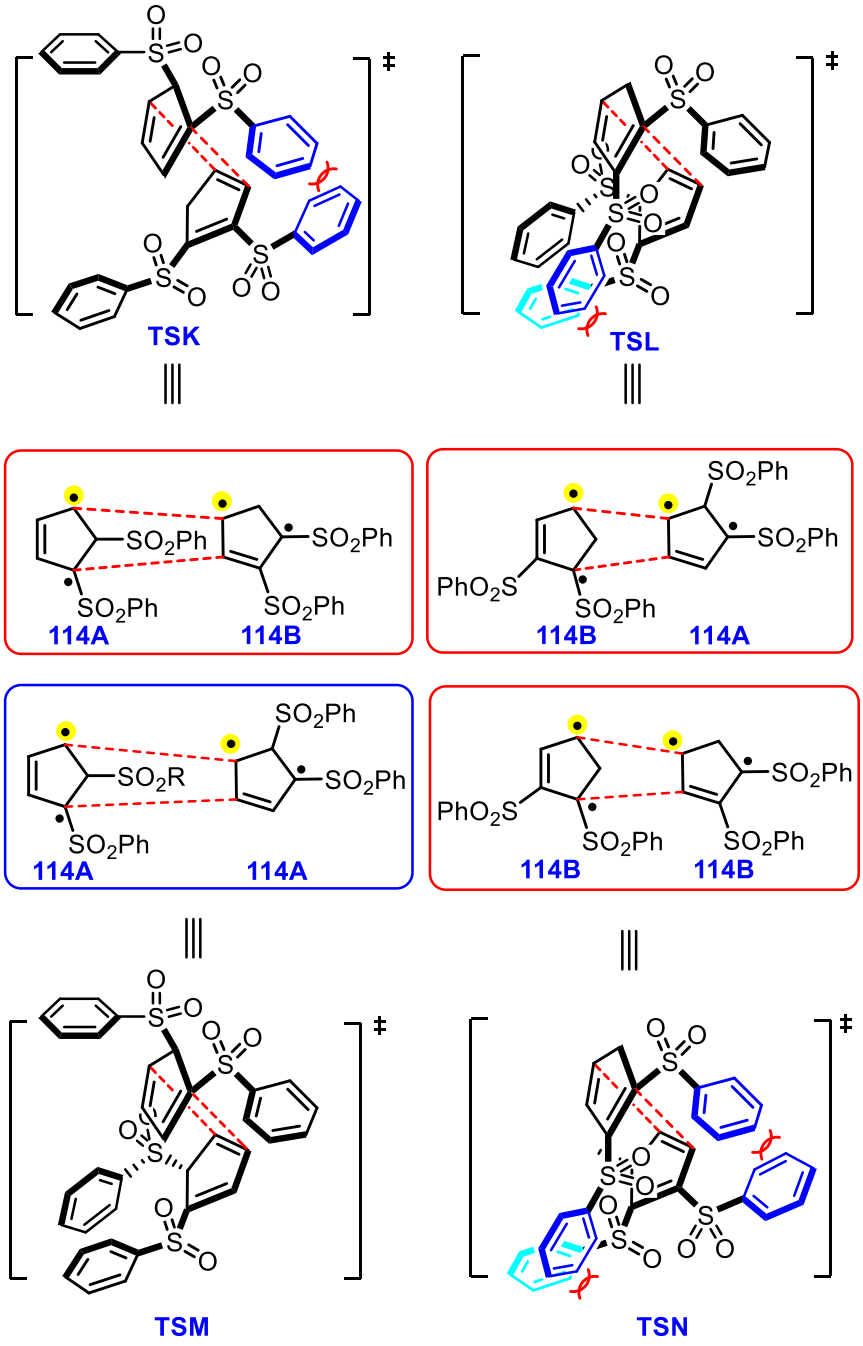

Figure 28: Electronically favoured combinations for the formation of tetrakis-sulfonylated dicyclopentadienes and their transition states. Yellow highlighting indicates the least stabilized radical for each structure. Transition states were approximated through observations of plastic models.

3.3.3. "Half" Thiele's ester

Peters reported that carboxylated cyclopentadiene **6** can heterodimerize efficiently with the parent, unsubstituted cyclopentadiene to provide two regioisomeric Diels–Alder products **61** and **116**[66]. We

repeated this reaction under similar conditions to our Thiele's ester methodology. A mixture of **61** (which later became an important monomer precursor to functionalized polydicyclopentadiene, see Chapter 4) and **116** with a ratio of 1:1.5 in 60% total yield was achieved.

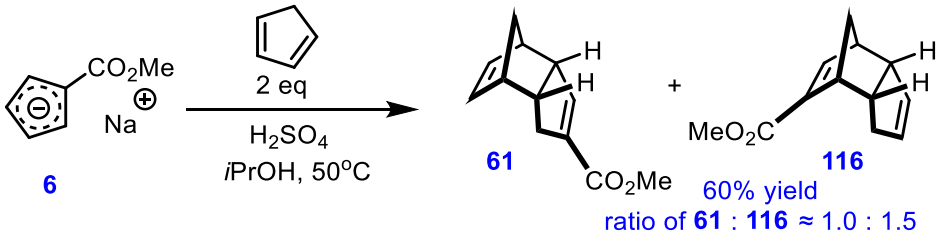

Scheme 30: Synthesis of "half Thiele's ester".

Owing to the negligible concentration of **5A**, only eight coupling possibilities need to be considered in this heterodimerization. The symmetrical cyclopentadiene, however, increases the amount of electronically favoured combinations. Five of the eight candidates shown in **Figure 29** moved on to the next stage for consideration of steric effects. Three pairings (in red boxes) which would result in the formation of a quaternary centre in their corresponding products were ruled out on the basis of steric factors. Once again, the remaining two combinations (in blue boxes) correctly predict the formation of the two isolated regioisomers **61** and **116**.

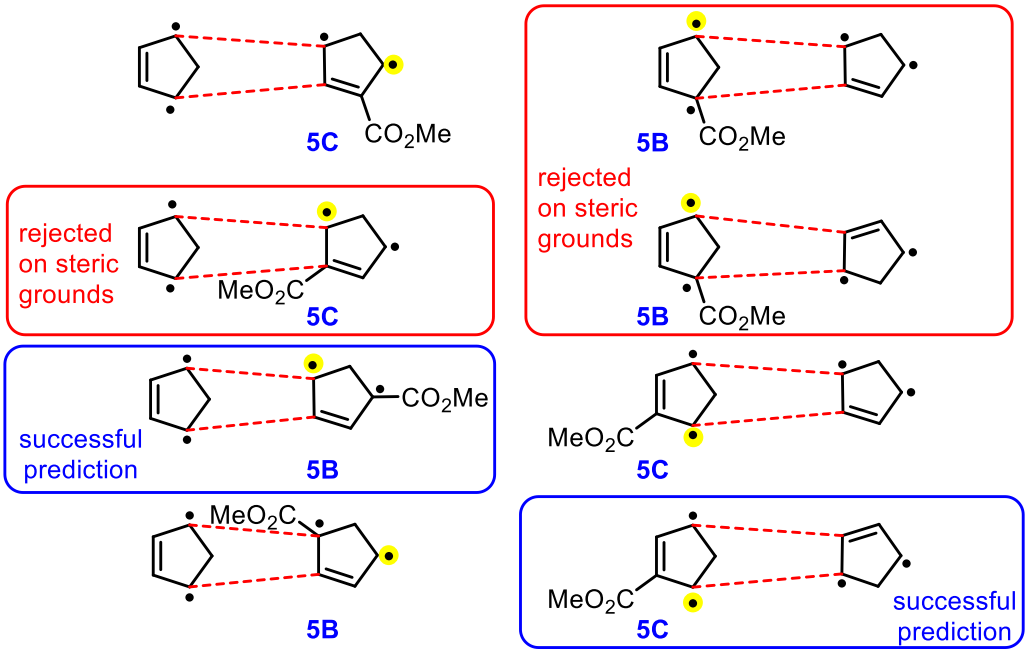

Figure 29: Predictions by radical stabilization algorithm. Yellow highlighting indicates the least stabilized radical for each structure.

3.4.0. Concluding remarks

With the help of 1D- and 2D NMR techniques, we eventually confirmed the structures of both minor regioisomers that arise from Thiele's ester formation as **7** and **8**. Both our spectral data and assignment matched to a very careful structural study by Marchand on the structures of the acid congeners. For the first time, we were able to conclusively report that the "acid first" and our "salt first" approach give the identical regiochemical outcomes.

Having the advantage of knowing the precise structures of three compounds from Thiele's ester dimerization, we found that radical stabilization arguments (based on Deslongchamps' seminal work) outperformed the classic frontier molecular orbital theory in terms of the regioselectivity of Thiele's ester dimerization. When this method was combined with simple steric arguments, we arrived at a general algorithm (summarized in **Chart 9**) to rationalize Thiele type dimerization. This new algorithm provided reliable predictions for all the known homo- and heterodimerizations in the literature. Unfortunately, just like most predictive tools, this algorithm has it own weakness. It does not provide any insight as to the relative distribution between all the predicted products. When there are multiple predictions that arise from our method, (*e.g.* Thiele's ester and "half" Thiele's ester), this algorithm has not yet been able to rank which one of those predictions would be the dominant species.

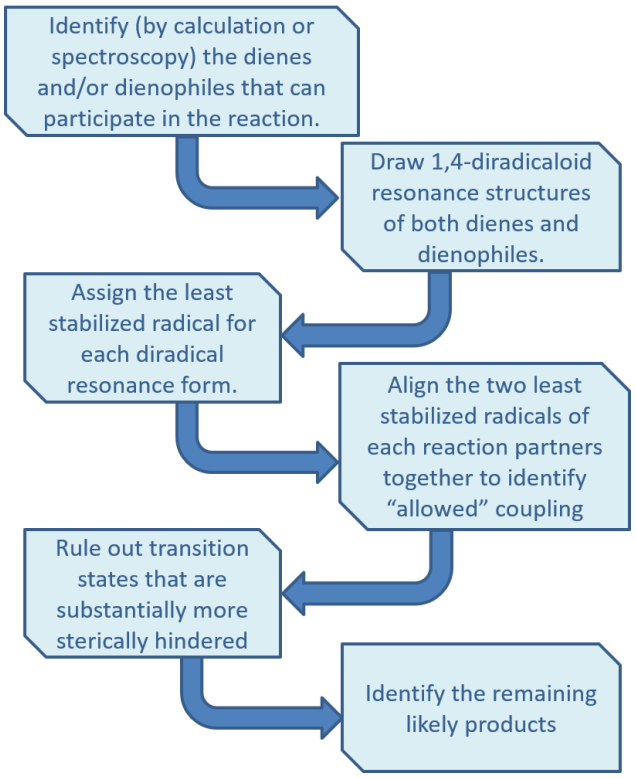

Chart 9: Algorithm for the application of radical stabilization logic to the rationalization of Diels-Alder outcomes.

While radical stabilization arguments undeniably constitute a useful predictive tool, we leave it for others to debate whether or not these results necessarily imply the existence of diradical (or diradicaloid) character in the Diels-Alder transition state, or whether “radical stabilization” merely functions as a convenient proxy for some other property (*e.g.* unanticipated FMO coefficient contributions, subdominant orbital interactions[19b], paralocalization energy[12d], etc.) that may be important in governing the reaction outcome.

Chapter Four: Functionalized Polydicyclopentadiene Polymer

The material in this chapter was adapted from: "A Thermally Crosslinked Functionalized Polydicyclopentadiene (*f*PDCPD) with a High T_g and Tunable Surface Energy" **J. Chen**, F. P. Burns, M.G. Moffitt, and J. E. Wulff * *ACS Omega*, **2016**, *1*, 532-540[18b]; "Functionalized Polydicyclopentadiene Polymer", J. E. Wulff *, **J. Chen**, F. P. Burns, and M.G. Moffitt, Provisional U.S. Patent No. 62/347,446 & No. 62/297,567[67] and "Correction to 'Thermally Crosslinked Functionalized Polydicyclopentadiene with a High T_g and Tunable Surface Energy'" T. J. Cuthbert, **J. Chen**, F. P. Burns, M.G. Moffitt, and J. E. Wulff * *ACS Omega,* **2017**, *2*, 2593[68].

All the synthesis, analysis and characterizations were performed by JC with the exception of the dynamic light scattering, gel permeation chromatography, differential scanning calorimetry, atomic force microscopy and spin-coating of polymers, which were conducted by Fraser Burns (the Moffitt group at University of Victoria). Dr. Ori Granot collected the HRMS data. Due to a calibration artefact associated with the differential scanning calorimeter at University of Victoria, Dr. Tyler J. Cuthbert (the Wulff group at University of Victoria) and Tristan D. Harrison (the Ragogna group at Western University) collected independent differential scanning calorimetry data at the University of Victoria and Western University, respectively[68].

4.0.0. Overview

The structure of the “half” Thiele’s esters **61** and **116** can be viewed as mono-ester substituted dicyclopentadienes. The parent compound—dicyclopentadiene—can be polymerized *via* ring-opening metathesis polymerization (ROMP) to afford the industrially important material polydicyclopentadiene (PDCPD)[35,51,69]. We envisioned that the monoester could be likewise polymerized *via* ROMP. The additional methyl ester functional group would bring some unique features that could overcome the limitations of the parent polymer PDCPD.

4.1.0. Polydicyclopentadiene

Dicyclopentadiene (DCPD) can be polymerized *via* ring opening metathesis polymerization (ROMP) using a variety of transition metal catalysts (for example through the use of complexes of Ru, Mo, Ti and W)[70] and even under metal-free conditions *via* photoredox catalysis[71]. It is known that the more strained norbornene moiety is polymerized initially to produce a soluble linear poly(dicyclopentadiene) (PDCPD) **117** (**Scheme 31**). Historically, researchers have generally assumed that a further olefin metathesis would occur on the less strained cyclopentene ring to produce the heavily crosslinked material. This reasonable assumption was accepted by the community for a long while until Wagener showed that this is often not representative of the exact mechanism for the crosslink. Instead, after the initial polymerization of the strained norbornene ring, the remaining pendant cyclopentene ring is inert to metathesis polymerization conditions (such as exposure to a Schrock alkylidene catalyst). Subsequent crosslinking steps might instead result from thermal (probably *via* a radical mechanism) addition reactions occurring between the remaining olefins in the linear polymer[70b]. Regardless of the debatable mechanism of crosslinking, polydicyclopendiene (PDCPD) is a heavily crosslinked organic polymer that has a very high impact resistance, coupled with a large resistance to chemical corrosion and a high heat deflection temperature. Because of the combination of these properties, PDCPD initially found applications in the automotive industry (such as for body panels, bumpers, and other components for trucks, buses, tractors, and construction equipment)[51,69a]. Recently, its other features (*e.g.* porosity and potential for microencapsulation) have been recognized and studied towards the development of tissue engineering, gas storage and self-healing material[69b,c,72].

However, PDCPD still suffers from a few disadvantages that have limited its broader application as an industrial material: (1) As a low surface energy material, it is hard to attach to machined parts and to be painted without further processing; (2) it is not chemically tunable, so its physical and chemical properties are somewhat restricted; (3) it inherits a strong acrid odour from its monomer DCPD which limits its indoor utilization; (4) it is not recyclable since the crosslinks in the polymer are not chemically reversible.

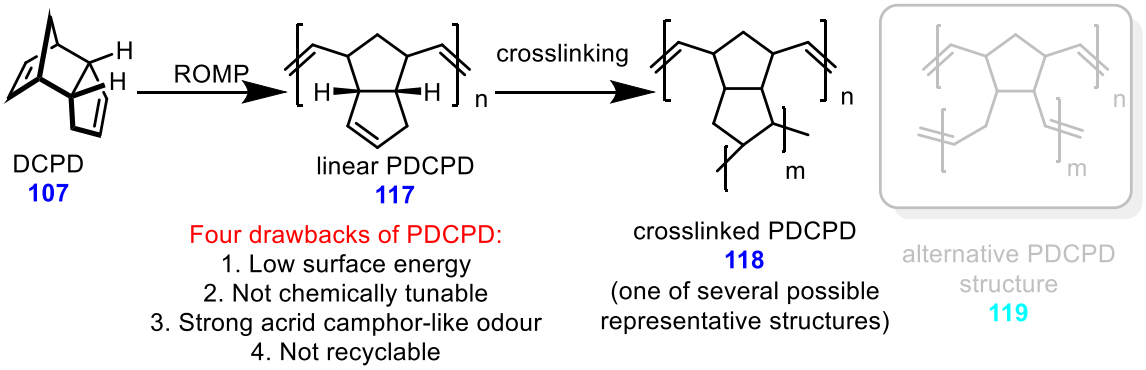

Scheme 31: Conventional synthesis of PDCPD.

4.2.0. Existing functionalized poly(dicyclopentadiene) (*f*PDCPD)

Each of these issues could presumably be solved by bringing functionality to PDCPD. The resulting functionalized poly(dicyclopentadiene) (*f*PDCPD) will naturally have a higher surface energy (owing to the presence of a functional group), tunable properties (since the functional group could be modified), a reduced odor (owing to a higher molecular weight of the monomer) and may even raise the possibility of a different crosslinking and decrosslinking strategy to develop a recyclable PDCPD. Indeed, there are many groups who have reported the post-polymerization functionalization of PDCPD by modifying the remaining alkenes in the backbone after polymerization. A variety of reactions have been used for this purpose such as bromination[73], epoxidation[74], inverse electron demand Diels−Alder[72a], radical-initiated thiol−ene addition[72b], etc. Each of these depends, however, on the ability of reagents to access the olefin in the polymer; as a result, these strategies are largely limited to the functionalization of PDCPD foams, or else to functionalization solely at the surface. The alternative way would be pre-functionalizing the monomer—DCPD—first and then triggering the polymerization.

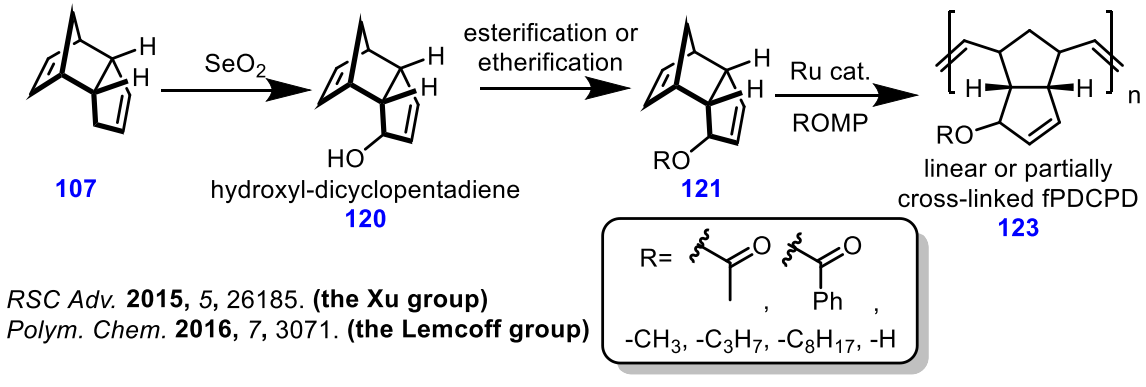

Scheme 32: 1-Hydroxydicyclopentadiene-based *f*PDCPD.

Prior to our own work, there were only two publications that described pre-functionalization of the DCPD monomer. In both reports, 1-hydroxydicyclopentaidene **120** was prepared by a known SeO_2-mediated allylic oxidation on DCPD[75], followed by further esterification or etherification and Ru-

catalyzed ROMP to achieve a new family of odourless *f*PDCPD polymers[76]. These odourless *f*PDCPD polymers showed glass transition temperatures (T_g) that ranged from 80 to 143 °C (most of them were under 100 °C)[76b] which is significantly higher than the linear PDCPD (T_g at 53 °C), but lower than crosslinked PDCPD (T_g ~ 155 °C). Since both groups assumed further metathesis of the cyclopentene olefin to underpin the crosslinking mechanism of PDCPD, these 1-hydroxydicylopentadiene based polymers were initially designed as a linear polymers[76a] (it is known that the allylic acetoxy group disfavours for metathesis)[77]. Their relatively low T_g data did suggest that these polymers were linear, or at least not extensively crosslinked. In addition, due to the nature of allylic acetoxy or ether group (being a good leaving group), substantial weight losses were observed at temperatures above 220 °C during both groups' thermogravimetric analyses (TGA) studies.

4.3.0. Selective polymerization of half "Thiele's ester"

Although these 1-hydroxydicylopentadiene based polymers **121** enrich the diversity of PDCPD-type materials, the additional functional groups (acetoxy or ether) do reduce the thermal stabilities of these polymers, and further complicate issues surrounding the crosslinking step. Thus, we envisioned that replacing the acetoxy group with a functional group which connects to the polymeric backbone with a more stable C-C bond could potentially solve this drawback. As mentioned above, the required monomer necessary to achieve such materials (compound **61** in **Scheme 33**) has already been reported by several groups[18a,31a,66].

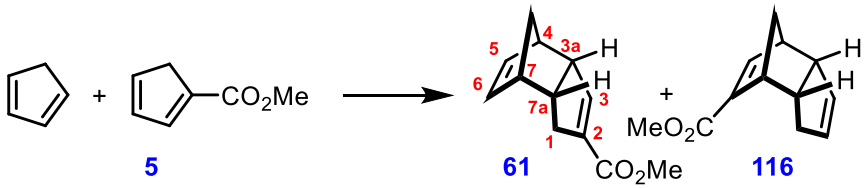

Scheme 33: Synthesis of mono-ester substituted dicyclopentadiene by other groups.

We hypothesized that the C2-methyl ester substituted DCPD monomer could strategically change both the chemical and physical properties of the resulting polymer which would be beneficial to broaden the future applications of *f*PDCPD:

(1) The fruity odours of esters[78], along with the extra molecular weight of **61** relative to **107**, would be likely to address any concern about the residual volatile monomer in the final material.

(2) Unlike the allylic acetoxy or ether groups in Xu's and Lemcoff's work, the C-linked ester cannot function as a leaving group. Thus, the resulting polymers should have a thermal stability closer to that of the parent PDCPD.

(3) The additional electron-withdrawing ester group on the unstrained olefin of DCPD should inhibit any olefin metathesis at the C2-C3 alkene (at least for modest reaction temperatures)[79]. Therefore, we could minimize the possibility of metathesis crosslinking. This should allow us to stop at the linear polymer stage (for use as a soft material) or else intentionally trigger crosslinking by thermal

or photochemical methods (to provide a tough, harder material). Furthermore, instead of the ambiguous structural assignment of the crosslinked PDCPD, our material would most likely crosslink through a radical mechanism to provide the crosslinked material shown as structure **125** (**Scheme 34**).

(4) The positioning of an ester at C2 of DCPD would essentially allow us bury a methyl methacrylate motif into the chemical framework of the post-metathesis linear polymer. Methyl methacrylate is known to be thermally polymerized *via* self-initiated radical processes to provide predominantly a head-to-tail polymerization[80]. Our linear polymer **124** would be expected to have a similar crosslinking mechanism as methyl methacrylate (**Scheme 34**) which would let one get access to a highly crosslinked *f*PDCPD **125**. More importantly, in contrast to unfunctionalized PDCPD (wherein presumably all of the residual olefins can react equally in the thermal crosslinking step), the regiochemical control in the crosslinking step will provide a less ambiguous structure of the crosslinked polymer. Knowing the exact structure of the crosslinked polymer **125** may also open up a new path to develop a decrosslinking method towards a recyclable material (such as going through a retro Michael addition mechanism).

(5) The resulting thermally crosslinked polymer **125** would bear an ester group at a quaternary center. This increased steric hindrance (relative to unmodified PDCPD) to bond rotation should result in an increased T_g.[81]

(6) The chemically tunable ester group would make it possible to adjust both the chemical and physical properties of the final polymer material.

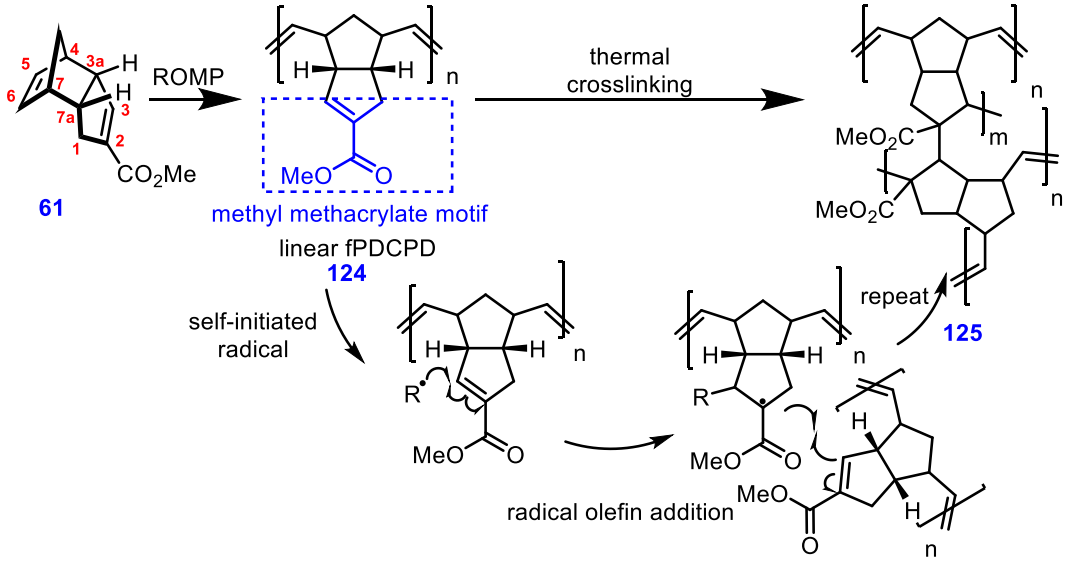

Scheme 34: Proposed *f*PDCPD formed via controllable thermal crosslinking.

Firstly, we started with the synthesis of the desired monomer **61** by using our own cyclopentadienylide salt-based route (see Chapter 2) to ester-containing derivatives of dicyclopentadiene. A mixture of regioisomers **116** and **61** (in a ~1.5:1 ratio) was achieved in 60%

yield. Notably, this reaction could also be scaled up to a 45 g scale with a consistent isolated yield. As we expected, the resulting mixture also bears a fruity odour due to the presence of the ester.

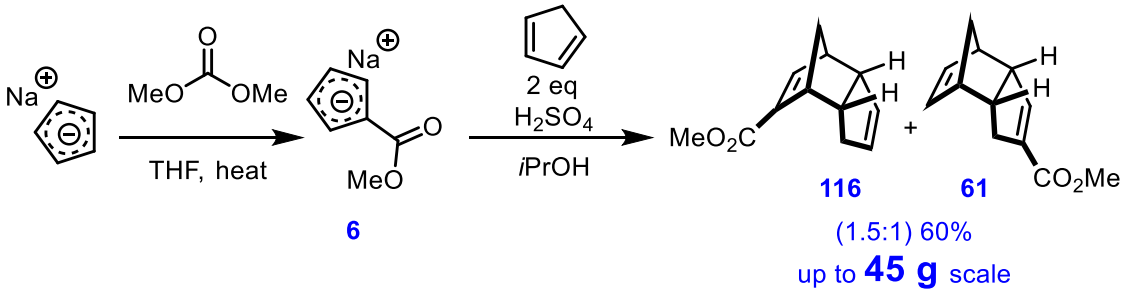

Scheme 35: Synthesis of the ester-containing monomer.

At first glance, the separation of these two regioisomers might seem to be very problematic. In fact, we can only achieve the regioisomerically pure **61** by trapping **116** *via* another chemical reaction. However, between the four alkenes in the mixture of **61** and **116**, there is only one strained and electron-rich alkene which is reactive under standard (room temperature) ruthenium-based olefin metathesis conditions. Compared to the other three alkenes (either unstrained or electron-poor), the electron-rich strained C5-C6 double bond (labelled with cyan square in **Scheme 36**) should be polymerized selectively under these conditions.

This hypothesis was quickly proven by reacting the monomer mixture with the Grubbs second-generation catalyst at room temperature. From the ^{1}H-NMR of the crude reaction mixture, we can see that **61** reacts much more rapidly than **116** under the applied conditions in **Scheme 36** after an hour. All the alkene protons of **124** were significantly broadened which indicated the occurrence of the polymerization. More importantly, the fact that only the electron-rich strained norbornene protons on **61** experienced a significant change in chemical shift (from around 6.0 ppm to 5.3 ppm) proved that the olefin metathesis did take place at the position that we predicted. After endcapping the resulting polymer **124** with ethyl vinyl ether, the two products were separated by the addition of diethyl ether to precipitate the polymer. While the solid that would be recovered from subsequent centrifugation provided us pure polymer (**Scheme 36C**), the remaining supernatant only contained unreacted **116** (**Scheme 36D**). The retro-Diels-Alder reaction of dicyclopentadienes with alkyl or ester functional groups has already been reported by Franklin[82], which suggests that the unreacted monomer **116** can be recycled back to the original mixture of **61** and **116** under thermal conditions. The molecular weight of **124** was determined as approximately 45,000 g/mol by comparing the ^{1}H NMR integration of the phenyl end-group and the internal vinyl protons. This estimation was also found to be close to the gel permeation chromatography (GPC) result (**Figure 30**) that we acquired from a freshly-prepared (~4-hour-old) sample of polymer **124**. All of these characterization data, coupled with the great solubility of the fresh prepared polymer suggested a negligible degree of crosslinking for polymer **124**.

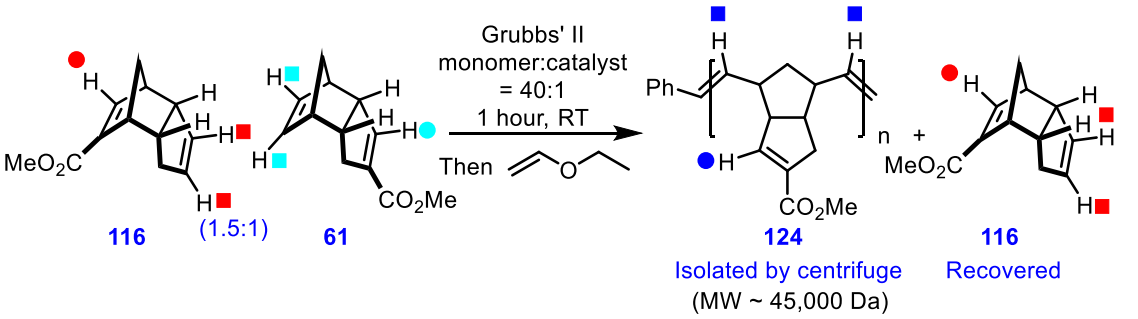

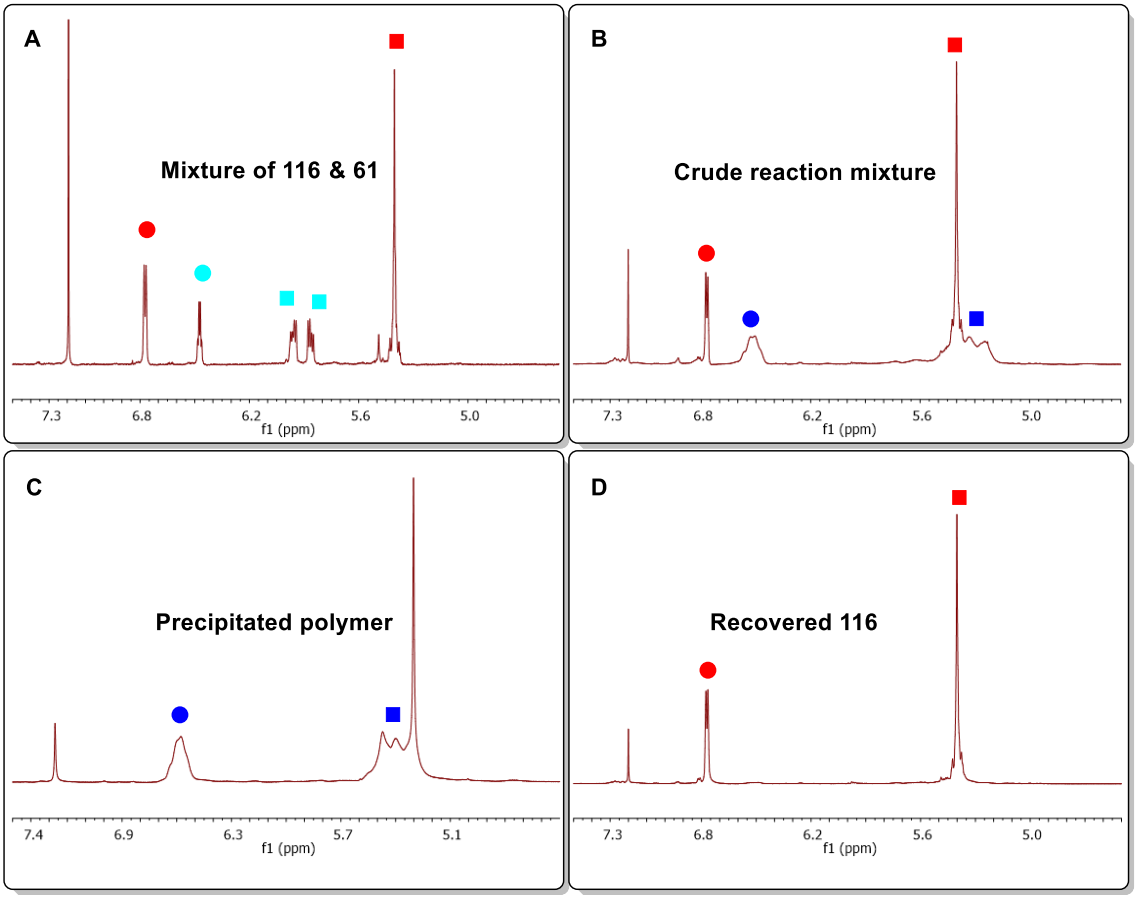

Scheme 36: Selective polymerization from the mixture of 61 and 116. A: Initial monomer mixture. B: Crude mixture of polymer product and unreacted monomer following selective polymerization. C: Polymer product isolated by precipitation from ether. D: Recovered unreacted monomer 116 from the supernatant.

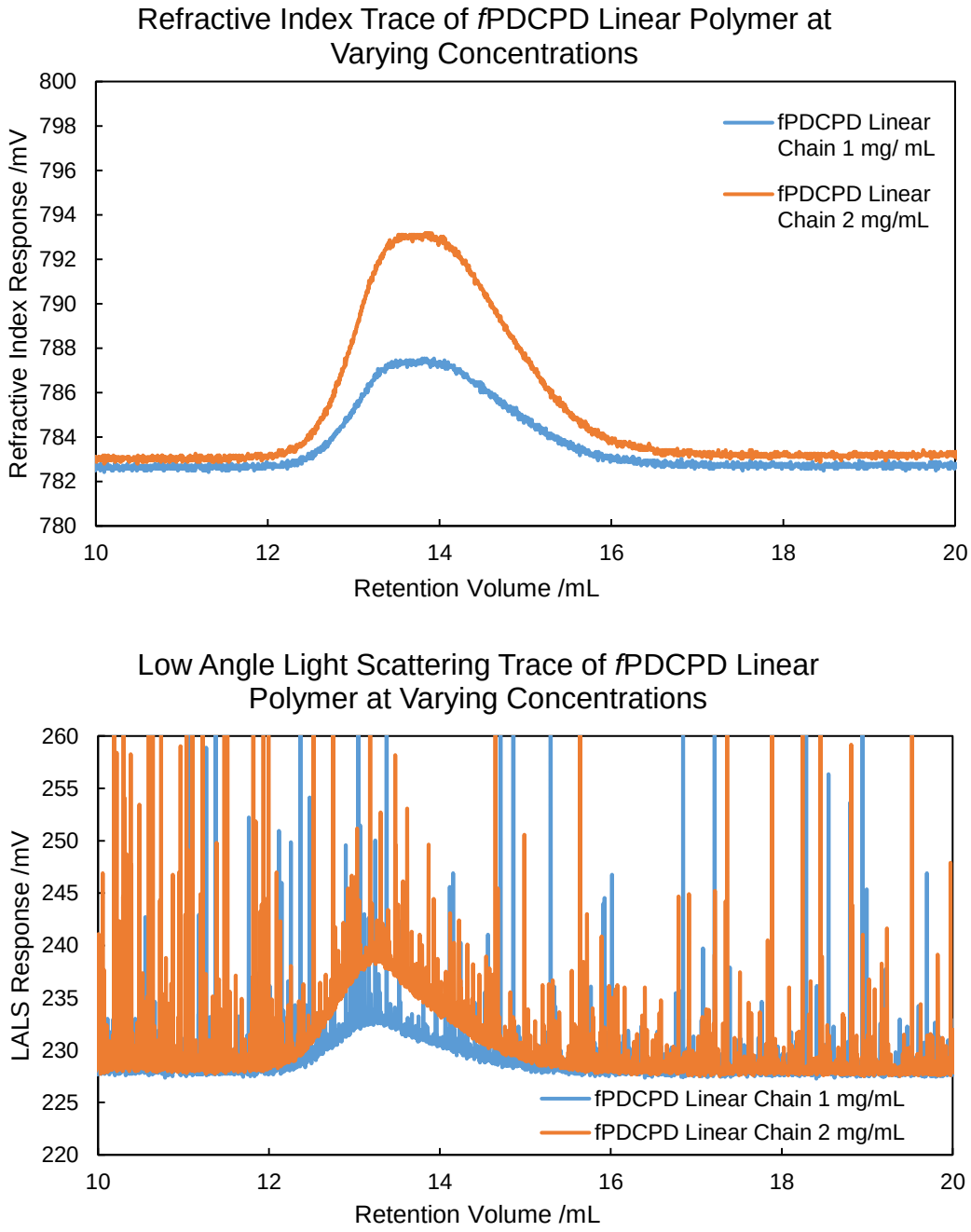

Figure 30: A. GPC traces of a freshly-prepared (~4-hour-old) sample of polymer 124. Top trace: refractive index detection. Bottom trace: low angle light scattering detection. Calculated data: 1 mg/mL sample: Mw = 94445 Da, Mn = 39824 Da, PDI = 2.37, dn/dc = 0.103; 2 mg/mL Sample: Mw = 93290 Da, Mn = 47684 Da, PDI = 1.96, dn/dc = 0.108.

However, similar to the parent polydicyclopentadiene[72b,83], **124** also exhibits a slow oxidative crosslinking behavior upon exposure to atmospheric conditions. It was found that the size of polymer **124** (monitored by dynamic light scattering) was growing over time. This was further proven by our GPC data from a 2-day-old **124** (molecular weight was up to ~30 000 000 Da for a 2-day-old sample) as well as by the observation that after 2−3 days samples (maintained in THF solution) became distinctly cloudier.

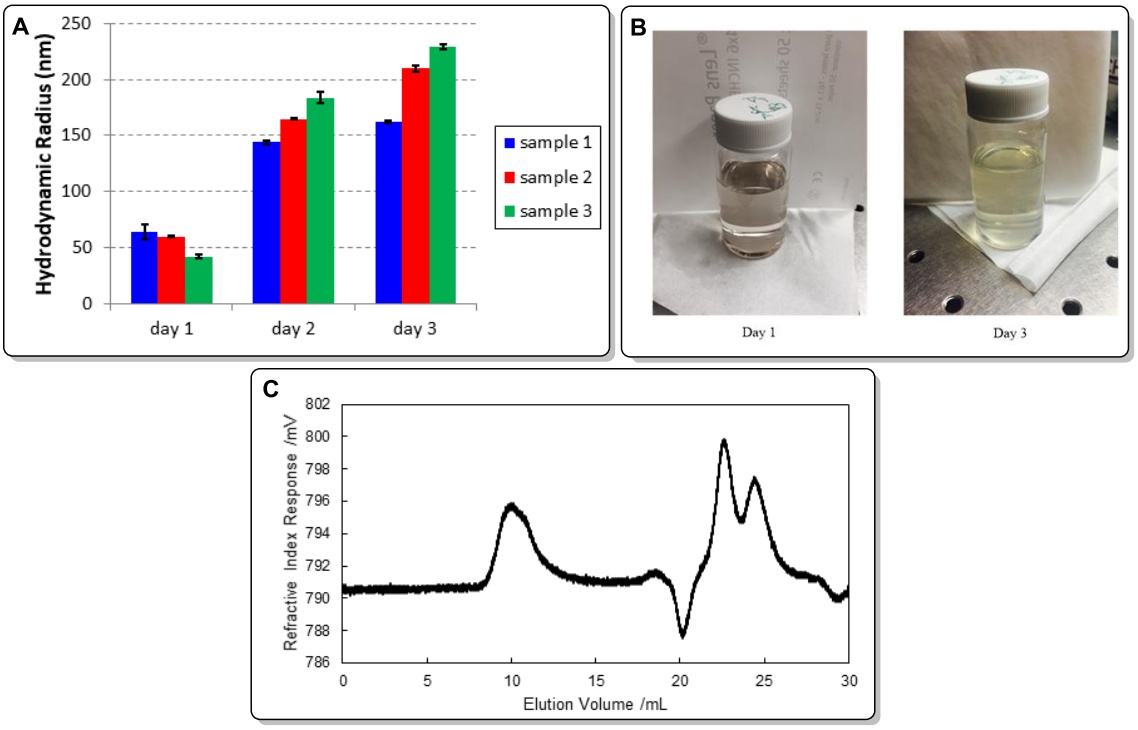

Figure 31: A: Oxidative crosslinking leading to a slow growth in hydrodynamic radius. B: Comparison between fresh-prepared polymer 124 solution and 3-day-old solution. C: GPC refractive index trace of a 2-day-old sample of polymer 124, peak at 10 mL elution volume corresponds to M_n and M_W values of ~3x10^7 Da, but this number is not particularly meaningful given the amount of oxidative crosslinking that the sample has evidently experienced prior to analysis.

4.4.0. Characterization of cross-linked *f*PDCPD

As we expected, after thermal curing at 180 °C overnight, the linear polymer **124** turned into a hard and completely insoluble material. The glass-transition temperature (T_g) of this insoluble material was found at 172 ± 3 °C (average data from 4 runs, acquired on two separate instruments). This is the highest T_g ever reported for an unaged polydicyclopentadiene[84]. Although we did not initially have conclusive proof of the structure of our crosslinked polymer, the poor solubility and high T_g did suggest that this material is crosslinked. Owing to the fact that our design of monomer **61** should

inhibit the metathesis crosslinking on the cyclopentene ring, it leaves us to propose that the structure of our crosslinked polymer should be as **125** (shown in **Scheme 37**). In addition to this, the thermal stability of **125** was revealed by the measurement of the percent mass loss of material via thermogravimetric analysis (TGA). Unlike Lemcoff's and Xu's 1-hydroxydicylopentadiene-based polymers **123** which all suffer from substantial weight losses at temperature above 220 °C,[76] our crosslinked material **125** appears to be extremely stable up to >300 °C. The 10% weight loss temperature of **125** is 411 °C which is significantly higher than any of the previously reported *f*PDCPD material (the previous highest is 254 °C) and only 40°C lower than the parent PDCPD[76b]. This observation is consistent with our earlier hypothesis that replacing the *O*-linked acetate with the *C*-linked ester would contribute to increasing the thermal stability of *f*PDCPD.

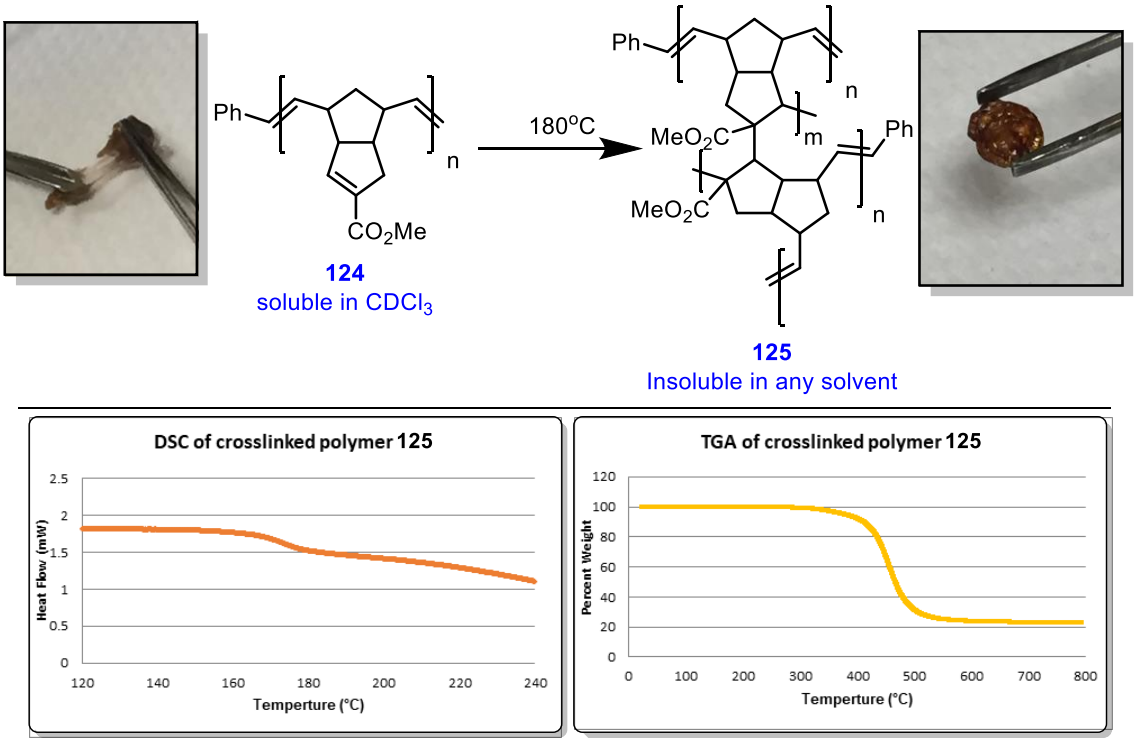

Scheme 37: Thermal curing of *f*PDCPD and TGA/DSC analysis from polymer 125.

4.5.0. Probing of the tunable surface energy of *f*PDCPD

After the synthesis and characterization of both linear and crosslinked polymers, we next focused on the modification of the surface chemistry. In order to systematically study the surface energy of our *f*PDCPD, we decided to measure the contact angles of our modified polymers with different solvents. Thus, we spin-coated the linear polymer **124** onto a series of glass slides and then incubated each slide in a 180 °C oven to achieve crosslinking. Some slides were then suspended in a solution of methanolic sodium hydroxide, followed by a solution of aqueous HCl. The surface roughness (R_a) of each slide was measured by atomic force microscopy (AFM) as shown in **Figure**

32B to ensure the precision of the subsequent contact angle measurements. It appears that the spin-coated thin films of all three modified polymers were as smooth as the surface of the naked glass slide used as a control.

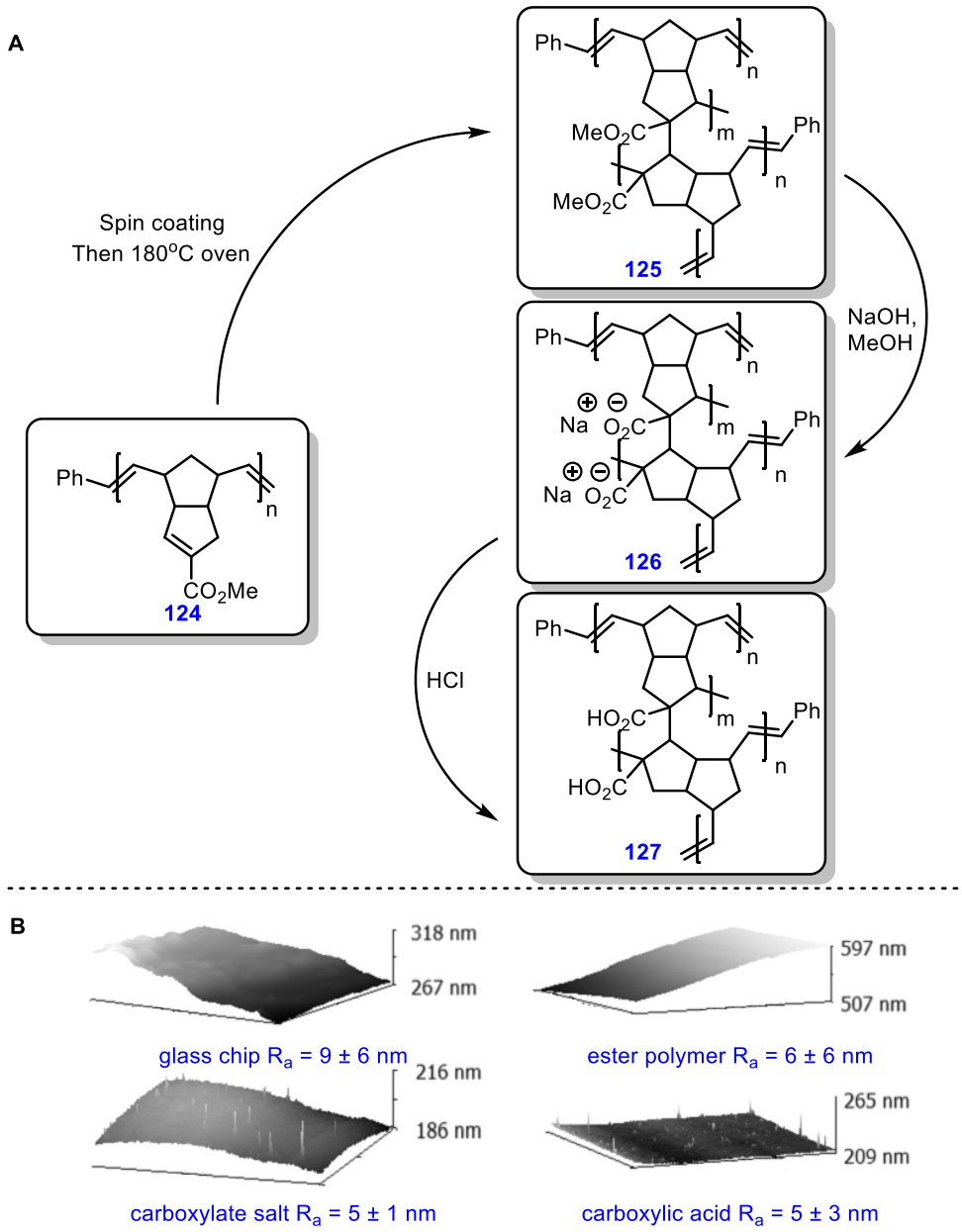

Figure 32: A: Saponification/acidification protocol used to alter surface energy. B: Surface roughness determined for each sample, as well as a control of glass chip.

Finally, the contact angle measurements were obtained with water as polar liquid and diiodomethane as dispersive liquid. Data are reported in **Table 7**. As we expected, a dramatic difference was found between the parent PDCPD and three functionalized polymers. Water contact angles ranged from nearly 120° for a sample of commercial PDCPD obtained from Product Rescue

BVBA) to approximately 30° for the carboxylic acid polymer **127**. The clear tendency for the contact angle to decrease from additional operations suggests that only partial hydrolysis was achieved at each stage of the protocol.

Table 7: Contact angles of *f*PDCPD and PDCPD.

polymer	left (°)	right (°)	overall (°)
methyl ester (H_2O) **125**	87.0 ± 1.1	87.4 ± 0.8	87.2 ± 0.9
carboxylate salt (H_2O) **126**	63.3 ± 3.0	63.9 ± 2.2	63.6 ± 2.5
carboxylic acid (H_2O) **127**	28.8 ± 1.1	29.2 ± 1.2	29.0 ± 1.1
methyl ester (CH_2I_2) **125**	46.0 ± 0.8	45.6 ± 1.0	45.8 ± 0.9
carboxylate salt (CH_2I_2) **126**	46.1 ± 1.7	46.6 ± 1.5	46.4 ± 1.5
carboxylic acid (CH_2I_2) **127**	52.0 ± 1.6	52.4 ± 1.3	52.2 ± 1.4
PDCPD (H_2O)	119.4 ± 1.2	120.1 ± 1.5	119.8 ± 1.3

All the measurements were triplicated and the standard deviations of these data were used to generate measurement errors.

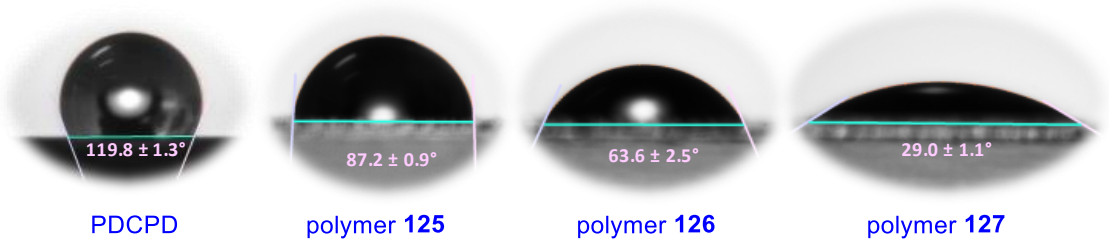

Figure 33: Representative water contact angle measurements for each sample.

With all the contact angle data in hand, dispersion surface tension (γ_{sv}^{d}), polar surface tension (γ_{sv}^{p}) and overall surface tension (γ_{sv}) was calculated by the combination of the OWRK equation **(1)** and equation **(2)**[85].

$$0.5\,\gamma_{lv}(1+\cos\theta) = \sqrt{\gamma_{sv}^{d}\gamma_{lv}^{d}} + \sqrt{\gamma_{sv}^{p}\gamma_{lv}^{p}} \qquad \textbf{(1)}$$

$$\gamma_{sv} = \gamma_{sv}^{d} + \gamma_{sv}^{p} \qquad \textbf{(2)}$$

$H_2O\ \gamma_{lv} = 72.8$ mN/m, $H_2O\ \gamma_{lv}^{d} = 21.8$ mN/m, $H_2O\ \gamma_{lv}^{p} = 50.0$ mN/m

$CH_2I_2\ \gamma_{lv} = 50.8$ mN/m, $CH_2I_2\ \gamma_{lv}^{d} = 50.8$ mN/m, $CH_2I_2\ \gamma_{lv}^{p} = 0.0$ mN/m

θ = contact angle

Gratifyingly, we observed a clear increase of γ_{sv}^{p} and decrease of γ_{sv}^{d} with increasing ester hydrolysis (as shown in **Table 8**). More importantly, the overall γ_{sv} values were enhanced from 38.5 mN/m (for the methyl ester) to 66.6 mN/m (for the carboxylic acid). This is a much greater range of surface energies than is available to unfunctionalized PDCPD, which has a γ_{sv} value of 36−38

mN/m when freshly made[51], increasing to 48−52 mN/m following oxidation[51,86]. Indeed, to the best of our knowledge, polymers **125-127** represent the largest (and therefore most tunable) range of surface energies known for any polydicyclopentadiene-based homopolymer.

Table 8: Calculated surface tension for the three *f*PDCPD polymers.

polymer	γ_{sv}^{d} (mN/m)	γ_{sv}^{p} (mN/m)	γ_{sv} (mN/m)
methyl ester **125**	36.6 ± 0.5	1.9 ± 0.1	38.5 ± 0.6
carboxylate salt **126**	36.2 ± 0.8	11.8 ± 1.1	48.0 ± 1.9
carboxylic acid **127**	33.0 ± 0.5	33.6 ± 0.1	66.6 ± 0.7

In order to better illustrate the drastic hydrophobicity difference between unmodified and modified polymers, a glass slide which was coated with polymer **125** was half-immersed in a solution of methanolic NaOH. The resulting half-**125** half-**126** coated glass slide was then wetted with water containing green food dye (**Figure 34**). Upon depositing onto the prepared slide, all the water shifted swiftly from the unmodified methyl ester polymer **125** side to the modified carboxylate salt polymer **126** side. Within a few seconds, all of the water accumulated on the portion of the sample that had been exposed to saponification conditions, as shown in **Figure 34**. The ability to tune surface tension so dramatically may open the door toward the use of *f*PDCPD in microfluidic applications.

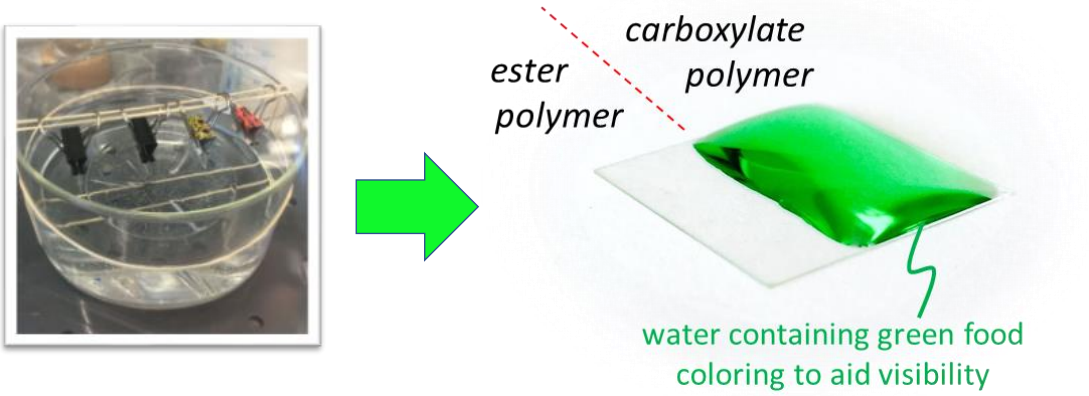

Figure 34: Macroscopic observation of changes in surface hydrophobicity following ester hydrolysis.

4.6.0. Concluding remarks

In this work, we described the first example of a polymer derived from a carboxyl-functionalized dicyclopentadiene monomer and its subsequent thermal crosslinking. The resulting crosslinked material has the highest glass-transition temperature reported for a polydicyclopentadiene, good thermal stability, no unpleasant odour and allows for the facile manipulation of the surface chemistry through alteration of the embedded functional group.

Chapter Five: *N*-substituted de-guanidinylated peramivir derivatives to target the 150-cavity of viral neuraminidase

All the synthesis, analysis and characterization of data were performed by JC with the exception of the synthesis of **152**, which was partially contributed by Deepak Jaswal and Cameron Zheng under the supervision of JC.

5.0.0. Overview

One of our long-term goals for the application of Thiele's ester's chemistry is utilizing Thiele's ester as the bicyclic core of a conformationally constrained neuraminidase inhibitor to mimic the enzyme-bound conformation of peramivir. The resulting inhibitor (which could be viewed as a rigidified form of peramivir) would provide reduced conformational flexibility to enhance the target specificity (such as towards different strains of viral or human neuraminidases). However, unlike the other two commercial drugs (oseltamivir and zanamivir), peramivir (the most potent commercially available viral neuraminidase inhibitor) has never been used as a ring scaffold to exploit both the catalytic site and the nearby 150-cavity. In this chapter, we describe our efforts toward the development of a new series of *N*-substituted de-guanidinylated peramivir analogues for probing the target specificity towards the 150-cavity of group 1 viral neuraminidase. It is expected that lessons learned from this sub-project could contribute to our eventual design of an optimized Thiele's ester-based neuraminidase inhibitor.

5.1.0. Introduction to the neuraminidase enzyme

Neuraminidase (also called sialidase) enzymes are a class of glycoside hydrolase enzymes that cleave the glycosidic linkages of terminal sialic acid residues of glycoconjugates. Different forms of neuraminidases in this enzyme family are found in a range of organisms including bacteria, fungi, protozoa, mycoplasma, mammals and viruses[87]. Many of these enzymes are known to play important roles in various human pathologies such as cancer,[88] cholera,[89] pneumonia,[90] and influenza.[91] Among all neuraminidases, influenza virus neuraminidase is the best known and has been studied since the 1950s. Thus, previous research results arising from the targeting of viral neuraminidase could be applied to develop inhibitors for other neuraminidase targets.

5.1.1. Viral neuraminidase

Influenza viruses are RNA viruses in the family of orthomyxoviridae that include three genera: influenza viruses A, B and C[92]. Influenza virus A infects multiple species (birds and some mammals), while influenza viruses B and C almost exclusively infect humans. Among the three types, influenza A viruses are particularly variable and have the potential to outwit the human immune system due to mechanisms of antigenic shift[93]. In fact, pandemics have all been caused by influenza virus A.

Influenza A viruses contain three membrane proteins: hemagglutinin (HA), neuraminidase (NA), and matrix 2 (M2) protein[94] along with an inner shell of matrix protein and nucleocapsids of the viral genome at the center[92]. Each subtype is sub-classified by its two major surface proteins variants: hemagglutinin (HA) which is responsible for sialic acid-receptor binding at the initial stage of infection and the fusion of virus and cell membranes[95], and neuraminidase (NA) which cleaves terminal sialic acid residues from the cell to release viral progeny[95-96]. It is estimated that each virion

contains approximately 100 copies of neuraminidase and 300 copies of hemagglutinin on its surface. There are at least 18 different hemagglutinin antigens that have been characterized (H1 to H18)[97] and 9 neuraminidases (N1 to N9)[98]. Influenza viruses are characterized by the combinations of hemagglutinin and neuraminidase subtypes. Three major pandemics in the 20th century were caused by viruses containing H1N1 in 1918, H2N2 in 1957, and H3N2 in 1968, respectively. The recent emergence of two novel avian influenza viruses (H7N9, H5N1) with high mortality (30% and 59% respectively) is also noteworthy[99]. Furthermore, a number of other point mutations of neuraminidase are known to confer drug resistances between the majority of influenza viruses and three commercially available drugs[100].

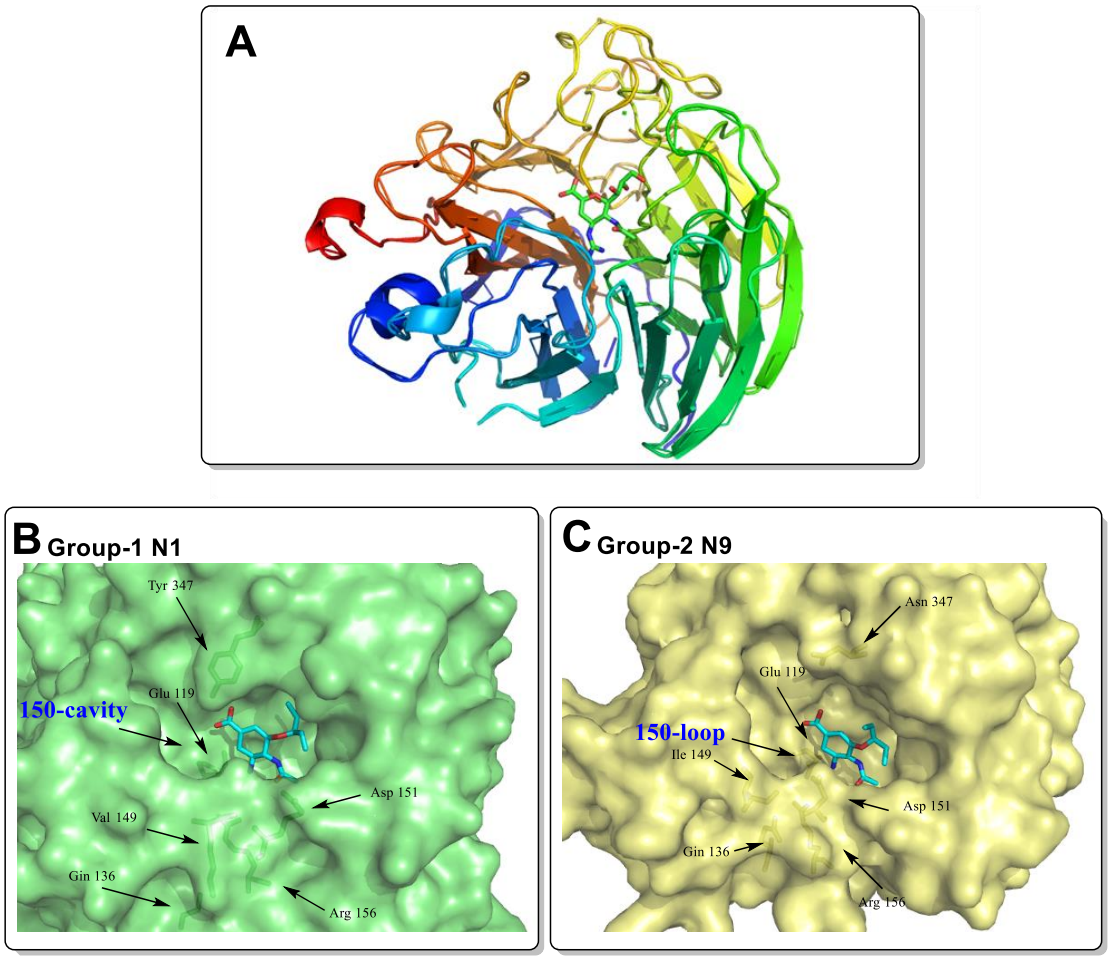

Figure 35: Structures of inhibitor bound neuraminidase enzymes. A: Influenza virus neuraminidase subtype N9 complexed with zanamivir[101]. B: Group-1 (N1) neuraminidase with oseltamivir. C: Group-2 (N9) neuraminidase with oseltamivir[102].

The most clinically successful anti-influenza drugs target the neuraminidase enzyme. Neuraminidases are found in a wide range of organisms including bacteria, fungi, protozoa, mycoplasma, mammals and the best known: viruses. The structure of influenza neuraminidase was first revealed as a 240 kD tetramer in 1983 at 2.9 Å resolution (**Figure 35A**)[103].

Studies of neuraminidase−inhibitor co-crystal structures illustrated that active sites of neuraminidase have very polar amino acid side chain residues including Arg 118, Arg 292, Arg 371, Asp 151, Glu 277, and Tyr 406. Based on phylogenetic trees, influenza A virus neuraminidase proteins can fall into two subtypes: group 1 (N1, N4, N5 and N8) and group 2 (N2, N3, N6, N7 and N9). By acquiring X-ray crystal structures of both types, Russell and coworkers found that in the group 1 enzymes, a loop of amino acids (residues 147-152, also known as the 150-loop) bear different conformations compared to group 2 enzymes. As a result, a 10 Å long, 5 Å wide and 5 Å deep cavity (also known as the 150-cavity) that locates very close to the catalytic cavity becomes accessible in the case of group 1 enzymes (**Figure 35B and 35C**), which opens a new door to novel selective inhibitors towards group 1 neuraminidases[102a].

5.1.1.1. Mechanism of neuraminidase catalyzed hydrolysis of sialidase

The catalytic pathway for neuraminidase is believed to contain three major steps[104].

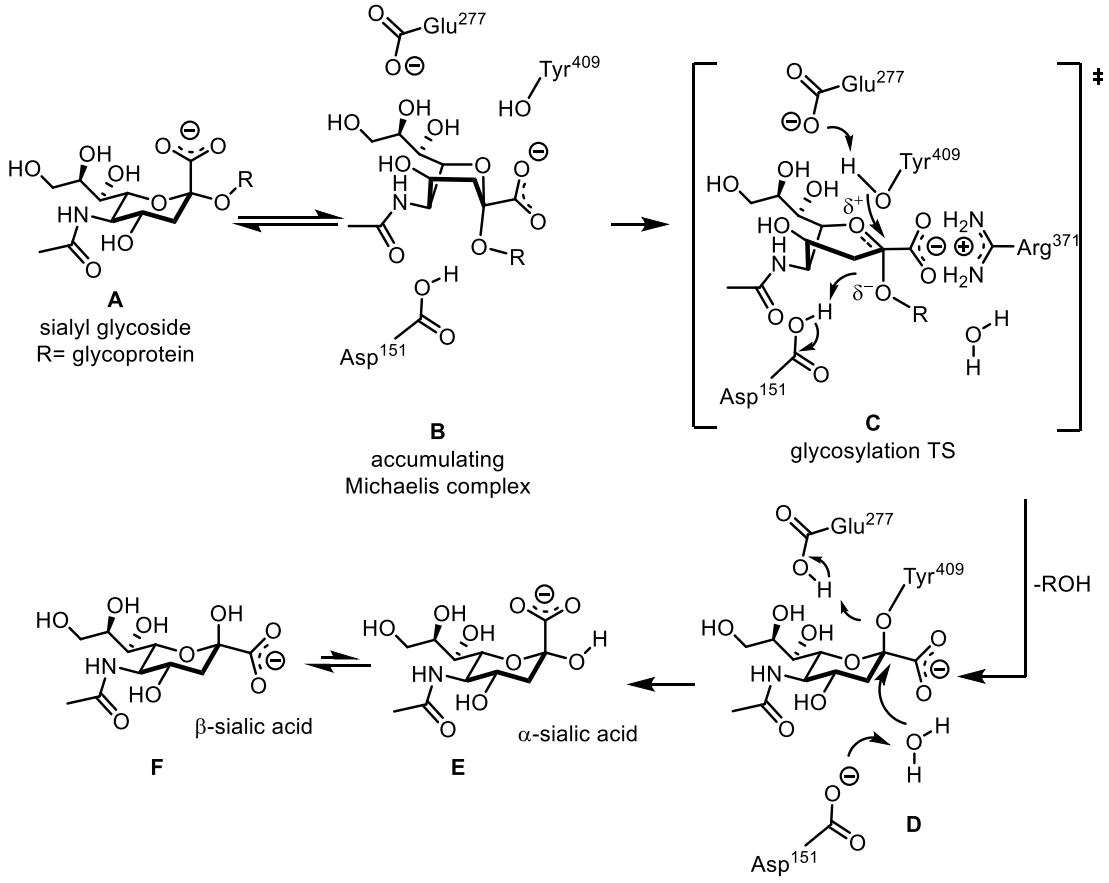

Figure 36: Proposed catalytic mechanism of viral neuraminidase.

The first step involves considerable distortion of the $^{2}C_{5}$ chair conformation pyranose ring **A** to a pseudoboat conformation when the sialyl glycoside binds to neuraminidase to form a Michaelis complex **B** (skew-boat conformation). Then the glycosidic bond is cleaved from the resulting Michaelis complex through a $^{4}H_{5}$ half-chair transition state **C** to afford a covalently linked sialosyl-

neuraminidase intermediate **D** ($^2C_5$ chair conformation). In the third step, the sialosyl−neuraminidase conjugate is hydrolyzed through catalysis by a nearby Asp 151 residue to release α-Neu5Ac **E** (α-sialic acid) which mutarotates to the more favorable anomer β-Neu5Ac **F** (β-sialic acid) spontaneously (**Figure 36**)[105].

5.1.1.2. Viral neuraminidase inhibitors

After decades of structure activity relationship studies of viral neuraminidases, the binding targets of a neuraminidase inhibitor can be generally divided into four subsites as described in Chapter 2 (**Figure 15B**).

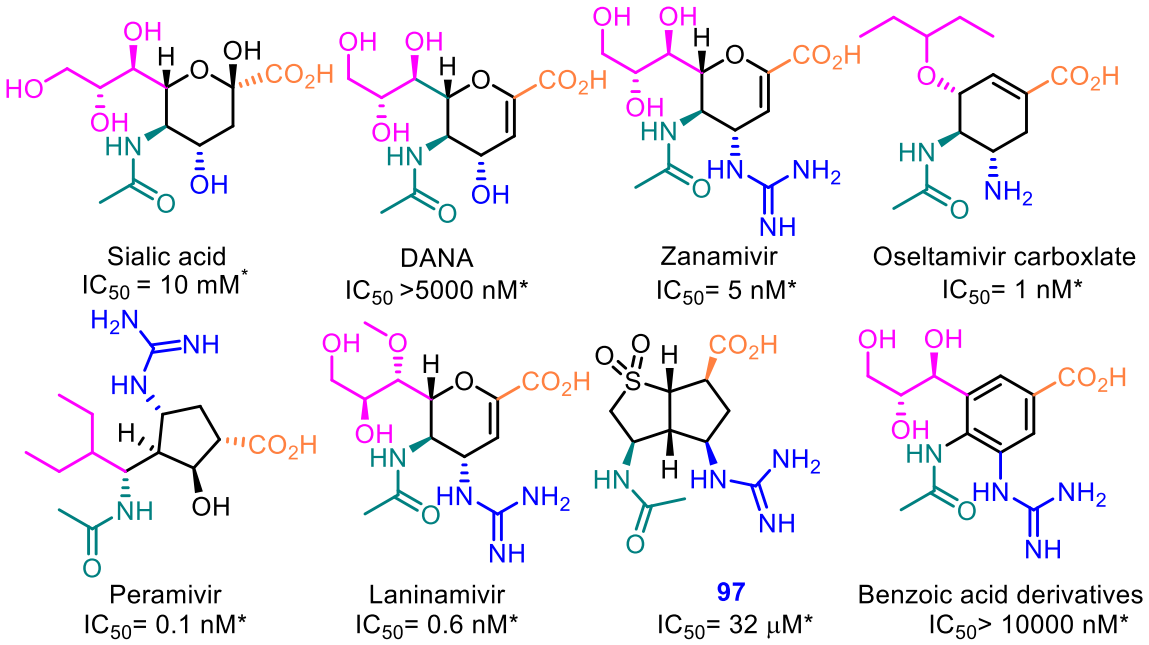

* Typical IC_{50} values vs. influenza neuraminidases (across the different subtypes, strains, etc.)

Figure 37: Summary of important neuraminidase inhibitors. (Colours indicate corresponding subsites in Figure 15B)

Various cyclic cores have been coopted for designing different generations of viral neuraminidase inhibitors, including aromatic rings[106], cyclohexenes[107], cyclopentanes[108], dihydropyrans[109], tetrahydropyrroles[110] and [3.3.0]bicycles[52]. These central cores do not interact directly with the enzyme at all. They merely project functionalities outward from themselves to four sub-pockets of the neuraminidase active sites.

Both zanamivir and oseltamivir (two of three commercially available viral neuraminidase inhibitors) benefit from the presence of an alkene in the cyclic core to mimic the skew-boat shaped Michaelis complex[104-105]. The dramatic difference of the IC_{50} value between two of them and the benzoic acid-based neuraminidase inhibitors (**Figure 37**) indicate the importance of the native conformation of the ring scaffold. In the case of the most potent commercially available viral neuraminidase inhibitor—peramivir—it still needs to endure a small amount of conformational switch (about 4.5 kJ/mol) between its free solution state and its enzyme-bound state[111]. Wulff and co-workers were

intrigued by this fact and designed a rigid sulfone-based bicyclic viral neuraminidase inhibitor to mimic the conformation of enzyme-bound peramivir. The 3-site inhibitor **97** was superior to analogous monocyclic 3-site inhibitors, but unfortunately it proved difficult to install the fourth substituent necessary for optimal potency.

5.1.1.3. Existing studies for probing the selectivity towards the 150-cavity of viral neuraminidase

The discovery of the 150-cavity encouraged many groups to design novel group-1 specific neuraminidase inhibitors which could be used against the potential pandemic threat posed by avian influenza virus H5N1 and swine flu virus H1N1[59a,112].

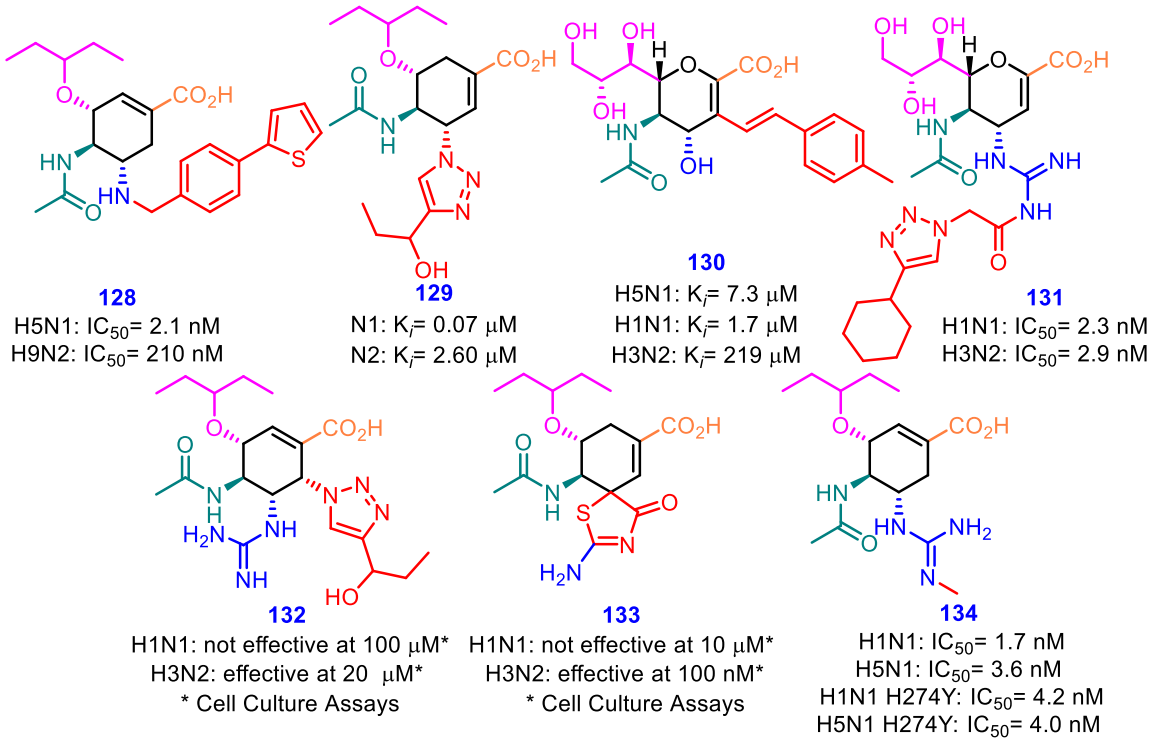

Figure 38: Summary of representative existing compounds targeting the 150-cavity (red colour indicates the additional function groups that were designed to interact with the 150-cavity).

In most of these cases, researchers have taken advantage of the existing inhibitors as templates and attach additional functional groups onto them to probe the 150-cavity. Iso-oseltamivir, oseltamivir and zanamivir have all been studied as scaffolds for this purpose. In the cases of compounds **128**, **129** and **130**, after fine tunings of the size, shape and hydrophobicity of additional groups, the resulting compounds were all found to have certain levels of selectivity between two groups of neuraminidases[112b,d,f,g]. However, compounds **131, 132**, **133** and **134** did not show any selectivity for group 1 over group 2 neuraminidase as shown in **Figure 38**[59a,112c,e].

5.1.2. Human neuraminidase

In addition to viral neuraminidase, human and bacterial neuraminidase also have been considered as a novel target for different diseases, such as cancer,[113] bacterial infections by streptococcus penumoniae,[90] cholera,[89] *etc.* Currently, human neuraminidases can be further divided into NEU1, NEU2, NEU3, and NEU4. The overall amino acid identity of NEU1 to the others neuraminidase is relatively low (19-24%), while NEU2, NEU3 and NEU4 exhibit approximately 34-40% homology to each other[88]. These isoenzymes exhibit in a diverse range of physiological functions within cells. Lysosomal sialidase, NEU1, is found primarily in the lysosome and plasma membrane and is generally accepted as a target gene for sialidosis. It also shows a narrow substrate specificity with oligosaccharides and glycopeptides in *in vitro* sialidase activity assays[114]. By contrast, NEU2 and NEU4 are able to hydrolyze glycoproteins and gangliosides[88]. The plasma sialidase, NEU3, hydrolyzes gangliosides almost exclusively. Notably, a high expression of NEU3 in some cancer cells has been reported[115]. The specific functions and locations of each of the four human neuraminidases are summarized in **Table 9**[114].

Table 9: A summary of the major locations and functions of the four human neuraminidases.

Neuraminidase	Locations	Functions	Major Substrates
NEU1	Lysosome	Muscle differentiation, Immune function, Lysosomal catabolism, Exocytosis, Phagocytosis, Elastogenesis	Oligosaccharides, Glycopeptides
NEU2	Cytosol	Myoblast differentiation, Neural differentiation	Glycoproteins, Gangliosides
NEU3	Plasma membrane	Apoptosis, Adhesion, Neuronal differentiation	Gangliosides
NEU4	Lysosomes, Mitochondria, Endoplasmic reticulum,	Apoptosis, Adhesion, Neuronal differentiation	Glycoproteins, Gangliosides

In terms of active sites, the neuraminidase enzymes are relatively similar across species. For instance, in human neuraminidase, there are several similar active site residues: a triad of arginine residues, a Tyr-Glu pair, and an Asp residue (**Figure 39**)[111]. However, most of the known viral neuraminidase inhibitors appear to have very weak activity against human NEU[116]. Also the complexity of the human NEU family has limited the design of selective inhibitors.

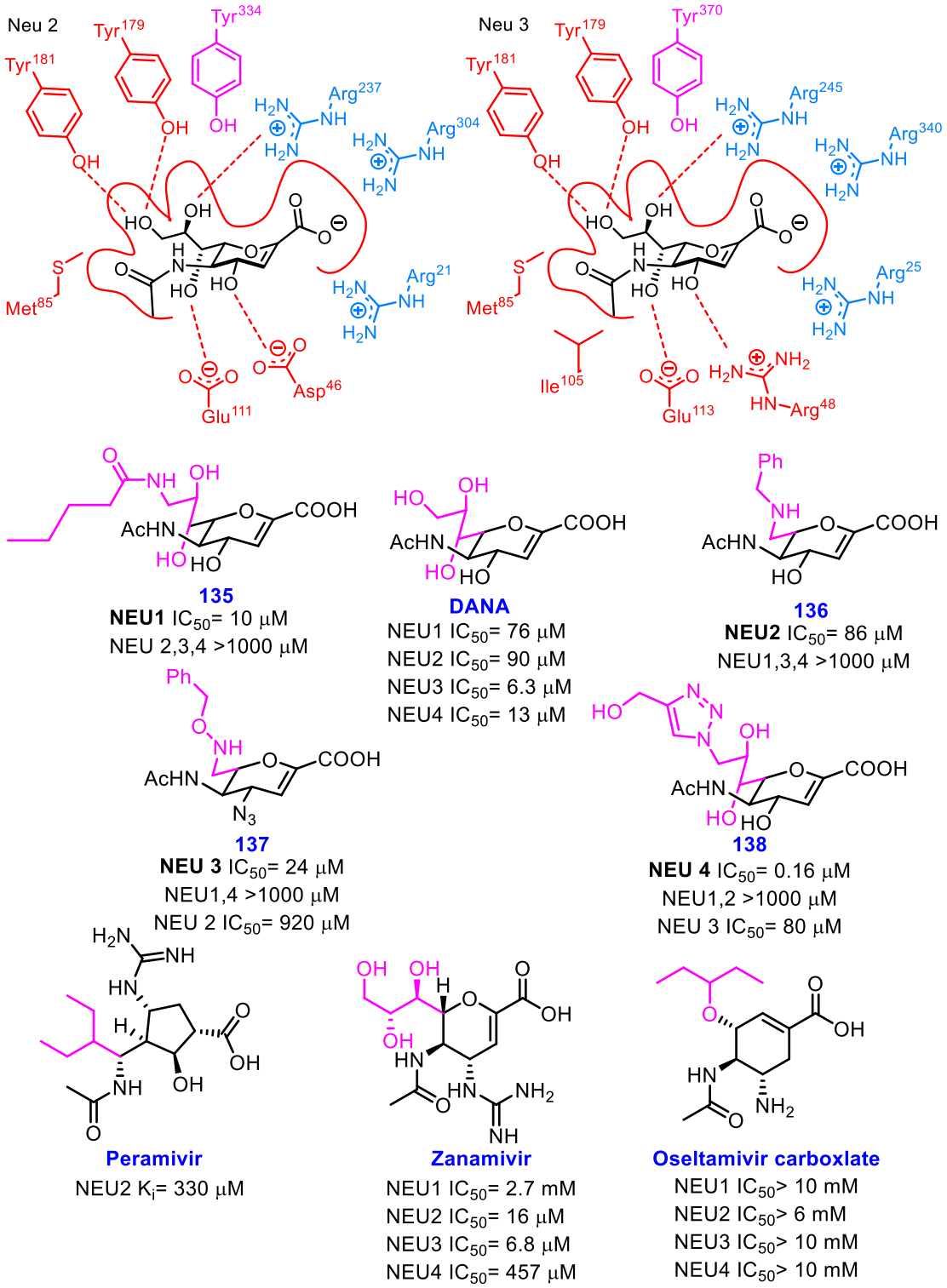

Figure 39: Binding site interactions of human neuraminidase Neu2 and Neu 3, and inhibitors for human neuraminidases.

Among all compounds displaying selectivity for NEU1, compounds that bear small alkyl or aryl groups for the **S4** pocket showed the best potency. Compound **135** (IC_{50} = 10 μM) showed a 100-

fold selectivity for NEU1 over NEU3[117d], while DANA has a 12-fold selectivity for NEU3 over NEU1[117b]. That might suggest that the selectivity amongst all 4 isoenzymes can be achieved by controlling the hydrophobicity of the side chain for **S4** pocket. Indeed, the Cairo group also identified inhibitors **136** and **137** that display up to 38-fold selectivity for NEU3 and 12-fold selectivity for NEU2 over all other isoenzymes. The most potent and selective inhibitor for NEU4 is a triazole derivative **138** of DANA which has a 500-fold selectivity for NEU4 over the other human neuraminidases.

5.2.0. Our goals

One of our long-term goals is utilizing Thiele's ester as the bicyclic core of a conformationally constrained neuraminidase inhibitor to mimic the enzyme-bound peramivir. The enhanced rigidity of the resulting compound could reduce the range of vectors across which dependant functional groups project, which would maximize the target specificity of our inhibitors. However, unlike DANA, iso-oseltamivir, oseltamivir and zanamivir, peramivir has not yet been studied as a ring scaffold towards probing the target selectivity in viral or human neuraminidases. In order to design a Thiele's ester-based conformationally constrained inhibitor that has improved target specificities, we first need to better understand the structure activity relationships of the parent compound—peramivir—towards different strains of viral or human neuraminidases.

Firstly, in an attempt to establish the selectivity between two groups of viral neuraminidases, we hypothesized that the hydrophobic 150-cavity of the group 1 viral neuraminidase can be accommodated by extending various aromatic rings or alkyl chains from the primary amine of de-guanidinylated peramivir. In addition to this, due to the fact that the catalytic site of neuraminidases contains an abundance of polar amino acid residues, all the three commercially available neuraminidase inhibitors were designed to have very high polarities. The high polarity of these compounds was thought to be the primary reasons for low oral absorption, hence these additional lipophilic groups should reduce the overall polarity and significantly improve the oral bioavailability of these peramivir analogues.

Secondly, although the three most widely used commercial neuraminidase inhibitors (zanamivir, oseltamivir, and peramivir) in the treatment of influenza have brought us huge benefits, they are still limited by multiple significant drawbacks. Oseltamivir is ineffective against mutation induced resistance (owing to the iso-pentane group). Fortunately, zanamivir is less susceptible to the H274Y mutation, but it has poor bioavailability (due to the polarity of the triol side chain and guanidinyl group). Meanwhile peramivir suffers from both drawbacks. We hypothesized that we can optimize the side chain for the S4 pocket (by finding the balance between polar alcohol groups and lipophilic alkyl chains) as well as a functional group (such as free amine/guanidine or substituted amine/ guanidine) for the S2 pocket to a series of hybrid neuraminidase inhibitors **140-143** (**Figure 40**).

These improved inhibitors which can inherit high potency (from peramivir), oral bioavailability (from oseltamivir), and a low susceptibility for mutation induced resistance (from zanamivir) is one of our synthetic goals.

Last but not the least, based on the pioneering work from the Cairo group, they found that the side chain for the S4 pocket plays a crucial role in targeting selectivity between 4 human neuraminidases. By manipulating the functionalities on this side chain, they achieved a good level of target specificity against human neuraminidases. Therefore, we hypothesized that the additional functionality (*e.g.* primary alcohol) from the side chains of our hybrid neuraminidase inhibitors can be further modified to those functional groups that already showed their impacts on the target specificity against human neuraminidases. These resulting peramivir-based analogues can be compared with those DANA analogues (from the Cario group) to evaluate the influence of different central ring scaffolds towards potency and target specificity against human neuraminidases.

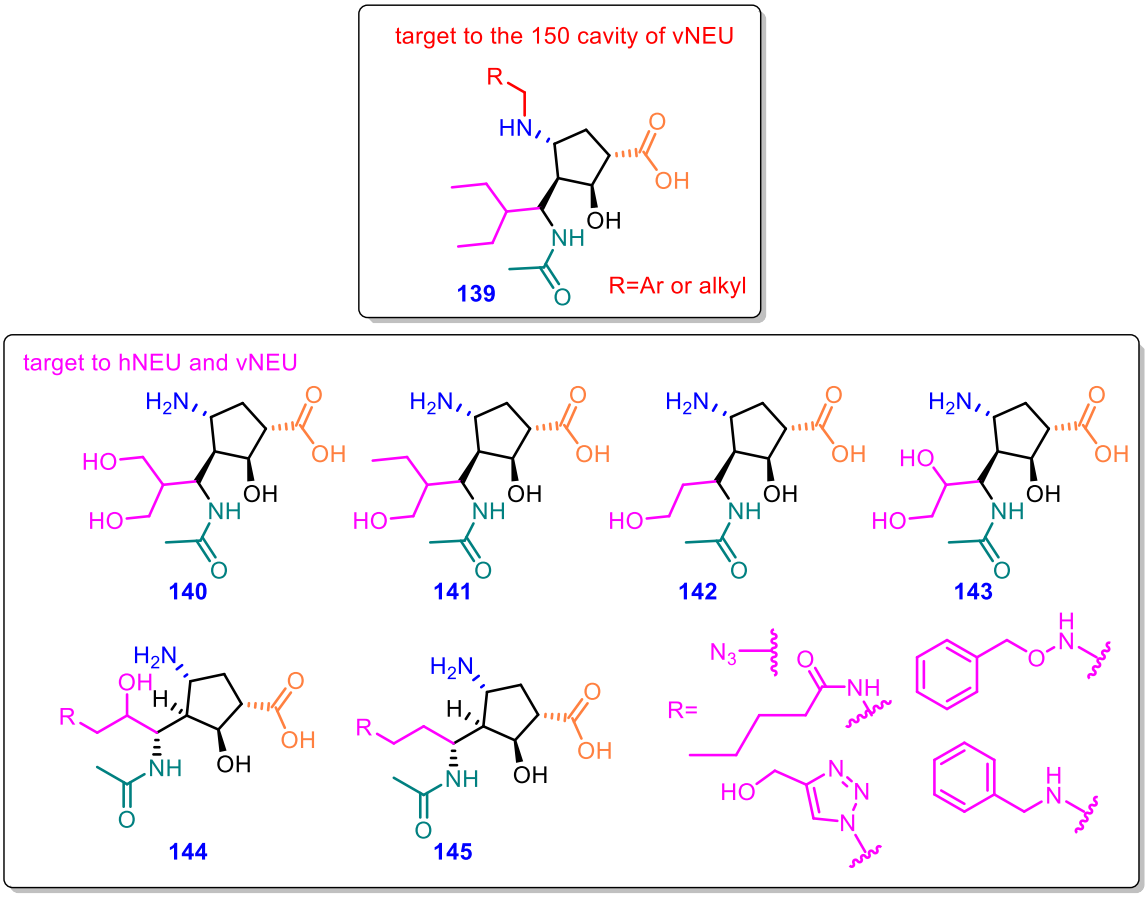

Figure 40: Proposed viral and human neuraminidase inhibitor library.

After utilizing the 5-membered central ring scaffold of peramivir to probe the target specificity towards both viral and human neuraminidase, we would apply the knowledge that we learn from our activity-based probes toward the design of a Thiele's ester based bicyclic inhibitors scaffold.

The ultimate goal would be to employ this scaffold in the creation of novel inhibitors with specificity to both viral and human neuraminidase targets.

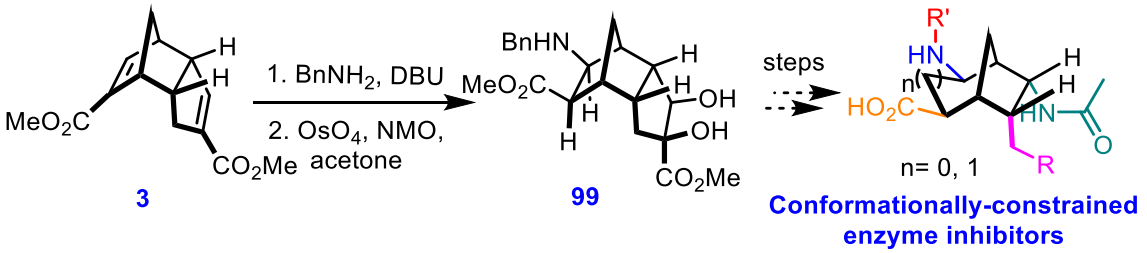

Scheme 38: Synthetic scheme leading to the production of conformationally-constrained neuraminidase inhibitors.

5.3.0. Synthesis of *N*-substituted de-guanidinylated peramivir analogues

The synthesis of de-guanidinylated peramivir was carried out according to the literature procedure for peramivir, but omitting the final guanidinylation steps[118,108]. The precursors for [3+2] dipolar cycloaddtion, oxime **147** and cyclopentene **14**, were prepared from commercially available aldehyde **146** and (1*S*,4*R*)-2-azabicyclo[2.2.1]hept-5-en-3-one **148** respectively**.** Due to the highly reactive nitrile oxide intermediate (which gives unwanted dimerization or rearrangement to isocyanates), the reaction was carried out with a slow addition of **147** to give the desired compound **150**. This isoxazoline ring was then subjected to hydrogenolysis in MeOH containing PtO_2. Subsequent acetylation and deprotection furnished precursor **151** to the key intermediate product **152**. A wide range of alkyl chains and aromatic rings were then installed on the primary amine *via* reductive amination. After subsequent hydrolysis, the resulting compounds **153** were purified by LCMS to provide us a handful *N*-substituted de-guanidinylated peramivir analogues as our screening library to study the structure activity relationship towards the 150-cavity of viral neuraminidase (**Scheme 39**).

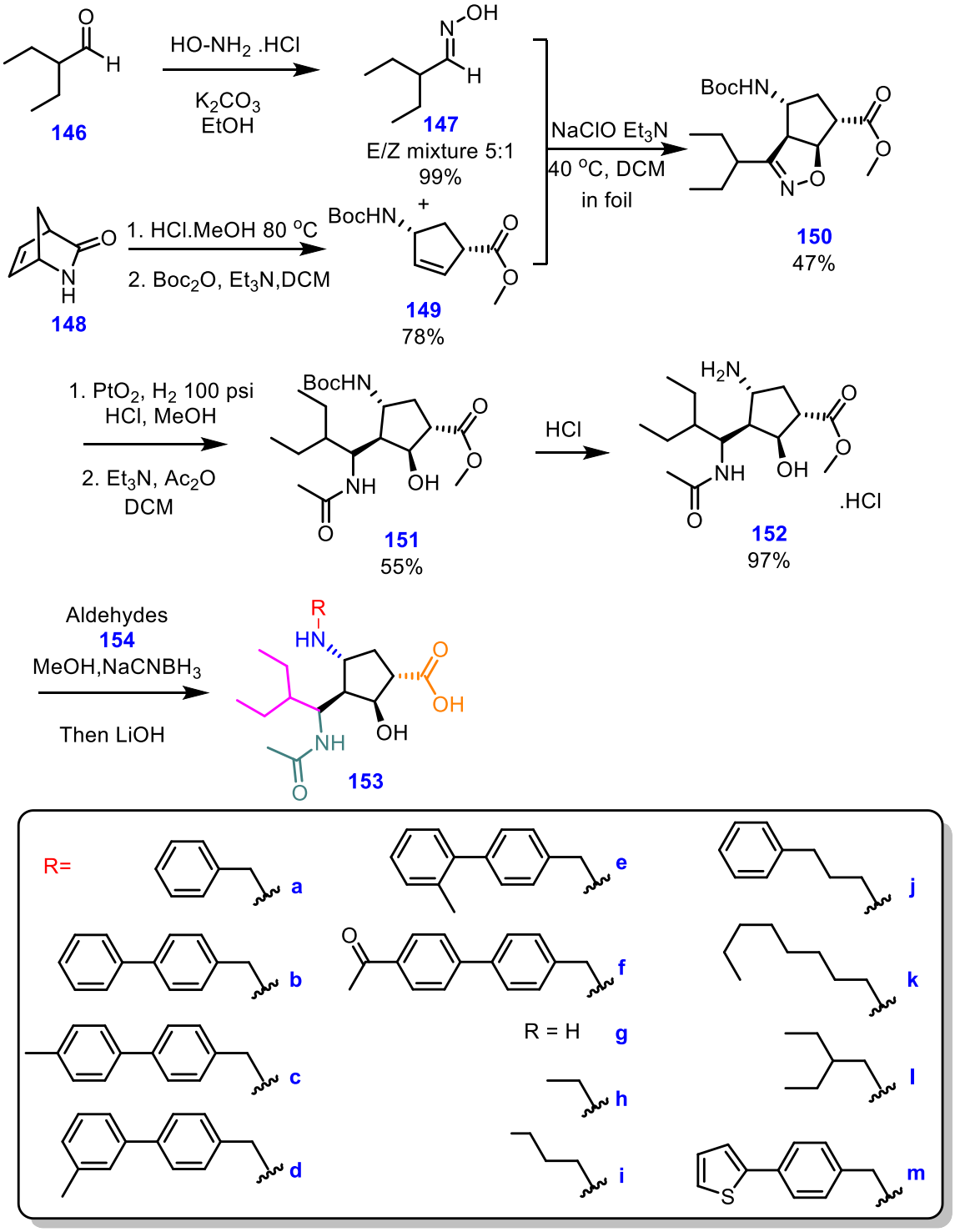

Scheme 39: Synthesis of *N*-substituted de-guanidinylated peramivir analogues.

5.4.0. Biological activity

In order to determine the selectivity of **153a-m** against two groups of viral neuraminidases, we made use of a standard literature protocol involving the enzymatic cleavage reaction of 2'-4-(methylumbelliferyl)-Neu5Ac with two types of viral neuraminidases. The product of the enzymatic cleavage is the fluorescent 4-methylumbelliferyl anion. By monitoring the rate of emission of the cleavage product over time with varying concentrations of inhibitor present, the percent inhibition for each specific concentration of inhibitor was determined by dividing the rate (slope, measured in fluorescent units per second) by the blank (uninhibited reaction). The IC_{50} (half maximal inhibitory concentration) of **153a-m** against the neuraminidase enzyme was determined through fitting the triplicate measurements of percent inhibition versus the concentration of the inhibitor to a sigmoidal model.

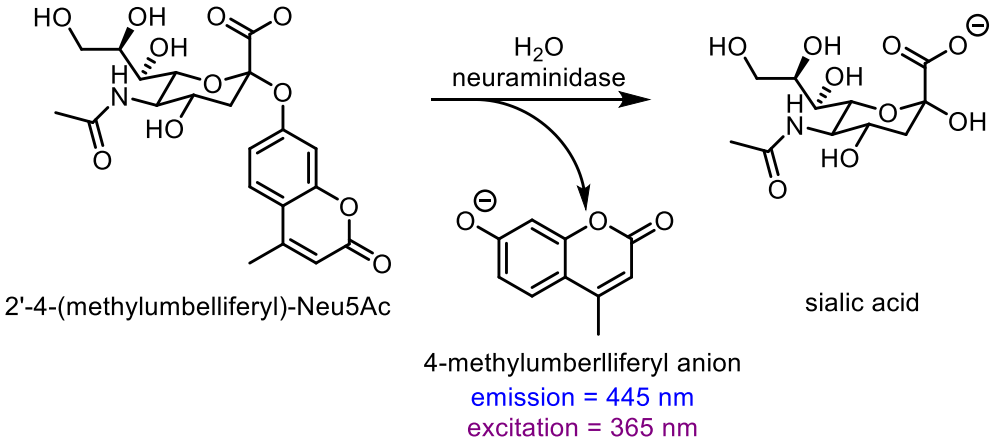

Scheme 40: Action of neuraminidase on the fluorescent substrate.

Influenza A virus H1N1 (A/California/04/2009) and H3N2 (A/Babol/36/2005) were the representatives of group-1 and group-2 neuraminidase for the inhibition assays. As shown in **Table 10**, peramivir was found to be more potent against N1, which is consistent with the literature data[119]. Although the IC_{50} of **153g** (3.14 nM) was found to have a similar value as our early reported data against H1N1 (A/Brisbane/59/2007) (IC_{50} = 7 nM)[120], compound **153g** did show an even stronger potency against H3N2. In an attempt to probe the selectivity towards 150-cavity, additional functional groups such as aromatic rings, alkyl chains with different length and substitution patterns were synthesized. All the compounds were tested in the neuraminidase assays with the exception of compound **153d** and **153f**, which were insoluble in the required buffer. Among all the compounds that we tested, none of them showed selectivity against H1N1. This might due to the different ring geometry between peramivir and oseltamivir/zanamivir. As shown in **Figure 41**, due to the similarity of their six-membered ring scaffolds, both enzyme-bound conformations of oseltamivir and zanamivir are highly overlapped. The amine group (from oseltamivir) and guanidine group (from zanamivir) are projected from the central core at a very similar degree. However, in the case of peramivir *vs* zanamivir/oseltamivir, we can see that the guanidine group (from peramivir) is

vectored in a significantly different fashion. In addition, in Amaro and co-workers' paper, they suggest that a key salt bridge (between Asp147 and His150) is crucial in controlling the formation of the 150-cavity across both subtypes[121]. It is likely that this ionic contact locks Ile149 in the space of the 150-cavity. In fact, the loss of Asp147-His150 salt bridge allows the 150-loop to move to the open position. From our data, we can see that other than compound **153k** which bears a long octyl side chain (which perhaps does not fit into the 150-cavity at all), the rest of the compounds all showed hundred nanomolar-range IC_{50} values. Furthermore, all of our de-guanidinylated peramivir analogues demonstrated selectivities (2.1 to 6.6 fold) against the group-2 neuraminidase over the group-1 neuraminidase. This surprising inverse selectivity was not seen with peramivir itself. This perhaps can be attributed to the stronger interactions between more basic guanidine (from peramivir) and amino acid residues (Asp147-His150) that may lock the 150-loop to its closed position. The observed target specificities against the group-2 neuraminidases suggest that these novel analogues may actually allow the 150-loop of H3N2 to have an even more opened conformation than the one of H1N1.

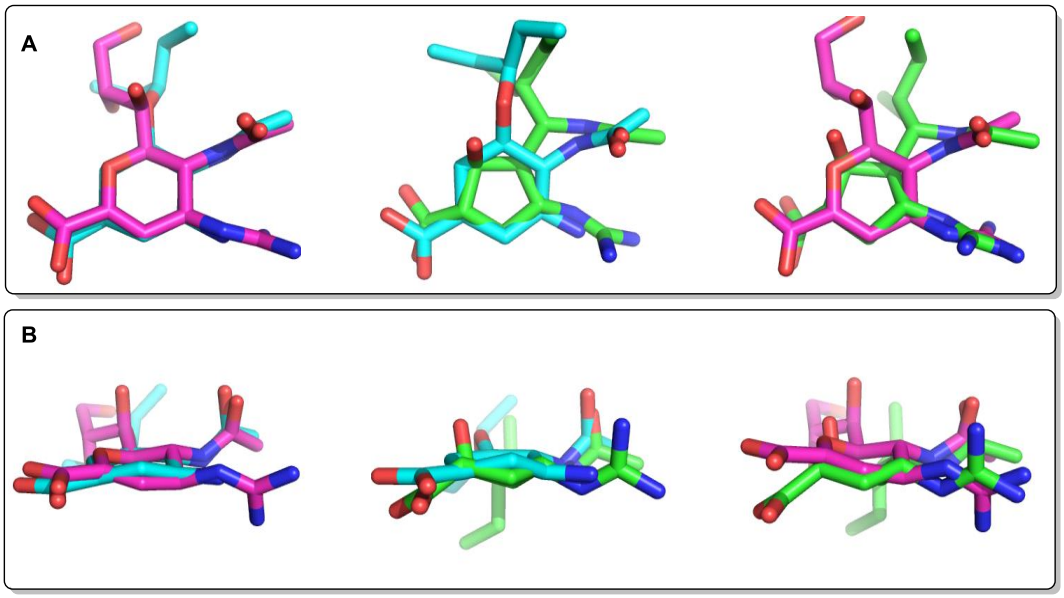

Figure 41: Structural comparisons between peramivir (green), oseltamivir (cyan) and zanamivir (pink). A: top views. B: side views. All substrates are shown in their enzyme-bound conformations.

Regardless of the target selectivity, most of these compounds still remained good nanomolar-range IC_{50} values. With the additional lipophilic groups on the ring, we hypothesize these compounds can improve the poor oral bioavailability of the parent compound (peramivir). In future work, parallel artificial membrane permeability assays will be run against the collected compounds to evaluate the permeability of these peramivir analogues.

Table 10: Inhibitory activities against H1N1 and H3N2 viral neuraminidases.

neuraminidase inhibition, IC_{50} (nM)

Entry	H1N1	H3N2	ratio N1:N2	Entry	H1N1	H3N2	ratio N1:N2
a	576 ± 60	216 ± 73	2.7	**g**	3.14 ± 0.79	0.95 ± 0.10	3.3
b	265 ± 66	126 ± 10	2.1	**h**	367 ± 77	56 ± 6.8	6.6
c	521 ± 84	146 ± 17	3.6	**i**	370 ± 78	109 ± 12	3.4
d	-*	-*		**j**	1674 ± 395	687 ± 114	2.4
e	795 ± 65	188 ± 16	4.2	**k**	>20000	>2300	
f	-*	-*		**l**	576 ± 60	216 ± 73	2.7
peramivir	0.17 ± 0.01	0.45 ± 0.03	0.38	**m**	533 ± 65	199 ± 59	2.7

* compounds are insoluble

While IC_{50} (half maximal inhibitory concentration) is commonly used as a measure of drug potency in inhibiting a specific biological function, it is not a direct indicator of the binding affinity of the inhibitor. The relationship between IC_{50} and K_i (dissociation constants) can be converted by using the Cheng-Prusoff equation (**3**), where [S] is fixed substrate concentration, K_m is the concentration of substrate at which enzyme activity is at half maximal and $[E]_0$ is the total enzyme concentration. However, in a tight binding condition where $[E]_0$ is significantly bigger then K_i, this equation will not be reliable.[122] Thus, K_i is a preferred method to report inhibition since it is independent of substrate concentration and thus is more comparable between different assays/experiments.

$$IC_{50} = K_i\,(1 + [S]/K_m) + [E]_0/2 \qquad (\mathbf{3})$$

The Morrison equation (**4**) describes the fractional velocity of an enzymatic reaction as a function of inhibitor concentration, at fixed concentrations of enzyme and substrate. The form of K_i^{app} depends of the inhibitor type. For competitive inhibitors, the Ki value can be achieved through curve fitting of equation (**5**) by plotting the K_i^{app} *versus* the concentration of inhibitor. However, as a more mathematical treatment, it is difficult to extract inhibitor constants from this complicated equation. In order to use it as a straightforward graphical method, Henderson presented the derivation of a linearized form of the Morrison equation. By plotting the fractional velocity as a function of inhibitors concentration at a fixed substrate concentration, the equation (**6**) will allow one to determine both K_i and [E] by the graphing software. The data could be fit to a straight line with the slope of the line equal to K_i^{app} and y intercept equal to [E].

$$\frac{v_i}{V_0} = 1 - \frac{([E]+[I]+K_i^{app}) - \sqrt{([E]+[I]+K_i^{app})^2 - 4[E][I]}}{2[E]} \quad (4)$$

$$K_i^{app} = K_i\,(1 + \frac{[I]}{K_m}) \quad (5)$$

$$\frac{[I]}{1-\frac{v_i}{V_0}} = K_i^{app}\left(\frac{V_0}{V_i}\right) + [E] \quad (6)$$

Unfortunately, due to the fact that this data treatment introduces some degree of systematic error, the data that we achieved from the method were not necessarily meaningful. The resulting [E] values were negative and the K_i^{app} values (1647 nM) were even bigger the IC_{50} (576 nM), which strongly indicated that these data are not reliable (**Figure 42**).

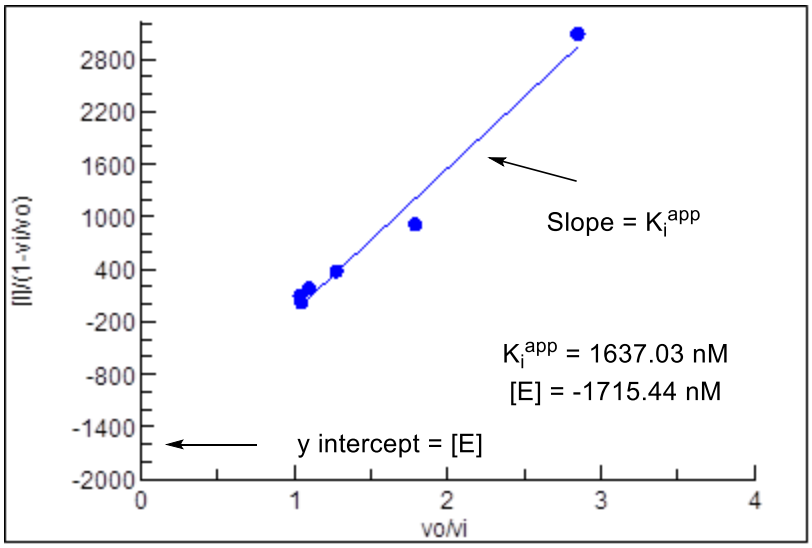

Figure 42 : Henderson plot for compound 153I against H1N1 neuraminidase

5.5.0. Concluding remarks

Our first attempt to synthesize *N*-substituted peramivir analogues successfully produced 12 compounds bearing alkyl chains or aromatic rings with different length and size. With a combination of the unique ring geometry (from the 5-membered ring scaffold of peramivir) and the weaker Asp147-His150 salt bridge (from the less basic amino group of de-guanidinylated peramivir analogues), we observed that our de-guanidinylated peramivir analogues showed a rare target specificity against the group-2 neuraminidases. This work indicated that the central ring scaffold of inhibitor as well as the strength of Asp147-His150 salt bridge between enzyme and inhibitor will likely present additional advances in the design of compounds that selectively target the 150-cavity. Moreover, most of these peramivir analogues still showed a nanomolar-range IC_{50} value against both N1 and N2 neuraminidases. The additional lyophilic groups may enhance the oral bioavailability relative to the parent agent.

Chapter Six: Context and Future Outlook

6.0.0. Overview

In this thesis, we described our contributions toward both Thiele's ester chemistry and the development of new neuraminidase inhibitors. The ultimate goal of this project is combining the knowledge that we learned from both the Thiele's ester chemistry and the peramivir analogues SAR study to develop a Thiele's ester based conformationally constrained bicyclic neuraminidase inhibitor for improved target specificity. While the works in this thesis have not yet reach this goal, they still provided us valuable lessons toward a Thiele-based neuraminidase inhibitor. Furthermore, during our exploration of the fundamental Thiele's ester chemistry, we expanded the applications of Thiele's ester to a wide range of research fields from biological to material.

6.1.0. Thiele's ester chemistry and applications

Building upon existing synthetic methods, we have optimized the synthesis of Thiele's methyl ester to an efficient and scalable methodology, including 5 novel Thiele's esters and ketones that incorporate synthetic handles for the attachment of additional functionality. In the study of the chemo- and regioselectivity in Thiele's ester chemistry, we found the C5−C6 alkene to be amenable to a variety of selective nucleophilic transformations, after which the C2−C3 alkene could be reacted with electrophiles. Conversely, the C2′ ester function was much more reactive than the C6′ ester, although the use of benzyl ester intermediates permits dual reactivity when desired. According to this selectivity study, we managed to design and synthesize a new suite of molecular scaffolds incorporating a broad range (from 123° to 176°) of cleft angles.

In addition to this, owing to our careful structural characterization for both minor regioisomers that arise during the formation of Thiele's ester, we were able to conclusively report for the first time that the traditional "acid first" and our "ester salt first" approach give the identical regiochemical outcomes. We compared two competing conceptual models for their ability to rationalize the selective formation of Thiele's ester and these two minor regioisomers. We found that radical stabilization arguments (based on Deslongchamps' seminal work) outperformed the classic frontier molecular orbital theory in terms of the regioselectivity of Thiele's ester dimerization. When this method was combined with simple steric arguments, we arrived at a general algorithm (summarized in **Chart 9**) to rationalize Thiele type dimerization. This new algorithm provided reliable predictions for all the known homo- and heterodimerizations in the literature as well as for our novel phosphine oxide containing Thiele acid analogues.

Last but not the least, in order to stimulate Thiele's ester chemistry in a diverse range of applications, we took advantage of our Thiele's ester methodology to achieve a mono ester-substituted dicyclopentadiene ("half" Thiele's ester) as the precursor of a novel functionalized polydicyclopentadiene ROMP polymer. The resulting *f*PDCPD has the highest glass-transition temperature reported for a polydicyclopentadiene and allows for the facile manipulation of the surface chemistry through alteration of the embedded functional group.

6.2.0. Neuraminidase inhibitors

The synthesis of a series of *N*-substituted de-guanidinylated peramivir analogues was accomplished. In an attempt to probe selectivity towards group-1 neuraminidases, we coupled a wide range of alkyl chains and aromatic rings with different length and size on the primary amine of de-guanidinylated peramivir. We found that our analogues showed a rare target specificity against the group-2 neuraminidases instead of the group-1 neuraminidases, which might due to the ring geometry of peramivir as well as the reduced electrostatic interaction between the amino group (from our analogues) and the Asp147-His150 (from the enzyme). This suggested that it is possible to allow the group-2 neuraminidases to have a more open 150-cavity state than the group-1 neuraminidases. Plus, the respectable IC_{50} value of these significantly less polar compounds may also efficiently enhance their bio-availability, relative to peramivir itself.

6.3.0. Future outlook

Proposed future directions can be grouped into two main categories.

6.3.1. Applications of Thiele's esters

As described in the earlier discussion at potential applications for Thiele's acid and ester (in Chapter 1), we can envision expanding the utility of Thiele's esters in multiple areas, as shown in **Figure 43**.

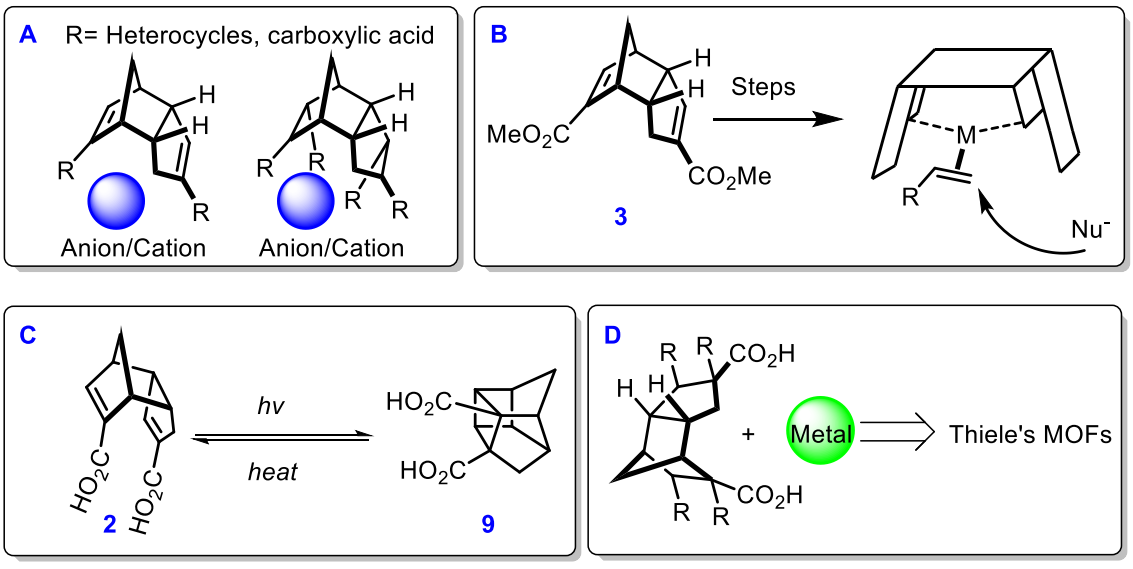

Figure 43: A: Thiele's acid-based anion/cation binders, B: Thiele's ester analogues as ligands in asymmetric synthesis, C: Photo-thermal controllable tweezers-like molecular machine, D: Thiele's acid derivatives as organic linkers towards Thiele's MOFs.

Furthermore, the molecular clefts that we developed can be easily converted to their corresponding amino acid congeners, which can be viewed as rigid templates with a broad range of cleft angles for the preparation of ß-hairpin peptidomimetics. In addition, the extraordinary reliability of our

radical stabilization algorithm for predicting the regiochemical outcomes of Thiele's type dimerizations encourages us to intentionally design more Thiele's type hetero-dimers, which might also lead to more interesting tricyclic scaffolds with different substitution partners.

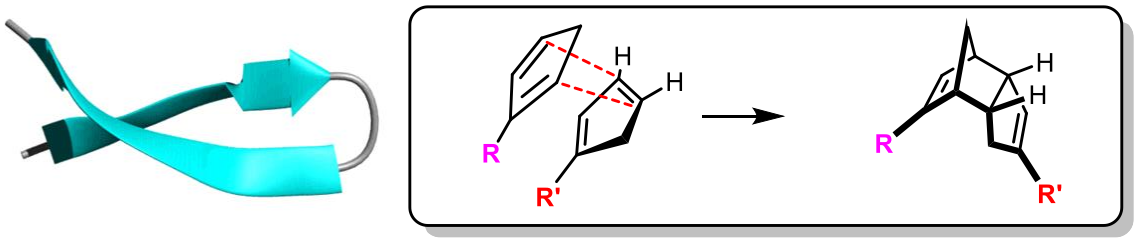

Figure 44: Thiele's ester analogues as templates for the preparation of ß-hairpin peptidomimetics and predictable Thiele's type hetero-dimerzation.

Regarding the *f*PDCPD, there are more unrevealed potentials behind this relatively new material. Firstly, we are interested in conducting more mechanistic studies to support our proposed structure of the crosslinked material as polymer **125**. Once a conclusive structure of our crosslinked polymer has been established, a wide range of strategies (either at the post-crosslinking or pre-crosslink stage) could be designed to create a chemically recyclable polymer. Secondly, with the chemical tunability of our *f*PDCPD, we anticipate that more functional groups other than methyl ester would be introduced to diversify the *f*PDCPD family. The resulting *f*PDCPD polymers would certainly have different physical and chemical properties, which could even open more research avenues. Currently, Dr. Tyler Cuthbert and Tong Li (in the Wulff group) are using solid state NMR, IR and Raman spectroscopy to study the structures of our crosslinked polymer and a pair of deuterated derivatives. In addition to these, more functional groups (such as, octyl, perfluorooctyl, adamantyl and triethylene glycol groups etc.) have been installed on our polymers. Both chemical and physical properties of these novel *f*PDCPDs will be tested by the Wulff group polymer team as well.

6.3.2. Peramivir analogues

As described in Chapter 5, we are also interested in using peramivir as the central ring scaffold to study the target selectivity between 4 human neuraminidases. Due to the fact that inhibitors with more polar side chains for the S4 pocket generally exhibit stronger potencies against human neuraminidase, we hypothesize those peramivir analogues with more polar side chains for the S4 pocket can be viewed as interesting synthetic targets. These polar side chains can be even further optimized to other functional groups that already showed their impacts for the target specificity against human neuraminidases.

After utilizing the 5-membered central ring scaffold of peramivir to probe the target specificity towards both viral and human neuraminidase, we would apply the lessons that we learn from our simple monocyclic analogues towards the design of a Thiele's ester based bicyclic inhibitor

scaffold. The ultimate goal would be to employ this scaffold in the creation of novel inhibitors with specificity to both viral and human neuraminidase targets.

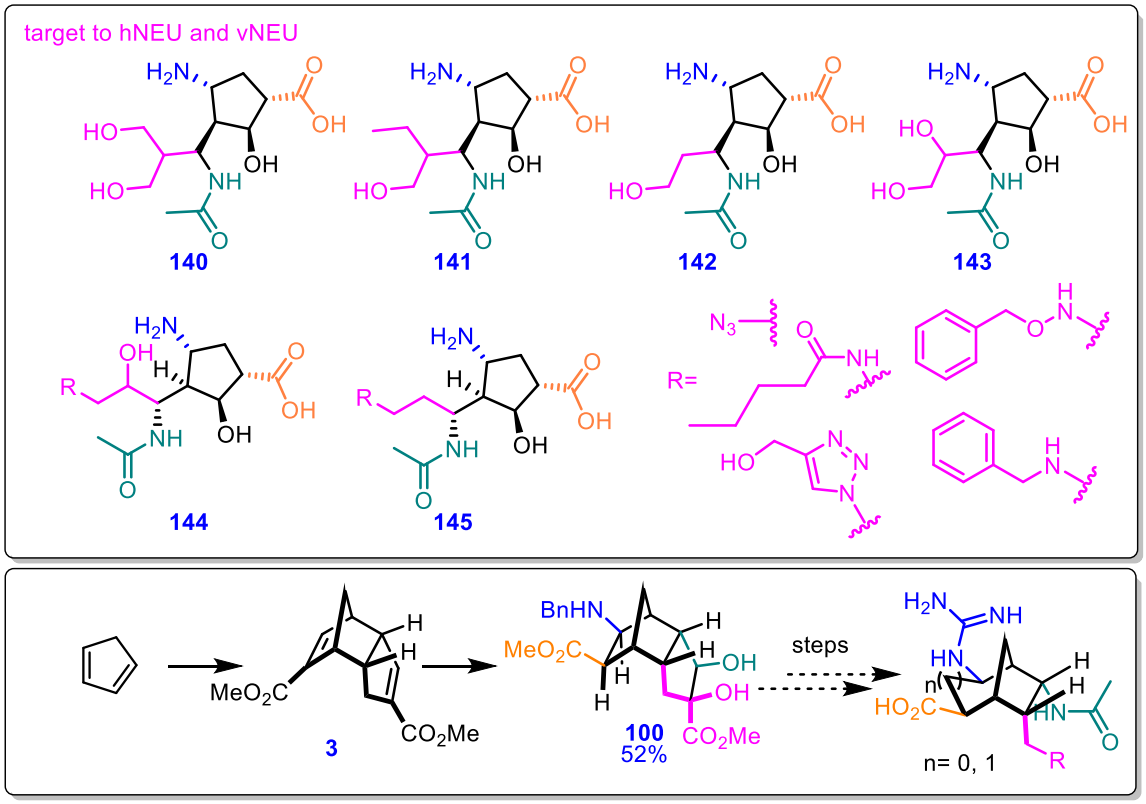

Figure 45: Proposed activity-based probes and synthetic scheme leading to the production of a new bicyclic neuraminidase inhibitor.

Chapter Seven: Experimental Section

General Methods. All reactions were performed in single-neck, flame-dried, round-bottom flasks fitted with rubber septa under a positive pressure of argon, unless otherwise noted. Liquid reagents were transferred via glass microsyringe. Solvents were transferred via syringe with a stainless-steel needle. Organic solutions were concentrated at 40 °C by rotary evaporation under vacuum. Analytical thin-layer chromatography (TLC) was performed using aluminum plates pre-coated with silica gel (0.20 mm, 60 Å pore-size, 230-400 mesh, Macherey-Nagel) impregnated with a fluorescent indicator (254 nm). TLC plates were visualized by exposure to ultraviolet light. Flash-column chromatography was performed over silica gel 60 (63-200 µM, Caledon) and silica gel (60 Å, 40-63 µM, SiliaFlash® F60).

Commercial solvents and reagents were used as received with the following exceptions. Tetrahydrofuran was dried by distillation over sodium and benzophenone. Dichloromethane was dried by passage through alumina in a commercial solvent purification system (SPS).

Proton nuclear magnetic resonance spectra (^{1}H NMR) were recorded at 300 MHz or 500 MHz at ambient temperature. Proton chemical shifts are expressed in parts per million (ppm, δ scale) downfield from tetramethylsilane, and are referenced to residual protium in the NMR solvent ($CDCl_3$, δ 7.26; D_2O, δ 4.79; DMSO-d_6, δ 2.50; MeOD, δ 3.31; acetone-d_6, δ 2.05). Data are represented as follows: chemical shift, multiplicity (s = singlet; d = doublet; t = triplet; dd = doublet of doublets, dt = doublet of triplets, ddd = doublet of doublet of doublets, ddt = doublet of doublet triplets, td = triplet of doublets, m = multiplet, br = broad)), coupling constant in Hertz, and integration. Carbon nuclear magnetic resonance spectra (^{13}C NMR) were recorded at 75 MHz or 125 MHz at ambient temperature. Carbon chemical shifts are reported in parts per million downfield from tetramethylsilane and are referenced to the carbon resonances of the solvent ($CDCl_3$, δ 77.16; DMSO-d_6, δ 39.52; MeOD, δ 49.00; acetone-d_6, δ 29.84). Phosphorus nuclear magnetic resonance spectra (^{31}P NMR) were recorded at 202 MHz at ambient temperature, and are uncalibrated. Infrared (IR) spectra were obtained using an FT-IR spectrometer referenced to a polystyrene standard. Accurate masses were obtained using an ion trap MS. Melting points were obtained using a Mel-Temp II apparatus, and are uncorrected.

Contact angles were obtained with a Holmarc contact angle meter (HO-IAD-CAM-01). The polar liquid was deionized water. The dispersive liquid was diiodomethane. DSC and TGA measurements were conducted on a TA Instruments Q600 SDT simultaneous thermal analyzer with samples being placed in aluminum oxide crucible, referenced against an empty aluminum oxide crucible. Data was collected with a ramp rate of 5 °C/min following temperature equalization at 50 °C under a nitrogen atmosphere flowing at 100 mL/min. For spin casting of polymer films a Best Tools, LLC model SC110-B Spin Coater was used. Atomic force microscopy (AFM)

measurements of the glass coverslips were performed on an Agilent Technologies 5500 Scanning Probe Microscope equipped with a Ted Pella TAP190-G AFM probe operating in tapping mode.

All GPC measurements were performed using a Viscotek Model 302 liquid chromatography system (Visckotek GPCmax + TDA 302 triple detector array) equipped with refractive index (RI), low angle light scattering (LALS, θ=7°), right-angle light scattering (RALS, θ = 90°). THF was used as the mobile phase at a flow rate of 1 mL/min, and the column temperature was set at 35 °C. All polymer solutions were filtered through membrane filters with a nominal pore size of 0.45 µm prior to injection into the GPC columns. The data was collected and analyzed using appropriate GPC software from Viscotek. The System was installed with a Tosoh Biosciences, LLC TSKgel H_{HR} series guard and two separation columns in series; specifically, H_{HR}-H guard column and G3000H_{HR} and GMH_{HR}-M columns respectively. Molecular weights were calculated from GPC data using an algorithm from Viscotek.

Dynamic light scattering (DLS) measurements were collected on a Brookhaven Instruments BI-200SM goniometer equipped with a BI-9000AT digital autocorrelator and a Brookhaven Instruments Mini-L30 compact diode laser (637 nm) with a 30 mW output. Samples were diluted with filtered THF into thoroughly washed glass cells. Measurements were carried out in cylindrical glass cells, thereby simplyifying corrections for variations in refractive index. Cells were immersed in a vat of decaline to minimize light refraction. Triplicate measurements collected at 90° were analyzed through the use of the CONTIN analysis package from Brookhaven, which provides the hydrodynamic radius (R_g) calculated from the translational diffusion coefficient.[123]

Liquid chromatography–mass spectrometry (LCMS) purifications were performed on a Thermo Scientific UltiMate 3000. All reactions purified by reverse phase LCMS were performed on a 4.6 x 150 mm Eclipse X DB-C18 5 µL column.

All enzyme assays were conducted on a SpectraMax M5 plate reader using standard sensitivity settings.

General Procedure A. A flame-dried round bottom flask fitted with an oven-dried condensor was charged with sodium cyclopentadienylide solution (2 M in THF, 1.0 equiv). To this solution was added the desired electrophile in THF, at room temperature with stirring. The reaction mixture was heated to reflux for 6 h, then cooled to room temperature and concentrated *in vacuo*. The resulting solid was suspended in ether and collected by vacuum filtration. The collected solid was washed with ether until the washings became colorless and then dried *in vacuo* to give intermediate salt **6** as a tan-brown air sensitive solid. In a separate step, the partially-purified salt **6** (1 equiv) was

added to a fresh round bottom flask, where it was combined with *i*PrOH (to 0.33 M) and sulfuric acid (0.55 equiv) at room temperature with stirring. Acidification was marked by a brown to orange color change. The solution was heated to 50 °C overnight. The reaction mixture was concentrated *in vacuo* and the resulting oil was dissolved in toluene, and loaded onto a silica gel column. Elution with hexanes-ethyl acetate provided the desired Thiele's ester.

General Procedure B. A flame-dried round bottom flask fitted with an oven-dried condensor was charged with sodium cyclopentadienylide solution (2 M in THF, 1.0 equiv). To this solution was added the desired electrophile in THF, at room temperature with stirring. The reaction mixture was heated to reflux for 6 hours, then cooled to room temperature. The supernatant was transferred by cannula to a fresh round bottom flask, and concentrated *in vacuo*. To the resulting solid was added *i*PrOH (to 0.33 M) and sulfuric acid (0.55 equiv) at room temperature with stirring. Acidification was marked by a brown to orange color change. The solution was heated to 50 °C overnight. The reaction mixture was concentrated *in vacuo* and the resulting oil was dissolved in toluene, and loaded onto a silica gel column. Elution with hexanes-ethyl acetate provided the desired Thiele's ester.

General Procedure C. To a solution of **152** (0.05 M in MeOH) was added $NaCNBH_3$. Then, aldehydes (solution in 2 mL MeOH) was added to the reaction during an hour. The mixture was stirred at room temperature for another 4 h, then concentrated *in vacuo*. The resulting solid was dissolved to a solution (0.05 M in MeOH and water 1:1). The reaction mixture was stirred for an hour and concentrated in *vacuo*. The resulting solid was purified by LCMS to provide the desired **153.**

General Procedure for enzyme assays. The following solutions were prepared for the enzyme assays:

1. Assay Buffer: 50 mM tris(hydroxymethyl)aminomethane, 5 mM $CaCl_2$, 200 mM NaCl, pH 7.5.
2. Protein Stock Solution: inactivated virus suspension (or purchased enzyme) was diluted in Assay Buffer at 4 °C to obtain a concentration which, when used in the assays described below, gave a slope of approximately 2 (fluorescence units *vs.* time in seconds) in the absence of inhibitors.
3. Substrate Stock Solution: 2'-4(methylumbelliferyl)-α-D-*N*-acetylneuraminic acid was dissolved in DMSO to a concentration of 10 mM (working stock).
4. Substrate Working Solution: 20 μL of the substrate stock solution was diluted to 1000 μL with assay buffer, with a final concentration of 200 μM (2% DMSO).
5. Inhibitor Solutions: Inhibitors were diluted in assay buffer to provide a range of working concentrations. Peramivir were used as positive controls.

Sample wells of a black 96-well plate (Nunc, optical bottom) were charged with 40 μL of protein stock solution, followed by 10 μL of inhibitor solution. The samples were incubated at room temperature for two hours, after which 50 μL of substrate working solution was added (i.e. final substrate concentration = 100 μM). The samples were mixed briefly by pipetting, and fluorescence was monitored over 5 min (λ_{exc} = 365 nm; λ_{em} =445 nm). IC_{50} values were obtained by plotting percent inhibition against inhibitor concentration using XLfit (IDBS software) and identifying the concentration required to achieve 50% inhibition of enzymatic activity. Estimates of error for IC_{50} values were obtained by plotting the data from three separate experiments (each of which was done in triplicate) and determining the "goodness of fit" to a sigmoidal function.

Thermal crosslinking

An oven dried vial was charged with linear polymer under an argon atmosphere. The reaction was heated to 180°C overnight. A tough, insoluble material was obtained.

Spin casting and functionalization of polymers

Spin casting was performed on freshly cleaned, 18x18 mm glass coverslips. Cleaning was performed as follows: 10 min of sonication in chloroform and 10 minutes in methanol followed by overnight drying under vacuum. Polymer samples were dissolved to 4 wt% in DCM and a 50 μL droplet was dropped onto a coverslip spinning at 2000 rpm. Following deposition, the film was allowed to spin for 60 s to ensure the majority of solvent had been removed.

Linear polymer **124** was spin coated on pre-cleaned glass slides. These coated glass slides were kept in a 180 °C oven under vacuum overnight to give cross-linked polymer **125**. These polymer **125** coated slides were immersed in solution of methanolic NaOH (MeOH/NaOH =1:1)) under vacuum. After 8 h, the slides were washed with water and MeOH, dried at 70 °C oven under vacuum overnight. The resulting polymer **126** coated slides were acidified with 10% HCl solution under vacuum for 30 min. All the slides were then washed with water and MeOH, dried at 70 °C oven under vacuum overnight to give polymer **127** coated slides.

Slides half coated with polymer **125** and half with polymer **126** were prepared by suspending half of the polymer **125** coated slides in a solution of methanolic NaOH (MeOH/NaOH =1:1) for 8 h under vacuum. (Figure E1) The resulting slides were washed with water and MeOH, and then dried at 70 °C oven under vacuum overnight.

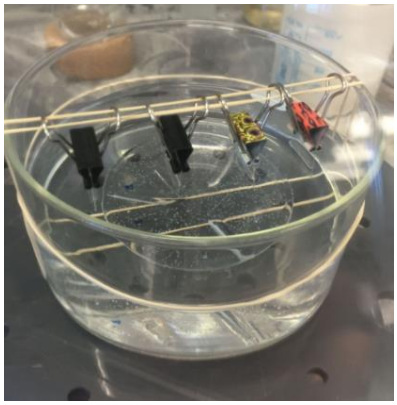

Figure E1 Preparation of slides half coated with polymer **125** and half with polymer **126**

Atomic force microscopy (AFM) measurements

Atomic force microscopy (AFM) measurements of the glass coverslips were performed on an Agilent Technologies 5500 Scanning Probe Microscope equipped with a Ted Pella TAP190-G AFM probe operating in tapping mode. In order to minimize vibrations, the microscope was covered in a vibration resistant case on a vibration isolation platform maintained at 80 psi. Each sample was imaged at 3 separate locations on the slide, surface roughness measurements being collected over a 10x10 µm area. Data was analyzed with the use of the Gwyddion data analysis software package. All images underwent slight modification to remove experimental artifacts such as sloped background, contrast alteration for ease of viewing – this was performed following measurements- and in some cases performing Fourier filtering of an unknown 10 Hz noise.

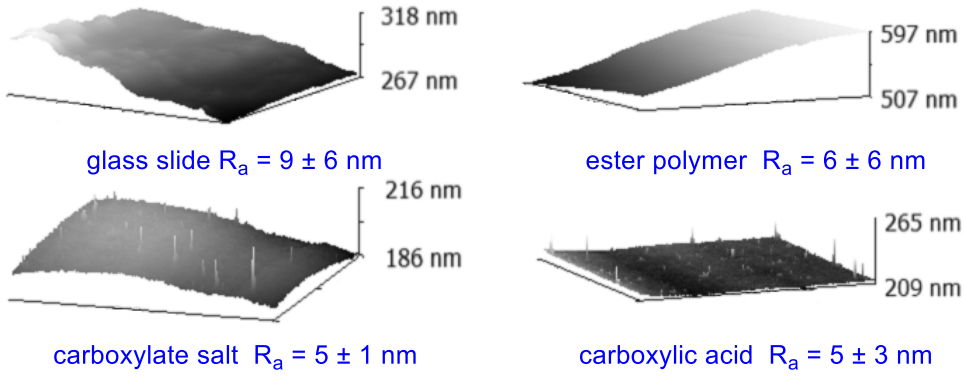

Figure E2 Average surface roughness of each polymer and glass slide by ATM

Contact angle measurement and surface tension

A drop of liquid (2 µL) was deposited on the freshly prepared substrate using a Hamilton microsyringe with a mechanical dispenser. Side view images of the drop on the substrate were taken by a high performance aberration corrected imaging lens with precise manual focus adjustment (CMOS sensor). Advancing contact angles were measured on these images. Two glass

chips were prepared for each substrate. Three drops of liquid were deposited at three different regions of each film. A mean contact angle and standard deviation were thus determined from the resulting measurements. (PDCPD was obtained from Product Rescue BVBA, Waarschoot, Belgium. It was polished with 400 grit sandpaper, then washed with water and MeOH, dried at 70 °C oven under vacuum overnight).

NMR data

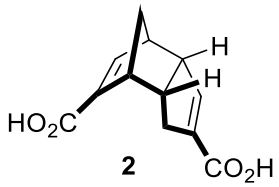

2

Compound **2**. To a solution of Thiele's ester **3** (270 mg, 1.1 mmol) in *i*PrOH (4 mL) was added KOH (10% solution, 4 mL) dropwise. After 5 h, *i*PrOH was removed *in vacuo*. The mixture was acidified to pH=1 by addition of HCl (2 M) and extracted twice with ethyl acetate. The combined organic layers were dried over $MgSO_4$ and concentrated *in vacuo* to afford Thiele's acid **3** as a white powder without further purification (184 mg, 76%; mp > 200 °C). ^{1}H NMR (300 MHz, D_2O) δ 6.60 (d, *J* = 3.1 Hz, 1H), 6.21 (q, *J* = 1.9 Hz, 1H), 3.39-3.48 (m, 1H), 3.13-3.20 (m, 1H), 3.04- 3.09 (m, 1H), 2.87-2.97 (m, 1H), 2.36 (ddt, *J* = 17.3, 10.5, 1.9 Hz, 1H), 1.88 (ddt, *J* = 17.3, 4.0, 2.0 Hz, 1H), 1.58 (dt, *J* = 8.4, 1.7 Hz, 1H), 1.36 (d, *J* = 8.4 Hz, 1H); ^{13}C NMR (75 MHz, D_2O) δ 174.7, 174.3, 143.8, 142.8, 139.6, 53.8, 50.3, 47.0, 46.9, 40.9, 34.0; IR (cm^{-1}, film) 2976, 2868, 1685, 1676, 1420, 1295, 1244, 949; HRMS (ESI) calcd for $[M+Na]^+$ $C_{12}H_{12}O_4Na$: 243.0628, found 243.0629.

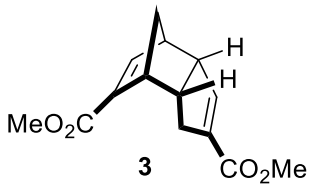

3

Compound **3**. Prepared according to general procedure A, using 20 mL sodium cyclopentadienylide (2 M in THF, 40 mmol), 16.8 mL dimethyl carbonate (100 mmol, in 20 mL THF), and 1.17 mL H_2SO_4 (22 mmol, in 120 mL *i*PrOH). Chromatography (hexanes-ethyl acetate, 20:1) afforded 3.18 g (65%) of **3** as a pale yellow solid (mp = 189-191 °C). ^{1}H NMR (300 MHz, $CDCl_3$) δ 6.83 (d, *J* = 3.1 Hz, 1H), 6.49 (q, *J* = 2.2 Hz ,1H), 3.71 (s, 3H), 3.65 (s, 3H), 3.44-3.52 (m, 1H), 3.32-3.37 (m, 1H), 3.10-3.14 (m, 1H), 2.91-3.01 (m, 1H), 2.47 (ddt, *J* = 17.9, 10.4, 2.0 Hz, 1H), 2.00 (ddt, *J* = 17.9, 4.0, 2.0 Hz, 1H), 1.67 (dt, *J* = 8.6, 1.7 Hz, 1H), 1.41 (dq, *J* = 8.8, 1.1 Hz, 1H); ^{13}C NMR (75 MHz, $CDCl_3$) δ 165.6, 165.4, 147.4, 142.8, 139.0, 138.1, 54.5, 51.6, 51.4, 51.0, 47.4, 46.8, 41.2, 33.1; IR (cm^{-1}, film) 2950, 1718, 1633, 1597, 1272, 1093, 765; HRMS (ESI) calcd for $[M+Na]^+$ $C_{14}H_{16}O_4Na$ 271.0941, found 271.0940.

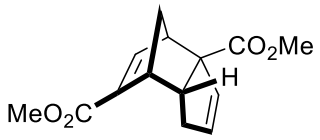

7a

Compound **7a**. Isolated as a yellow solid from the preparation of **3** described above (540 mg; 11% yield; mp = 73-77 °C). ^{1}H NMR (300 MHz, $CDCl_3$) δ 6.85 (dd, *J* = 3.2, 1.3 Hz ,1H), 5.56 (dt, *J* = 5.7, 2.4 Hz, 1H), 5.48 (dt, *J* = 5.7, 2.3 Hz, 1H), 3.71 (s, 3H), 3.70 (s, 3H), 3.30-3.35 (m, 2H), 3.21-3.28 (m, 1H), 2.40 (ddt, *J* = 18.3, 9.9, 2.2 Hz, 1H), 1.78 (dq, *J* = 18.3, 2.4 Hz, 1H), 1.65 (t, *J* = 1.5 Hz, 2H); ^{13}C NMR (75 MHz, $CDCl_3$) δ 175.8, 165.7, 147.9, 139.7, 134.9, 130.0, 70.3, 52.3, 51.6, 51.3, 49.1, 46.9, 46.0, 34.6; IR (cm^{-1}, film) 2954, 1733, 1717, 1653, 1559, 1436, 1272, 1089, 773; HRMS (ESI) calcd for $[M+Na]^+$ $C_{14}H_{16}O_4Na$ 271.0941, found 271.0941.

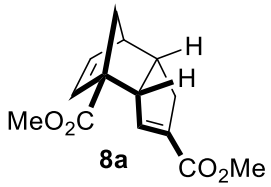

8a

Compound **8a**. Isolated as a white solid from the preparation of **3** described above (880 mg; 18% yield; mp = 98-102 °C). ^{1}H NMR (300 MHz, $CDCl_3$) δ 6.58 (q, *J* = 2.2 Hz ,1H), 6.09 (dd, *J* = 5.7, 2.7 Hz ,1H), 6.05 (d, *J* = 5.6, 2.7 Hz ,1H), 3.77 (s, 3H), 3.68 (s, 3H), 3.60-3.67 (m, 1H), 2.96-3.05 (m, 2H), 2.45 (ddt, *J* = 17.6, 9.9, 2.1 Hz, 1H), 1.94 (dtd, *J* = 17.6, 3.6, 2.0 Hz, 1H), 1.77 (dd, *J* = 8.3, 1.8 Hz, 1H), 1.67 (d, *J* = 8.2 Hz, 1H); ^{13}C NMR (75 MHz, $CDCl_3$) δ 174.4, 165.4, 142.2, 138.5, 134.6, 133.6, 61.2, 59.0, 53.5, 52, 51.5, 46.9, 42.7, 33.8; IR (cm^{-1}, film) 2955, 1734, 1718, 1653, 1559, 1275, 1096, 736; HRMS (ESI) calcd for $[M+Na]^+$ $C_{14}H_{16}O_4Na$ 271.0941 Found 271.0941.

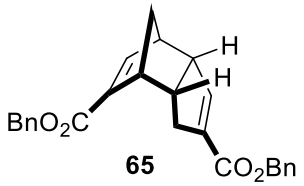

65

Compound **65**. Prepared according to general procedure B, using 2.5 mL sodium cyclopentadienylide (2 M in THF, 5 mmol), 1.83 g dibenzyl carbonate (7.5 mmol, in 5 mL THF), and 147 μL H_2SO_4 (2.75 mmol, in 15 mL *i*PrOH). Chromatography (hexanes-ethyl acetate, 5:1) afforded 540 mg (54%) of **65** as a yellow oil. ^{1}H NMR (300 MHz, $CDCl_3$) δ 7.37-7.27 (m, 10H), 6.90 (d, *J* = 3.1 Hz, 1H), 6.55 (q, *J* = 2.1 Hz ,1H), 5.15 (s, 2H), 5.06 (d, *J* = 12.7, 1H), 5.14 (d, *J* = 12.7, 1H), 3.46-3.54 (m, 1H), 3.36-3.41 (m,1H), 3.11-3.16 (m, 1H), 2.91-3.01 (m, 1H), 2.51 (ddt, *J* = 17.9, 10.4, 2.0 Hz, 1H), 2.10 (ddt, *J* = 17.9, 3.9, 2.1 Hz, 1H), 1.69 (dt, *J* = 8.8, 1.7 Hz, 1H), 1.41 (dq, *J* = 8.5, 0.9 Hz, 1H); ^{13}C NMR (75 MHz, $CDCl_3$) δ 165.0, 164.7, 148.0, 143.3, 138.9, 138.2, 136.5, 136.4, 128.6, 128.1, 128.0, 127.9, 66.1, 65.9, 54.5, 50.9, 47.5, 46.8, 41.2, 33.2; IR (cm^{-1}, film) 2944,

1708, 1454, 1268, 1231, 1074, 749; HRMS (ESI) calcd for $[M+H]^+$ $C_{26}H_{25}O_4$ 401.1748, found 401.1748.

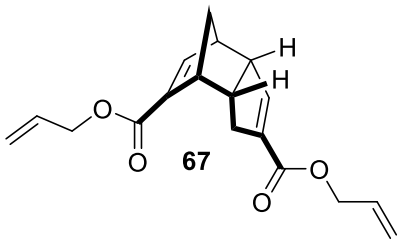

Compound **67**. Prepared according to general procedure A, from 2 mL sodium cyclopentadienylide (2 M in THF, 4 mmol), 580 µL diallyl carbonate (4 mmol, in 2 mL THF), and 117 µL H_2SO_4 (2.2 mmol, in 3 mL *i*PrOH). Chromatography (hexanes-ethyl acetate, 10:1) afforded 186 mg (31%) of **67** as a yellow oil. ^{1}H NMR (300 MHz, $CDCl_3$) δ 6.88 (d, *J* = 3.2 Hz, 1H), 6.54 (q, *J* = 2.2 Hz, 1H), 5.82-5.98 (m, 2H), 5.27 (dm, *J* = 17.3 Hz, 2H), 5.20 (dq, *J* = 10.4, 1.4 Hz, 2H), 4.60-4.65 (m, 2H), 4.54-4.59 (m, 2H), 3.46-3.54 (m, 1H), 3.36-3.40 (m, 1H), 3.11-3.17 (m, 1H), 2.91-3.02 (m, 1H), 2.50 (ddt, *J* = 17.9, 10.4, 2.0 Hz, 1H), 2.06 (dtd, *J* = 17.9, 4.1, 2.2 Hz, 1H), 1.69 (dt, *J* = 8.8, 1.8 Hz, 1H), 1.36 (dd, *J* = 8.8,1.0 Hz, 1H); ^{13}C NMR (75 MHz, $CDCl_3$) δ 164.8, 164.6, 147.8, 143.1, 139.0, 138.2, 132.6, 132.5, 117.9, 117.8, 65.0, 64.9, 54.5, 50.9, 47.5, 46.8, 41.2, 33.2; IR (cm^{-1}, film) 2939, 1717, 1701, 1268, 1231, 1087, 765; HRMS (ESI) calcd for $[M+Na]^+$ $C_{18}H_{20}O_4Na$ 323.1254, found 323.1254.

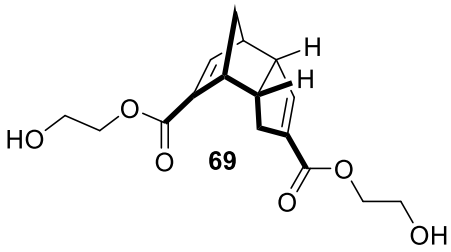

Compound **69**. Prepared according to general procedure A, from 5 mL sodium cyclopentadienylide (2 M in THF, 10 mmol), 890 mg ethylene carbonate (10 mmol, in 5 mL THF), and 293 µL H_2SO_4 (5.5 mmol, in 7 mL *i*PrOH). Chromatography (hexanes-ethyl acetate, 2:1) afforded 786 mg (51%) of **69** as a yellow oil. ^{1}H NMR (300 MHz, $CDCl_3$) δ 6.89 (d, *J* = 3.3 Hz, 1H), 6.54 (q, *J* = 2.1 Hz, 1H), 4.25-4.33 (m, 3H), 4.11 (ddd, *J* = 11.9, 4.8, 4.1 Hz, 1H), 3.77-3.84 (m, 4H), 3.49-3.56 (m, 1H), 3.37-3.41 (m, 1H), 3.15-3.20 (m, 1H), 2.91-3.01 (m, 1H), 2.61 (br, 2H), 2.48 (ddt, *J* = 17.9, 10.3, 2.0 Hz, 1H), 2.15 (dtd, *J* = 18.0, 3.9, 2.2 Hz, 1H), 1.68 (dt, *J* = 8.7, 1.8 Hz, 1H), 1.42 (dq, *J* = 8.5,0.9 Hz, 1H); ^{13}C NMR (75 MHz, $CDCl_3$) δ 165.7, 165.5, 148.5, 143.7, 138.3, 137.9, 66.2, 65.8, 61.6, 61.3, 54.3, 50.3, 47.5, 46.8, 41.0, 33.1; IR (cm^{-1}, film) 3416, 2943, 1707, 1630, 1272, 1235, 1068, 766; HRMS (ESI) calcd for $[M+Na]^+$ $C_{16}H_{20}O_6Na$ 331.1152, found 331.1148.

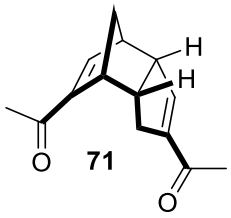

Compound **71**. Prepared according to general procedure B, from 5 mL sodium cyclopentadienylide (2 M in THF, 10 mmol), 2.4 mL methyl acetate (30 mmol, in 5 mL THF), and 293 µL H_2SO_4 (5.5 mmol, in 10 mL *i*PrOH). Chromatography (hexanes-ethyl acetate, 1:1) afforded 545 mg (51%) of **71** as a brown oil. ^{1}H NMR (300 MHz, $CDCl_3$) δ 6.73 (d, *J* = 3.3 Hz, 1H), 6.43 (q, *J* = 2.1 Hz, 1H), 3.52-3.60 (m, 1H), 3.42-3.48 (m, 1H), 3.17-3.22 (m, 1H), 2.86-2.93 (m, 1H), 2.39 (ddt, *J* = 18.0, 10.4, 2.0 Hz, 1H), 2.17 (s, 3H), 2.16 (s, 3H), 1.85 (dtd, *J* = 18.1, 3.9, 2.0 Hz, 1H), 1.64 (dt, *J* = 8.7, 1.9 Hz, 1H), 1.42 (dq, *J* = 8.6,0.9 Hz, 1H); ^{13}C NMR (75 MHz, $CDCl_3$) δ 196.6, 195.7, 148.3, 147.5, 147.1, 142.6, 55.0, 50.5, 47.9, 45.6, 40.6, 32.6, 27.0, 25.7; IR (cm^{-1}, film) 2939, 1702, 1664, 1641, 1372, 1272, 950; HRMS (ESI) calcd for $[M+Na]^+$ $C_{14}H_{16}O_2Na$ 239.1042, found 239.1040.

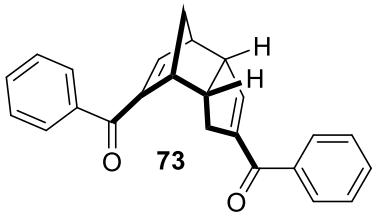

Compound **73**. Prepared according to general procedure B, from 5 mL sodium cyclopentadienylide (2 M in THF, 10 mmol), 3.8 mL methyl benzoate (30 mmol, in 5 mL THF), and 293 µL H_2SO_4 (5.5 mmol, in 15 mL *i*PrOH). Chromatography (hexanes-ethyl acetate, 5:1) afforded 584 mg (35%) of **73** as a yellow oil. ^{1}H NMR (300 MHz, $CDCl_3$) δ 7.58-7.63 (m, 2H), 7.51-7.56 (m, 2H), 7.44-7.50 (m, 2H), 7.30-7.37 (m, 4H), 6.62 (d, *J* = 3.3 Hz, 1H), 6.23 (q, *J* = 2.2 Hz, 1H), 3.66-3.73 (m, 2H), 3.27-3.32 (m, 1H), 3.03-3.14 (m, 1H), 2.70 (ddt, *J* = 18.2, 10.3, 1.9 Hz, 1H), 2.38 (dtd, *J* = 18.0, 3.8, 2.0 Hz, 1H), 1.82 (dt, *J* = 8.7, 1.7 Hz, 1H), 1.54 (dd, *J* = 8.8,0.8 Hz, 1H); ^{13}C NMR (75 MHz, $CDCl_3$) δ 193.7, 193.3, 150.3, 147.0, 146.4, 144.7, 138.9, 138.8, 132.0, 131.8, 128.8, 128.7, 128.2, 55.4, 50.6, 48.6, 47.0, 40.8, 33.9; IR (cm^{-1}, film) 3060, 2938, 1687, 1636, 1578, 1446, 1353, 1277, 918; HRMS (ESI) calcd for $[M+Na]^+$ $C_{24}H_{20}O_2Na$: 363.1355, found 363.1357.

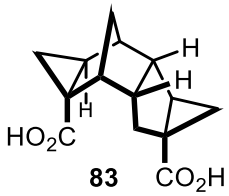

Compound **83**. To a solution of **92** (30 mg, 0.14 mmol) in a mixture of CCl_4 (0.5 mL), MeCN (0.5 mL), and water (0.75 mL) was added $NaIO_4$ (584 mg, 2.74 mmol), and $RuCl_3 \cdot XH_2O$ (5.7 mg). The reaction mixture was stirred overnight, then was partitioned between aqueous HCl (10%) and ethyl acetate. The aqueous layer was extracted twice with ethyl acetate and the combined organic layers were dried over Na_2SO_4 and concentrated *in vacuo*. Chromatography (dichloromethane-methanol, 20:1) afforded **83** as a white solid (33 mg, 99%). ^{1}H NMR (300 MHz, D_2O) δ 2.50-2.55 (m, 1H), 2.32-2.48 (m, 4H), 1.80 (dd, *J* = 9.1, 5.1 Hz, 1H), 1.65-1.75 (m, 2H), 1.26 (d, *J* = 10.4 Hz, 1H), 1.19 (dd, *J* = 9.1, 3.0 Hz, 1H), 1.14 (t, *J* = 4.4 Hz, 1H), 0.83 (d, *J* = 11.0 Hz, 1H), 0.44 (dd, *J* = 7.7, 5.0 Hz, 1H), 0.37 (dd, *J* = 5.0, 3.8 Hz, 1H); ^{13}C NMR (75 MHz, D_2O) δ 185.7, 184.9, 51.3, 48.2, 41.1, 41.0, 39.7, 32.2, 29.2, 28.0, 27.6, 24.0, 17.9, 12.8; IR (cm^{-1}, film) 3351, 1685, 1540, 1423, 830; HRMS (ESI) calcd for $[M+Na]^+$ $C_{14}H_{16}O_4Na$ 271.0941, found 271.0940.

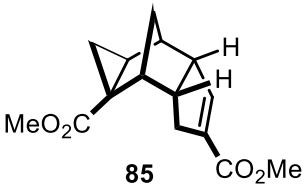

85

Compound **85**. To a stirred solution of trimethylsulfoxonium iodide (273 mg, 1.24 mmol) and DBU (341 mg, 2.24 mmol) in MeCN (5 mL) was added Thiele's ester **3** (140 mg, 0.56 mmol) in 1 mL of MeCN. The reaction mixture was heated to 60 °C for 36 h, then returned to room temperature. The resulting mixture was diluted with ethyl acetate, filtered through filter paper, and dried over $MgSO_4$. The solvent was removed *in vacuo*, and the residue was purified by chromatography (hexanes-ethyl acetate, 4:1) to afford **16** as a white solid (91 mg, 62%). ^{1}H NMR (300 MHz, $CDCl_3$) δ 6.63 (q, *J* = 2.0 Hz, 1H), 3.68 (s, 3H), 3.57 (s, 3H), 3.19-3.27 (m, 1H), 2.62-2.75 (m, 3H), 2.53-2.58 (m, 1H), 2.40 (ddt, *J* = 18.7, 10.5, 2.7 Hz, 1H), 1.35 (dd, *J* = 7.7, 4.0 Hz, 1H), 1.22 (dt, *J* = 11.0, 1.6 Hz, 1H), 1.12 (dd, *J* = 5.1, 4.6 Hz, 1H), 0.89 (dd, *J* = 11.0, 1.2 Hz, 1H), 0.56 (dd, *J* = 7.7, 5.4 Hz, 1H); ^{13}C NMR (75 MHz, $CDCl_3$) δ 175.4, 165.4, 142.7, 137.4, 53.8, 51.5, 51.4, 44.5, 40.4, 39.8, 31.1, 30.9, 25.2, 21.5, 13.6; IR (cm^{-1}, film) 2954, 1707, 1442, 1293, 1230, 1150, 1095, 951; HRMS (ESI) calcd for $[M+H]^+$ $C_{15}H_{19}O_4$: 263.1278, found 263.1276.

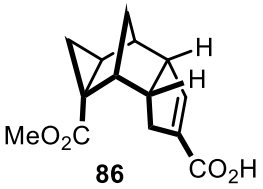

86

Compound **86**. To a stirring solution of **85** (41 mg, 0.16 mmol) in 1 mL of MeOH was added NaOH (10% solution, 1 mL) slowly. The reaction was stirred overnight. MeOH was removed *in vacuo*, and the mixture was acidified to pH=1 by addition of aqueous HCl (2 M), extracted twice with ethyl acetate, dried over $MgSO_4$, and concentrated *in vacuo*. Chromatography (hexanes-ethyl acetate,

2:1) afforded **86** as a white solid (38 mg, 97%, mp = 193-196 °C). ^{1}H NMR (300 MHz, $CDCl_3$) δ 6.79 (q, *J* = 1.9 Hz, 1H), 3.61 (s, 3H), 3.22-3.31 (m, 1H), 2.65-2.79 (m, 3H), 2.59-2.62 (m, 1H), 2.43 (ddt, *J* = 18.6, 10.2, 2.6 Hz, 1H), 1.38 (dd, *J* = 7.7, 4.3 Hz, 1H),1.25 (dt, *J* = 11.0, 1.7 Hz, 1H), 1.15 (t, *J* = 5.0, Hz, 1H), 0.93 (dd, *J* = 11.1, 1.0 Hz, 1H), 0.60 (dd, *J* = 7.8, 5.3 Hz, 1H); ^{13}C NMR (75 MHz, $CDCl_3$) δ 175.5, 169.6, 145.5, 137.0, 54.0, 51.7, 44.6, 40.4, 39.9, 31.1, 30.6, 25.3, 21.6, 13.6; IR (cm^{-1}, film) 2935, 1710, 1673, 1423, 1295, 1129, 1116, 749; HRMS (ESI) calcd for $[M+H]^+$ $C_{14}H_{17}O_4$ 249.1122, found 249.1121.

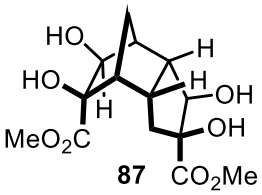

87

Compound **87**. To a solution of Thiele's ester **3** (400 mg, 1.61 mmol) in 20 mL of acetone was added 4-methylmorpholine-*N*-oxide (565 mg, 4.83 mmol) and OsO_4 (4% in H_2O, 1.02 mL, 0.16 mmol) at 0 °C. The reaction was quenched by the addition of aqueous $Na_2S_2O_3$, and acetone was removed *in vacuo*. The resulting mixture was extracted twice with ethyl acetate, and the combined organic layers were dried over Na_2SO_4 and concentrated *in vacuo*. Chromatography (5% methanol in dichloromethane) afforded **87** as a yellow oil (382 mg, 75%). ^{1}H NMR (300 MHz, MeOD) δ 4.60 (d, *J* = 2.1 Hz,1H), 4.25 (d, *J* = 8.7 Hz ,1H), 3.73 (s, 3H), 3.72 (s, 3H), 2.65-2.79 (m, 1H), 2.39-2.51 (m, 2H), 2.35 (dt, *J* = 10.3, 1.7 Hz, 1H), 2.16-2.21 (m, 1H), 1.43-1.63 (m, 3H); ^{13}C NMR (75 MHz, MeOD) δ 175.3, 175.0, 87.2, 81.3, 75.6, 71.4, 52.7, 52.6, 51.0, 50.3, 46.2, 41.5, 41.3, 34.9; IR (cm^{-1}, film) 3408, 2959, 1728, 1644, 1439, 1273, 1073, 728; HRMS (ESI) calcd for $[M + Na]^+$ $C_{14}H_{20}O_8Na$ 339.1050, found 339.1049.

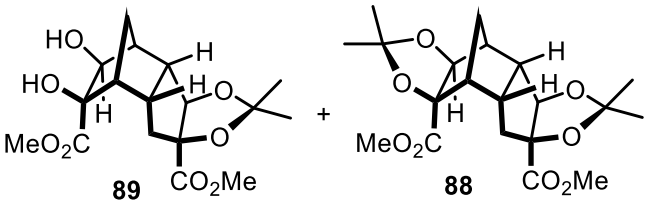

89 **88**

Compounds **88** and **89**. To a solution of **87** (64 mg, 0.20 mmol) in 3 mL of acetone was added 2,2-dimethoxypropane (0.4 mL) and *p*-toluenesulfonic acid (32 mg, 0.16 mmol). The reaction was stirred at room temperature overnight. Solvent was removed *in vacuo*, and the residue was purified by chromatography (hexanes-ethyl acetate, 1:1) to afford **89** (28 mg, 40%) and **88** (38 mg, 48%) as colorless oils. For compound **88**: ^{1}H NMR (300 MHz, $CDCl_3$) δ 5.09 (d, *J* = 5.0 Hz, 1H), 4.93 (d, *J* = 1.9 Hz, 1H), 3.79 (s, 3H), 3.73 (s, 3H), 2.93-3.05 (m, 1H), 2.70 (dt, *J* = 12.8, 5.1 Hz, 1H), 2.49-2.56 (m, 2H), 2.10-2.17 (m, 2H), 1.51 (s, 3H), 1.47-1.55 (m,1H), 1.47 (s, 3H), 1.40 (d, *J* = 10.5 Hz,

1H), 1.30 (s, 3H), 1.29 (s, 3H); ^{13}C NMR (75 MHz, $CDCl_3$) δ 172.8, 172.1, 113.1, 110.7, 96.5, 89.1, 82.1, 79.1, 52.6, 52.4, 51.7, 47.6, 44.5, 41.5, 40.1, 33.1, 29.2, 27.5, 26.4, 26.0; IR (cm^{-1}, film) 2990, 2953, 1742, 1457, 1373, 1256, 1072, 1036, 749; HRMS (ESI) calcd for $[M+Na]^+$ $C_{20}H_{28}O_8Na$ 419.1676, found 419.1674. For compound **89**: ^{1}H NMR (300 MHz, $CDCl_3$) δ 5.05 (d, *J* = 1.9 Hz, 1H), 4.30 (t, *J* = 8.7 Hz, 1H), 3.80 (s, 3H), 3.78 (s, 3H), 3.49 (s, 1H), 2.68-2.82 (m, 1H), 2.43-2.55 (m, 3H), 2.17 (d, *J* = 10.3 Hz, 1H), 2.12 (d, *J* = 9.0 Hz, 1H), 1.71 (dd, *J* = 14.5, 9.3 Hz, 1H), 1.53 (dd, *J* = 14.5, 10.4 Hz, 1H), 1.48 (s, 3H), 1.32 (s, 3H); ^{13}C NMR (75 MHz, $CDCl_3$) δ 174.0, 172.7, 110.4, 88.9, 85.8, 79.8, 74.1, 53.0, 52.6, 47.9, 47.0, 42.3, 40.7, 39.5, 32.3, 26.2, 25.8; IR (cm^{-1}, film) 3445, 2992, 2955, 1737, 1654, 1437, 1258, 1070, 731; HRMS (ESI) calcd for $[M+H]^+$ $C_{17}H_{25}O_8$ 357.1544, found 357.1544.

Direct access to compound **88** from **87**. To a stirred solution of **87** (90 mg, 0.28 mmol) in 4 mL of dichloromethane was added 2,2-dimethoxypropane (0.8 mL) and camphorsulfonic acid (160 mg, 0.68 mmol) at 0 °C. The reaction was allowed to warm to room temperature with stirring. After 16 h, the reaction mixture was cooled back to 0 °C, and the reaction was quenched by the addition of aqueous $NaHCO_3$. The resulting mixture was extracted twice with dichloromethane, and the combined organic layers were dried over $NaSO_4$ and concentrated *in vacuo*. Chromatography (hexanes-ethyl acetate, 6:1) afforded **88** (103 mg, 88%) as a colorless oil, with spectral properties identical to those reported above.

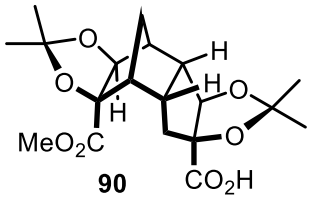

90

Compound **90**. To a stirring solution of **88** (44 mg, 0.11 mmol) in 1 mL of MeOH was added NaOH (10% solution, 1 mL) slowly. The reaction was stirred overnight. MeOH was removed *in vacuo*, and the mixture was acidified to pH=1 by addition of aqueous HCl (2 M), extracted twice with ethyl acetate, dried over $MgSO_4$, and concentrated *in vacuo* to afford **90** as a white solid (41 mg, 96%, mp = 161-162 °C). ^{1}H NMR (300 MHz, $CDCl_3$) δ 5.07 (d, *J* = 4.9 Hz, 1H), 4.93 (d, *J* = 1.9 Hz, 1H), 3.75 (s, 3H), 2.93-3.06 (m, 1H), 2.71 (dt, *J* = 12.8, 5.0 Hz, 1H), 2.57 (d, *J* = 4.4 Hz, 1H), 2.51 (d, *J* = 4.4 Hz, 1H), 2.11-2.23 (m, 2H), 1.61 (dd, *J* = 16.2, 8.7 Hz, 1H), 1.53 (s, 3H), 1.47 (s, 3H), 1.42 (d, *J* = 11.9 Hz, 1H), 1.36 (s, 3H), 1.31 (s, 3H); ^{13}C NMR (75 MHz, $CDCl_3$) δ 175.4, 173.0, 113.6, 110.9, 96.3, 89.2, 82.3, 79.0, 52.8, 51.8, 47.6, 44.6, 41.6, 40.2, 33.2, 29.2, 27.7, 26.5, 26.1; IR (cm^{-1}, film) 3056, 2978, 2941, 1716, 1639, 1598, 1578, 1447, 1353, 1277, 732; HRMS (ESI) calcd for $[M+Na]^+$ $C_{19}H_{26}O_8Na$ 405.1520, found 405.1521.

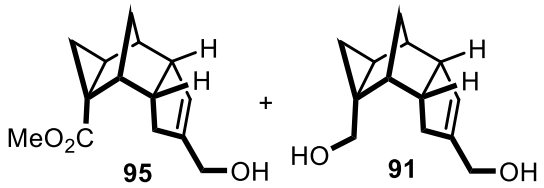

Compounds **91** and **95**. To a solution of **85** (162 mg, 0.62 mmol) in ether (10 mL) was added $LiAlH_4$ (58.7 mg, 2.48 mmol) at 0 °C. After addition the reaction was warmed to room temperature and stirred overnight. Next day, the reaction was quenched by the addition of water, and extracted with ethyl acetate. The organic layer was dried over $MgSO_4$, and concentrated *in vacuo*. Chromatography (hexanes-ethyl acetate, 1:1 to 1:3) afforded **95** (72 mg, 50%) and **91** (49 mg, 39%). For compound **95** (colorless oil): ^{1}H NMR (300 MHz, $CDCl_3$) δ 5.48-5.52 (m, 1H), 4.16 (dd, *J* = 12.7, 3.6 Hz,1H), 3.90- 3.99 (m, 1H), 3.67 (s, 3H), 3.07-3.17 (m, 1H), 2.60-2.70 (m, 2H), 2.42-2.47 (m, 1H), 2.38 (d, *J* = 18.5 Hz,1H), 2.20 (dd, *J* = 18.1, 9.7 Hz,1H), 1.66 (dd, *J* = 8.2, 4.0 Hz,1H), 1.43 (dd, *J* = 8.0, 4.6 Hz,1H), 1.22 (dt, *J* = 11.0, 1.7 Hz,1H), 1.14 (t, *J* = 5.1 Hz,1H), 0.91 (dd, *J* =11.0, 1.2 Hz,1H), 0.53 (dd, *J* = 7.9, 5.2 Hz,1H); ^{13}C NMR (75 MHz, $CDCl_3$) δ 177.0, 145.7, 126.7, 62.2, 53.0, 51.9, 44.8, 40.4, 39.3, 31.7, 31.3, 25.5, 21.4, 14.0; IR (cm^{-1}, film) 3427, 2950, 1705, 1438, 1294, 1164, 1017, 923, 751; HRMS (ESI) calcd for $[M+Na]^+$ $C_{14}H_{18}O_3Na$ 257.1148, found 257.1148. For compound **91** (pale yellow crystalline solid, mp = 105-110 °C): ^{1}H NMR (300 MHz, $CDCl_3$) δ 5.57 (s, 1H), 4.14 (s, 2H), 4.07 (dd, *J* = 11.6, 1.0 Hz, 1H), 3.22 (d, *J* = 11.6 Hz, 1H), 3.07-3.16 (m, 1H), 2.54-2.69 (m, 2H), 2.27-2.44 (m, 3H), 1.83 (br, 2H) 1.19 (dt, *J* = 10.7, 1.8 Hz, 1H), 0.77-0.85 (m, 3H), -0.12 (dd, *J* = 6.9, 5.0 Hz, 1H); ^{13}C NMR (75 MHz, $CDCl_3$) δ 144.8, 127.1, 66.6, 62.1, 52.9, 45.6, 40.5, 39.1, 33.5, 32.1, 25.3, 17.7, 9.3; IR (cm^{-1}, film) 3407, 1645, 1260, 1016; HRMS (ESI) calcd for $[M-H]^-$ $C_{13}H_{17}O_2$: 205.1234, found 205.1235.

Direct access to compound **91** from **85**. To a solution of **85** (96 mg, 0.36 mmol) in ether (5 mL) was added $LiAlH_4$ (140 mg, 3.66 mmol) at 0 °C. After addition the reaction was warmed to room temperature and stirred overnight. Next day, the reaction was quenched by the addition of water, and extracted with ethyl acetate. The organic layer was dried over $MgSO_4$, and concentrated *in vacuo*. Chromatography (hexanes-ethyl acetate, 1:1 to 1:3) afforded **91** (75 mg, 99%) as a pale yellow crystalline solid, with spectral properties identical to those reported above.

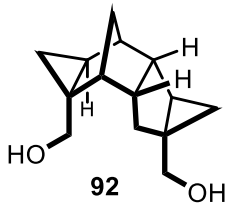

Compound **92**. To a solution of **91** (61 mg, 0.28 mmol) in dichloromethane (3 mL) was added Et_2Zn (1 M in hexane, 0.6 mL, 0.6 mmol) at 0 °C. After 15 min, CH_2I_2 (48 µL, 0.6 mmol) was injected into

the mixture. The reaction was then heated to 40 °C for 18 h, then returned to room temperature. Additional Et_2Zn (1 M in hexane, 0.6 mL, 0.6 mmol) and CH_2I_2 (48 µL, 0.6 mmol) was added, and the reaction was heated to 40 °C overnight. The following day, the reaction was cooled to room temperature and quenched by the addition of saturated NH_4Cl. The resulting mixture was extracted twice with dichloromethane, washed with brine, dried over $NaSO_4$, and concentrated *in vacuo* to afford **92** as a colorless oil with no further purification (63 mg, 97%). ^{1}H NMR (300 MHz, $CDCl_3$) δ 4.34 (d, *J* = 11.4 Hz, 1H), 3.68 (d, *J* = 4.0 Hz, 1H), 3.65 (d, *J* = 4.0 Hz, 1H), 3.48 (d, *J* = 11.3 Hz, 1H), 2.26-2.44 (m, 5H), 1.72 (dd, *J* = 14.1, 9.6 Hz, 1H), 1.36 (d, *J* = 7.4 Hz, 1H), 1.20-1.27 (m, 2H), 0.84 (dd, *J* = 5.0, 2.5 Hz, 1H), 0.73 (d, *J* = 10.5 Hz, 1H), 0.66 (ddd, *J* = 8.6, 4.2, 1.2 Hz, 1H), 0.05 (dd, *J* = 7.2, 2.8 Hz, 1H), -0.02 (dd, *J* = 7.2, 5.3 Hz, 1H); ^{13}C NMR (75 MHz, $CDCl_3$) δ 68.0, 66.4, 52.5, 50.6, 41.7, 40.8, 37.1, 33.6, 30.6, 26.4, 24.1, 20.1, 16.2, 8.0; IR (cm^{-1}, film) 3324, 2933, 1456, 1261, 1024, 913; HRMS (ESI) calcd for $[M-H]^-$ $C_{14}H_{19}O_2$ 219.1390, found 219.1383.

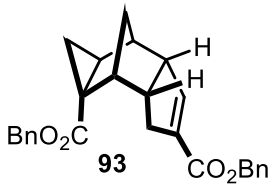

93

Compound **93**. To a stirred solution of trimethylsulfoxonium iodide (99 mg, 0.45 mmol) and DBU (69 mg, 0.45 mmol) in MeCN (5 mL) was added **65** (90 mg, 0.225 mmol) in MeCN (1 mL). The reaction was heated to 60 °C for 36 h. The resulting mixture was diluted with ethyl acetate, filtered through filter paper, dried over $MgSO_4$, and concentrated *in vacuo*. The residue was purified by chromatography (hexanes-ethyl acetate, 2:1) to afford **93** as a yellow oil (67 mg, 72%). ^{1}H NMR (300 MHz, $CDCl_3$) δ 7.13-7.29 (m, 10H), 6.67 (q, *J* = 2.2 Hz, 1H), 5.10 (d, *J* = 12.7 Hz, 1H), 4.95 (d, *J* = 12.7 Hz ,1H), 4.89 (d, *J* = 12.6 Hz, 1H), 4.78 (d, *J* = 12.6 Hz, 1H), 3.13-3.23 (m, 1H), 2.69-2.80 (m, 2H), 2.58-2.68 (m, 1H), 2.48- 2.53 (m, 1H), 2.39 (ddt, *J* = 18.2, 10.3, 2.7 Hz, 1H), 1.36 (dd, *J* = 7.6, 4.2 Hz, 1H), 1.17 (dt, *J* = 10.7, 1.7 Hz, 1H), 1.08 (dd, *J* = 5.4, 4.5 Hz, 1H), 0.84 (dd, *J* = 10.9, 1.0 Hz, 1H), 0.54 (dd, *J* = 7.7, 5.3 Hz, 1H); ^{13}C NMR (75 MHz, $CDCl_3$) δ 164.8 (2C), 143.3, 137.5, 136.4, 136.2, 128.6, 128.5, 128.1, 128.0, 66.3, 65.9, 53.9, 44.5, 40.4, 39.9, 31.2, 31.0, 25.5, 21.7, 13.8; IR (cm^{-1}, film) 2955, 1714, 1630, 1455, 1280, 1230, 1135, 746; HRMS (ESI) calcd for $[M+Na]^+$ $C_{27}H_{26}O_4Na$: 437.17232 Found 437.17228.

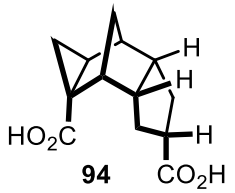

94

Compound **94**. To a solution of **93** (68 mg, 0.17 mmol) in 10 mL of MeOH was added Pd/C 10% (~30 mg). The reaction mixture was pressurized inside a Parr reactor to 200 psi of H_2 and was stirred for 16 h. The product mixture was filtered through cotton, then concentrated *in vacuo*. The

residue was purified by chromatography (hexanes-ethyl acetate, 2:1) to afford **94** as a white solid (30 mg, 75%, mp > 200 °C). ^{1}H NMR (300 MHz, D_2O) δ 2.56-2.67 (m, 1H), 2.44-2.49 (m, 1H), 2.37-2.44 (m, 2H), 2.19-2.24 (m, 1H), 1.54-1.82 (m, 4H), 1.39 (d, *J* = 10.7 Hz, 1H), 1.23-1.34 (m, 1H), 1.19 (t, *J* = 4.6 Hz, 1H), 1.04 (d, *J* = 11.1 Hz, 1H), 0.52 (dd, *J* = 7.7, 4.9 Hz, 1H); ^{13}C NMR (75 MHz, D_2O) δ 185.7, 185.0, 52.8, 47.3, 46.2, 39.4, 38.8, 34.2, 31.7, 28.7, 28.7, 18.7, 12.7; IR (cm^{-1}, film) 3421, 2926, 1701, 1560, 1438, 1295; HRMS (ESI) calcd for $[M+Na]^+$ $C_{13}H_{16}O_4Na$ 259.0941, found 259.0941.

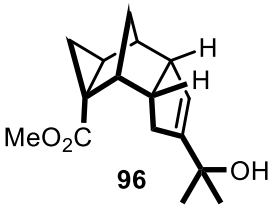

96

Compound **96**. To a solution of **85** (40 mg, 0.15 mmol) in THF (6 mL) was added MeMgBr (3.0 M in THF, 0.1 mL, 0.3 mmol) dropwise. The reaction was stirred overnight. The mixture was quenched by the addition of saturated NH_4Cl, and extracted with ether. The aqueous layer was washed with brine, dried over $MgSO_4$, and concentrated *in vacuo*. Chromatography (hexanes-ethyl acetate, 4:1) afforded **96** as a colorless oil (34 mg, 70%). ^{1}H NMR (300 MHz, $CDCl_3$) δ 5.43 (q, *J* = 1.9 Hz, 1H), 3.67 (s, 3H), 3.07-3.16 (m, 1H), 2.58-2.70 (m, 2H), 2.38-2.48 (m, 2H), 2.30 (ddt, *J* = 18.2, 10.1, 2.7 Hz, 1H), 1.81 (br, 1H), 1.43 (dd, *J* = 7.9, 4.6 Hz, 1H), 1.36 (s, 3H), 1.18-1.26 (m, 4H), 1.16 (t, *J* = 4.7 Hz, 1H), 0.91 (dd, *J* = 10.7, 1.0 Hz, 1H), 0.55 (dd, *J* = 7.6, 5.3 Hz, 1H); ^{13}C NMR (75 MHz, $CDCl_3$) δ 177.0, 152.8, 123.0, 70.0, 53.2, 51.9, 44.4, 40.4, 39.5, 31.4, 30.3, 29.6, 28.3, 25.6, 21.4, 14.2; IR (cm^{-1}, film) 3429, 2974, 1701, 1647, 1439, 1292, 1157, 750; HRMS (ESI) calcd for $[M+Na]^+$ $C_{16}H_{22}O_3Na$: 285.1461, found 285.1456.

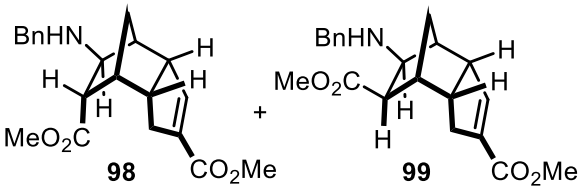

98 **99**

Compounds **98** and **99**. To a solution of Thiele's ester **3** (100 mg, 0.40 mmol) in MeCN (3 mL) was added benzyl amine (129.6 mg, 1.21 mmol) and DBU (61.4 mg, 0.80 mmol). The mixture was heated to 70 °C and stirred overnight. After cooling to room temperature, the reaction was quenched by the addition of saturated NH_4Cl and extracted twice with ethyl acetate. The combined organic layers were dried over $MgSO_4$ and concentrated *in vacuo*. Chromatography (hexanes-ethyl acetate, 4:1) afford 75 mg of **98** (53%) and 27 mg of **99** (19%). For compound **98** (brown solid; mp = 83-85 °C): ^{1}H NMR (300 MHz, $CDCl_3$) δ 7.27-7.32 (m, 4H) 7.20-7.25 (m, 1H), 6.60 (q, *J* = 2.0 Hz

,1H), 3.74 (d, *J* = 12.8 Hz, 1H), 3.73 (s, 3H), 3.65 (d, *J* = 12.8 Hz, 1H), 3.62 (s, 3H), 3.25-3.30 (m, 1H), 3.24 (dd, *J* = 4.9, 1.7 Hz, 1H), 2.76 (t, *J* = 4.0 Hz, 1H), 2.70 (tt, *J* = 10.6, 4.0 Hz, 1H), 2.48-2.39 (m, 3H), 2.27 (ddt, *J* = 18.4, 3.1, 1.6 Hz, 1H), 1.86 (dt, *J* = 10.0, 1.4 Hz, 1H), 1.48 (dq, *J* = 10.0, 1.5 Hz, 1H); ^{13}C NMR (75 MHz, $CDCl_3$) δ 173.6, 165.3, 143.1, 140.7, 136.6, 128.4, 128.3, 127.0, 57.9, 54.6, 52.8, 52.1, 51.6, 51.5, 45.8, 44.3, 41.8, 40.5, 31.0; IR (cm^{-1}, film) 3436, 2959, 1720, 1639, 1438, 1273, 1081; HRMS (ESI) calcd for $[M+H]^+$ $C_{21}H_{26}NO_4$ 356.1857, found 356.1860. For compound **99** (brown oil): ^{1}H NMR (300 MHz, $CDCl_3$) δ 7.22-7.33 (m, 5H), 6.61 (q, *J* = 2.0 Hz ,1H), 3.76 (d, *J* = 12.3 Hz, 1H), 3.75 (s, 3H), 3.68 (s, 3H), 3.66 (d, *J* = 12.3 Hz, 1H), 3.22-3.28 (m, 1H), 2.98 (dd, *J* = 8.1, 1.2 Hz, 1H), 2.69 (dd, *J* = 8.1, 1.2 Hz, 1H), 2.63 (ddt, *J* = 9.9, 4.2, 2.7 Hz, 1H), 2.53 (ddt, *J* = 17.5, 9.9, 2.5 Hz, 1H), 2.48 (d, *J* = 5.7 Hz, 1H), 2.37-2.44 (m, 2H), 2.07 (dt, *J* = 10.7, 1.6 Hz, 1H), 1.44 (dt, *J* = 10.6, 1.5 Hz, 1H); ^{13}C NMR (75 MHz, $CDCl_3$) δ 174.0, 165.4, 144.1, 140.7, 136.4, 128.4, 128.0, 127.0 60.6, 52.8, 52.5, 51.6, 51.5, 46.3, 44.2, 44.1, 41.6, 37.7, 31.4; IR (cm^{-1}, film) 3419, 2950, 1717, 1633, 1436, 1274, 1094; HRMS (ESI) calcd for $[M+H]^+$ $C_{21}H_{26}NO_4$ 356.1857, found 356.1853.

Isomerization of **98** to **99**. To a solution of **98** (40 mg, 0.11 mmol) in toluene (3 ml) was added DBU (31 µL, 0.22 mmol). The mixture was heated to 110 °C and stirred for 2 d. After cooling to room temperature, the reaction was quenched by the addition of saturated NH_4Cl and extracted twice with ethyl acetate. The combined organic layers were dried over $MgSO_4$ and concentrated *in vacuo*. Chromatography (hexanes-ethyl acetate, 4:1) afforded **99** as a brown oil (21 mg, 52 %). Spectral details were identical to those provided above.

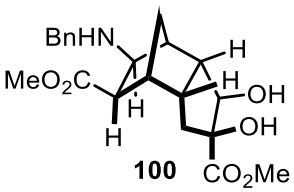

100

Compound **100**. To a solution of **99** (50 mg, 0.14 mmol) in 3 mL acetone was added 4-methylmorpholine-*N*-oxide (25.7 mg, 0.22 mmol) and OsO_4 (4% in H_2O, 45 µL, 0.007 mmol) at 0 °C. The mixture was warmed to room temperature and stirred for 6 h. The reaction was quenched by the addition of aqueous $Na_2S_2O_3$, and acetone was removed *in vacuo*. The resulting mixture was extracted twice with ethyl acetate, and the combined organic layers were dried over Na_2SO_4 and concentrated *in vacuo*. Chromatography (hexanes-ethyl acetate, 1:1) afforded **100** as a yellow oil (28 mg, 52%). ^{1}H NMR (300 MHz, $CDCl_3$) δ 7.13-7.29 (m, 5H), 4.07 (d, *J* = 8.6 Hz, 1H), 3.80 (d, *J* = 13.3 Hz, 1H), 3.77 (s, 3H), 3.69 (d, *J* = 13.3 Hz, 1H), 3.67 (s, 3H), 3.38 (dd, *J* = 8.3, 1.3 Hz, 1H), 2.94 (dd, *J* = 8.2, 1.4 Hz, 1H), 2.66 (ddd, *J* = 21.8, 9.4, 4.1 Hz, 1H), 2.28-2.40 (m, 3H), 2.22 (dt, *J* = 10.4, 1.8 Hz, 1H), 1.80 (dd, *J* = 14.1, 9.6 Hz, 1H), 1.70 (dd, *J* = 14.1, 9.6 Hz, 1H), 1.56 (d,

J = 10.6 Hz, 1H); ^{13}C NMR (75 MHz, $CDCl_3$) δ 175.5, 173.6, 140.5, 128.4, 128.0, 127.0, 86.2, 74.9, 58.9, 53.2, 52.9, 51.5, 50.8, 46.6, 42.3, 42.0, 41.1 33.4; IR (cm^{-1}, film) 3436, 2954, 1726, 1642, 1452, 1275, 1171, 1083, 748; HRMS (ESI) calcd for $[M+H]^+$ $C_{21}H_{28}NO_6$ 390.1911, found 390.1908.

Procedure for the Preparation of Racemic Thiele's Acid. To a solution of Thiele's ester in *i*PrOH was added 10% KOH solution (10 mL / g of Thiele's ester) dropwise. After 5 h, *i*PrOH was removed *in vacuo*. The mixture was acidified to pH=1 by the addition of 2 M HCl, then extracted twice with ethyl acetate. The combined organic layers were dried over $MgSO_4$ and concentrated *in vacuo* to afford Thiele's acid, (±)-**2**, as a white powder without further purification. Spectral data were identical to those reported previously, while yields were consistently >90%.

Resolution of Thiele's acid. A 100 mL round bottomed flask was charged with racemic Thiele's acid (**2**, 1.10 g, 5.00 mmol) and methanol (20 mL). The suspension was warmed to 80 °C to provide a clear solution. To this hot solution was added brucine (**105**, 3.94 g, 10.0 mmol). An additional 10 mL of methanol was added to facilitate complete dissolution. The resulting solution was filtered to remove a small amount of residual insolubles, and then cooled in a freezer at 0 °C. Brown crystals of crude **2•105**$_2$ were formed within 2 h. NMR analysis of the crude salt revealed a ~3.6:1 ratio of diastereomers. This ratio varied only slightly across multiple trials. The crude salt was filtered from the mother liquor, added to 25 mL of methanol, and warmed until all of the solid dissolved. The solution was then cooled in the freezer. Crystals of purified **2•105**$_2$ were formed within 2 h. This recrystallization was repeated twice more, and the final, thrice recrystallized solid was obtained by suction filtration to provide 1.86 g (1.84 mmol, 37%) of **2•105**$_2$ as a pale brown solid after drying *in vacuo*. MP = 147 °C (dec).

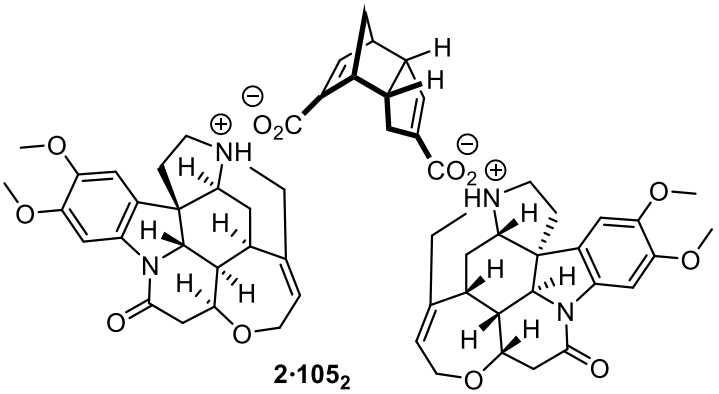

2·105$_2$

^{1}H NMR (500 MHz, $CDCl_3$: C_6D_6 = 1:8.3) δ 8.22 (s, 2H), 7.07 (d, *J* = 2.9 Hz, 0.95H, **Major**), 7.02 (d, *J* = 2.9 Hz, 0.05H, **Minor**), 6.90 (s, 2H), 6.63 (s, 1H), 5.40 (s, 2H), 4.16 (s, 2H), 3.74 (dd, *J* = 14.0, 7.1 Hz, 2H), 3.69 (d, *J* = 14.4, 2H), 3.58-3.64 (m, 8H), 3.53-3.57 (m, 8H), 3.47 (dd, *J* = 13.5, 6.0 Hz, 2H), 3.12-3.22 (m, 3H), 3.01-3.09 (m, 2H), 2.81 (s, 1H), 2.66-2.77 (m, 3H), 2.61 (dd, *J* = 17.5, 2.2 Hz, 2H), 2.35-2.46 (m, 4H), 2.32 (s, 2H), 2.09 (d, *J* = 14.7 Hz, 2H), 1.89 (dt, *J* = 13.0, 7.9 Hz,

2H), 1.60 (d, *J* = 8.1 Hz, 1H), 1.42 (dd, *J* = 12.8, 5.9 Hz, 2H), 1.10 (d, *J* = 8.4 Hz, 1H), 0.97 (d, *J* = 14.4 Hz, 2H), 0.49 (d, *J* = 10.3 Hz, 2H); ^{13}C NMR (75 MHz, $CDCl_3$:C_6D_6 = 1:8.3) δ 171.3, 169.9, 168.7, 150.8, 147.3, 144.6, 142.4, 141.4, 137.9, 136.9, 130.3, 122.3, 107.3, 101.9, 77.7, 64.2, 60.1, 59.9, 54.6, 52.2, 52.1, 50.4, 50.3, 48.9, 47.7, 47.6, 42.6, 41.8, 41.6, 34.1, 31.1, 26.0; IR (cm^{-1}, film) 3400, 2939, 1641, 1602, 1555, 1501, 1448, 1398, 1198, 987, 847; HRMS (ESI) calcd for [**2•105**+H]$^+$ $C_{35}H_{39}N_2O_8$ 615.2706, found 615.2702.

The isolated salt was added to 30 mL of 10% aqueous HCl, and extracted with 60 mL of ethyl acetate three times. The combined organic layers were dried over $MgSO_4$. After removal of the solvent *in vacuo*, (–)-Thiele's acid was isolated as a light brown solid (398 mg, 1.81 mmol, 98% from the intermediate salt; 72% recovery of (–)-**2** from the initial racemic mixture). Spectral data were consistent with the racemic compound that has been described previously in the literature[53]. $[\alpha]_D^{28.6}$ = –228 deg mL dm^{-1} g^{-1} (*c* = 0.25, 1 M KOH). MP = 180–182 °C.

Esterification of Optically Active Thiele's acids. To a solution of (–)-**2** (220 mg; 1.00 mmol) in CH_2Cl_2 (20 mL) was added DMAP (24 mg, 0.2 mmol) and MeOH (0.4 mL, 10 mmol). DCC (460 mg, 2.2 mmol) was then added at 0 °C. The mixture was allowed to warm to room temperature, and was stirred overnight. The product mixture was washed with 1 M HCl and saturated $NaHCO_3$, dried over $MgSO_4$, and concentrated *in vacuo*. Chromatography (hexanes-ethyl acetate, 4:1) afforded (–)-Thiele's ester **3** as a white solid (200 mg, 81%). Spectral data were consistent with the racemic compound that has been described previously in the literature[53]. $[\alpha]_D^{25}$ = –216 deg mL dm^{-1} g^{-1} (*c* = 0.25, ethanol). MP = 87–89 °C.

(+)-Thiele's ester **3** was prepared by the same procedure, beginning from crude (+)-**2** recovered from the crystalization mother liquor. Spectral data were identical, but a lower melting point (51–53 °C) was attributed to the presence of minor impurities. $[\alpha]_D^{24}$ = +269 deg mL dm^{-1} g^{-1} (*c* = 0.25, ethanol).

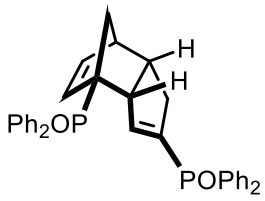

Compound **110a**. A flame dried round bottom flask under argon atmosphere was charged with diphenylphosphinic chloride (236 mg, 1 mmol) and THF (3 mL). To this solution was added sodium cyclopentadienylide (2 M in THF, 1 mmol) at 0 °C with stirring. After 30 min, the reaction was quenched by water, extracted with DCM and dried over $MgSO_4$. After the removal of solvent, the neat mixture was heated to 50 °C overnight. The resulting deep purple mixture was loaded onto a

silica gel column and eluted with DCM/MeOH (20:1 to 10:1) to give **110a** as a brown oil (159 mg, 60%). ^{1}H NMR (500 MHz, $CDCl_3$) δ 7.80-7.84 (m, 2H), 7.71-7.77 (m, 2H), 7.47-7.59 (m, 7H), 7.33-7.47 (m, 7H), 7.29 (td, *J* = 7.7, 2.7 Hz, 2H), 6.19-6.24 (m, 2H), 5.38 (dd, *J* = 10.5, 2.0 Hz, 1H), 3.91-3.97 (m, 1H), 3.06- 3.10 (m,1H), 2.97-3.03 (m, 1H), 2.50 (ddd, *J* = 17.6, 10.4, 1.7 Hz, 1H), 1.89 (d, *J* = 17.6 Hz, 1H), 1.85 (dd, *J* = 8.7, 1.7 Hz, 1H), 1.68 (d, *J* = 8.7 Hz, 1H); ^{13}C NMR (125 MHz, $CDCl_3$) δ 146.5 (d, *J* = 12.9 Hz), 140.6 (d, *J* = 99.5 Hz), 135.4 (d, *J* = 11.2 Hz), 133.7 (d, *J* = 4.7 Hz), 132.6 (d, *J* = 86.6 Hz), 132.2-131.2 (m), 128.6-128.4 (m), 58.1 (d, *J* = 16.2 Hz), 57.7 (d, *J* = 87.7 Hz), 52.6, 46.9 (d, *J* = 13.9 Hz), 43.7 (dd, *J* = 9.4, 5.6 Hz), 34.7 (d, *J* = 11.2 Hz); ^{31}P NMR (202 MHz, $CDCl_3$) δ 29.9, 23.6; IR (cm^{-1}, film) 3056, 2929, 1607, 1436, 1176, 1116; HR-ESIMS calculated for $[M+Na]^+$ $C_{34}H_{30}O_2P_2Na$ 555.1613 Found 555.1612.

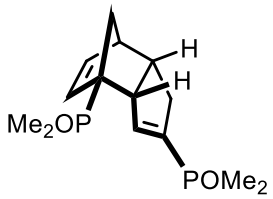

Compound **110b.** In a glove box, a vial was charged with dimethylphosphinic chloride (56.3 mg, 0.5 mmol) and THF (3 mL). To this solution was added sodium cyclopentadienylide (2 M in THF, 0.5 mmol) at room temperature with stirring. After 30 min, the reaction mixture was concentrated and the resulting neat oil was heated to 50 °C overnight. The reaction mixture was then loaded onto a silica gel column and eluted with DCM/MeOH (10:1 to 5:1) to give **110b** as a pale-yellow oil (46 mg, 65%). ^{1}H NMR (500 MHz, MeOD) δ 6.37 (dd, *J* = 10.3, 2.0 Hz, 1H), 6.31-6.34 (m, 1H), 6.04 (dd, *J* = 5.9, 4.0, 1H), 3.79-3.85 (m, 1H), 3.15-3.23 (m, 2H), 2.50 (ddd, *J* = 16.9, 9.8, 1.9 Hz, 1H), 2.00 (d, *J* = 17.2 Hz, 1H), 1.68 (d, *J* = 8.5 Hz, 1H), 1.59-1.66 (m, 7H), 1.55 (dd, *J* = 13.3, 2.8 Hz, 6H); ^{13}C NMR (75 MHz, MeOD) δ 144.5 (d, *J* = 10.9 Hz), 142.3 (d, *J* = 95.4 Hz), 137.0 (d, *J* = 10.9 Hz), 133.2 (d, *J* = 4.5 Hz), 58.2 (d, *J* = 16.5 Hz), 57.7 (d, *J* = 85.9 Hz), 52.3, 48.3 (d, *J* = 14.4 Hz), 45.2 (dd, *J* = 8.7, 5.2 Hz), 35.2 (d, *J* = 12.4 Hz), 16.0 (d, *J* = 73.0 Hz), 14.5 (d, *J* = 68.5 Hz), 13.6 (d, *J* = 69.8 Hz); ^{31}P NMR (202 MHz, MeOD) δ 50.6, 36.3; IR (cm^{-1} , film) 2926, 1645, 1421, 1296, 1129; HR-ESIMS calculated for $[M+H]^+$ $C_{14}H_{23}O_2P_2$ 285.1168 Found 285.1165.

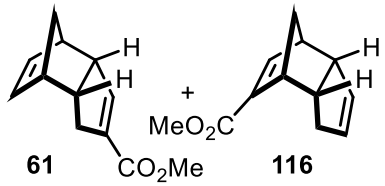

Compound **61** and **116**. A flame-dried round bottom flask fitted with an oven-dried condensor was charged with 7 mL sodium cyclopentadienylide solution (2 M in THF, 14.0 mmol). To this solution was added 5.9 mL dimethylcarbonate (70 mmol), at room temperature with stirring. The reaction mixture was heated to reflux for 6 h, then cooled to room temperature. The mixture was

concentrated *in vacuo*. To the resulting solid was added *i*PrOH (to 0.33 M), 0.41 mL sulfuric acid (0.55 equiv, 7.7 mmol) and 2.35 mL of freshly cracked cyclopentadiene (28 mmol) at room temperature with stirring. Acidification was marked by a brown to orange color change. The solution was heated to 50 °C overnight. The reaction mixture was concentrated *in vacuo* and the resulting oil was dissolved in toluene, and loaded onto a silica gel column. Elution with hexanes-ethyl acetate provided 1.60 g of a mixture of **61** and **116** (60%).

Major compound **116**

^{1}H NMR (300 MHz, $CDCl_3$) δ 6.84 (d, *J* = 3.5 Hz ,1H), 5.45-5.50 (m ,2H), 3.72 (s, 3H), 3.35-3.40 (m, 1H), 3.28-3.31 (m, 1H), 3.01-3.04 (m, 1H), 2.23 (ddq, *J* = 18.3,10.3, 1.9 Hz, 1H), 1.70-1.77 (m, 1H), 1.64 (dt, *J* = 8.2, 1.8 Hz, 1H), 1.30 (d, *J* = 8.2 Hz, 1H). ^{13}C NMR (75 MHz, $CDCl_3$) δ 166.9, 148.5, 133.1, 133.1, 130.8, 54.2, 51.4, 50.6, 47.1, 46.4, 40.8, 34.2.

Minor compound **61**

^{1}H NMR (300 MHz, $CDCl_3$) δ 6.54 (d, *J* = 2.3 Hz ,1H), 6.03 (dd, *J* = 5.7, 3.0 Hz ,1H), 5.93 (dd, *J* = 5.7, 3.0 Hz,1H), 3.68 (s, 3H), 2.92-2.96 (m, 1H), 2.89-2.92 (m, 1H), 2.80-2.88 (m, 2H), 2.42 (ddt, *J* = 17.3, 10.3, 2.0 Hz, 1H), 1.91 (dtd, *J* = 17.3, 4.0, 2.0 Hz, 1H), 1.49 (dt, *J* = 8.2, 1.7 Hz, 1H), 1.30 (d, *J* = 8.2 Hz, 1H). ^{13}C NMR (75 MHz, $CDCl_3$) δ 166.7, 144.5, 137.1, 135.7, 133.0, 55.0, 51.3, 50.3, 46.3, 45.6, 41.3, 33.6. IR (cm^{-1}, film) 2955, 1732, 1717, 1634, 1439, 1268, 1096, 735.

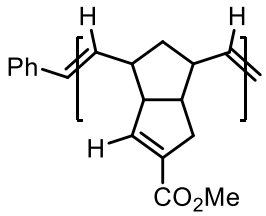

124

Compound **124**. To a mixture of **61** and **116** (190 mg, 1 mmol) in 3 mL DCM was added 8 mg Grubbs second generation catalyst (monomer : catalyst = 40 : 1). The mixture was allowed to stir at room temperature for 40 min. To this solution was added 1 mL ethyl vinyl ether. The reaction was stirred for an additional 1 h. To the reaction was added 10 mL of ether. White precipitate indicated the formation of the polymer. The resulting mixture was centrifuged in 3000 rpm at 4 °C for 5 min. The polymer **124** was isolated as a precipitate (64 mg, 90%) and unreacted **116** was obtained in the ether supernatant. ^{1}H NMR (500 MHz, $CDCl_3$) δ 6.52-6.65 (br, 1H), 5.22-5.55 (br, 2H), 3.69-3.75 (br, 3H), 3.33-3.42 (br, 1H), 2.85-3.02 (br, 2H), 2.47-2.73 (br, 2H), 1.59-1.76 (br, 1H), 1.20-1.34 (br, 1H). ^{13}C NMR (75 MHz, $CDCl_3$) δ 165.3, 143.9, 136.6, 131.5, 130.7, 56.0, 51.4 (the rest of carbons showed as multiple signals from 47.3 to 34.2 ppm).

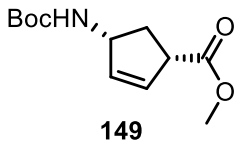

149

Compound **149**. Compound **148** (432 mg, 3.96 mmol) was heated to reflux for 18 h in methanolic hydrochloride (10 mL). The solvent was removed in *vacuo* to yield a white solid. To a mixture of the crude hydrochloride salt and di-*tert*-butyl dicarbonate (963 mg, 4.41 mmol) in 30 mL anhydrous dichloromethane at 0 °C was added triethylamine (610 µL, 4.36 mmol) dropwise via syringe. After stirring for 1 hour the solvent was removed in *vacuo* to yield a crude white solid, which was further purified by washing with 4:1 hexanes:ethyl acetate. The filtrate was collected and concentrated under reduced pressure to provide compound **149** as a white solid (956 mg, 3.96 mmol, quantitative over two steps). Spectral data were consistent with that reported in the literature.[118]

^{1}H NMR (300 MHz, $CDCl_3$) δ 5.81-5.88 (m, 2H), 4.87 (br, 1H), 4.71-4.82 (m, 1H), 3.69 (s, 3H), 3.46 (ddd, *J* = 8.5, 4.4, 0.8 Hz, 1H), 2.49 (dt, *J* = 13.8, 8.5 Hz, 1H), 1.84 (dt, *J* = 13.8, 4.1 Hz, 1H), 1.42 (s, 9H).

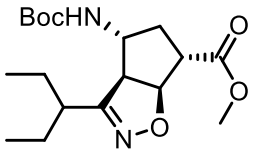

150

Compound **150**. A solution of sodium hypochlorite (5% solution in water, 12.7 mL, 8.55 mmol) and a solution of 2-ethyl butyraldehyde oxime (**147**; 499 mg, 4.33 mmol) in 12 mL dichloromethane were added dropwise via a syringe pump over two d to a mixture of compound **149** (229 mg, 0.950 mmol) and triethylamine (40 µL, 0.29 mmol) in 20 mL dichloromethane and heated to reflux. The solution was stirred at reflux for an additional 24 h before being quenched with 40 mL saturated brine. The aqueous layer was extracted with 3 x 40 mL dichloromethane, and the combined organic phases were dried over anhydrous sodium sulphate and concentrated in vacuo to yield a yellow oil. Flash-column chromatography afforded compound **150** as a colourless oil (180 mg, 0.508 mmol, 53.5%). Spectral data were consistent with that reported in literature.[118]

^{1}H NMR (300 MHz, $CDCl_3$) δ 5.57 (d, *J* = 7.5 Hz), 5.18 (dd, *J* = 9.1, 0.9 Hz, 1H), 4.15-4.24 (m, 1H), 3.74 (s, 3H), 3.56 (d, *J* = 9.2 Hz, 1H), 3.18 (d, *J* = 6.4 Hz, 1H), 2.42-2.55 (m, 1H), 2.10 (ddd, *J* = 14.4, 7.5, 1.0 Hz, 1H), 1.99 (dt, *J* = 14.1, 2.8 Hz, 1H), 1.53-1.78 (m, 4H), 1.42 (s, 9H), 0.90 (t, *J* = 7.0, 3H), 0.86 (t, *J* = 7.0 Hz, 3H).

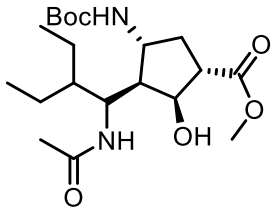

151

Compound **151**. To **150** (17 mg, 0.048 mmol) in 2 mL anhydrous methanol were added concentrated hydrochloric acid (4 µL, 0.048 mmol) and platinum (VI) oxide. The mixture was stirred vigorously at 100 psi hydrogen pressure (Parr reactor) for 24 h. The catalyst was removed by filtration through a minimum amount of celite and the filtrate was concentrated in *vacuo* to give a pale-yellow oil, which was used crude for acetylation.

To the amine hydrochloride in 2 mL anhydrous dichloromethane were added triethylamine (7 µL, 0.05 mmol) and acetic anhydride (5 µL, 0.05 mmol) at room temperature. The mixture was stirred for 2 h and then washed with 10 mL distilled water. The aqueous layer was extracted with 3 x 15 mL dichloromethane, and the combined organic layer was dried over anhydrous sodium sulphate and concentrated in vacuo to yield a colourless oil. Flash-column chromatography afforded compound **151** as a colourless oil (12 mg, 0.031 mmol, 64% over two steps). Spectral data were consistent with that reported in the literature.[118]

^{1}H NMR (300 MHz, $CDCl_3$) δ 7.59 (d, *J* = 9.5 Hz, 1H), 4.72 (d, *J* = 9.4 Hz, 1H), 4.21 (dd, *J* = 4.6, 1.2 Hz, 1H), 4.07-4.15 (m, 1H), 3.96-4.05 (m, 1H), 3.68 (s, 3H), 2.80 (ddd, *J* = 9.0, 8.9, 1.7 Hz, 1H), 2.47 (dt, *J* = 13.7, 7.9 Hz, 1H), 2.07 (s, 3H), 1.96 (dd, *J* = 10.8, 4.3 Hz, 1H), 1.60-1.73 (m, 1H), 1.42 (s, 9H), 1.18-1.30 (m, 6H), 0.83 (t, *J* = 7.0 Hz, 3H), 0.77 (t, *J* = 7.0 Hz, 3H).

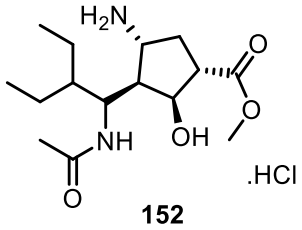

152

Compound **152**. To a solution of **151** (4.9 g, 12.3 mmol) in 250 mL MeOH was added hydrochloric acid (2.0 M aq., 61.3 mL, 123 mmol) at room temperature. The mixture was stirred for 5 h and the solvent was removed in *vacuo* to yield compound **152** as a brown solid. The crude compound was used without any further purifications. (4.0 g, 0.031 mmol, 97%).

^{1}H NMR (300 MHz, $CDCl_3$) δ 4.53 (dd, *J* = 10.2, 2.4 Hz, 1H), 4.37 (dd, *J* = 5.0, 1.2 Hz, 1H), 3.77 (s, 3H), 3.60-3.69 (m, 1H), 3.02 (ddd, *J* = 9.0, 3.0, 2.0 Hz, 1H), 2.56-2.69 (m, 1H), 2.37-2.46 (m, 1H), 2.10 (s, 3H), 1.96-2.01 (m, 1H), 1.43-1.52 (m, 4H), 0.82-1.02 (m, 8H).

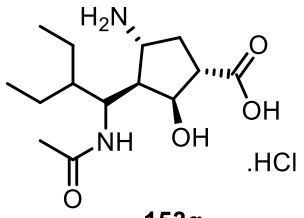

153g

Compound **153g**. To a solution of **152** (100 mg, 0.25 mmol) in MeOH was added LiOH (52.5 mg, 1.25 mmol) at room temperature. The mixture was stirred for 1 h and the solvent was removed in *vacuo*. Then the reaction mixture was dissolved in MeOH again. The resulting solution was added hydrochloric acid (1.0 M aq., 2.5 mL, 2.5 mmol). The mixture was stirred for 1 h and the solvent was removed in *vacuo*. After LCMS purification, compound **153g** was afforded as a while power (63.3 mg, 84%). Spectral data were consistent with that reported in the literature.[120]

^{1}H NMR (300 MHz, D_2O) δ 4.52 (dd, *J* = 5.1, 1.5 Hz, 1H), 4.38 (dd, *J* = 10.5, 2.3 Hz, 1H), 3.61-3.72 (m, 1H), 3.02-3.08 (m, 1H), 2.54-2.77 (m, 1H), 2.36-2.47 (m, 1H), 2.05 (s, 3H) 1.97-2.01 (m, 1H), 1.36-1.57 (m, 4H), 0.82-0.98 (m, 8H). HR-ESIMS calculated for $[M+H]^+$ $C_{14}H_{27}N_2O_4$ 286.1893 Found 287.1962.

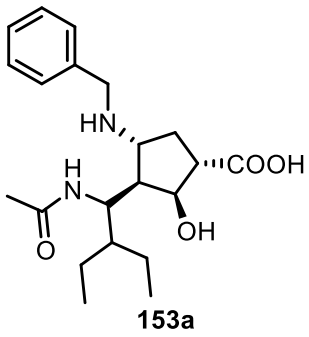

153a

Compound **153a**. Prepared according to general procedure C, using 60 mg **154a** (0.18 mmol), 33.7 mg $NaCNBH_3$ (0.54 mmol), 38.0 mg benzaldehyde (0.36 mmol), 37.8 mg $LiOH.H_2O$ (0.90 mmol). Reverse phase chromatography (LCMS) afforded 4.1 mg of **153a** as a white powder.

^{1}H NMR (300 MHz, CD_3OD) δ 7.22-7.38 (m, 5H), 4.42 (dd, *J* = 11.0, 2.2 Hz, 1H), 4.31 (d, *J* = 4.9 Hz, 1H), 3.06 (td, *J* = 7.5, 3.5 Hz, 1H), 2.69-2.74 (m, 1H), 2.30 (dt, *J* = 13.6, 8.0 Hz, 1H), 2.10-2.19 (m, 1H), 2.05 (dt, *J* = 13.6, 3.0 Hz, 1H), 1.84 (s, 3H), 1.50-1.63 (m, 1H), 1.34-1.48 (m, 2H), 0.89-1.16 (m, 8H). ^{13}C NMR (75 MHz, CD_3OD) δ 182.4, 173.1, 140.4, 129.9, 129.6, 128.3, 77.7, 62.7, 57.5, 53.4, 52.0, 51.2, 45.6, 33.2, 24.5, 22.9, 22.6, 13.0, 12.5; HR-ESIMS calculated for $[M+H]^+$ $C_{21}H_{33}N_2O_4$ 377.2435 Found 377.2433.

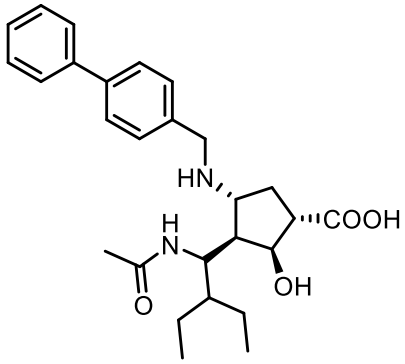

153b

Compound **153b.** Prepared according to general procedure C, using 60 mg **152** (0.18 mmol), 33.7 mg $NaCNBH_3$ (0.54 mmol), 65.5 mg **154b** (0.36 mmol), 37.8 mg $LiOH.H_2O$ (0.90 mmol). Reverse phase chromatography (LCMS) afforded 6.0 mg of **153b** as a white powder.

^1H NMR (300 MHz, CD_3OD) δ 7.58-7.68 (m, 4H), 7.40-7.53 (m, 4H), 7.31-7.38 (m,1H), 4.45 (dd, *J* = 11.2, 1.7 Hz, 1H), 4.34 (d, *J* = 4.9 Hz, 1H), 4.19 (d, *J* = 13.2 Hz, 1H), 3.93 (d, *J* = 13.2 Hz, 1H), 3.32-3.37 (m, 1H), 2.86 (d, *J* = 6.7 Hz, 1H), 2.26-2.43 (m, 2H), 2.17 (d, *J* = 14.2 Hz, 1H), 1.81 (s, 3H), 1.38-1.60 (m, 3H), 0.89-1.08 (m, 8H). ^{13}C NMR (75 MHz, CD_3OD) δ 182.0, 173.3, 142.7, 141.7, 131.1, 129.9, 128.6, 128.0, 77.5, 62.6, 58.6, 51.9, 51.4, 50.7, 45.2, 31.7, 24.5, 22.9, 22.4, 13.1, 12.4; HR-ESIMS calculated for $[M+H]^+$ $C_{27}H_{37}N_2O_4$ 453.2748 Found 453.2745.

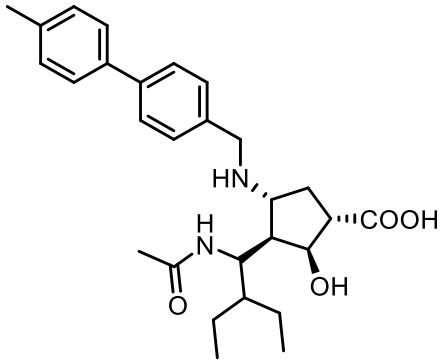

153c

Compound **153c**. Prepared according to general procedure C, using 60 mg **152** (0.18 mmol), 33.7 mg $NaCNBH_3$ (0.54 mmol), 70.0 mg **153c** (0.36 mmol), 37.8 mg $LiOH.H_2O$ (0.90 mmol). Reverse phase chromatography (LCMS) afforded 5.0 mg of **153c** as a white powder.

^1H NMR (300 MHz, CD_3OD) δ 7.66 (d, *J* = 8.1 Hz, 2H), 7.51 (d, *J* = 8.1 Hz, 2H), 7.49 (d, *J* = 8.1 Hz, 2H), 7.26 (d, *J* = 8.1 Hz, 2H), 4.45 (d, *J* = 11.2 Hz, 1H), 4.35 (d, *J* = 4.9 Hz, 1H), 4.27 (d, *J* = 13.2 Hz, 1H), 4.03 (d, *J* = 13.2 Hz, 1H), 3.42 (dd, *J* = 7.5, 5.1 Hz, 1H), 2.92 (d, *J* = 6.2 Hz, 1H), 2.30-2.47 (m, 5H), 2.23 (d, *J* = 14.6 Hz, 1H), 1.77 (s, 3H), 1.38-1.55 (m, 3H), 0.88-1.00 (m, 8H). ^{13}C NMR (75 MHz, CD_3OD) δ 186.4, 173.4, 143.3, 138.9, 138.5, 131.4, 130.7, 128.7, 127.9, 77.4,

62.6, 59.4, 51.9, 50.5, 50.4, 44.9, 30.7, 24.5, 22.9, 22.2, 21.2, 13.2, 12.4; HR-ESIMS calculated for $[M+H]^+$ $C_{28}H_{39}N_2O_4$ 467.2905 Found 467.2904.

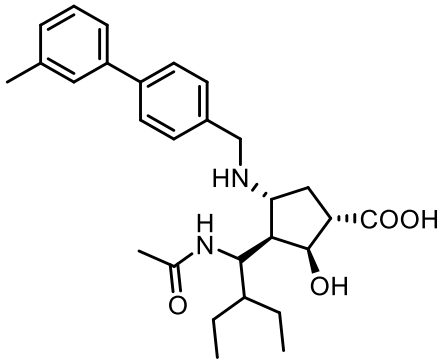

153d

Compound **153d**. Prepared according to general procedure C, using 60 mg **152** (0.18 mmol), 33.7 mg $NaCNBH_3$ (0.54 mmol), 70.0 mg **154d** (0.36 mmol), 37.8 mg $LiOH.H_2O$ (0.90 mmol). Reverse phase chromatography (LCMS) afforded 3.5 mg of **153d** as a white powder.

^{1}H NMR (300 MHz, CD_3OD) δ 7.67 (d, *J* = 8.2 Hz, 2H), 7.50 (d, *J* = 8.2 Hz, 2H), 7.49 (d, *J* = 8.1 Hz, 2H), 7.38-7.44 (m, 2H), 7.32 (t, *J* = 7.4 Hz, 1H), 7.18 (d, *J* = 7.4 Hz, 1H), 4.45 (d, *J* = 11.6 Hz, 1H), 4.35 (d, *J* = 4.8 Hz, 1H), 4.27 (d, *J* = 13.4 Hz, 1H), 4.02 (d, *J* = 13.4 Hz, 1H), 3.42 (dd, *J* = 7.6, 5.3 Hz, 1H), 2.92 (d, *J* = 6.2 Hz, 1H), 2.30-2.46 (m, 5H), 2.23 (d, *J* = 14.6 Hz, 1H), 1.77 (s, 3H), 1.38-1.55 (m, 3H), 0.88-1.05 (m, 8H). ^{13}C NMR (75 MHz, CD_3OD) δ 181.8, 173.4, 143.5, 141.3, 139.8, 132.7, 131.4, 129.9, 129.5, 128.8, 128.6, 127.9, 125.1, 77.3, 62.5, 59.2, 51.9, 50.4, 50.3, 44.9, 30.7, 24.4, 22.8, 22.2, 21.5, 13.1, 12.3; HR-ESIMS calculated for $[M+H]^+$ $C_{28}H_{39}N_2O_4$ 467.2905 Found 467.2904.

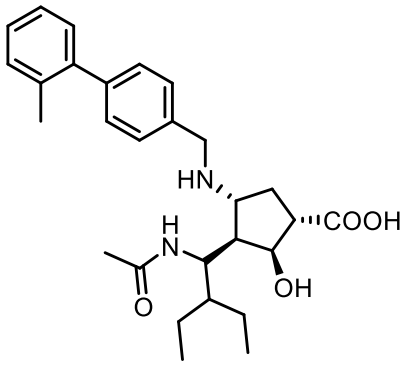

153e

Compound **153e**. Prepared according to general procedure C, using 60 mg **152** (0.18 mmol), 33.7 mg $NaCNBH_3$ (0.54 mmol), 70.0 mg **154e** (0.36 mmol), 37.8 mg $LiOH.H_2O$ (0.90 mmol). Reverse phase chromatography (LCMS) afforded 7.1 mg of **153e** as a white powder.

^{1}H NMR (300 MHz, CD_3OD) δ 7.50 (d, *J* = 8.1 Hz, 2H), 7.36 (d, *J* = 8.1 Hz, 2H), 7.13-7.28 (m, 4H), 4.48 (d, *J* = 11.4 Hz, 1H), 4.35 (d, *J* = 4.6 Hz, 1H), 4.23 (d, *J* = 13.1 Hz, 1H), 3.97 (d, *J* = 13.1 Hz,

1H), 3.34-3.41 (m, 1H), 2.88 (d, *J* = 6.4 Hz, 1H), 2.27-2.45 (m, 2H), 2.16-2.27 (m, 2H), 1.88 (s, 3H), 1.40-1.59 (m, 3H), 0.90-1.10 (m, 8H); ^{13}C NMR (75 MHz, CD_3OD) δ 181.9, 173.3, 144.0, 142.4, 136.2, 134.2, 131.4, 131.0, 130.6, 130.4, 128.6, 126.9, 77.4, 62.9, 58.9, 52.0, 51.2, 50.7, 45.1, 31.3, 24.5, 23.0, 22.4, 20.6, 13.1, 12.4; HR-ESIMS calculated for $[M+H]^+$ $C_{28}H_{39}N_2O_4$ 467.2905 Found 467.2906.

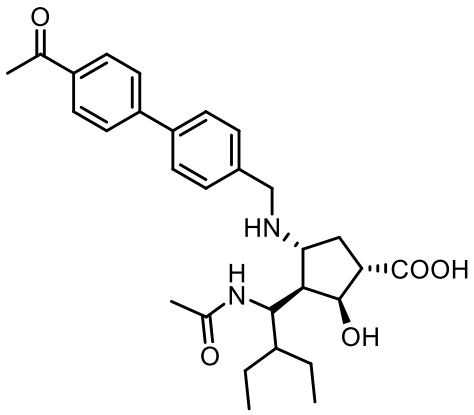

153f

Compound **153f**. Prepared according to general procedure C, using 60 mg **152** (0.18 mmol), 33.7 mg $NaCNBH_3$ (0.54 mmol), 80.0 mg **154f** (0.36 mmol), 37.8 mg $LiOH.H_2O$ (0.90 mmol). Reverse phase chromatography (LCMS) afforded 3.0 mg of **153f** as a white powder.

^{1}H NMR (300 MHz, CD_3OD) δ 8.08 (d, *J* = 8.5 Hz, 2H), 7.78 (d, *J* = 8.5 Hz, 2H), 7.74 (d, *J* = 8.5 Hz, 2H), 7.54 (d, *J* = 8.5 Hz, 2H), 4.44 (dd, *J* = 11.3, 1.8 Hz, 1H), 4.35 (d, *J* = 5.0 Hz, 1H), 4.17 (d, *J* = 13.0 Hz, 1H), 3.92 (d, *J* = 13.0 Hz, 1H), 3.27-3.30 (m, 1H) (hid under solvent peak), 2.84 (d, *J* = 6.4 Hz, 1H), 2.65 (s, 3H), 2.31-2.44 (m, 1H), 2.21-2.31 (m, 1H), 2.16 (d, *J* = 13.9 Hz, 1H), 1.81 (s, 3H), 1.38-1.59 (m, 3H), 0.88-1.10 (m, 8H); ^{13}C NMR (75 MHz, CD_3OD) δ 200.6, 182.0, 173.3, 146.5, 137.5, 131.2, 130.3, 128.9, 128.2, 77.5, 62.6, 58.5, 52.0, 51.4, 50.8, 45.2, 31.7, 24.5, 22.9, 22.4, 13.1, 12.4; HR-ESIMS calculated for $[M+H]^+$ $C_{29}H_{39}N_2O_5$ 495.2854 Found 495.2859.

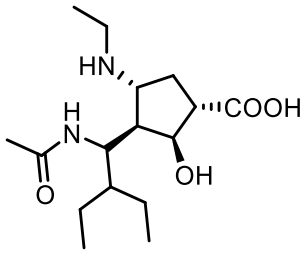

153h

Compound **153h**.Prepared according to general procedure C, using 60 mg **152** (0.18 mmol), 33.7 mg $NaCNBH_3$ (0.54 mmol), 16.0 mg **154h** (0.36 mmol), 37.8 mg $LiOH.H_2O$ (0.90 mmol). Reverse phase chromatography (LCMS) afforded 2.5 mg of **153h** as a white powder.

^{1}H NMR (300 MHz, MeOD) δ 4.50 (dd, *J* = 11.4, 1.8 Hz, 1H), 4.33 (d, *J* = 5.0 Hz, 1H), 3.33-3.37 (m, 1H) (hid under solvent peak), 3.06 (dq, *J* = 12.3, 7.5 Hz, 1H), 2.82-2.95 (m, 2H), 2.24-2.40 (m, 2H), 1.97-2.07 (m, 4H), 1.42-1.59 (m, 3H), 1.25 (t, *J* = 7.1 Hz, 1H), 0.88-1.05 (m, 8H); ^{13}C NMR (75 MHz, MeOD) δ 181.7, 173.5, 77.4, 62.6, 59.1, 52.0, 44.8, 42.1, 31.2, 24.5, 23.0, 22.3, 13.2, 12.5, 12.3; HR-ESIMS calculated for $[M+H]^+$ $C_{16}H_{31}N_2O_4$ 315.2279 Found 315.2279

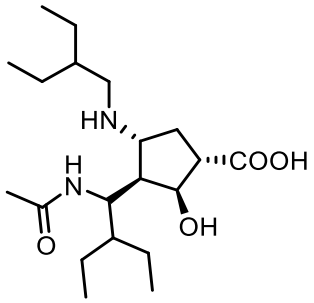

153i

Prepared according to general procedure C, using 60 mg **152** (0.18 mmol), 33.7 mg $NaCNBH_3$ (0.54 mmol), 36.0 mg **154i** (0.36 mmol), 37.8 mg $LiOH.H_2O$ (0.90 mmol). Reverse phase chromatography (LCMS) afforded 4.5 mg of **153i** as a white powder.

^{1}H NMR (300 MHz, CD_3OD) δ 4.48 (dd, *J* = 11.7, 1.5 Hz, 1H), 4.33 (d, *J* = 4.9 Hz, 1H), 3.37 (dd, *J* = 7.9, 5.1 Hz, 1H), 2.94 (dd, *J* = 12.6, 7.2 Hz, 1H), 2.88 (d, *J* = 6.2 Hz, 1H), 2.77 (dd, *J* = 12.6, 7.2 Hz, 1H), 2.30-2.45 (m, 2H), 2.00-2.08 (m, 4H), 1.35-1.63 (m, 8H), 0.89-1.08 (m, 14H). ^{13}C NMR (75 MHz, CD_3OD) δ 181.6, 173.4, 77.3, 64.5, 59.2, 51.2, 50.8, 50.7, 44.8, 40.4, 31.3, 24.5, 24.4, 24.2, 23.0, 22.3, 13.1, 12.3, 11.0, 10.6; HR-ESIMS calculated for $[M+H]^+$ $C_{20}H_{39}N_2O_4$ 371.2905 Found 371.2900.

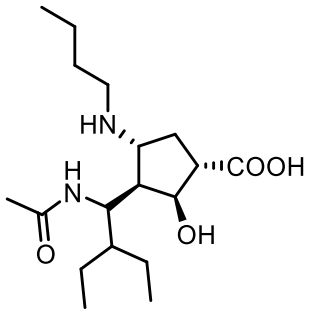

153i

Compound **153i**. Prepared according to general procedure C, using 60 mg **152** (0.18 mmol), 33.7 mg $NaCNBH_3$ (0.54 mmol), 26.0 mg **154i** (0.36 mmol), 37.8 mg $LiOH.H_2O$ (0.90 mmol). Reverse phase chromatography (LCMS) afforded 3.4 mg of **153i** as a white powder.

^{1}H NMR (300 MHz, CD_3OD) δ 4.50 (d, *J* = 11.4 Hz, 1H), 4.34 (d, *J* = 5.0 Hz, 1H), 3.33-3.37 (m, 1H) (hid under solvent peak), 2.90-3.06 (m, 1H), 2.79-2.92 (m, 2H), 2.24-2.40 (m, 2H), 2.18-2.43 (m, 2H), 1.92-2.07 (m, 4H), 1.29-1.67 (m, 7H), 0.88-1.05 (m, 11H); ^{13}C NMR (75 MHz, CD_3OD) δ 181.7, 173.4, 77.4, 63.3, 59.0, 52.1, 50.7, 44.9, 31.5, 30.6, 24.5, 23.0, 22.3, 21.0 ,14.0, 13.1 , 12.3; HR-ESIMS calculated for $[M+H]^+$ $C_{18}H_{35}N_2O_4$ 343.2592 Found 343.2591.

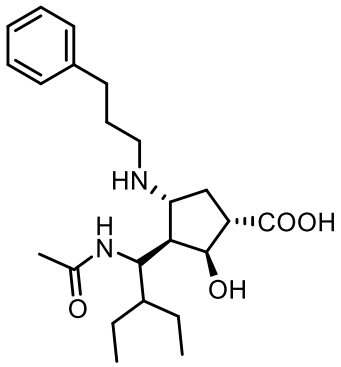

153j

Compound **153j**. Prepared according to general procedure C, using 60 mg **152** (0.18 mmol), 33.7 mg $NaCNBH_3$ (0.54 mmol), 53.6 mg **154j** (0.36 mmol), 37.8 mg $LiOH.H_2O$ (0.90 mmol). Reverse phase chromatography (LCMS) afforded 3.7 mg of **153j** as a white powder.

^{1}H NMR (300 MHz, CD_3OD) δ 7.20-7.32 (m, 5H), 4.48 (dd, *J* = 11.6, 1.3 Hz, 1H), 4.32 (d, *J* = 4.8 Hz, 1H), 3.30-3.35 (m, 1H) (hid under solvent peak), 2.77-3.04 (m, 3H), 2.68-2.75 (m, 2H), 2.23-2.36 (m, 2H), 1.99 (d, *J* = 13.8, 1.3 Hz, 1H), 1.91 (s, 3H), 1.43-1.56 (m, 3H), 1.25-1.38 (m, 2H), 0.88-1.08 (m, 10H); ^{13}C NMR (75 MHz, CD_3OD) δ 181.6, 173.4, 142.0, 129.6, 129.5, 127.3, 77.4, 63.4, 59.1, 52.0, 50.6, 46.9, 44.8, 33.6, 31.4, 30.1 ,24.5, 23.0 , 13.2, 12.3; HR-ESIMS calculated for $[M+H]^+$ $C_{23}H_{36}N_2O_4$ 405.2748 Found 405.2748.

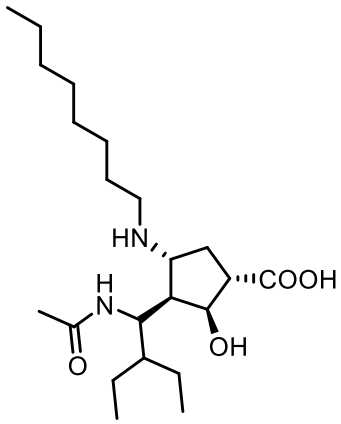

153k

Compound **153k**. Prepared according to general procedure C, using 60 mg **152** (0.18 mmol), 33.7 mg $NaCNBH_3$ (0.54 mmol), 46.0 mg **154k** (0.36 mmol), 37.8 mg $LiOH.H_2O$ (0.90 mmol). Reverse phase chromatography (LCMS) afforded 4.5 mg of **153k** as a white powder.

^1H NMR (300 MHz, CD_3OD) δ 4.49 (dd, *J* = 11.6, 1.4 Hz, 1H), 4.33 (d, *J* = 4.9 Hz, 1H), 3.30-3.35 (m, 1H) (hid under solvent peak), 2.92-3.03 (m, 3H), 2.76-2.88 (m, 2H), 2.23-2.40 (m, 2H), 1.96-2.07 (m, 4H), 1.25-1.78 (m, 16H), 0.88-1.08 (m, 11H); ^{13}C NMR (75 MHz, CD_3OD) δ 181.7, 173.4, 77.4, 63.3, 59.0, 52.1, 50.7, 47.7, 44.8, 32.9, 31.3, 30.3, 30.2, 28.4, 27.8, 24.5, 23.7, 23.0, 22.3, 14.4, 13.1, 12.3; HR-ESIMS calculated for $[M+H]^+$ $C_{22}H_{43}N_2O_4$ 399.3218 Found 399.3218.

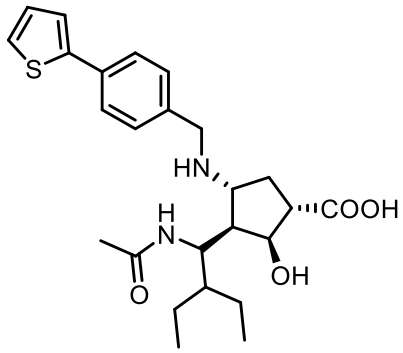

153m

Compound **153m**. Prepared according to general procedure C, using 60 mg **152** (0.18 mmol), 33.7 mg $NaCNBH_3$ (0.54 mmol), 67.7 mg **154m** (0.36 mmol), 37.8 mg $LiOH.H_2O$ (0.90 mmol). Reverse phase chromatography (LCMS) afforded 3.0 mg of **153m** as a white powder.

^1H NMR (300 MHz, CD_3OD) δ 7.65 (d, *J* = 8.2 Hz, 2H), 7.36-7.45 (m, 4H), 7.09 (dd, *J* = 5.3, 3.8 Hz, 1H), 4.48 (dd, *J* = 11.4, 1.8 Hz, 1H), 4.33 (d, *J* = 5.0 Hz, 1H), 4.09 (d, *J* = 13.0 Hz, 1H), 3.82 (d, *J* = 13.0 Hz, 1H), 3.22-3.28 (m, 1H), 2.82 (d, *J* = 6.7 Hz, 1H), 2.29-2.41 (m, 1H), 2.19-2.29 (m, 1H), 2.15 (d, *J* = 13.8 Hz, 1H), 1.83 (s, 3H), 1.38-1.59 (m, 3H), 0.90-1.10 (m, 8H); ^{13}C NMR (75 MHz, CD_3OD) δ 182.1, 173.2, 144.7, 135.8, 131.1, 129.2, 127.2, 126.2, 124.6, 77.5, 62.6, 58.5, 52.0, 51.6, 50.8, 45.3, 31.9, 24.5, 22.9, 22.4, 13.1, 12.4; HR-ESIMS calculated for $[M+H]^+$ $C_{25}H_{35}N_2O_4S$ 459.2312 Found 459.2314.

Bibliography

(1) Thiele, J. *Ber. Dtsch. Chem.* **1901**, *34*, 68.
(2) Ziegler, K.; Froitzheim-Kühlhorn, H.; Hafner, K. *Chem. Ber.* **1956**, *89*, 434.
(3) Top, S.; Lehn, J.-S.; Morel, P.; Jaouen, G. *J. Organomet. Chem.* **1999**, *583*, 63.
(4) Courtot, C. *Ann. Chim. Appl* **1915**, *4*, 68.
(5) Marchand, A. P.; Namboothiri, I. N. N.; Lewis, S. B.; Watson, W. H.; Krawiec, M. *Tetrahedron* **1998**, *54*, 12691.
(6) Finnegan, R. A.; McNees, R. S. *J. Org. Chem.* **1964**, *29*, 3234.
(7) Minter, D. E.; Smith, W. B.; Marchand, A. P.; Etukala, J. R.; Sivappa, R. *J. Phys. Org. Chem.* **2004**, *17*, 174.
(8) Peters, D. *J. Chem. Soc.* **1959**, 1761.
(9) Dive, G.; Robiette, R.; Chenel, A.; Ndong, M.; Meier, C.; Desouter-Lecomte, M. *Theor. Chem. Acc.* **2012**, *131*, 1236.
(10) Dunn, G. L.; Donohue, J. K. *Tetrahedron Lett.* **1968**, *9*, 3485.
(11) (a) Corey, E. J. *Angew. Chem. Int. Ed.* **2002**, *41*, 1650; (b) Nicolaou, K. C.; Snyder, S. A.; Montagnon, T.; Vassilikogiannakis, G. *Angew. Chem. Int. Ed.* **2002**, *41*, 1668.
(12) (a) Fleming, I. In *Molecular Orbitals and Organic Chemical Reactions*; John Wiley & Sons, Ltd: 2010, p 253; (b) Deslongchamps, G.; Deslongchamps, P. *Tetrahedron* **2013**, *69*, 6022; (c) Spino, C.; Rezaei, H.; Dory, Y. L. *J. Org. Chem.* **2004**, *69*, 757; (d) Spino, C.; Pesant, M.; Dory, Y. *Angew. Chem. Int. Ed.* **1998**, *37*, 3262.
(13) Fukui, K.; Yonezawa, T.; Shingu, H. *The Journal of Chemical Physics* **1952**, *20*, 722.
(14) Fukui, K. *Acc. Chem. Res.* **1971**, *4*, 57.
(15) Houk, K. N. *J. Am. Chem. Soc.* **1973**, *95*, 4092.
(16) (a) Hoffmann, R.; Woodward, R. B. *J. Am. Chem. Soc.* **1965**, *87*, 2046; (b) Salem, L. *J. Am. Chem. Soc.* **1968**, *90*, 553; (c) Woodward, R. B.; Katz, T. J. *Tetrahedron* **1959**, *5*, 70.
(17) (a) Pauling, L. *J. Am. Chem. Soc.* **1931**, *53*, 1367; (b) Schultz, P. A.; Messmer, R. P. *J. Am. Chem. Soc.* **1993**, *115*, 10925; (c) Squillacote, M. E.; Sheridan, R. S.; Chapman, O. L.; Anet, F. A. L. *J. Am. Chem. Soc.* **1979**, *101*, 3657; (d) Loncharich, R. J.; Brown, F. K.; Houk, K. N. *J. Org. Chem.* **1989**, *54*, 1129; (e) Deslongchamps, G.; Deslongchamps, P. *Org. Biomol. Chem.* **2011**, *9*, 5321.
(18) (a) Alder, K.; Flock, F. H.; Hausweiler, A.; Reeber, R. *Chem. Ber.* **1954**, *87*, 1752; (b) Chen, J.; Burns, F. P.; Moffitt, M. G.; Wulff, J. E. *ACS Omega* **2016**, *1*, 532.
(19) (a) Spino, C.; Crawford, J. *Can. J. Chem.* **1993**, *71*, 1094; (b) Spino, C.; Crawford, J.; Cui, Y.; Gugelchuk, M. *J. Chem. Soc., Perkin Trans. 2* **1998**, 1499; (c) Inukai, T.; Kojima, T. *J. Org. Chem.* **1971**, *36*, 924.
(20) Brown, R. D. *J. Chem. Soc.* **1950**, 691.
(21) Dewar, M. J. S.; Olivella, S.; Stewart, J. J. P. *J. Am. Chem. Soc.* **1986**, *108*, 5771.
(22) Rúnarsson, Ö. V.; Artacho, J.; Wärnmark, K. *Eur. J. Org. Chem.* **2012**, *2012*, 7015.
(23) Adrian, J. C.; Wilcox, C. S. *J. Am. Chem. Soc.* **1989**, *111*, 8055.
(24) Hansson, A. P.; Norrby, P.-O.; Wärnmark, K. *Tetrahedron Lett.* **1998**, *39*, 4565.
(25) Cowart, M. D.; Sucholeiki, I.; Bukownik, R. R.; Wilcox, C. S. *J. Am. Chem. Soc.* **1988**, *110*, 6204.
(26) Whiting, A. L.; Dubicki, K. I.; Hof, F. *Eur. J. Org. Chem.* **2013**, *2013*, 6802.
(27) Paliwal, S.; Geib, S.; Wilcox, C. S. *J. Am. Chem. Soc.* **1994**, *116*, 4497.
(28) Yu-Mei, S.; Mei-Xin, Z.; Jiaxi, X.; Yian, S. *Angew. Chem. Int. Ed.* **2006**, *45*, 8005.

(29) Tatibouet, A.; Demeunynck, M.; Andraud, C.; Collet, A.; Lhomme, J. *Chem. Commun.* **1999**, 161.
(30) Top, S.; Tang, J.; Vessieres, A.; Carrez, D.; Provot, C.; Jaouen, G. *Chem. Commun.* **1996**, 955.
(31) (a) Liu, Y.; Spingler, B.; Schmutz, P.; Alberto, R. *J. Am. Chem. Soc.* **2008**, *130*, 1554; (b) Wald, J.; Alberto, R.; Ortner, K.; Candreia, L. *Angew. Chem. Int. Ed.* **2001**, *40*, 3062.
(32) Dhingra, K. *Invest. New Drugs* **1999**, *17*, 285.
(33) Jaouen, G.; Top, S.; Vessieres, A.; Pigeon, P.; Leclercq, G.; Laios, I. *Chem. Commun.* **2001**, 383.
(34) Can, D.; Spingler, B.; Schmutz, P.; Mendes, F.; Raposinho, P.; Fernandes, C.; Carta, F.; Innocenti, A.; Santos, I.; Supuran, C. T.; Alberto, R. *Angew. Chem. Int. Ed.* **2012**, *51*, 3354.
(35) Streib, M.; Kräling, K.; Richter, K.; Xie, X.; Steuber, H.; Meggers, E. *Angew. Chem. Int. Ed.* **2014**, *53*, 305.
(36) Sulieman, S.; Can, D.; Mertens, J.; N'Dongo, H. W. P.; Liu, Y.; Schmutz, P.; Bauwens, M.; Spingler, B.; Alberto, R. *Organometallics* **2012**, *31*, 6880.
(37) Chen, X.; Dam, M. A.; Ono, K.; Mal, A.; Shen, H.; Nutt, S. R.; Sheran, K.; Wudl, F. *Science* **2002**, *295*, 1698.
(38) (a) Mercier, C.; Soucy, P.; Rosen, W.; Deslongchamps, P. *Synth. Commun.* **1973**, *3*, 161; (b) Russo, R.; Lambert, Y.; Deslongchamps, P. *Can. J. Chem.* **1971**, *49*, 531; (c) Deslongchamps, P.; Cheriyan, U. O.; Lambert, Y.; Mercier, J.-C.; Ruest, L.; Russo, R.; Soucy, P. *Can. J. Chem.* **1978**, *56*, 1687.
(39) Steed, J. W.; Atwood, J. L. In *Supramolecular Chemistry*; John Wiley & Sons, Ltd: 2009, p 1.
(40) Davis, A. M.; Teague, S. J. *Angew. Chem. Int. Ed.* **1999**, *38*, 736.
(41) Kassem, S.; van Leeuwen, T.; Lubbe, A. S.; Wilson, M. R.; Feringa, B. L.; Leigh, D. A. *Chem. Soc. Rev.* **2017**, *46*, 2592.
(42) Koumura, N.; Zijlstra, R. W. J.; van Delden, R. A.; Harada, N.; Feringa, B. L. *Nature* **1999**, *401*, 152.
(43) Feringa, B. L. *Angew. Chem. Int. Ed.* **2017**, *56*, 11060.
(44) Jellema, E.; Budzelaar, P. H. M.; Reek, J. N. H.; de Bruin, B. *J. Am. Chem. Soc.* **2007**, *129*, 11631.
(45) (a) Miller, T. M.; Izumi, A. N.; Shih, Y. S.; Whitesides, G. M. *J. Am. Chem. Soc.* **1988**, *110*, 3146; (b) Bennett, M. A.; McMahon, I. J.; Pelling, S.; Robertson, G. B.; Wickramasinghe, W. A. *Organometallics* **1985**, *4*, 754.
(46) (a) Champness, N. R. *Nat. Mater.* **2017**, *16*, 283; (b) Yang, D.; Gates, B. C. *Nat. Mater.* **2017**, *advance online publication*; (c) Noro, S.-I.; Nakamura, T. *NPG Asia Mater.* **2017**, *9*, e433; (d) Gallagher, J. **2016**, *1*, 16167; (e) Yi, F.-Y.; Chen, D.; Wu, M.-K.; Han, L.; Jiang, H.-L. *ChemPlusChem* **2016**, *81*, 675; (f) Huang, Y.-B.; Liang, J.; Wang, X.-S.; Cao, R. *Chem. Soc. Rev.* **2017**, *46*, 126.
(47) Lu, W.; Wei, Z.; Gu, Z.-Y.; Liu, T.-F.; Park, J.; Park, J.; Tian, J.; Zhang, M.; Zhang, Q.; Gentle Iii, T.; Bosch, M.; Zhou, H.-C. *Chem. Soc. Rev.* **2014**, *43*, 5561.
(48) Cook, T. R.; Zheng, Y.-R.; Stang, P. J. *Chem. Rev.* **2013**, *113*, 734.
(49) Peindy N'Dongo, H. W.; Liu, Y.; Can, D.; Schmutz, P.; Spingler, B.; Alberto, R. *J. Organomet. Chem.* **2009**, *694*, 981.
(50) (a) Chen, B.; Eddaoudi, M.; Reineke, T. M.; Kampf, J. W.; O'Keeffe, M.; Yaghi, O. M. *J. Am. Chem. Soc.* **2000**, *122*, 11559; (b) Fang, Q.; Zhu, G.; Xue, M.; Sun, J.; Tian, G.; Wu, G.; Qiu, S. *Dalton Trans.* **2004**, 2202.
(51) Vervacke, D. *An Introduction to PDCPD*; Product Rescue, 2008.
(52) Brant, M. G.; Wulff, J. E. *Org. Lett.* **2012**, *14*, 5876.
(53) Chen, J.; Kilpatrick, B.; Oliver, A. G.; Wulff, J. E. *J. Org. Chem.* **2015**, *80*, 8979.
(54) Chen, J.; Sun, X.; Oliver, A. G.; Wulff, J. E. *Can. J. Chem.* **2017**, *95*, 234.

(55) Murphy, E. B.; Bolanos, E.; Schaffner-Hamann, C.; Wudl, F.; Nutt, S. R.; Auad, M. L. *Macromolecules* **2008**, *41*, 5203.
(56) (a) Chen, C. W.; Whitlock, H. W. *J. Am. Chem. Soc.* **1978**, *100*, 4921; (b) Rebek, J. *Angew. Chem. Int. Ed. Engl.* **1990**, *29*, 245; (c) Klärner, F.-G.; Panitzky, J.; Bläser, D.; Boese, R. *Tetrahedron* **2001**, *57*, 3673.
(57) William H. Watson; Alan P. Marchand; Sivappa, a. R. *ARKIVOC* **2004**, *iii*.
(58) Shie, J.-J.; Fang, J.-M.; Wang, S.-Y.; Tsai, K.-C.; Cheng, Y.-S. E.; Yang, A.-S.; Hsiao, S.-C.; Su, C.-Y.; Wong, C.-H. *J. Am. Chem. Soc.* **2007**, *129*, 11892.
(59) (a) Mooney, C. A.; Johnson, S. A.; 't Hart, P.; Quarles van Ufford, L.; de Haan, C. A. M.; Moret, E. E.; Martin, N. I. *J. Med. Chem.* **2014**, *57*, 3154; (b) Stoll, V.; Stewart, K. D.; Maring, C. J.; Muchmore, S.; Giranda, V.; Gu, Y.-g. Y.; Wang, G.; Chen, Y.; Sun, M.; Zhao, C.; Kennedy, A. L.; Madigan, D. L.; Xu, Y.; Saldivar, A.; Kati, W.; Laver, G.; Sowin, T.; Sham, H. L.; Greer, J.; Kempf, D. *Biochemistry* **2003**, *42*, 718.
(60) (a) Collins, P. J.; Haire, L. F.; Lin, Y. P.; Liu, J.; Russell, R. J.; Walker, P. A.; Skehel, J. J.; Martin, S. R.; Hay, A. J.; Gamblin, S. J. *Nature* **2008**, *453*, 1258; (b) Gubareva, L. V.; Sleeman, K.; Guo, Z.; Yang, H.; Hodges, E.; Davis, C. T.; Baranovich, T.; Stevens, J. *J. Infect. Dis.* **2017**, *216*, S566.
(61) (a) Wilen, S. H.; Qi, J. Z.; Williard, P. G. *J. Org. Chem.* **1991**, *56*, 485; (b) Allen, P. R.; Reek, J. N. H.; Try, A. C.; Crossley, M. J. *Tetrahedron: Asymmetry* **1997**, *8*, 1161; (c) Jameson, D. L.; Field, T.; Schmidt, M. R.; DeStefano, A. K.; Stiteler, C. J.; Venditto, V. J.; Krovic, B.; Hoffman, C. M.; Ondisco, M. T.; Belowich, M. E. *J. Org. Chem.* **2013**, *78*, 11590; (d) Rúnarsson, Ö. V.; Benkhäuser, C.; Christensen, N. J.; Ruiz, J. A.; Ascic, E.; Harmata, M.; Snieckus, V.; Rissanen, K.; Fristrup, P.; Lützen, A.; Wärnmark, K. *J. Org. Chem.* **2015**, *80*, 8142.
(62) Chen, J.; Wulff, J. E. *Org. Biomol. Chem.* **2016**, *14*, 10170.
(63) Chen, J.; Lu, L.; Wulff, J. E. *Synlett* **2017**, *28*, 2777.
(64) Fleming, I. *Frontier Orbitals and Organic Chemical Reactions: student Edition*; John Wiley & Sons, 2009.
(65) (a) Hartke, K.; Jung, M. H.; Zerbe, H.; Kämpchen, T. *Annalen* **1986**, *1986*, 1268; (b) Bridges, A. J.; Fischer, J. W. *J. Chem. Soc., Perkin Trans. 1* **1983**, 2359.
(66) Peters, D. *J. Chem. Soc.* **1961**, 1037.
(67) Wulff, J. E.; Chen, J.; Burns, F. P.; Moffitt, M. G., Provisional U.S. Patent No. 62/347,446 & No. 62/297,567
(68) Cuthbert, T. J.; Chen, J.; Burns, F. P.; Moffitt, M. G.; Wulff, J. E. *ACS Omega* **2017**, *2*, 2593.
(69) (a) Mol, J. C. *J. Mol. Catal. A: Chem.* **2004**, *213*, 39; (b) Kovacic, S.; Jerabek, K.; Krajnc, P.; Slugovc, C. *Polym. Chem.* **2012**, *3*, 325; (c) White, S. R.; Sottos, N. R.; Geubelle, P. H.; Moore, J. S.; Kessler, M. R.; Sriram, S. R.; Brown, E. N.; Viswanathan, S. *Nature* **2001**, *409*, 794.
(70) (a) Autenrieth, B.; Jeong, H.; Forrest, W. P.; Axtell, J. C.; Ota, A.; Lehr, T.; Buchmeiser, M. R.; Schrock, R. R. *Macromolecules* **2015**, *48*, 2480; (b) Davidson, T. A.; Wagener, K. B. *J. Mol. Catal. A: Chem.* **1998**, *133*, 67; (c) Grubbs, R. H.; Gilliom, L. R., U.S. Patent No. 4,607,112; (d) Pacreau, A.; Fontanille, M. *Makromol. Chem.* **1987**, *188*, 2585; (e) Rule, J. D.; Moore, J. S. *Macromolecules* **2002**, *35*, 7878.
(71) Goetz, A. E.; Boydston, A. J. *J. Am. Chem. Soc.* **2015**, *137*, 7572.
(72) (a) Knall, A.-C.; Kovacic, S.; Hollauf, M.; Reishofer, D.; Saf, R.; Slugovc, C. *Chem. Commun.* **2013**, *49*, 7325; (b) Kovacic, S.; Krajnc, P.; Slugovc, C. *Chem. Commun.* **2010**, *46*, 7504.
(73) Perring, M.; Bowden, N. B. *Langmuir* **2008**, *24*, 10480.
(74) Perring, M.; Long, T. R.; Bowden, N. B. *J. Mater. Chem.* **2010**, *20*, 8679.
(75) Rosenblum, M. *J. Am. Chem. Soc.* **1957**, *79*, 3179.

(76) (a) Gong, L.; Liu, K.; Ou, E.; Xu, F.; Lu, Y.; Wang, Z.; Gao, T.; Yang, Z.; Xu, W. *RSC Adv.* **2015**, *5*, 26185; (b) Saha, S.; Ginzburg, Y.; Rozenberg, I.; Iliashevsky, O.; Ben-Asuly, A.; Gabriel Lemcoff, N. *Polym. Chem.* **2016**, *7*, 3071.
(77) Hejl, A.; Scherman, O. A.; Grubbs, R. H. *Macromolecules* **2005**, *38*, 7214.
(78) Surburg, H.; Panten, J. *Common Fragrance and Flavor Materials*; Wiley-VCH, 2006.
(79) Chatterjee, A. K.; Choi, T.-L.; Sanders, D. P.; Grubbs, R. H. *J. Am. Chem. Soc.* **2003**, *125*, 11360.
(80) (a) Walling, C.; Briggs, E. R. *J. Am. Chem. Soc.* **1946**, *68*, 1141; (b) Stickler, M.; Meyerhoff, G. *Makromol. Chem.* **1978**, *179*, 2729; (c) Srinivasan, S.; Lee, M. W.; Grady, M. C.; Soroush, M.; Rappe, A. M. *J. Phys. Chem. A* **2011**, *115*, 1125.
(81) Mathias, L. J.; Lewis, C. M.; Wiegel, K. N. *Macromolecules* **1997**, *30*, 5970.
(82) Franklin, W. E. *J. Org. Chem.* **1970**, *35*, 1794.
(83) Yang, Y.-S.; Lafontaine, E.; Mortaigne, B. *J. Appl. Polym. Sci.* **1996**, *60*, 2419.
(84) Vidavsky, Y.; Navon, Y.; Ginzburg, Y.; Gottlieb, M.; Lemcoff, N. G. *Beilstein J. Org. Chem.* **2015**, *11*, 1469.
(85) Kwok, D. Y.; Neumann, A. W. *Adv. Colloid Interface Sci.* **1999**, *81*, 167.
(86) Lučić, B.; Trinajstić, N. *J. Chem. Inf. Comput. Sci.* **1999**, *39*, 121.
(87) Taylor, N. R.; von Itzstein, M. *J. Med. Chem.* **1994**, *37*, 616.
(88) Miyagi, T.; Wada, T.; Yamaguchi, K.; Shiozaki, K.; Sato, I.; Kakugawa, Y.; Yamanami, H.; Fujiya, T. *PROTEOMICS* **2008**, *8*, 3303.
(89) Galen, J. E.; Ketley, J. M.; Fasano, A.; Richardson, S. H.; Wasserman, S. S.; Kaper, J. B. *Infection and Immunity* **1992**, *60*, 406.
(90) Xu, G.; Kiefel, M. J.; Wilson, J. C.; Andrew, P. W.; Oggioni, M. R.; Taylor, G. L. *J. Am. Chem. Soc.* **2011**, *133*, 1718.
(91) Hata, K.; Koseki, K.; Yamaguchi, K.; Moriya, S.; Suzuki, Y.; Yingsakmongkon, S.; Hirai, G.; Sodeoka, M.; von Itzstein, M.; Miyagi, T. *Antimicrobial Agents and Chemotherapy* **2008**, *52*, 3484.
(92) Yoon, S.-W.; Webby, R.; Webster, R. In *Influenza Pathogenesis and Control - Volume I*; Compans, R. W., Oldstone, M. B. A., Eds.; Springer International Publishing: 2014; Vol. 385, p 359.
(93) Hilleman, M. R. *Vaccine* **2002**, *20*, 3068.
(94) McKimm-Breschkin, J. L. *Influenza and Other Respiratory Viruses* **2013**, *7*, 25.
(95) Russell, R. J.; Kerry, P. S.; Stevens, D. J.; Steinhauer, D. A.; Martin, S. R.; Gamblin, S. J.; Skehel, J. J. *Proc. Natl. Acad. Sci. U.S.A.* **2008**, *105*, 17736.
(96) Sui, J.; Hwang, W. C.; Perez, S.; Wei, G.; Aird, D.; Chen, L.-m.; Santelli, E.; Stec, B.; Cadwell, G.; Ali, M.; Wan, H.; Murakami, A.; Yammanuru, A.; Han, T.; Cox, N. J.; Bankston, L. A.; Donis, R. O.; Liddington, R. C.; Marasco, W. A. *Nat. Struct. Mol. Biol.* **2009**, *16*, 265.
(97) (a) Tong, S.; Zhu, X.; Li, Y.; Shi, M.; Zhang, J.; Bourgeois, M.; Yang, H.; Chen, X.; Recuenco, S.; Gomez, J.; Chen, L.-M.; Johnson, A.; Tao, Y.; Dreyfus, C.; Yu, W.; McBride, R.; Carney, P. J.; Gilbert, A. T.; Chang, J.; Guo, Z.; Davis, C. T.; Paulson, J. C.; Stevens, J.; Rupprecht, C. E.; Holmes, E. C.; Wilson, I. A.; Donis, R. O. *PLoS Pathog.* **2013**, *9*, e1003657; (b) Fouchier, R. A. M.; Munster, V.; Wallensten, A.; Bestebroer, T. M.; Herfst, S.; Smith, D.; Rimmelzwaan, G. F.; Olsen, B.; Osterhaus, A. D. M. E. *J. Virol.* **2005**, *79*, 2814.
(98) Russell, R. J.; Haire, L. F.; Stevens, D. J.; Collins, P. J.; Lin, Y. P.; Blackburn, G. M.; Hay, A. J.; Gamblin, S. J.; Skehel, J. J. *Nature* **2006**, *443*, 45.
(99) (a) WHO.int. *Cumulative number of confirmed human cases for avian influenza A(H5N1) reported to WHO, 2003-2014* **2014**; (b) Donaldson, L. J.; Rutter, P. D.; Ellis, B. M.; Greaves, F. E. C.; Mytton, O. T.; Pebody, R. G.; Yardley, I. E. *BMJ* **2009**, *339*, b5213; (c) Li, Q.; Zhou, L.; Zhou, M.;

Chen, Z.; Li, F.; Wu, H.; Xiang, N.; Chen, E.; Tang, F.; Wang, D.; Meng, L.; Hong, Z.; Tu, W.; Cao, Y.; Li, L.; Ding, F.; Liu, B.; Wang, M.; Xie, R.; Gao, R.; Li, X.; Bai, T.; Zou, S.; He, J.; Hu, J.; Xu, Y.; Chai, C.; Wang, S.; Gao, Y.; Jin, L.; Zhang, Y.; Luo, H.; Yu, H.; He, J.; Li, Q.; Wang, X.; Gao, L.; Pang, X.; Liu, G.; Yan, Y.; Yuan, H.; Shu, Y.; Yang, W.; Wang, Y.; Wu, F.; Uyeki, T. M.; Feng, Z. *N. Engl. J. Med.* **2014**, *370*, 520.

(100) WHO.int. *Summary of neuraminidase amino acid substitutions associated with reduced inhibition by neuraminidase inhibitors (NAI)*, 2016.

(101) Varghese, J. N.; Epa, V. C.; Colman, P. M. *Protein Sci* **1995**, *4*, 1081.

(102) (a) Russell, R. J.; Haire, L. F.; Stevens, D. J.; Collins, P. J.; Lin, Y. P.; Blackburn, G. M.; Hay, A. J.; Gamblin, S. J.; Skehel, J. J. *Nature* **2006**, *443*, 45; (b) Wu, Y.; Bi, Y.; Vavricka, C. J.; Sun, X.; Zhang, Y.; Gao, F.; Zhao, M.; Xiao, H.; Qin, C.; He, J.; Liu, W.; Yan, J.; Qi, J.; Gao, G. F. *Cell Res.* **2013**, *23*, 1347.

(103) Varghese, J. N.; Laver, W. G.; Colman, P. M. *Nature* **1983**, *303*, 35.

(104) Shidmoossavee, F. S.; Watson, J. N.; Bennet, A. J. *J. Am. Chem. Soc.* **2013**, *135*, 13254.

(105) Chan, J.; Lewis, A. R.; Gilbert, M.; Karwaski, M.-F.; Bennet, A. J. *Nat. Chem. Biol.* **2010**, *6*, 405.

(106) Atigadda, V. R.; Brouillette, W. J.; Duarte, F.; Babu, Y. S.; Bantia, S.; Chand, P.; Chu, N.; Montgomery, J. A.; Walsh, D. A.; Sudbeck, E.; Finley, J.; Air, G. M.; Luo, M.; Laver, G. W. *Biorg. Med. Chem.* **1999**, *7*, 2487.

(107) Kim, C. U.; Lew, W.; Williams, M. A.; Liu, H.; Zhang, L.; Swaminathan, S.; Bischofberger, N.; Chen, M. S.; Mendel, D. B.; Tai, C. Y.; Laver, W. G.; Stevens, R. C. *J. Am. Chem. Soc.* **1997**, *119*, 681.

(108) Babu, Y. S.; Chand, P.; Bantia, S.; Kotian, P.; Dehghani, A.; El-Kattan, Y.; Lin, T.-H.; Hutchison, T. L.; Elliott, A. J.; Parker, C. D.; Ananth, S. L.; Horn, L. L.; Laver, G. W.; Montgomery, J. A. *J. Med. Chem.* **2000**, *43*, 3482.

(109) von Itzstein, M.; Wu, W.-Y.; Kok, G. B.; Pegg, M. S.; Dyason, J. C.; Jin, B.; Phan, T. V.; Smythe, M. L.; White, H. F.; Oliver, S. W.; Colman, P. M.; Varghese, J. N.; Ryan, D. M.; Woods, J. M.; Bethell, R. C.; Hotham, V. J.; Cameron, J. M.; Penn, C. R. *Nature* **1993**, *363*, 418.

(110) Hanessian, S.; Bayrakdarian, M.; Luo, X. *J. Am. Chem. Soc.* **2002**, *124*, 4716.

(111) Richards, M. R.; Brant, M. G.; Boulanger, M. J.; Cairo, C. W.; Wulff, J. E. *Med. Chem. Comm.* **2014**, *5*, 1483.

(112) (a) Amaro, R. E.; Minh, D. D. L.; Cheng, L. S.; Lindstrom, W. M.; Olson, A. J.; Lin, J.-H.; Li, W. W.; McCammon, J. A. *J. Am. Chem. Soc.* **2007**, *129*, 7764; (b) Mohan, S.; McAtamney, S.; Haselhorst, T.; von Itzstein, M.; Pinto, B. M. *J. Med. Chem.* **2010**, *53*, 7377; (c) Adabala, P. J. P.; LeGresley, E. B.; Bance, N.; Niikura, M.; Pinto, B. M. *J. Org. Chem.* **2013**, *78*, 10867; (d) Xie, Y.; Xu, D.; Huang, B.; Ma, X.; Qi, W.; Shi, F.; Liu, X.; Zhang, Y.; Xu, W. *J. Med. Chem.* **2014**, *57*, 8445; (e) Mohan, S.; Kerry, P. S.; Bance, N.; Niikura, M.; Pinto, B. M. *Angew. Chem. Int. Ed.* **2014**, *53*, 1076; (f) Das, A.; Adak, A. K.; Ponnapalli, K.; Lin, C.-H.; Hsu, K.-C.; Yang, J.-M.; Hsu, T.-A.; Lin, C.-C. *Eur. J. Med. Chem.* **2016**, *123*, 397; (g) Rudrawar, S.; Dyason, J. C.; Rameix-Welti, M.-A.; Rose, F. J.; Kerry, P. S.; Russell, R. J. M.; van der Werf, S.; Thomson, R. J.; Naffakh, N.; von Itzstein, M. *Nat. Comm.* **2010**, *1*, 113.

(113) (a) Kakugawa, Y.; Wada, T.; Yamaguchi, K.; Yamanami, H.; Ouchi, K.; Sato, I.; Miyagi, T. *Proc. Natl. Acad. Sci.* **2002**, *99*, 10718; (b) Shiozaki, K.; Yamaguchi, K.; Takahashi, K.; Moriya, S.; Miyagi, T. *J. Biol. Chem.* **2011**, *286*, 21052.

(114) Miyagi, T.; Takahashi, K.; Hata, K.; Shiozaki, K.; Yamaguchi, K. *Glycoconj J* **2012**, *29*, 567.

(115) Miyata, M.; Kambe, M.; Tajima, O.; Moriya, S.; Sawaki, H.; Hotta, H.; Kondo, Y.; Narimatsu, H.; Miyagi, T.; Furukawa, K.; Furukawa, K. *Cancer Science* **2011**, *102*, 2139.

(116) Cairo, C. W. *Med. Chem. Comm.* **2014**, *5*, 1067.

(117) (a) Chavas, L. M. G.; Kato, R.; Suzuki, N.; von Itzstein, M.; Mann, M. C.; Thomson, R. J.; Dyason, J. C.; McKimm-Breschkin, J.; Fusi, P.; Tringali, C.; Venerando, B.; Tettamanti, G.; Monti, E.; Wakatsuki, S. *J. Med. Chem.* **2010**, *53*, 2998; (b) Albohy, A.; Zhang, Y.; Smutova, V.; Pshezhetsky, A. V.; Cairo, C. W. *ACS Med. Chem. Lett.* **2013**, *4*, 532; (c) Zhang, Y.; Albohy, A.; Zou, Y.; Smutova, V.; Pshezhetsky, A. V.; Cairo, C. W. *J. Med. Chem.* **2013**, *56*, 2948; (d) Magesh, S.; Moriya, S.; Suzuki, T.; Miyagi, T.; Ishida, H.; Kiso, M. *Bioorg. Med. Chem. Lett.* **2008**, *18*, 532.
(118) Mineno, T.; Miller, M. J. *J. Org. Chem.* **2003**, *68*, 6591.
(119) (a) Pizzorno, A.; Abed, Y.; Bouhy, X.; Beaulieu, É.; Mallett, C.; Russell, R.; Boivin, G. *Antimicrob. Agents Chemother.* **2012**, *56*, 1208; (b) Zürcher, T.; Yates, P. J.; Daly, J.; Sahasrabudhe, A.; Walters, M.; Dash, L.; Tisdale, M.; McKimm-Breschkin, J. L. *J. Antimicrob. Chemother.* **2006**, *58*, 723.
(120) Bromba, C. M.; Mason, J. W.; Brant, M. G.; Chan, T.; Lunke, M. D.; Petric, M.; Boulanger, M. J.; Wulff, J. E. *Bioorg. Med. Chem. Lett.* **2011**, *21*, 7137.
(121) Amaro, R. E.; Swift, R. V.; Votapka, L.; Li, W. W.; Walker, R. C.; Bush, R. M. *Nat. Comm.* **2011**, *2*, 388.
(122) Cha, S. *Biochem. Pharmacol.* **1975**, *24*, 2177.
(123) Marcelo, G.; J. V. Prazeres, T.; Charreyre, M.-T.; Martinho, J. M. G.; Farinha, J. P. S. *Macromolecules* **2010**, *43*, 501.

Appendix

Appendix A: Crystallographic Parameters

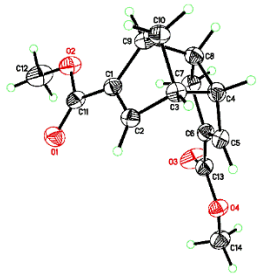

Table A1 Crystal data and structure refinement for compound **3**.

Identification code	uvic1522
Empirical formula	$C_{14}H_{16}O_4$
Formula weight	248.27
Temperature	120(2) K
Wavelength	1.54184 Å
Crystal system	Orthorhombic
Space group	$P2_12_12_1$
Unit cell dimensions	a = 6.08420(10) Å α = 90°
	b = 11.5373(2) Å β = 90°
	c = 17.6400(3) Å γ = 90°
Volume	1238.24(4) $Å^3$
Z	4
Density (calculated)	1.332 $g.cm^{-3}$
Absorption coefficient (μ)	0.803 mm^{-1}
F(000)	528
Crystal color, habit	colorless, blade
Crystal size	0.256 × 0.077 × 0.035 mm^3
θ range for data collection	4.579 to 72.208°
Index ranges	$-7 \leq h \leq 7$, $-14 \leq k \leq 14$, $-21 \leq l \leq 21$
Reflections collected	34320
Independent reflections	2441 [R_{int} = 0.0526]
Completeness to θ = 67.679°	100.0 %
Absorption correction	Numerical
Max. and min. transmission	1.0000 and 0.8044
Refinement method	Full-matrix least-squares on F^2
Data / restraints / parameters	2441 / 0 / 165
Goodness-of-fit on F^2	1.087
Final R indices [I>2σ(I)]	R_1 = 0.0335, wR_2 = 0.0868
R indices (all data)	R_1 = 0.0355, wR_2 = 0.0887
Absolute structure parameter	0.04(8)
Extinction coefficient	n/a
Largest diff. peak and hole	0.117 and -0.174 $e^-.Å^{-3}$

Table A2. Atomic coordinates and equivalent isotropic displacement parameters ($Å^2$) for compound **3**. U(eq) is defined as one third of the trace of the orthogonalized U_{ij} tensor.

	x	y	z	U(eq)
O(1)	0.2076(3)	0.83038(14)	0.39625(8)	0.037(1)
O(2)	-0.1016(2)	0.73975(13)	0.35918(8)	0.034(1)
O(3)	0.3563(3)	0.41502(17)	0.46870(9)	0.047(1)
O(4)	0.7017(2)	0.45251(13)	0.43231(7)	0.031(1)
C(1)	0.2027(3)	0.72601(16)	0.27988(10)	0.025(1)
C(2)	0.4133(3)	0.73814(16)	0.25922(11)	0.025(1)
C(3)	0.4481(3)	0.66744(17)	0.18864(11)	0.026(1)
C(4)	0.4356(3)	0.53710(17)	0.21516(11)	0.027(1)
C(5)	0.5557(3)	0.50811(17)	0.28704(11)	0.026(1)
C(6)	0.4201(3)	0.47784(16)	0.34285(11)	0.025(1)
C(7)	0.1827(3)	0.47561(17)	0.31900(11)	0.028(1)
C(8)	0.1873(3)	0.52178(17)	0.23646(11)	0.027(1)
C(9)	0.0940(3)	0.64548(17)	0.22288(10)	0.026(1)
C(10)	0.2206(3)	0.67932(17)	0.15073(11)	0.028(1)
C(11)	0.1091(3)	0.77160(17)	0.35081(11)	0.027(1)
C(12)	-0.2061(4)	0.7753(3)	0.42907(13)	0.049(1)
C(13)	0.4847(3)	0.44581(18)	0.42081(11)	0.029(1)
C(14)	0.7785(4)	0.4155(2)	0.50644(11)	0.036(1)
H(2)	0.5212	0.7833	0.2846	0.030
H(3)	0.5778	0.6890	0.1568	0.031
H(4)	0.4785	0.4833	0.1732	0.033
H(5)	0.7110	0.5110	0.2921	0.032
H(7A)	0.0925	0.5263	0.3519	0.034
H(7B)	0.1230	0.3958	0.3209	0.034
H(8)	0.1156	0.4650	0.2015	0.033
H(9)	-0.0698	0.6511	0.2195	0.032
H(10A)	0.1888	0.7593	0.1337	0.034
H(10B)	0.1986	0.6239	0.1086	0.034
H(12A)	-0.3649	0.7621	0.4254	0.074
H(12B)	-0.1780	0.8578	0.4378	0.074
H(12C)	-0.1462	0.7300	0.4713	0.074
H(14A)	0.9395	0.4180	0.5077	0.055
H(14B)	0.7285	0.3362	0.5162	0.055
H(14C)	0.7194	0.4675	0.5454	0.055

Table A3. Anisotropic displacement parameters ($Å^2$) for compound **3**.
The anisotropic displacement factor exponent takes the form:
$-2\pi^2[h^2a^{*2}U_{11} + ... + 2hka^*b^*U_{12}]$

	U_{11}	U_{22}	U_{33}	U_{23}	U_{13}	U_{12}
O(1)	0.0357(7)	0.0430(9)	0.0320(8)	-0.0092(6)	-0.0014(6)	0.0013(7)
O(2)	0.0257(7)	0.0505(9)	0.0257(7)	0.0004(6)	0.0022(6)	0.0026(6)
O(3)	0.0319(8)	0.0751(12)	0.0334(8)	0.0189(8)	0.0049(7)	-0.0005(8)
O(4)	0.0265(7)	0.0392(8)	0.0264(7)	0.0035(6)	-0.0011(6)	0.0027(6)
C(1)	0.0246(9)	0.0249(9)	0.0243(9)	0.0031(7)	-0.0010(8)	0.0003(7)
C(2)	0.0259(9)	0.0245(9)	0.0247(9)	0.0018(7)	-0.0015(8)	-0.0022(7)
C(3)	0.0258(9)	0.0282(10)	0.0237(9)	0.0019(7)	0.0016(7)	-0.0009(7)
C(4)	0.0287(10)	0.0277(9)	0.0249(9)	-0.0016(7)	0.0018(8)	0.0013(8)
C(5)	0.0253(9)	0.0261(9)	0.0274(9)	0.0001(7)	0.0014(8)	0.0024(7)
C(6)	0.0253(9)	0.0233(8)	0.0271(9)	0.0013(7)	0.0001(8)	0.0008(7)
C(7)	0.0268(9)	0.0279(10)	0.0304(10)	0.0052(8)	-0.0010(8)	-0.0036(8)
C(8)	0.0284(10)	0.0261(9)	0.0276(9)	-0.0002(7)	-0.0021(8)	-0.0030(8)
C(9)	0.0226(8)	0.0305(9)	0.0261(9)	0.0026(7)	-0.0021(8)	-0.0020(8)
C(10)	0.0293(9)	0.0329(10)	0.0231(9)	0.0014(7)	-0.0029(8)	-0.0012(8)
C(11)	0.0256(10)	0.0309(9)	0.0260(9)	0.0030(8)	-0.0016(8)	0.0034(8)
C(12)	0.0340(12)	0.0854(19)	0.0278(11)	-0.0015(11)	0.0081(10)	0.0086(13)
C(13)	0.0266(9)	0.0310(10)	0.0281(10)	0.0008(8)	0.0012(8)	0.0021(7)
C(14)	0.0362(11)	0.0470(12)	0.0261(10)	0.0016(9)	-0.0051(9)	0.0068(9)

Table A4. Bond lengths [Å] for compound **3**.

atom-atom	distance	atom-atom	distance
O(1)-C(11)	1.209(2)	O(2)-C(11)	1.341(2)
O(2)-C(12)	1.447(3)	O(3)-C(13)	1.204(3)
O(4)-C(13)	1.338(3)	O(4)-C(14)	1.453(2)
C(1)-C(2)	1.339(3)	C(1)-C(11)	1.472(3)
C(1)-C(9)	1.521(3)	C(2)-C(3)	1.503(3)
C(2)-H(2)	0.9500	C(3)-C(10)	1.543(3)
C(3)-C(4)	1.577(3)	C(3)-H(3)	1.0000
C(4)-C(5)	1.501(3)	C(4)-C(8)	1.566(3)
C(4)-H(4)	1.0000	C(5)-C(6)	1.331(3)
C(5)-H(5)	0.9500	C(6)-C(13)	1.477(3)
C(6)-C(7)	1.504(3)	C(7)-C(8)	1.551(3)
C(7)-H(7A)	0.9900	C(7)-H(7B)	0.9900
C(8)-C(9)	1.555(3)	C(8)-H(8)	1.0000
C(9)-C(10)	1.538(3)	C(9)-H(9)	1.0000
C(10)-H(10A)	0.9900	C(10)-H(10B)	0.9900
C(12)-H(12A)	0.9800	C(12)-H(12B)	0.9800
C(12)-H(12C)	0.9800	C(14)-H(14A)	0.9800
C(14)-H(14B)	0.9800	C(14)-H(14C)	0.9800

Table A5. Bond angles [°] for compound **3**.

atom-atom-atom	angle	atom-atom-atom	angle
C(11)-O(2)-C(12)	115.86(18)	C(13)-O(4)-C(14)	115.91(16)
C(2)-C(1)-C(11)	124.34(18)	C(2)-C(1)-C(9)	107.47(17)
C(11)-C(1)-C(9)	127.73(18)	C(1)-C(2)-C(3)	107.66(17)
C(1)-C(2)-H(2)	126.2	C(3)-C(2)-H(2)	126.2
C(2)-C(3)-C(10)	100.62(15)	C(2)-C(3)-C(4)	105.37(15)
C(10)-C(3)-C(4)	99.78(15)	C(2)-C(3)-H(3)	116.2
C(10)-C(3)-H(3)	116.2	C(4)-C(3)-H(3)	116.2
C(5)-C(4)-C(8)	103.99(15)	C(5)-C(4)-C(3)	116.07(16)
C(8)-C(4)-C(3)	103.03(15)	C(5)-C(4)-H(4)	111.1
C(8)-C(4)-H(4)	111.1	C(3)-C(4)-H(4)	111.1
C(6)-C(5)-C(4)	112.42(17)	C(6)-C(5)-H(5)	123.8
C(4)-C(5)-H(5)	123.8	C(5)-C(6)-C(13)	126.08(18)
C(5)-C(6)-C(7)	113.12(16)	C(13)-C(6)-C(7)	120.78(17)
C(6)-C(7)-C(8)	103.84(15)	C(6)-C(7)-H(7A)	111.0
C(8)-C(7)-H(7A)	111.0	C(6)-C(7)-H(7B)	111.0
C(8)-C(7)-H(7B)	111.0	H(7A)-C(7)-H(7B)	109.0
C(7)-C(8)-C(9)	116.96(16)	C(7)-C(8)-C(4)	106.35(15)
C(9)-C(8)-C(4)	102.23(15)	C(7)-C(8)-H(8)	110.3
C(9)-C(8)-H(8)	110.3	C(4)-C(8)-H(8)	110.3
C(1)-C(9)-C(10)	100.02(15)	C(1)-C(9)-C(8)	107.46(15)
C(10)-C(9)-C(8)	100.22(15)	C(1)-C(9)-H(9)	115.7
C(10)-C(9)-H(9)	115.7	C(8)-C(9)-H(9)	115.7
C(9)-C(10)-C(3)	93.91(14)	C(9)-C(10)-H(10A)	112.9
C(3)-C(10)-H(10A)	112.9	C(9)-C(10)-H(10B)	112.9
C(3)-C(10)-H(10B)	112.9	H(10A)-C(10)-H(10B)	110.4
O(1)-C(11)-O(2)	123.68(19)	O(1)-C(11)-C(1)	124.89(18)
O(2)-C(11)-C(1)	111.43(17)	O(2)-C(12)-H(12A)	109.5
O(2)-C(12)-H(12B)	109.5	H(12A)-C(12)-H(12B)	109.5
O(2)-C(12)-H(12C)	109.5	H(12A)-C(12)-H(12C)	109.5
H(12B)-C(12)-H(12C)	109.5	O(3)-C(13)-O(4)	123.43(19)
O(3)-C(13)-C(6)	123.64(19)	O(4)-C(13)-C(6)	112.92(17)
O(4)-C(14)-H(14A)	109.5	O(4)-C(14)-H(14B)	109.5
H(14A)-C(14)-H(14B)	109.5	O(4)-C(14)-H(14C)	109.5
H(14A)-C(14)-H(14C)	109.5	H(14B)-C(14)-H(14C)	109.5

Table A6. Torsion angles [°] for compound **3**.

atom-atom-atom-atom	angle	atom-atom-atom-atom	angle
C(11)-C(1)-C(2)-C(3)	173.16(17)	C(9)-C(1)-C(2)-C(3)	0.4(2)
C(1)-C(2)-C(3)-C(10)	32.87(19)	C(1)-C(2)-C(3)-C(4)	-70.48(19)
C(2)-C(3)-C(4)-C(5)	-43.7(2)	C(10)-C(3)-C(4)-C(5)	-147.64(16)
C(2)-C(3)-C(4)-C(8)	69.24(18)	C(10)-C(3)-C(4)-C(8)	-34.73(17)
C(8)-C(4)-C(5)-C(6)	1.2(2)	C(3)-C(4)-C(5)-C(6)	113.56(19)
C(4)-C(5)-C(6)-C(13)	-179.14(18)	C(4)-C(5)-C(6)-C(7)	2.4(2
C(5)-C(6)-C(7)-C(8)	-4.8(2)	C(13)-C(6)-C(7)-C(8)	176.56(17)
C(6)-C(7)-C(8)-C(9)	-108.16(18)	C(6)-C(7)-C(8)-C(4)	5.2(2)
C(5)-C(4)-C(8)-C(7)	-4.0(2)	C(3)-C(4)-C(8)-C(7)	-125.55(16)
C(5)-C(4)-C(8)-C(9)	119.11(15)	C(3)-C(4)-C(8)-C(9)	-2.39(18)
C(2)-C(1)-C(9)-C(10)	-33.51(19)	C(11)-C(1)-C(9)-C(10)	154.01(18)
C(2)-C(1)-C(9)-C(8)	70.63(19)	C(11)-C(1)-C(9)-C(8)	-101.8(2)
C(7)-C(8)-C(9)-C(1)	50.7(2)	C(4)-C(8)-C(9)-C(1)	-65.03(18)
C(7)-C(8)-C(9)-C(10)	154.66(16)	C(4)-C(8)-C(9)-C(10)	38.97(17)
C(1)-C(9)-C(10)-C(3)	49.77(17)	C(8)-C(9)-C(10)-C(3)	-60.19(16)
C(2)-C(3)-C(10)-C(9)	-49.97(16)	C(4)-C(3)-C(10)-C(9)	57.84(16)
C(12)-O(2)-C(11)-O(1)	-3.0(3)	C(12)-O(2)-C(11)-C(1)	177.01(18)
C(2)-C(1)-C(11)-O(1)	4.4(3)	C(9)-C(1)-C(11)-O(1)	175.66(19)
C(2)-C(1)-C(11)-O(2)	-175.66(18)	C(9)-C(1)-C(11)-O(2)	-4.4(3)
C(14)-O(4)-C(13)-O(3)	2.4(3)	C(14)-O(4)-C(13)-C(6)	-176.44(16)
C(5)-C(6)-C(13)-O(3)	-177.3(2)	C(7)-C(6)-C(13)-O(3)	1.1(3)
C(5)-C(6)-C(13)-O(4)	1.6(3)	C(7)-C(6)-C(13)-O(4)	179.98(17)

Table A7. Hydrogen bonds for compound **3** [Å and °].

D-H...A	d(D-H)	d(H...A)	d(D...A)	<(DHA)
C(12)-H(12C)...O(1)#1	0.98	2.60	3.355(3)	134.4
C(14)-H(14A)...O(3)#2	0.98	2.63	3.578(3)	163.4
C(14)-H(14C)...O(1)#3	0.98	2.55	3.425(3)	148.5

Symmetry transformations used to generate equivalent atoms:
#1 x-1/2,-y+3/2,-z+1 #2 x+1,y,z #3 x+1/2,-y+3/2,-z+1

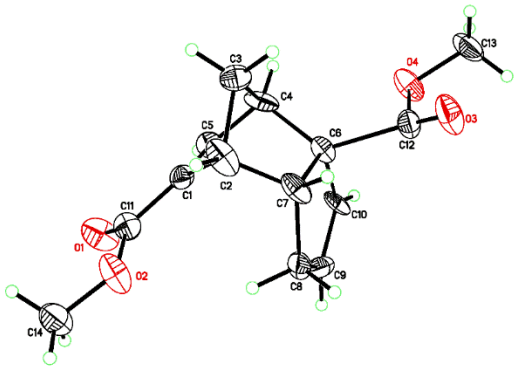

Table B1. Crystal data and structure refinement for **compound 7**.

Identification code	uvic1521a	
Empirical formula	$C_{14}H_{16}O_4$	
Formula weight	248.27	
Temperature	120(2) K	
Wavelength	1.54184 Å	
Crystal system	Monoclinic	
Space group	Pc	
Unit cell dimensions	*a* = 8.5158(7) Å	α = 90°
	b = 6.0532(5) Å	β = 95.954(3)°
	c = 11.8232(10) Å	γ = 90°
Volume	606.17(9) $Å^3$	
Z	2	
Density (calculated)	1.360 $g.cm^{-3}$	
Absorption coefficient (μ)	0.820 mm^{-1}	
F(000)	264	
Crystal color, habit	colorless, block	
Crystal size	0.259 × 0.240 × 0.090 mm^3	
θ range for data collection	5.222 to 72.099°	
Index ranges	$-10 \leq h \leq 10$, $-7 \leq k \leq 7$, $-14 \leq l \leq 14$	
Reflections collected	15713	
Independent reflections	2257 [R_{int} = 0.0297]	
Completeness to θ = 67.679°	97.5 %	
Absorption correction	Numerical	
Max. and min. transmission	1.0000 and 0.9075	
Refinement method	Full-matrix least-squares on F^2	
Data / restraints / parameters	2257 / 305 / 310	
Goodness-of-fit on F^2	1.118	
Final R indices [I>2σ(I)]	R_1 = 0.0531, wR_2 = 0.1454	
R indices (all data)	R_1 = 0.0537, wR_2 = 0.1471	
Absolute structure parameter	0.14(7)	
Extinction coefficient	n/a	
Largest diff. peak and hole	0.246 and -0.307 $e^-.Å^{-3}$	

Table B2. Atomic coordinates and equivalent isotropic displacement parameters ($Å^2$) for compound **7**. U(eq) is defined as one third of the trace of the orthogonalized U_{ij} tensor.

	x	y	z	U(eq)
O(1)	-0.1105(13)	0.703(2)	0.9674(10)	0.046(2)
O(3)	0.6656(11)	0.7923(18)	0.7064(10)	0.044(2)
O(4)	0.609(2)	0.422(3)	0.7611(14)	0.036(3)
C(1)	0.0816(8)	0.7412(12)	0.8358(5)	0.024(1)
C(2)	0.1726(13)	0.8704(16)	0.7548(9)	0.034(2)
C(3)	0.1892(12)	0.6761(12)	0.6667(6)	0.031(2)
C(4)	0.2553(11)	0.5145(11)	0.7611(5)	0.027(1)
C(5)	0.1395(9)	0.5353(10)	0.8410(6)	0.027(1)
C(6)	0.4056(9)	0.6628(9)	0.8122(5)	0.022(1)
C(7)	0.3405(10)	0.9053(11)	0.8043(6)	0.029(1)
C(8)	0.3617(11)	1.0008(12)	0.9228(7)	0.032(2)
C(9)	0.4227(10)	0.8207(12)	0.9995(7)	0.029(2)
C(10)	0.4570(11)	0.6330(13)	0.9340(6)	0.025(2)
C(11)	-0.0380(11)	0.8174(17)	0.9077(8)	0.028(2)
C(12)	0.5946(11)	0.6715(16)	0.7615(9)	0.029(2)
C(13)	0.743(3)	0.366(4)	0.705(2)	0.043(5)
O(1A)	0.6068(13)	0.7684(19)	0.6875(11)	0.052(3)
O(2A)	0.599(2)	0.456(3)	0.7579(17)	0.043(4)
O(3A)	-0.0499(15)	0.725(2)	0.9842(15)	0.069(4)
C(1A)	0.4820(10)	0.7556(15)	0.8358(7)	0.038(2)
C(2A)	0.3931(16)	0.625(2)	0.9294(13)	0.056(3)
C(3A)	0.3579(16)	0.795(3)	1.0016(11)	0.070(3)
C(4A)	0.2918(12)	0.9722(15)	0.9127(8)	0.039(2)
C(5A)	0.4192(10)	0.9657(14)	0.8352(7)	0.038(2)
C(6A)	0.1521(12)	0.8225(16)	0.8647(9)	0.048(2)
C(7A)	0.2242(13)	0.5927(14)	0.8729(9)	0.049(2)
C(8A)	0.1905(18)	0.519(3)	0.7288(13)	0.078(4)
C(9A)	0.1213(14)	0.684(2)	0.6809(11)	0.057(3)
C(10A)	0.1137(15)	0.864(2)	0.7387(12)	0.048(3)
C(11A)	0.5458(11)	0.6272(17)	0.7419(9)	0.028(2)
C(12A)	0.0116(12)	0.8558(16)	0.9325(9)	0.032(2)
C(13A)	0.729(3)	0.371(3)	0.693(2)	0.037(4)
O(2)	-0.0475(3)	1.0537(4)	0.9120(3)	0.043(1)
C(14)	-0.1731(5)	1.1261(6)	0.9743(4)	0.043(1)
H(2A)	0.1180	1.0057	0.7219	0.041
H(3A)	0.0868	0.6282	0.6270	0.037
H(3B)	0.2653	0.7094	0.6111	0.037
H(4A)	0.2790	0.3612	0.7364	0.032
H(5A)	0.1091	0.4214	0.8895	0.032
H(7A)	0.3992	0.9953	0.7516	0.035

H(8A)	0.4374	1.1253	0.9265	0.039
H(8B)	0.2596	1.0556	0.9447	0.039
H(9A)	0.4368	0.8291	1.0802	0.035
H(10A)	0.5073	0.5034	0.9653	0.030
H(13A)	0.7245	0.4088	0.6245	0.064
H(13B)	0.7613	0.2065	0.7103	0.064
H(13C)	0.8361	0.4444	0.7406	0.064
H(2B)	0.4476	0.4924	0.9652	0.068
H(3C)	0.4534	0.8486	1.0485	0.083
H(3D)	0.2776	0.7498	1.0518	0.083
H(4B)	0.2645	1.1200	0.9429	0.047
H(5B)	0.4519	1.0869	0.7922	0.045
H(7B)	0.1632	0.4944	0.9203	0.059
H(8C)	0.2914	0.4891	0.6969	0.093
H(8D)	0.1231	0.3856	0.7191	0.093
H(9B)	0.0760	0.6761	0.6041	0.069
H(10B)	0.0873	1.0049	0.7063	0.058
H(13D)	0.7043	0.4023	0.6119	0.056
H(13E)	0.7400	0.2107	0.7043	0.056
H(13F)	0.8290	0.4432	0.7208	0.056
H(14A)	-0.1618	1.0581	1.0499	0.064
H(14B)	-0.2745	1.0826	0.9336	0.064
H(14C)	-0.1692	1.2872	0.9820	0.064
H(14D)	-0.1438	1.1025	1.0557	0.064
H(14E)	-0.2689	1.0418	0.9498	0.064
H(14F)	-0.1928	1.2836	0.9599	0.064

Table B3. Anisotropic displacement parameters ($Å^2$) for compound **7**.
The anisotropic displacement factor exponent takes the form:
$-2\pi^2[h^2a^{*2}U_{11} + ... + 2hka^*b^*U_{12}]$

	U_{11}	U_{22}	U_{33}	U_{23}	U_{13}	U_{12}
O(1)	0.063(6)	0.033(3)	0.046(3)	0.006(2)	0.026(4)	-0.004(4)
O(3)	0.037(5)	0.038(4)	0.062(5)	0.005(3)	0.027(4)	0.000(4)
O(4)	0.039(4)	0.027(5)	0.044(4)	0.007(3)	0.016(3)	0.019(3)
C(1)	0.023(3)	0.027(3)	0.022(3)	0.000(2)	0.004(2)	-0.006(2)
C(2)	0.043(5)	0.025(3)	0.038(4)	0.020(3)	0.023(4)	0.008(3)
C(3)	0.038(5)	0.034(3)	0.020(3)	0.003(2)	0.001(3)	0.000(3)
C(4)	0.052(4)	0.020(3)	0.010(2)	0.006(2)	0.007(2)	0.013(3)
C(5)	0.032(3)	0.014(3)	0.034(3)	0.003(2)	0.005(2)	0.001(2)
C(6)	0.027(3)	0.013(2)	0.029(3)	0.0038(18)	0.013(2)	0.001(2)
C(7)	0.037(3)	0.016(2)	0.037(3)	0.005(2)	0.019(3)	0.009(2)
C(8)	0.021(4)	0.018(3)	0.058(4)	-0.014(3)	0.007(3)	0.001(3)
C(9)	0.031(5)	0.030(3)	0.025(3)	-0.008(2)	-0.003(3)	-0.002(3)
C(10)	0.034(4)	0.021(3)	0.023(3)	0.002(2)	0.021(3)	0.003(3)
C(11)	0.031(4)	0.031(4)	0.023(4)	0.006(3)	0.003(3)	0.003(3)
C(12)	0.022(5)	0.027(4)	0.038(5)	-0.002(3)	0.008(3)	0.000(3)
C(13)	0.038(8)	0.058(9)	0.033(5)	-0.006(5)	0.012(4)	0.020(6)
O(1A)	0.044(5)	0.040(4)	0.077(6)	0.019(4)	0.029(5)	0.002(4)
O(2A)	0.032(5)	0.034(6)	0.070(6)	0.019(4)	0.033(4)	0.009(4)
O(3A)	0.071(7)	0.041(5)	0.105(9)	0.021(5)	0.061(7)	0.019(5)
C(1A)	0.034(3)	0.040(3)	0.041(3)	0.004(3)	0.007(3)	0.001(3)
C(2A)	0.052(6)	0.050(5)	0.074(6)	0.012(4)	0.037(5)	0.003(5)
C(3A)	0.053(7)	0.108(8)	0.051(5)	0.021(5)	0.023(5)	0.022(6)
C(4A)	0.028(4)	0.041(4)	0.048(4)	-0.005(3)	0.004(3)	-0.008(3)
C(5A)	0.033(4)	0.036(4)	0.043(4)	-0.008(3)	0.005(3)	-0.012(3)
C(6A)	0.032(4)	0.050(4)	0.064(5)	-0.017(3)	0.020(3)	-0.011(3)
C(7A)	0.053(4)	0.028(3)	0.069(5)	0.000(3)	0.020(4)	-0.006(3)
C(8A)	0.071(8)	0.068(6)	0.093(8)	-0.038(6)	0.000(6)	0.002(5)
C(9A)	0.032(5)	0.079(6)	0.062(6)	-0.022(4)	0.012(4)	-0.005(4)
C(10A)	0.043(6)	0.054(5)	0.049(5)	-0.008(4)	0.012(4)	-0.004(5)
C(11A)	0.020(4)	0.029(4)	0.036(4)	-0.002(3)	0.005(3)	-0.005(3)
C(12A)	0.035(5)	0.026(4)	0.034(5)	-0.002(3)	0.006(4)	-0.001(3)
C(13A)	0.013(5)	0.033(6)	0.069(11)	0.000(6)	0.019(5)	0.003(4)
O(2)	0.0400(14)	0.0365(14)	0.0555(16)	0.0114(12)	0.0234(11)	0.0110(11)
C(14)	0.043(2)	0.0364(18)	0.050(2)	-0.0056(18)	0.0151(16)	0.0020(16)

Table B4. Bond lengths [Å] for compound **7**.

atom-atom	distance	atom-atom	distance
O(1)-C(11)	1.203(15)	O(3)-C(12)	1.185(16)
O(4)-C(13)	1.42(3)	O(4)-C(12)	1.51(2)
C(1)-C(5)	1.340(9)	C(1)-C(11)	1.467(13)
C(1)-C(2)	1.512(12)	C(2)-C(7)	1.502(16)
C(2)-C(3)	1.587(14)	C(2)-H(2A)	1.0000
C(3)-C(4)	1.546(9)	C(3)-H(3A)	0.9900
C(3)-H(3B)	0.9900	C(4)-C(5)	1.440(11)
C(4)-C(6)	1.627(11)	C(4)-H(4A)	1.0000
C(5)-H(5A)	0.9500	C(6)-C(10)	1.473(10)
C(6)-C(7)	1.568(8)	C(6)-C(12)	1.776(12)
C(7)-C(8)	1.509(12)	C(7)-H(7A)	1.0000
C(8)-C(9)	1.478(11)	C(8)-H(8A)	0.9900
C(8)-H(8B)	0.9900	C(9)-C(10)	1.423(10)
C(9)-H(9A)	0.9500	C(10)-H(10A)	0.9500
C(11)-O(2)	1.434(11)	C(13)-H(13A)	0.9800
C(13)-H(13B)	0.9800	C(13)-H(13C)	0.9800
O(1A)-C(11A)	1.218(16)	O(2A)-C(11A)	1.14(2)
O(2A)-C(13A)	1.50(3)	O(3A)-C(12A)	1.158(17)
C(1A)-C(5A)	1.379(12)	C(1A)-C(11A)	1.503(14)
C(1A)-C(2A)	1.611(16)	C(2A)-C(3A)	1.39(2)
C(2A)-C(7A)	1.53(2)	C(2A)-H(2B)	1.0000
C(3A)-C(4A)	1.565(16)	C(3A)-H(3C)	0.9900
C(3A)-H(3D)	0.9900	C(4A)-C(5A)	1.491(15)
C(4A)-C(6A)	1.555(13)	C(4A)-H(4B)	1.0000
C(5A)-H(5B)	0.9500	C(6A)-C(10A)	1.513(18)
C(6A)-C(7A)	1.519(12)	C(6A)-C(12A)	1.522(15)
C(7A)-C(8A)	1.755(18)	C(7A)-H(7B)	1.0000
C(8A)-C(9A)	1.266(19)	C(8A)-H(8C)	0.9900
C(8A)-H(8D)	0.9900	C(9A)-C(10A)	1.292(18)
C(9A)-H(9B)	0.9500	C(10A)-H(10B)	0.9500
C(12A)-O(2)	1.312(11)	C(13A)-H(13D)	0.9800
C(13A)-H(13E)	0.9800	C(13A)-H(13F)	0.9800
O(2)-C(14)	1.428(5)	C(14)-H(14A)	0.9800
C(14)-H(14B)	0.9800	C(14)-H(14C)	0.9800
C(14)-H(14D)	0.9800	C(14)-H(14E)	0.9800
C(14)-H(14F)	0.9800		

Table B5. Bond angles [°] for compound **7**.

atom-atom-atom	angle	atom-atom-atom	angle
C(13)-O(4)-C(12)	108.1(17)	C(5)-C(1)-C(11)	122.7(7)
C(5)-C(1)-C(2)	107.4(7)	C(11)-C(1)-C(2)	129.6(7)
C(7)-C(2)-C(1)	110.8(7)	C(7)-C(2)-C(3)	102.3(8)
C(1)-C(2)-C(3)	96.8(7)	C(7)-C(2)-H(2A)	114.9
C(1)-C(2)-H(2A)	114.9	C(3)-C(2)-H(2A)	114.9
C(4)-C(3)-C(2)	92.6(6)	C(4)-C(3)-H(3A)	113.2
C(2)-C(3)-H(3A)	113.2	C(4)-C(3)-H(3B)	113.2
C(2)-C(3)-H(3B)	113.2	H(3A)-C(3)-H(3B)	110.5
C(5)-C(4)-C(3)	101.3(7)	C(5)-C(4)-C(6)	105.9(6)
C(3)-C(4)-C(6)	97.6(5)	C(5)-C(4)-H(4A)	116.5
C(3)-C(4)-H(4A)	116.5	C(6)-C(4)-H(4A)	116.5
C(1)-C(5)-C(4)	109.0(6)	C(1)-C(5)-H(5A)	125.5
C(4)-C(5)-H(5A)	125.5	C(10)-C(6)-C(7)	103.9(6)
C(10)-C(6)-C(4)	116.0(6)	C(7)-C(6)-C(4)	103.6(5)
C(10)-C(6)-C(12)	98.4(6)	C(7)-C(6)-C(12)	106.2(6)
C(4)-C(6)-C(12)	126.6(6)	C(2)-C(7)-C(8)	115.7(7)
C(2)-C(7)-C(6)	102.0(7)	C(8)-C(7)-C(6)	107.2(5)
C(2)-C(7)-H(7A)	110.5	C(8)-C(7)-H(7A)	110.5
C(6)-C(7)-H(7A)	110.5	C(9)-C(8)-C(7)	106.8(5)
C(9)-C(8)-H(8A)	110.4	C(7)-C(8)-H(8A)	110.4
C(9)-C(8)-H(8B)	110.4	C(7)-C(8)-H(8B)	110.4
H(8A)-C(8)-H(8B)	108.6	C(10)-C(9)-C(8)	109.5(6)
C(10)-C(9)-H(9A)	125.2	C(8)-C(9)-H(9A)	125.2
C(9)-C(10)-C(6)	112.2(6)	C(9)-C(10)-H(10A)	123.9
C(6)-C(10)-H(10A)	123.9	O(1)-C(11)-O(2)	121.2(10)
O(1)-C(11)-C(1)	126.1(10)	O(2)-C(11)-C(1)	112.3(7)
O(3)-C(12)-O(4)	124.5(12)	O(3)-C(12)-C(6)	137.4(9)
O(4)-C(12)-C(6)	92.8(10)	O(4)-C(13)-H(13A)	109.5
O(4)-C(13)-H(13B)	109.5	H(13A)-C(13)-H(13B)	109.5
O(4)-C(13)-H(13C)	109.5	H(13A)-C(13)-H(13C)	109.5
H(13B)-C(13)-H(13C)	109.5	C(11A)-O(2A)-C(13A)	122.1(17)
C(5A)-C(1A)-C(11A)	130.0(8)	C(5A)-C(1A)-C(2A)	104.3(9)
C(11A)-C(1A)-C(2A)	119.1(9)	C(3A)-C(2A)-C(7A)	96.3(11)
C(3A)-C(2A)-C(1A)	101.9(11)	C(7A)-C(2A)-C(1A)	104.5(10)
C(3A)-C(2A)-H(2B)	117.1	C(7A)-C(2A)-H(2B)	117.0
C(1A)-C(2A)-H(2B)	117.0	C(2A)-C(3A)-C(4A)	100.4(11)
C(2A)-C(3A)-H(3C)	111.7	C(4A)-C(3A)-H(3C)	111.7
C(2A)-C(3A)-H(3D)	111.7	C(4A)-C(3A)-H(3D)	111.7
H(3C)-C(3A)-H(3D)	109.5	C(5A)-C(4A)-C(6A)	109.8(8)
C(5A)-C(4A)-C(3A)	99.2(9)	C(6A)-C(4A)-C(3A)	93.1(8)
C(5A)-C(4A)-H(4B)	117.0	C(6A)-C(4A)-H(4B)	117.0
C(3A)-C(4A)-H(4B)	117.0	C(1A)-C(5A)-C(4A)	109.1(8)

C(1A)-C(5A)-H(5B)	125.4	C(4A)-C(5A)-H(5B)	125.5
C(10A)-C(6A)-C(7A)	105.1(9)	C(10A)-C(6A)-C(12A)	113.3(9)
C(7A)-C(6A)-C(12A)	115.0(9)	C(10A)-C(6A)-C(4A)	109.9(8)
C(7A)-C(6A)-C(4A)	102.8(8)	C(12A)-C(6A)-C(4A)	110.1(8)
C(6A)-C(7A)-C(2A)	105.4(9)	C(6A)-C(7A)-C(8A)	98.4(9)
C(2A)-C(7A)-C(8A)	120.4(9)	C(6A)-C(7A)-H(7B)	110.5
C(2A)-C(7A)-H(7B)	110.5	C(8A)-C(7A)-H(7B)	110.5
C(9A)-C(8A)-C(7A)	104.8(10)	C(9A)-C(8A)-H(8C)	110.8
C(7A)-C(8A)-H(8C)	110.8	C(9A)-C(8A)-H(8D)	110.8
C(7A)-C(8A)-H(8D)	110.8	H(8C)-C(8A)-H(8D)	108.9
C(8A)-C(9A)-C(10A)	118.5(12)	C(8A)-C(9A)-H(9B)	120.7
C(10A)-C(9A)-H(9B)	120.7	C(9A)-C(10A)-C(6A)	111.2(12)
C(9A)-C(10A)-H(10B)	124.4	C(6A)-C(10A)-H(10B)	124.4
O(2A)-C(11A)-O(1A)	122.8(14)	O(2A)-C(11A)-C(1A)	121.1(14)
O(1A)-C(11A)-C(1A)	103.5(10)	O(3A)-C(12A)-O(2)	122.4(12)
O(3A)-C(12A)-C(6A)	127.7(12)	O(2)-C(12A)-C(6A)	109.3(8)
O(2A)-C(13A)-H(13D)	109.5	O(2A)-C(13A)-H(13E)	109.5
H(13D)-C(13A)-H(13E)	109.5	O(2A)-C(13A)-H(13F)	109.5
H(13D)-C(13A)-H(13F)	109.5	H(13E)-C(13A)-H(13F)	109.5
C(12A)-O(2)-C(14)	118.6(6)	C(14)-O(2)-C(11)	111.9(5)
O(2)-C(14)-H(14A)	109.5	O(2)-C(14)-H(14B)	109.5
H(14A)-C(14)-H(14B)	109.5	O(2)-C(14)-H(14C)	109.5
H(14A)-C(14)-H(14C)	109.5	H(14B)-C(14)-H(14C)	109.5
O(2)-C(14)-H(14D)	109.5	O(2)-C(14)-H(14E)	109.5
H(14D)-C(14)-H(14E)	109.5	O(2)-C(14)-H(14F)	109.5
H(14D)-C(14)-H(14F)	109.5	H(14E)-C(14)-H(14F)	109.5

Table B6. Torsion angles [°] for compound **7**.

atom-atom-atom-atom	angle	atom-atom-atom-atom	angle
C(5)-C(1)-C(2)-C(7)	-68.7(9)	C(11)-C(1)-C(2)-C(7)	105.5(10)
C(5)-C(1)-C(2)-C(3)	37.4(8)	C(11)-C(1)-C(2)-C(3)	-148.4(8)
C(7)-C(2)-C(3)-C(4)	61.7(7)	C(1)-C(2)-C(3)-C(4)	-51.4(7)
C(2)-C(3)-C(4)-C(5)	50.9(8)	C(2)-C(3)-C(4)-C(6)	-57.1(7)
C(11)-C(1)-C(5)-C(4)	-179.3(7)	C(2)-C(1)-C(5)-C(4)	-4.6(9)
C(3)-C(4)-C(5)-C(1)	-31.6(8)	C(6)-C(4)-C(5)-C(1)	69.8(7)
C(5)-C(4)-C(6)-C(10)	46.4(7)	C(3)-C(4)-C(6)-C(10)	150.5(7
C(5)-C(4)-C(6)-C(7)	-66.8(6)	C(3)-C(4)-C(6)-C(7)	37.3(7)
C(5)-C(4)-C(6)-C(12)	170.7(6)	C(3)-C(4)-C(6)-C(12)	-85.2(8)
C(1)-C(2)-C(7)-C(8)	-51.5(9)	C(3)-C(2)-C(7)-C(8)	-153.9(6)
C(1)-C(2)-C(7)-C(6)	64.4(8)	C(3)-C(2)-C(7)-C(6)	-37.9(7)
C(10)-C(6)-C(7)-C(2)	-121.0(7)	C(4)-C(6)-C(7)-C(2)	0.7(7)
C(12)-C(6)-C(7)-C(2)	135.8(6)	C(10)-C(6)-C(7)-C(8)	1.0(9)
C(4)-C(6)-C(7)-C(8)	122.6(7)	C(12)-C(6)-C(7)-C(8)	-102.2(7)
C(2)-C(7)-C(8)-C(9)	108.3(8)	C(6)-C(7)-C(8)-C(9)	-4.7(10)
C(7)-C(8)-C(9)-C(10)	6.9(10)	C(8)-C(9)-C(10)-C(6)	-6.6(10)
C(7)-C(6)-C(10)-C(9)	3.3(9)	C(4)-C(6)-C(10)-C(9)	-109.6(8)
C(12)-C(6)-C(10)-C(9)	112.4(7)	C(5)-C(1)-C(11)-O(1)	-9.6(15)
C(2)-C(1)-C(11)-O(1)	177.0(11)	C(5)-C(1)-C(11)-O(2)	162.8(7)
C(2)-C(1)-C(11)-O(2)	-10.6(13)	C(13)-O(4)-C(12)-O(3)	12(2)
C(13)-O(4)-C(12)-C(6)	170.3(16)	C(10)-C(6)-C(12)-O(3)	-125.4(14
C(7)-C(6)-C(12)-O(3)	-18.2(16)	C(4)-C(6)-C(12)-O(3)	103.1(14)
C(10)-C(6)-C(12)-O(4)	81.7(9)	C(7)-C(6)-C(12)-O(4)	-171.1(8)
C(4)-C(6)-C(12)-O(4)	-49.7(10)	C(5A)-C(1A)-C(2A)-C(3A)	-27.9(13)
C(11A)-C(1A)-C(2A)-C(3A)	178.0(10)	C(5A)-C(1A)-C(2A)-C(7A)	71.9(11)
C(11A)-C(1A)-C(2A)-C(7A)	-82.2(11)	C(7A)-C(2A)-C(3A)-C(4A)	-60.6(11)
C(1A)-C(2A)-C(3A)-C(4A)	45.7(12)	C(2A)-C(3A)-C(4A)-C(5A)	-48.5(12)
C(2A)-C(3A)-C(4A)-C(6A)	62.1(11)	C(11A)-C(1A)-C(5A)-C(4A)	145.9(10)
C(2A)-C(1A)-C(5A)-C(4A)	-4.3(11)	C(6A)-C(4A)-C(5A)-C(1A)	-65.8(10)
C(3A)-C(4A)-C(5A)-C(1A)	30.9(11)	C(5A)-C(4A)-C(6A)-C(10A)	-45.6(10)
C(3A)-C(4A)-C(6A)-C(10A)	-146.6(10)	C(5A)-C(4A)-C(6A)-C(7A)	65.9(9)
C(3A)-C(4A)-C(6A)-C(7A)	-35.1(10)	C(5A)-C(4A)-C(6A)-C(12A)	-171.1(8)
C(3A)-C(4A)-C(6A)-C(12A)	87.9(10)	C(10A)-C(6A)-C(7A)-C(2A)	117.9(10)
C(12A)-C(6A)-C(7A)-C(2A)	-116.8(10)	C(4A)-C(6A)-C(7A)-C(2A)	2.8(11)
C(10A)-C(6A)-C(7A)-C(8A)	-7.0(11)	C(12A)-C(6A)-C(7A)-C(8A)	118.3(10)
C(4A)-C(6A)-C(7A)-C(8A)	-122.1(9)	C(3A)-C(2A)-C(7A)-C(6A)	35.6(12)
C(1A)-C(2A)-C(7A)-C(6A)	-68.4(11)	C(3A)-C(2A)-C(7A)-C(8A)	145.3(11)
C(1A)-C(2A)-C(7A)-C(8A)	41.3(13)	C(6A)-C(7A)-C(8A)-C(9A)	-0.3(14)
C(2A)-C(7A)-C(8A)-C(9A)	-113.8(12)	C(7A)-C(8A)-C(9A)-C(10A)	9.7(18)
C(8A)-C(9A)-C(10A)-C(6A)	-15.5(17)	C(7A)-C(6A)-C(10A)-C(9A)	13.4(12)
C(12A)-C(6A)-C(10A)-C(9A)	-112.9(11)	C(4A)-C(6A)-C(10A)-C(9A)	123.4(11)
C(13A)-O(2A)-C(11A)-O(1A)	-14(3)	C(13A)-O(2A)-C(11A)-C(1A)	-149.1(17)
C(5A)-C(1A)-C(11A)-O(2A)	177.1(14)	C(2A)-C(1A)-C(11A)-O(2A)	-36.4(18)
C(5A)-C(1A)-C(11A)-O(1A)	34.5(14)	C(2A)-C(1A)-C(11A)-O(1A)	-179.0(11)
C(10A)-C(6A)-C(12A)-O(3A)	116.9(18)	C(7A)-C(6A)-C(12A)-O(3A)	-4(2)
C(4A)-C(6A)-C(12A)-O(3A)	-119.6(16)	C(10A)-C(6A)-C(12A)-O(2)	-54.3(11)
C(7A)-C(6A)-C(12A)-O(2)	-175.2(8)	C(4A)-C(6A)-C(12A)-O(2)	69.2(10)
O(3A)-C(12A)-O(2)-C(14)	13.2(17)	C(6A)-C(12A)-O(2)-C(14)	-175.1(6)
O(1)-C(11)-O(2)-C(14)	-12.1(12)	C(1)-C(11)-O(2)-C(14)	175.0(5)

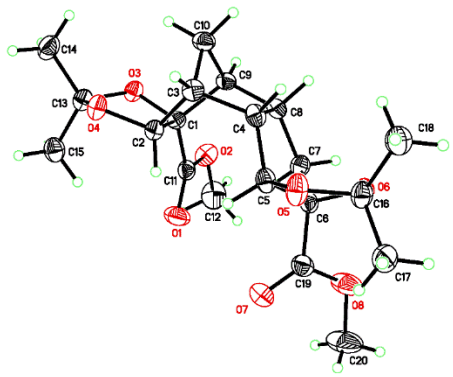

Table C1. Crystal data and structure refinement for compound **90**.

Identification code	uvic1409a	
Empirical formula	$C_{20}H_{28}O_8$	
Formula weight	396.42	
Temperature	120(2) K	
Wavelength	1.54184 Å	
Crystal system	Monoclinic	
Space group	$P2_1/n$	
Unit cell dimensions	a = 6.7876(2) Å	α = 90°
	b = 21.2855(5) Å	β = 94.6000(14)°
	c = 13.9033(4) Å	γ = 90°
Volume	2002.24(10) $Å^3$	
Z	4	
Density (calculated)	1.315 $g.cm^{-3}$	
Absorption coefficient (μ)	0.849 mm^{-1}	
F(000)	848	
Crystal color, habit	colorless, tablet	
Crystal size	0.151 × 0.082 × 0.035 mm^3	
θ range for data collection	3.806 to 71.860°	
Index ranges	$-8 \le h \le 7$, $-26 \le k \le 26$, $-16 \le l \le 17$	
Reflections collected	39788	
Independent reflections	3869 [R_{int} = 0.0391]	
Completeness to θ = 67.679°	99.4 %	
Absorption correction	Numerical	
Max. and min. transmission	1.0000 and 0.8772	
Refinement method	Full-matrix least-squares on F^2	
Data / restraints / parameters	3869 / 0 / 259	
Goodness-of-fit on F^2	1.026	
Final R indices [I>2σ(I)]	R_1 = 0.0387, wR_2 = 0.0968	
R indices (all data)	R_1 = 0.0428, wR_2 = 0.0999	
Extinction coefficient	n/a	
Largest diff. peak and hole	0.369 and -0.239 $e^-.Å^{-3}$	

Table C2. Atomic coordinates and equivalent isotropic displacement parameters ($Å^2$) for compound **90**. U(eq) is defined as one third of the trace of the orthogonalized U_{ij} tensor.

	x	y	z	U(eq)
O(1)	0.29491(15)	0.57692(6)	0.23864(8)	0.040(1)
O(2)	0.51703(15)	0.63690(5)	0.17073(7)	0.030(1)
O(3)	0.66155(14)	0.64603(4)	0.36500(7)	0.024(1)
O(4)	0.59117(15)	0.57761(4)	0.48285(7)	0.026(1)
O(5)	0.61665(17)	0.34787(4)	0.30324(7)	0.033(1)
O(6)	0.67225(14)	0.36898(4)	0.14580(7)	0.025(1)
O(7)	0.20170(17)	0.41709(7)	0.18779(10)	0.049(1)
O(8)	0.32150(17)	0.40168(7)	0.04513(8)	0.049(1)
C(1)	0.62811(18)	0.58735(6)	0.31571(9)	0.019(1)
C(2)	0.5889(2)	0.54020(6)	0.39708(9)	0.021(1)
C(3)	0.7729(2)	0.49810(6)	0.40292(10)	0.024(1)
C(4)	0.7707(2)	0.45340(6)	0.31601(10)	0.024(1)
C(5)	0.5870(2)	0.41392(6)	0.28722(10)	0.025(1)
C(6)	0.5546(2)	0.41966(6)	0.17762(10)	0.024(1)
C(7)	0.6424(2)	0.48260(6)	0.14877(10)	0.024(1)
C(8)	0.80465(19)	0.49848(6)	0.22965(9)	0.023(1)
C(9)	0.82341(19)	0.56403(6)	0.27905(9)	0.021(1)
C(10)	0.9332(2)	0.54469(7)	0.37604(10)	0.026(1)
C(11)	0.4583(2)	0.59828(6)	0.23889(10)	0.023(1)
C(12)	0.3653(3)	0.65384(9)	0.09628(12)	0.044(1)
C(13)	0.5771(2)	0.64220(6)	0.45648(10)	0.024(1)
C(14)	0.7061(2)	0.68031(8)	0.52838(11)	0.035(1)
C(15)	0.3634(2)	0.66348(7)	0.44821(11)	0.032(1)
C(16)	0.6734(2)	0.31937(6)	0.21607(10)	0.028(1)
C(17)	0.5213(2)	0.26920(7)	0.18607(13)	0.037(1)
C(18)	0.8808(2)	0.29390(7)	0.23049(12)	0.036(1)
C(19)	0.3391(2)	0.41274(7)	0.13915(11)	0.029(1)
C(20)	0.1212(3)	0.39428(12)	0.00173(15)	0.057(1)
H(2)	0.4631	0.5162	0.3838	0.025
H(3)	0.8020	0.4771	0.4668	0.029
H(4)	0.8870	0.4246	0.3257	0.029
H(5)	0.4697	0.4295	0.3193	0.030
H(7A)	0.5394	0.5156	0.1439	0.029
H(7B)	0.6998	0.4790	0.0858	0.029
H(8)	0.9355	0.4879	0.2056	0.027
H(9)	0.8943	0.5961	0.2422	0.026
H(10A)	1.0616	0.5241	0.3680	0.031
H(10B)	0.9513	0.5801	0.4220	0.031
H(12A)	0.4217	0.6815	0.0493	0.066
H(12B)	0.2579	0.6757	0.1254	0.066

H(12C)	0.3136	0.6158	0.0637	0.066
H(14A)	0.8422	0.6647	0.5305	0.053
H(14B)	0.6567	0.6764	0.5924	0.053
H(14C)	0.7029	0.7245	0.5088	0.053
H(15A)	0.2863	0.6367	0.4019	0.047
H(15B)	0.3558	0.7072	0.4259	0.047
H(15C)	0.3098	0.6604	0.5114	0.047
H(17A)	0.3894	0.2882	0.1789	0.055
H(17B)	0.5243	0.2363	0.2355	0.055
H(17C)	0.5521	0.2508	0.1245	0.055
H(18A)	0.9727	0.3283	0.2483	0.055
H(18B)	0.9169	0.2744	0.1705	0.055
H(18C)	0.8879	0.2624	0.2821	0.055
H(20A)	0.1249	0.3808	-0.0655	0.086
H(20B)	0.0512	0.4345	0.0038	0.086
H(20C)	0.0522	0.3626	0.0376	0.086

Table C3. Anisotropic displacement parameters ($Å^2$) for compound **90**.
The anisotropic displacement factor exponent takes the form:
$-2\pi^2[h^2a^{*2}U_{11} + ... + 2hka^*b^*U_{12}]$

	U_{11}	U_{22}	U_{33}	U_{23}	U_{13}	U_{12}
O(1)	0.0211(5)	0.0649(8)	0.0326(6)	0.0017(5)	-0.0004(4)	-0.0050(5)
O(2)	0.0368(6)	0.0257(5)	0.0247(5)	0.0063(4)	-0.0045(4)	0.0022(4)
O(3)	0.0303(5)	0.0183(4)	0.0224(5)	-0.0007(3)	0.0041(4)	-0.0059(4)
O(4)	0.0376(6)	0.0197(5)	0.0206(5)	0.0006(4)	0.0054(4)	-0.0012(4)
O(5)	0.0511(7)	0.0183(5)	0.0301(5)	0.0014(4)	0.0117(5)	0.0026(4)
O(6)	0.0267(5)	0.0217(5)	0.0272(5)	-0.0025(4)	0.0052(4)	0.0046(4)
O(7)	0.0263(6)	0.0629(8)	0.0581(8)	-0.0220(6)	0.0101(5)	-0.0016(5)
O(8)	0.0245(6)	0.0893(10)	0.0329(6)	0.0055(6)	-0.0030(5)	-0.0052(6)
C(1)	0.0205(6)	0.0165(6)	0.0211(6)	0.0001(5)	0.0013(5)	-0.0025(5)
C(2)	0.0242(7)	0.0186(6)	0.0198(6)	0.0002(5)	0.0028(5)	-0.0012(5)
C(3)	0.0258(7)	0.0236(6)	0.0217(6)	0.0043(5)	-0.0003(5)	0.0022(5)
C(4)	0.0252(7)	0.0224(6)	0.0247(7)	0.0029(5)	0.0035(5)	0.0058(5)
C(5)	0.0302(7)	0.0176(6)	0.0273(7)	0.0009(5)	0.0080(5)	0.0028(5)
C(6)	0.0227(7)	0.0211(6)	0.0279(7)	-0.0023(5)	0.0051(5)	0.0030(5)
C(7)	0.0277(7)	0.0224(6)	0.0230(6)	-0.0001(5)	0.0023(5)	0.0004(5)
C(8)	0.0204(6)	0.0239(6)	0.0236(6)	0.0017(5)	0.0032(5)	0.0026(5)
C(9)	0.0184(6)	0.0241(6)	0.0218(6)	0.0022(5)	0.0014(5)	-0.0026(5)
C(10)	0.0206(7)	0.0320(7)	0.0256(7)	0.0022(6)	-0.0012(5)	0.0001(5)
C(11)	0.0241(7)	0.0221(6)	0.0227(6)	-0.0023(5)	0.0019(5)	0.0039(5)
C(12)	0.0499(10)	0.0493(10)	0.0310(8)	0.0082(7)	-0.0077(7)	0.0202(8)
C(13)	0.0312(7)	0.0200(6)	0.0222(6)	0.0006(5)	0.0043(5)	-0.0048(5)
C(14)	0.0430(9)	0.0337(8)	0.0290(8)	-0.0069(6)	0.0060(6)	-0.0129(7)
C(15)	0.0358(8)	0.0271(7)	0.0324(8)	-0.0001(6)	0.0077(6)	0.0020(6)
C(16)	0.0351(8)	0.0210(7)	0.0295(7)	-0.0012(5)	0.0059(6)	0.0018(6)
C(17)	0.0385(9)	0.0259(7)	0.0467(9)	-0.0056(6)	0.0091(7)	-0.0026(6)
C(18)	0.0382(9)	0.0248(7)	0.0457(9)	-0.0003(6)	0.0007(7)	0.0064(6)
C(19)	0.0254(7)	0.0230(7)	0.0385(8)	-0.0010(6)	0.0050(6)	0.0008(5)
C(20)	0.0291(9)	0.0935(16)	0.0475(11)	0.0110(11)	-0.0098(8)	-0.0110(9)

Table C4. Bond lengths [Å] for compound **90**.

atom-atom	distance	atom-atom	distance
O(1)-C(11)	1.1980(17)	O(2)-C(11)	1.3393(17)
O(2)-C(12)	1.4460(18)	O(3)-C(1)	1.4340(15)
O(3)-C(13)	1.4388(16)	O(4)-C(13)	1.4240(16)
O(4)-C(2)	1.4330(15)	O(5)-C(5)	1.4351(16)
O(5)-C(16)	1.4354(17)	O(6)-C(6)	1.4329(15)
O(6)-C(16)	1.4383(17)	O(7)-C(19)	1.1990(19)
O(8)-C(19)	1.324(2)	O(8)-C(20)	1.451(2)
C(1)-C(11)	1.5252(18)	C(1)-C(9)	1.5400(18)
C(1)-C(2)	1.5512(17)	C(2)-C(3)	1.5341(18)
C(3)-C(4)	1.5372(19)	C(3)-C(10)	1.5403(19)
C(4)-C(5)	1.5300(19)	C(4)-C(8)	1.5684(18)
C(5)-C(6)	1.5269(19)	C(6)-C(19)	1.524(2)
C(6)-C(7)	1.5325(18)	C(7)-C(8)	1.5471(18)
C(8)-C(9)	1.5559(18)	C(9)-C(10)	1.5434(18)
C(13)-C(14)	1.5111(19)	C(13)-C(15)	1.515(2)
C(16)-C(18)	1.507(2)	C(16)-C(17)	1.520(2)
C(2)-H(2)	1.0000	C(3)-H(3)	1.0000
C(4)-H(4)	1.0000	C(5)-H(5)	1.0000
C(7)-H(7A)	0.9900	C(7)-H(7B)	0.9900
C(8)-H(8)	1.0000	C(9)-H(9)	1.0000
C(10)-H(10A)	0.9900	C(10)-H(10B)	0.9900
C(12)-H(12A)	0.9800	C(12)-H(12B)	0.9800
C(12)-H(12C)	0.9800	C(14)-H(14A)	0.9800
C(14)-H(14B)	0.9800	C(14)-H(14C)	0.9800
C(15)-H(15A)	0.9800	C(15)-H(15B)	0.9800
C(15)-H(15C)	0.9800	C(17)-H(17A)	0.9800
C(17)-H(17B)	0.9800	C(17)-H(17C)	0.9800
C(18)-H(18A)	0.9800	C(18)-H(18B)	0.9800
C(18)-H(18C)	0.9800	C(20)-H(20A)	0.9800
C(20)-H(20B)	0.9800	C(20)-H(20C)	0.9800

Table C5. Bond angles [°] for compound **90**.

atom-atom-atom	angle	atom-atom-atom	angle
C(11)-O(2)-C(12)	115.10(12)	C(1)-O(3)-C(13)	108.30(9)
C(13)-O(4)-C(2)	109.04(9)	C(5)-O(5)-C(16)	109.07(10)
C(6)-O(6)-C(16)	108.42(10)	C(19)-O(8)-C(20)	115.94(14)
O(3)-C(1)-C(11)	106.47(10)	O(3)-C(1)-C(9)	109.35(10)
C(11)-C(1)-C(9)	116.09(10)	O(3)-C(1)-C(2)	104.17(10)
C(11)-C(1)-C(2)	116.43(11)	C(9)-C(1)-C(2)	103.61(10)
O(4)-C(2)-C(3)	109.04(10)	O(4)-C(2)-C(1)	104.85(10)
C(3)-C(2)-C(1)	103.30(10)	C(2)-C(3)-C(4)	111.31(11)
C(2)-C(3)-C(10)	101.47(10)	C(4)-C(3)-C(10)	99.80(11)
C(5)-C(4)-C(3)	120.12(11)	C(5)-C(4)-C(8)	107.60(11)
C(3)-C(4)-C(8)	103.32(10)	O(5)-C(5)-C(6)	103.91(10)
O(5)-C(5)-C(4)	113.35(11)	C(6)-C(5)-C(4)	105.44(11)
O(6)-C(6)-C(19)	111.21(11)	O(6)-C(6)-C(5)	102.04(10)
C(19)-C(6)-C(5)	113.58(11)	O(6)-C(6)-C(7)	109.84(11)
C(19)-C(6)-C(7)	112.01(11)	C(5)-C(6)-C(7)	107.66(11)
C(6)-C(7)-C(8)	105.64(11)	C(7)-C(8)-C(9)	123.03(11)
C(7)-C(8)-C(4)	106.44(11)	C(9)-C(8)-C(4)	102.86(10)
C(1)-C(9)-C(10)	99.50(10)	C(1)-C(9)-C(8)	113.14(10)
C(10)-C(9)-C(8)	99.39(10)	C(3)-C(10)-C(9)	94.75(10)
O(1)-C(11)-O(2)	123.98(13)	O(1)-C(11)-C(1)	126.27(13)
O(2)-C(11)-C(1)	109.74(11)	O(4)-C(13)-O(3)	105.01(10)
O(4)-C(13)-C(14)	108.94(12)	O(3)-C(13)-C(14)	107.66(11)
O(4)-C(13)-C(15)	110.63(11)	O(3)-C(13)-C(15)	111.28(11)
C(14)-C(13)-C(15)	112.96(12)	O(5)-C(16)-O(6)	106.02(10)
O(5)-C(16)-C(18)	110.55(12)	O(6)-C(16)-C(18)	107.99(12)
O(5)-C(16)-C(17)	107.82(12)	O(6)-C(16)-C(17)	111.27(12)
C(18)-C(16)-C(17)	112.99(12)	O(7)-C(19)-O(8)	123.90(14)
O(7)-C(19)-C(6)	124.26(14)	O(8)-C(19)-C(6)	111.84(12)
O(4)-C(2)-H(2)	113.0	C(3)-C(2)-H(2)	113.0
C(1)-C(2)-H(2)	113.0	C(2)-C(3)-H(3)	114.2
C(4)-C(3)-H(3)	114.2	C(10)-C(3)-H(3)	114.2
C(5)-C(4)-H(4)	108.4	C(3)-C(4)-H(4)	108.4
C(8)-C(4)-H(4)	108.4	O(5)-C(5)-H(5)	111.3
C(6)-C(5)-H(5)	111.3	C(4)-C(5)-H(5)	111.3
C(6)-C(7)-H(7A)	110.6	C(8)-C(7)-H(7A)	110.6
C(6)-C(7)-H(7B)	110.6	C(8)-C(7)-H(7B)	110.6
H(7A)-C(7)-H(7B)	108.7	C(7)-C(8)-H(8)	107.9
C(9)-C(8)-H(8)	107.9	C(4)-C(8)-H(8)	107.9
C(1)-C(9)-H(9)	114.3	C(10)-C(9)-H(9)	114.3
C(8)-C(9)-H(9)	114.3	C(3)-C(10)-H(10A)	112.8
C(9)-C(10)-H(10A)	112.8	C(3)-C(10)-H(10B)	112.8
C(9)-C(10)-H(10B)	112.8	H(10A)-C(10)-H(10B)	110.2

O(2)-C(12)-H(12A)	109.5	O(2)-C(12)-H(12B)	109.5
H(12A)-C(12)-H(12B)	109.5	O(2)-C(12)-H(12C)	109.5
H(12A)-C(12)-H(12C)	109.5	H(12B)-C(12)-H(12C)	109.5
C(13)-C(14)-H(14A)	109.5	C(13)-C(14)-H(14B)	109.5
H(14A)-C(14)-H(14B)	109.5	C(13)-C(14)-H(14C)	109.5
H(14A)-C(14)-H(14C)	109.5	H(14B)-C(14)-H(14C)	109.5
C(13)-C(15)-H(15A)	109.5	C(13)-C(15)-H(15B)	109.5
H(15A)-C(15)-H(15B)	109.5	C(13)-C(15)-H(15C)	109.5
H(15A)-C(15)-H(15C)	109.5	H(15B)-C(15)-H(15C)	109.5
C(16)-C(17)-H(17A)	109.5	C(16)-C(17)-H(17B)	109.5
H(17A)-C(17)-H(17B)	109.5	C(16)-C(17)-H(17C)	109.5
H(17A)-C(17)-H(17C)	109.5	H(17B)-C(17)-H(17C)	109.5
C(16)-C(18)-H(18A)	109.5	C(16)-C(18)-H(18B)	109.5
H(18A)-C(18)-H(18B)	109.5	C(16)-C(18)-H(18C)	109.5
H(18A)-C(18)-H(18C)	109.5	H(18B)-C(18)-H(18C)	109.5
O(8)-C(20)-H(20A)	109.5	O(8)-C(20)-H(20B)	109.5
H(20A)-C(20)-H(20B)	109.5	O(8)-C(20)-H(20C)	109.5
H(20A)-C(20)-H(20C)	109.5	H(20B)-C(20)-H(20C)	109.5

Table C6. Torsion angles [°] for compound **90**.

atom-atom-atom-atom	angle	atom-atom-atom-atom	angle
C(13)-O(3)-C(1)-C(11)	103.08(11)	C(13)-O(3)-C(1)-C(9)	-130.76(11)
C(13)-O(3)-C(1)-C(2)	-20.52(13)	C(13)-O(4)-C(2)-C(3)	124.71(11)
C(13)-O(4)-C(2)-C(1)	14.63(13)	O(3)-C(1)-C(2)-O(4)	3.69(13)
C(11)-C(1)-C(2)-O(4)	-113.19(12)	C(9)-C(1)-C(2)-O(4)	118.07(11)
O(3)-C(1)-C(2)-C(3)	-110.48(11)	C(11)-C(1)-C(2)-C(3)	132.64(11)
C(9)-C(1)-C(2)-C(3)	3.90(12)	O(4)-C(2)-C(3)-C(4)	175.89(10)
C(1)-C(2)-C(3)-C(4)	-73.00(13)	O(4)-C(2)-C(3)-C(10)	-78.71(12)
C(1)-C(2)-C(3)-C(10)	32.40(12)	C(2)-C(3)-C(4)-C(5)	-49.96(16)
C(10)-C(3)-C(4)-C(5)	-156.46(11)	C(2)-C(3)-C(4)-C(8)	69.81(13)
C(10)-C(3)-C(4)-C(8)	-36.69(12)	C(16)-O(5)-C(5)-C(6)	20.30(14
C(16)-O(5)-C(5)-C(4)	-93.64(14)	C(3)-C(4)-C(5)-O(5)	-111.66(13)
C(8)-C(4)-C(5)-O(5)	130.73(11)	C(3)-C(4)-C(5)-C(6)	135.33(12)
C(8)-C(4)-C(5)-C(6)	17.72(13)	C(16)-O(6)-C(6)-C(19)	-90.40(13)
C(16)-O(6)-C(6)-C(5)	31.04(13)	C(16)-O(6)-C(6)-C(7)	145.04(11)
O(5)-C(5)-C(6)-O(6)	-30.93(13)	C(4)-C(5)-C(6)-O(6)	88.54(11)
O(5)-C(5)-C(6)-C(19)	88.86(13)	C(4)-C(5)-C(6)-C(19)	-151.67(11)
O(5)-C(5)-C(6)-C(7)	-146.53(11)	C(4)-C(5)-C(6)-C(7)	-27.06(14)
O(6)-C(6)-C(7)-C(8)	-84.65(13)	C(19)-C(6)-C(7)-C(8)	151.25(11)
C(5)-C(6)-C(7)-C(8)	25.70(14)	C(6)-C(7)-C(8)-C(9)	-132.09(12)
C(6)-C(7)-C(8)-C(4)	-14.14(13)	C(5)-C(4)-C(8)-C(7)	-2.20(14)
C(3)-C(4)-C(8)-C(7)	-130.23(11)	C(5)-C(4)-C(8)-C(9)	128.36(11
C(3)-C(4)-C(8)-C(9)	0.33(13)	O(3)-C(1)-C(9)-C(10)	72.05(12)
C(11)-C(1)-C(9)-C(10)	-167.51(11)	C(2)-C(1)-C(9)-C(10)	-38.56(12)
O(3)-C(1)-C(9)-C(8)	176.61(10)	C(11)-C(1)-C(9)-C(8)	-62.94(14)
C(2)-C(1)-C(9)-C(8)	66.00(13)	C(7)-C(8)-C(9)-C(1)	51.03(16)
C(4)-C(8)-C(9)-C(1)	-68.63(13)	C(7)-C(8)-C(9)-C(10)	155.66(12)
C(4)-C(8)-C(9)-C(10)	36.00(12)	C(2)-C(3)-C(10)-C(9)	-55.54(11)
C(4)-C(3)-C(10)-C(9)	58.76(11)	C(1)-C(9)-C(10)-C(3)	57.37(11)
C(8)-C(9)-C(10)-C(3)	-58.19(11)	C(12)-O(2)-C(11)-O(1)	2.3(2)
C(12)-O(2)-C(11)-C(1)	-176.66(12)	O(3)-C(1)-C(11)-O(1)	-110.85(15)
C(9)-C(1)-C(11)-O(1)	127.17(15)	C(2)-C(1)-C(11)-O(1)	4.8(2)
O(3)-C(1)-C(11)-O(2)	68.08(13)	C(9)-C(1)-C(11)-O(2)	-53.90(14)
C(2)-C(1)-C(11)-O(2)	-176.32(10)	C(2)-O(4)-C(13)-O(3)	-27.46(13)
C(2)-O(4)-C(13)-C(14)	-142.56(12)	C(2)-O(4)-C(13)-C(15)	92.70(13)
C(1)-O(3)-C(13)-O(4)	29.97(13)	C(1)-O(3)-C(13)-C(14)	145.95(11)
C(1)-O(3)-C(13)-C(15)	-89.76(12)	C(5)-O(5)-C(16)-O(6)	-1.63(15)
C(5)-O(5)-C(16)-C(18)	115.15(13)	C(5)-O(5)-C(16)-C(17)	-120.89(13)
C(6)-O(6)-C(16)-O(5)	-19.44(14)	C(6)-O(6)-C(16)-C(18)	-137.93(12)
C(6)-O(6)-C(16)-C(17)	97.52(13)	C(20)-O(8)-C(19)-O(7)	-0.4(3)
C(20)-O(8)-C(19)-C(6)	179.92(15)	O(6)-C(6)-C(19)-O(7)	131.11(15)
C(5)-C(6)-C(19)-O(7)	16.7(2)	C(7)-C(6)-C(19)-O(7)	-105.56(17)
O(6)-C(6)-C(19)-O(8)	-49.26(16)	C(5)-C(6)-C(19)-O(8)	-163.69(12)

C(7)-C(6)-C(19)-O(8)	74.08(15)

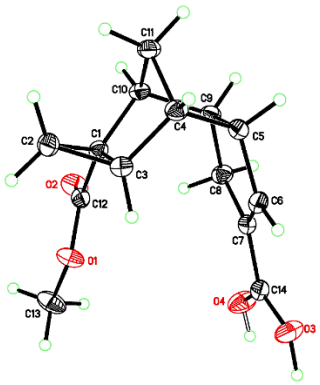

Table D1. Crystal data and structure refinement for compound **86**.

Identification code	uvic1404a	
Empirical formula	$C_{14}H_{16}O_4$	
Formula weight	248.27	
Temperature	120(2) K	
Wavelength	1.54184 Å	
Crystal system	Monoclinic	
Space group	$P2_1/c$	
Unit cell dimensions	a = 7.3209(2) Å	α = 90°
	b = 6.09350(10) Å	β = 92.0063(7)°
	c = 26.7101(6) Å	γ = 90°
Volume	1190.80(5) $Å^3$	
Z	4	
Density (calculated)	1.385 $g.cm^{-3}$	
Absorption coefficient (μ)	0.835 mm^{-1}	
F(000)	528	
Crystal color, habit	colorless, tablet	
Crystal size	0.234 × 0.109 × 0.065 mm^3	
θ range for data collection	3.311 to 71.782°	
Index ranges	$-9 \leq h \leq 8$, $-7 \leq k \leq 6$, $-32 \leq l \leq 32$	
Reflections collected	20313	
Independent reflections	2277 [R_{int} = 0.0244]	
Completeness to θ = 67.679°	98.1 %	
Absorption correction	Numerical	
Max. and min. transmission	0.9858 and 0.8600	
Refinement method	Full-matrix least-squares on F^2	
Data / restraints / parameters	2277 / 0 / 171	
Goodness-of-fit on F^2	1.081	
Final R indices [I>2σ(I)]	R_1 = 0.0358, wR_2 = 0.0930	
R indices (all data)	R_1 = 0.0363, wR_2 = 0.0936	
Extinction coefficient	n/a	
Largest diff. peak and hole	0.256 and -0.226 $e^-.Å^{-3}$	

Table D2. Atomic coordinates and equivalent isotropic displacement parameters ($Å^2$) for compound **86**. U(eq) is defined as one third of the trace of the orthogonalized U_{ij} tensor.

	x	y	z	U(eq)
O(1)	0.74225(11)	0.60789(14)	0.17944(3)	0.023(1)
O(2)	0.63600(12)	0.94329(15)	0.19732(4)	0.027(1)
O(3)	0.72690(13)	0.55047(16)	0.00226(3)	0.029(1)
O(4)	0.50289(13)	0.73032(19)	0.03948(4)	0.031(1)
C(1)	0.94904(15)	0.90236(19)	0.17773(4)	0.016(1)
C(2)	1.09729(16)	0.7809(2)	0.20936(4)	0.020(1)
C(3)	1.09811(15)	0.76632(19)	0.15363(4)	0.017(1)
C(4)	1.20727(15)	0.9361(2)	0.12525(4)	0.018(1)
C(5)	1.08653(16)	1.0092(2)	0.07918(4)	0.019(1)
C(6)	0.98427(16)	0.8328(2)	0.05111(4)	0.020(1)
C(7)	0.80356(16)	0.8559(2)	0.05360(4)	0.019(1)
C(8)	0.74832(16)	1.0580(2)	0.08204(4)	0.020(1)
C(9)	0.93261(16)	1.15200(19)	0.10290(4)	0.018(1)
C(10)	0.98271(15)	1.13734(19)	0.16012(4)	0.017(1)
C(11)	1.19254(16)	1.1446(2)	0.15749(4)	0.020(1)
C(12)	0.76052(15)	0.8256(2)	0.18550(4)	0.018(1)
C(13)	0.56277(17)	0.5185(2)	0.18818(5)	0.029(1)
C(14)	0.67135(16)	0.7019(2)	0.03022(4)	0.020(1)
H(3O)	0.627(7)	0.455(9)	-0.0134(17)	0.064(14)
H(4O)	0.439(5)	0.642(7)	0.0258(13)	0.024(8)
H(2A)	1.1936	0.8704	0.2264	0.024
H(2B)	1.0600	0.6489	0.2280	0.024
H(3)	1.0645	0.6245	0.1369	0.020
H(4)	1.3346	0.8912	0.1176	0.022
H(5)	1.1593	1.0996	0.0558	0.023
H(6)	1.0414	0.7176	0.0335	0.024
H(8A)	0.6670	1.0195	0.1096	0.024
H(8B)	0.6850	1.1648	0.0595	0.024
H(9)	0.9450	1.3076	0.0916	0.022
H(10A)	0.9281	1.2545	0.1811	0.020
H(11A)	1.2366	1.2775	0.1404	0.023
H(11B)	1.2549	1.1293	0.1908	0.023
H(13A)	0.5642	0.3595	0.1828	0.043
H(13B)	0.5299	0.5495	0.2227	0.043
H(13C)	0.4728	0.5861	0.1649	0.043

Table D3. Anisotropic displacement parameters ($Å^2$) for compound **86**.
The anisotropic displacement factor exponent takes the form:
$-2\pi^2[h^2a^{*2}U_{11} + ... + 2hka^*b^*U_{12}]$

	U_{11}	U_{22}	U_{33}	U_{23}	U_{13}	U_{12}
O(1)	0.0163(4)	0.0155(4)	0.0357(5)	0.0013(3)	0.0034(3)	-0.0021(3)
O(2)	0.0219(4)	0.0213(5)	0.0374(5)	-0.0020(4)	0.0095(4)	0.0023(3)
O(3)	0.0267(5)	0.0296(5)	0.0307(5)	-0.0129(4)	0.0014(4)	-0.0047(4)
O(4)	0.0194(5)	0.0372(6)	0.0361(5)	-0.0137(4)	0.0015(4)	-0.0064(4)
C(1)	0.0170(5)	0.0145(6)	0.0156(5)	-0.0008(4)	-0.0001(4)	0.0006(4)
C(2)	0.0197(6)	0.0209(6)	0.0196(6)	0.0028(4)	-0.0032(4)	0.0002(4)
C(3)	0.0149(5)	0.0155(6)	0.0197(6)	-0.0012(4)	0.0000(4)	0.0009(4)
C(4)	0.0151(5)	0.0197(6)	0.0201(5)	-0.0014(4)	0.0007(4)	-0.0024(4)
C(5)	0.0192(6)	0.0215(6)	0.0173(5)	0.0006(4)	0.0015(4)	-0.0055(5)
C(6)	0.0228(6)	0.0235(7)	0.0149(5)	-0.0021(4)	0.0020(4)	-0.0044(5)
C(7)	0.0219(6)	0.0195(6)	0.0145(5)	0.0012(4)	-0.0006(4)	-0.0041(4)
C(8)	0.0207(6)	0.0187(6)	0.0212(5)	0.0003(4)	-0.0053(4)	-0.0005(4)
C(9)	0.0210(6)	0.0140(6)	0.0200(6)	0.0019(4)	-0.0030(4)	-0.0028(4)
C(10)	0.0181(6)	0.0138(6)	0.0190(5)	-0.0023(4)	-0.0015(4)	-0.0016(4)
C(11)	0.0190(6)	0.0175(6)	0.0218(6)	-0.0010(4)	-0.0022(4)	-0.0042(4)
C(12)	0.0199(6)	0.0165(6)	0.0164(5)	0.0010(4)	0.0008(4)	0.0000(4)
C(13)	0.0169(6)	0.0227(7)	0.0461(8)	0.0079(6)	0.0012(5)	-0.0045(5)
C(14)	0.0218(6)	0.0216(6)	0.0156(5)	0.0000(4)	0.0001(4)	-0.0031(5)

Table D4. Bond lengths [Å] for compound **86**.

atom-atom	distance	atom-atom	distance
O(1)-C(12)	1.3427(15)	O(1)-C(13)	1.4488(14)
O(2)-C(12)	1.2104(15)	O(3)-C(14)	1.2635(15)
O(4)-C(14)	1.2781(15)	C(1)-C(12)	1.4787(15)
C(1)-C(10)	1.5297(16)	C(1)-C(3)	1.5302(15)
C(1)-C(2)	1.5412(15)	C(2)-C(3)	1.4915(15)
C(3)-C(4)	1.5252(16)	C(4)-C(11)	1.5406(16)
C(4)-C(5)	1.5549(16)	C(5)-C(6)	1.4959(16)
C(5)-C(9)	1.5744(16)	C(6)-C(7)	1.3344(17)
C(7)-C(14)	1.4712(16)	C(7)-C(8)	1.5097(17)
C(8)-C(9)	1.5511(15)	C(9)-C(10)	1.5617(15)
C(10)-C(11)	1.5408(15)	O(3)-H(3O)	1.01(6)
O(4)-H(4O)	0.79(4)	C(2)-H(2A)	0.9900
C(2)-H(2B)	0.9900	C(3)-H(3)	1.0000
C(4)-H(4)	1.0000	C(5)-H(5)	1.0000
C(6)-H(6)	0.9500	C(8)-H(8A)	0.9900
C(8)-H(8B)	0.9900	C(9)-H(9)	1.0000
C(10)-H(10A)	1.0000	C(11)-H(11A)	0.9900
C(11)-H(11B)	0.9900	C(13)-H(13A)	0.9800
C(13)-H(13B)	0.9800	C(13)-H(13C)	0.9800

Table D5. Bond angles [°] for compound **86**.

atom-atom-atom	angle	atom-atom-atom	angle
C(12)-O(1)-C(13)	116.05(10)	C(12)-C(1)-C(10)	120.02(10)
C(12)-C(1)-C(3)	124.79(10)	C(10)-C(1)-C(3)	104.64(9)
C(12)-C(1)-C(2)	114.46(10)	C(10)-C(1)-C(2)	120.00(10)
C(3)-C(1)-C(2)	58.10(7)	C(3)-C(2)-C(1)	60.58(7)
C(2)-C(3)-C(4)	118.43(10)	C(2)-C(3)-C(1)	61.32(7)
C(4)-C(3)-C(1)	103.61(9)	C(3)-C(4)-C(11)	103.49(9)
C(3)-C(4)-C(5)	107.12(9)	C(11)-C(4)-C(5)	99.06(9)
C(6)-C(5)-C(4)	116.85(10)	C(6)-C(5)-C(9)	104.25(9)
C(4)-C(5)-C(9)	103.58(9)	C(7)-C(6)-C(5)	112.27(11)
C(6)-C(7)-C(14)	123.39(11)	C(6)-C(7)-C(8)	113.24(10)
C(14)-C(7)-C(8)	123.37(11)	C(7)-C(8)-C(9)	103.71(9)
C(8)-C(9)-C(10)	120.13(10)	C(8)-C(9)-C(5)	106.09(9)
C(10)-C(9)-C(5)	102.44(9)	C(1)-C(10)-C(11)	102.26(9)
C(1)-C(10)-C(9)	108.64(9)	C(11)-C(10)-C(9)	98.87(9)
C(4)-C(11)-C(10)	95.24(8)	O(2)-C(12)-O(1)	122.95(11)
O(2)-C(12)-C(1)	124.37(11)	O(1)-C(12)-C(1)	112.65(10)
O(3)-C(14)-O(4)	123.09(11)	O(3)-C(14)-C(7)	119.74(11)
O(4)-C(14)-C(7)	117.16(11)	C(14)-O(3)-H(3O)	115(3)
C(14)-O(4)-H(4O)	112(2)	C(3)-C(2)-H(2A)	117.7
C(1)-C(2)-H(2A)	117.7	C(3)-C(2)-H(2B)	117.7
C(1)-C(2)-H(2B)	117.7	H(2A)-C(2)-H(2B)	114.8
C(2)-C(3)-H(3)	119.3	C(4)-C(3)-H(3)	119.3
C(1)-C(3)-H(3)	119.3	C(3)-C(4)-H(4)	115.1
C(11)-C(4)-H(4)	115.1	C(5)-C(4)-H(4)	115.1
C(6)-C(5)-H(5)	110.6	C(4)-C(5)-H(5)	110.6
C(9)-C(5)-H(5)	110.6	C(7)-C(6)-H(6)	123.9
C(5)-C(6)-H(6)	123.9	C(7)-C(8)-H(8A)	111.0
C(9)-C(8)-H(8A)	111.0	C(7)-C(8)-H(8B)	111.0
C(9)-C(8)-H(8B)	111.0	H(8A)-C(8)-H(8B)	109.0
C(8)-C(9)-H(9)	109.2	C(10)-C(9)-H(9)	109.2
C(5)-C(9)-H(9)	109.2	C(1)-C(10)-H(10A)	115.1
C(11)-C(10)-H(10A)	115.1	C(9)-C(10)-H(10A)	115.1
C(4)-C(11)-H(11A)	112.7	C(10)-C(11)-H(11A)	112.7
C(4)-C(11)-H(11B)	112.7	C(10)-C(11)-H(11B)	112.7
H(11A)-C(11)-H(11B)	110.2	O(1)-C(13)-H(13A)	109.5
O(1)-C(13)-H(13B)	109.5	H(13A)-C(13)-H(13B)	109.5
O(1)-C(13)-H(13C)	109.5	H(13A)-C(13)-H(13C)	109.5
H(13B)-C(13)-H(13C)	109.5		

Table D6. Torsion angles [°] for compound **86**.

atom-atom-atom-atom	angle	atom-atom-atom-atom	angle
C(12)-C(1)-C(2)-C(3)	117.08(11)	C(10)-C(1)-C(2)-C(3)	-89.11(11)
C(1)-C(2)-C(3)-C(4)	90.51(11)	C(12)-C(1)-C(3)-C(2)	-99.29(12)
C(10)-C(1)-C(3)-C(2)	116.49(10)	C(12)-C(1)-C(3)-C(4)	145.51(10)
C(10)-C(1)-C(3)-C(4)	1.29(11)	C(2)-C(1)-C(3)-C(4)	-115.21(10)
C(2)-C(3)-C(4)-C(11)	-32.52(13)	C(1)-C(3)-C(4)-C(11)	31.98(11)
C(2)-C(3)-C(4)-C(5)	-136.60(10)	C(1)-C(3)-C(4)-C(5)	-72.10(10)
C(3)-C(4)-C(5)-C(6)	-42.08(13)	C(11)-C(4)-C(5)-C(6)	-149.32(10)
C(3)-C(4)-C(5)-C(9)	71.88(11)	C(11)-C(4)-C(5)-C(9)	-35.36(10)
C(4)-C(5)-C(6)-C(7)	115.60(12)	C(9)-C(5)-C(6)-C(7)	2.02(13)
C(5)-C(6)-C(7)-C(14)	-178.57(10)	C(5)-C(6)-C(7)-C(8)	2.44(14
C(6)-C(7)-C(8)-C(9)	-5.81(13)	C(14)-C(7)-C(8)-C(9)	175.20(10)
C(7)-C(8)-C(9)-C(10)	-108.66(11)	C(7)-C(8)-C(9)-C(5)	6.59(11)
C(6)-C(5)-C(9)-C(8)	-5.41(11)	C(4)-C(5)-C(9)-C(8)	-128.14(10)
C(6)-C(5)-C(9)-C(10)	121.36(9)	C(4)-C(5)-C(9)-C(10)	-1.37(11)
C(12)-C(1)-C(10)-C(11)	179.72(9)	C(3)-C(1)-C(10)-C(11)	-33.96(10)
C(2)-C(1)-C(10)-C(11)	27.37(12)	C(12)-C(1)-C(10)-C(9)	-76.40(12)
C(3)-C(1)-C(10)-C(9)	69.91(11)	C(2)-C(1)-C(10)-C(9)	131.24(10)
C(8)-C(9)-C(10)-C(1)	48.51(13)	C(5)-C(9)-C(10)-C(1)	-68.63(10)
C(8)-C(9)-C(10)-C(11)	154.74(10)	C(5)-C(9)-C(10)-C(11)	37.60(10)
C(3)-C(4)-C(11)-C(10)	-51.42(10)	C(5)-C(4)-C(11)-C(10)	58.75(9)
C(1)-C(10)-C(11)-C(4)	51.63(10)	C(9)-C(10)-C(11)-C(4)	-59.77(10)
C(13)-O(1)-C(12)-O(2)	-0.32(17)	C(13)-O(1)-C(12)-C(1)	177.87(10)
C(10)-C(1)-C(12)-O(2)	-28.89(16)	C(3)-C(1)-C(12)-O(2)	-168.10(11)
C(2)-C(1)-C(12)-O(2)	124.91(12)	C(10)-C(1)-C(12)-O(1)	152.94(10)
C(3)-C(1)-C(12)-O(1)	13.73(15)	C(2)-C(1)-C(12)-O(1)	-53.26(13)
C(6)-C(7)-C(14)-O(3)	-6.94(18)	C(8)-C(7)-C(14)-O(3)	171.95(11)
C(6)-C(7)-C(14)-O(4)	173.29(11)	C(8)-C(7)-C(14)-O(4)	-7.82(17)

Table D7. Hydrogen bonds for compound **86** [Å and °].

D-H...A	d(D-H)	d(H...A)	d(D...A)	<(DHA)
O(3)-H(3O)...O(4)#1	1.01(6)	1.62(6)	2.6209(13)	170(4)
O(4)-H(4O)...O(3)#1	0.79(4)	1.83(4)	2.6209(13)	174(3)

Symmetry transformations used to generate equivalent atoms:
#1 -x+1,-y+1,-z

Appendix B: NMR Data for Selected Compounds

^{1}H and ^{13}C NMR spectra for compound **2**

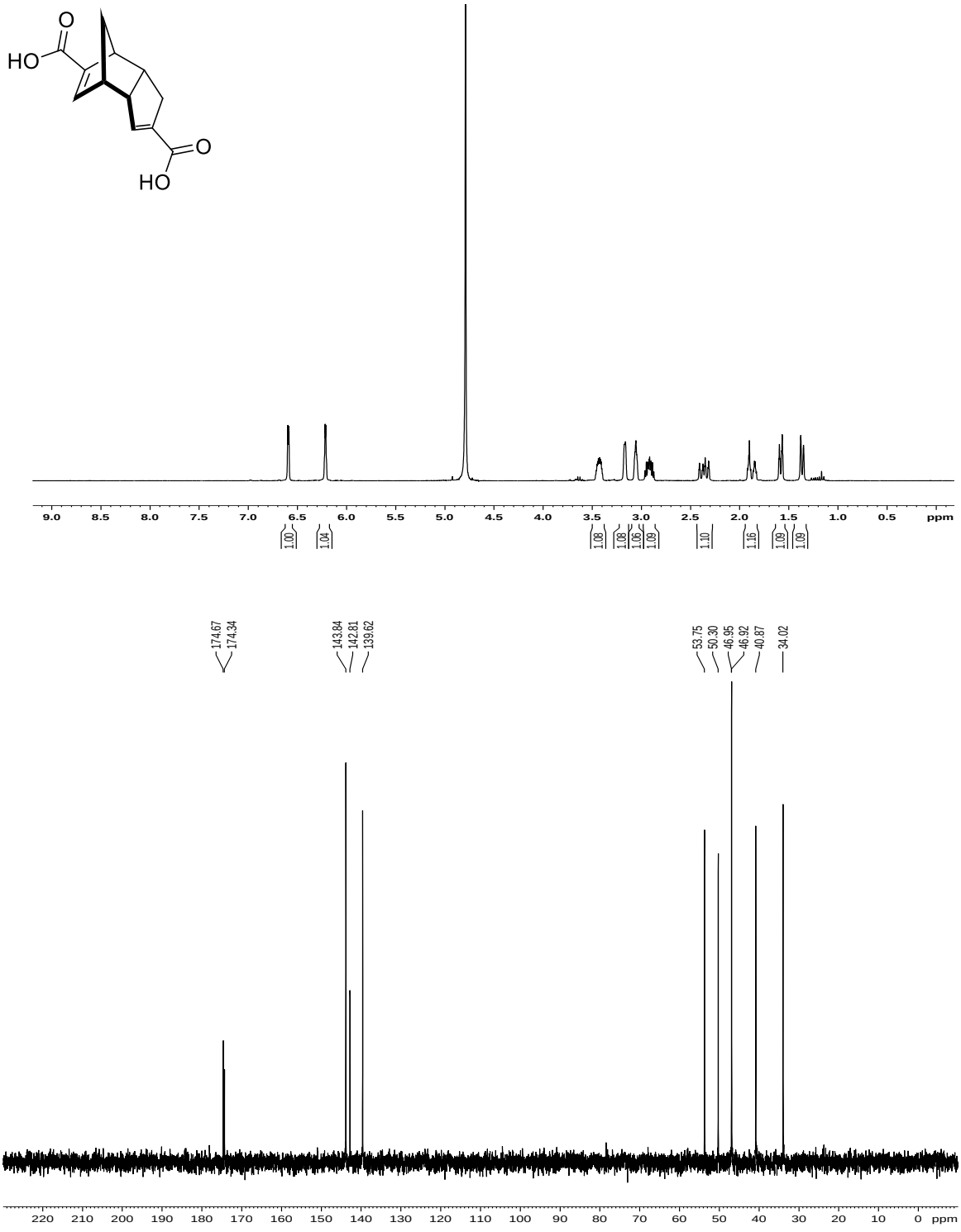

^{1}H and ^{13}C NMR spectra for compound **3**

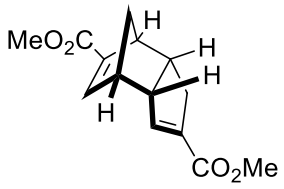

^{1}H and ^{13}C NMR spectra for compound **6**

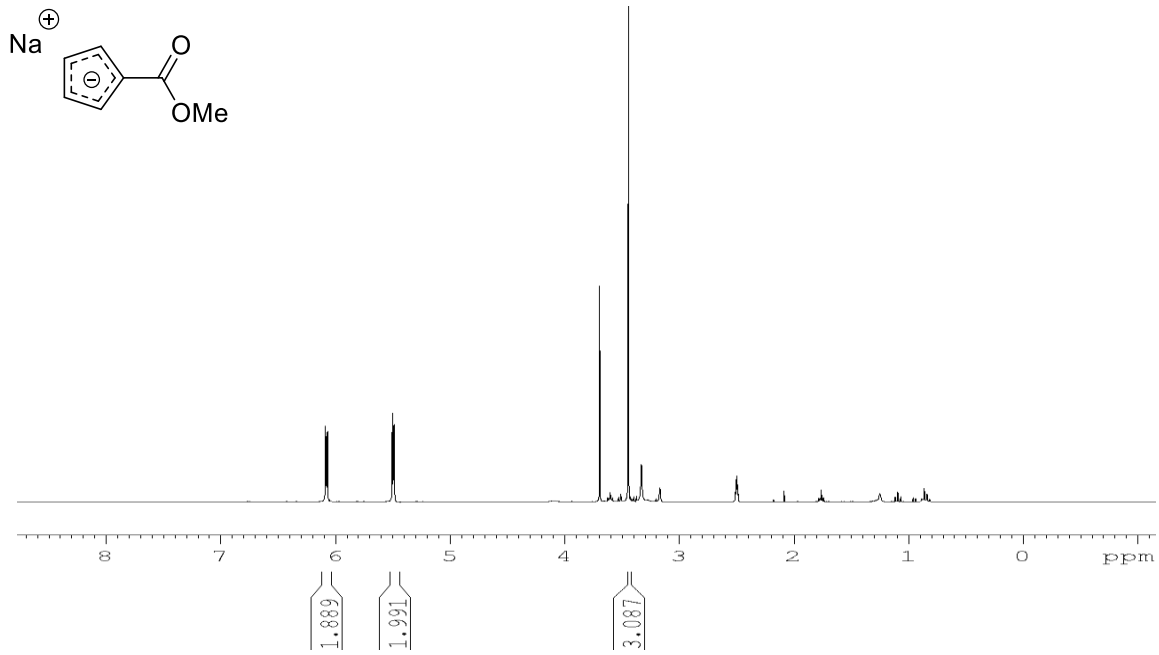

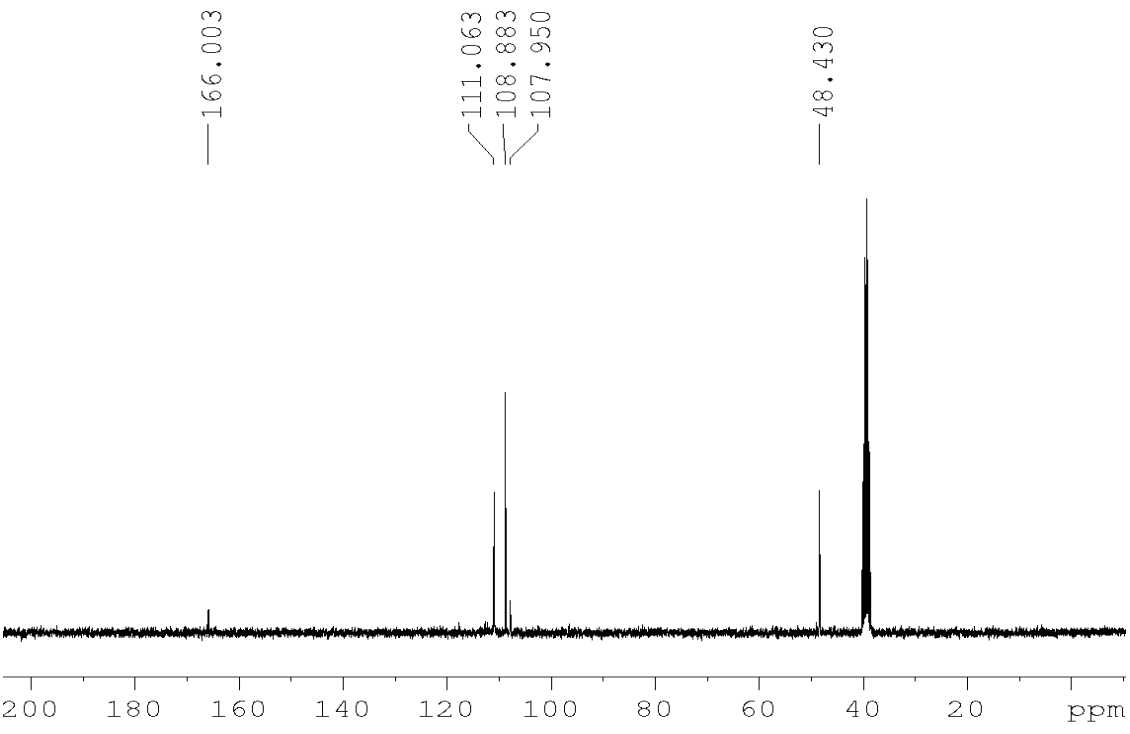

^{1}H and ^{13}C NMR spectra for compound **7**

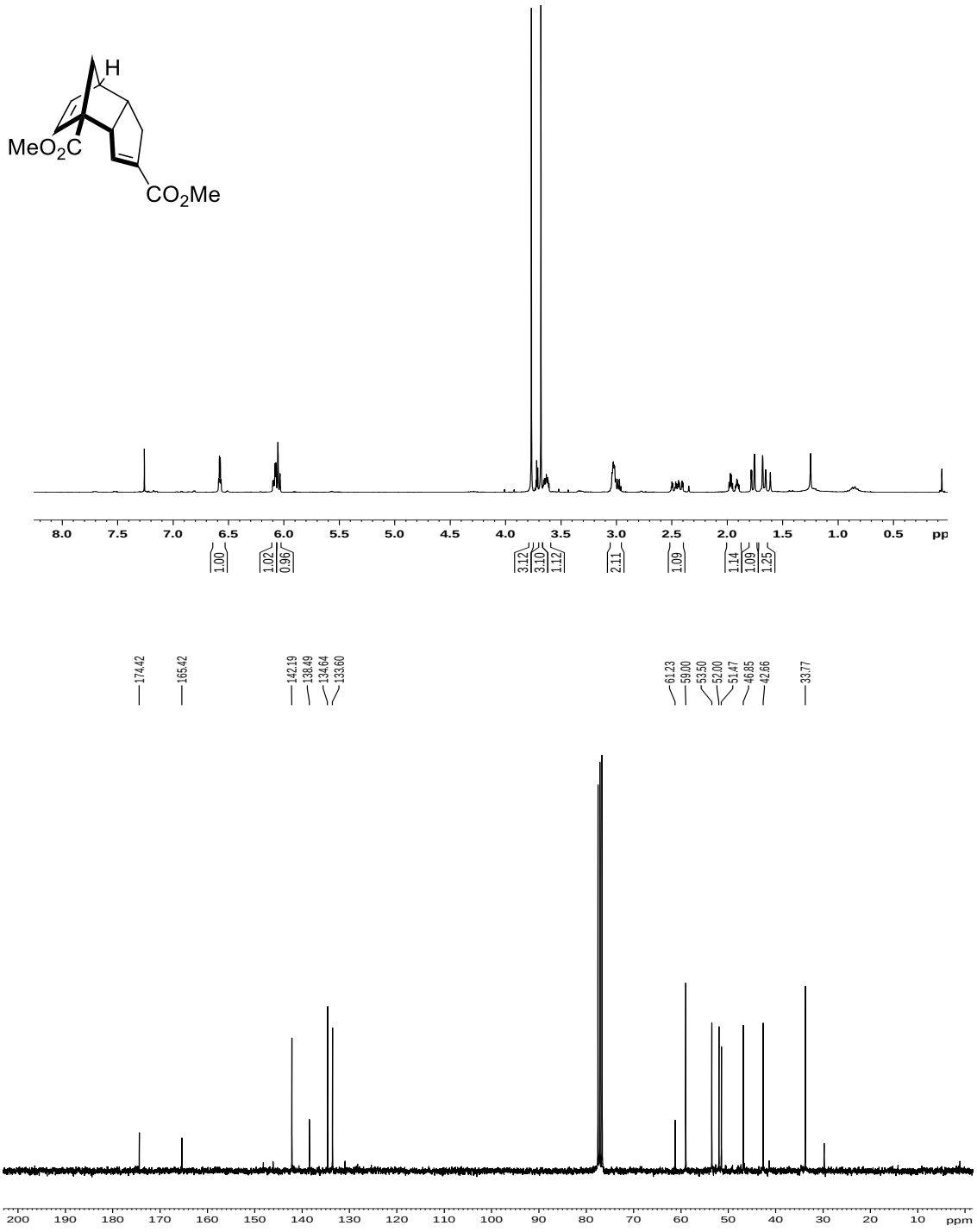

^{1}H and ^{13}C NMR spectra for compound **8**

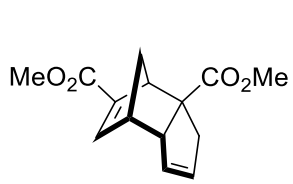

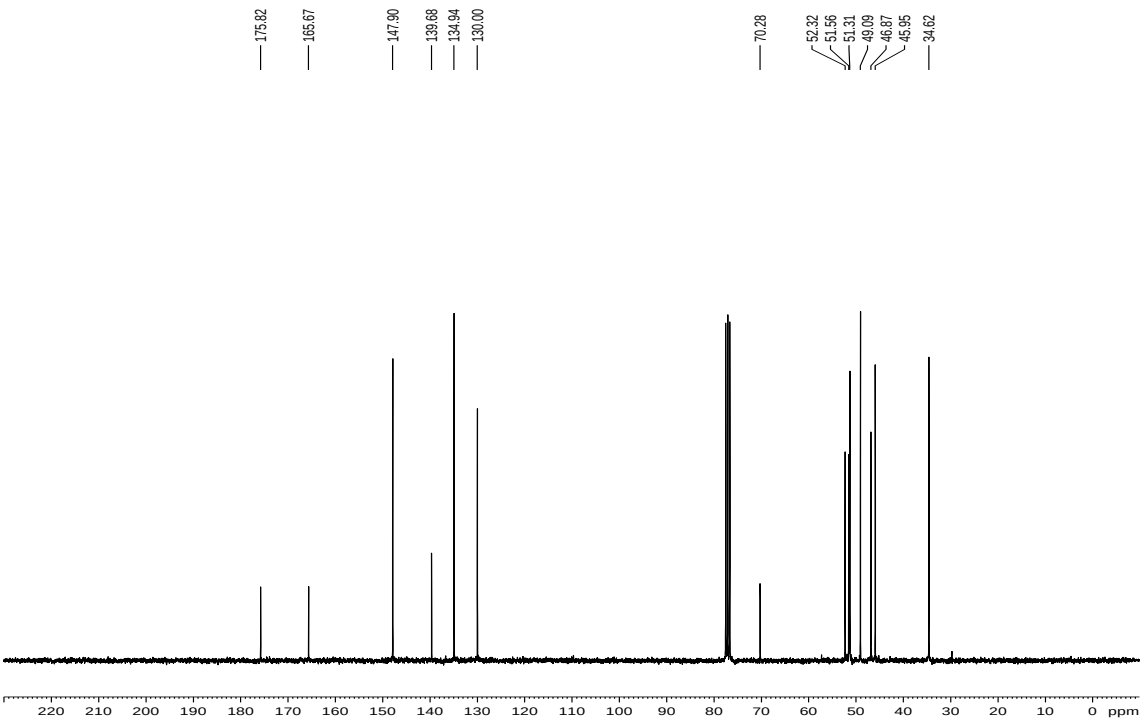

^{1}H and ^{13}C NMR spectra for compound **65**

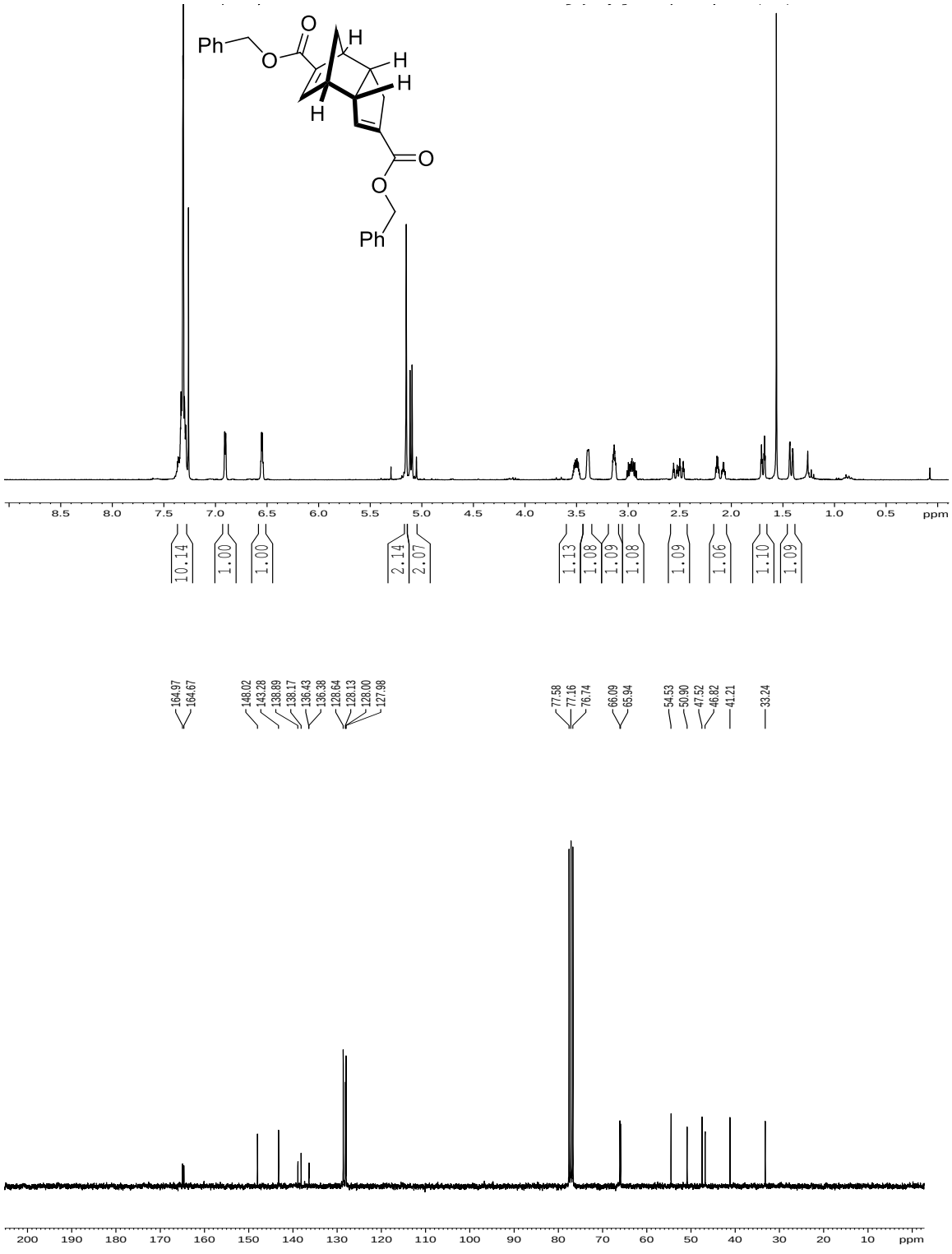

^{1}H and ^{13}C NMR spectra for compound **67**

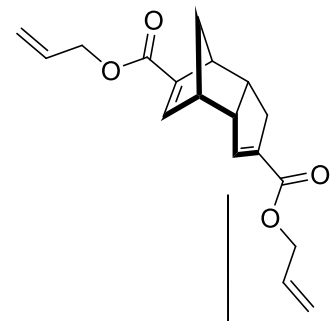

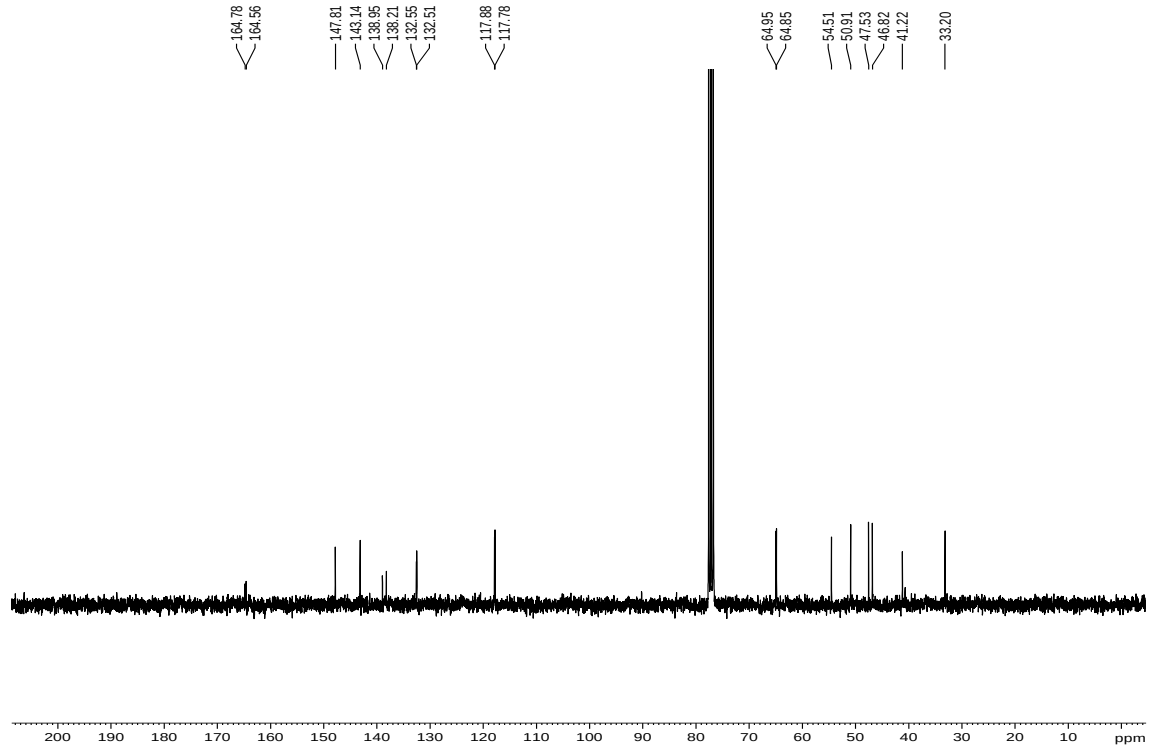

^{1}H and ^{13}C NMR spectra for compound **69**

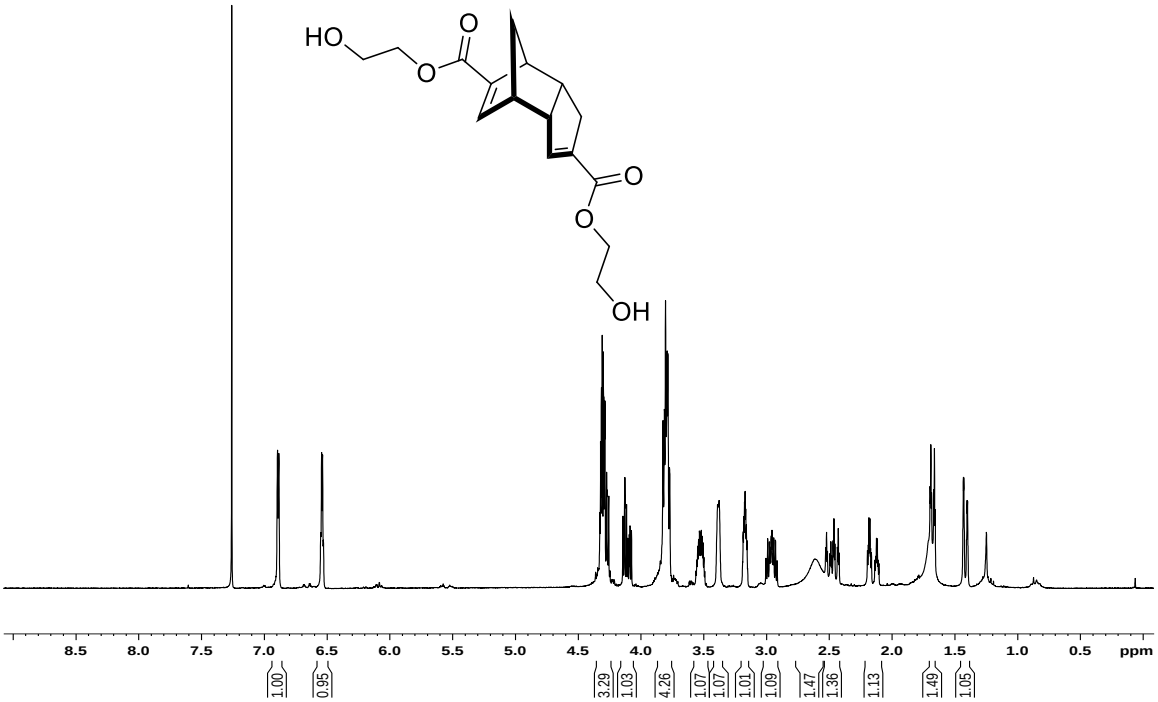

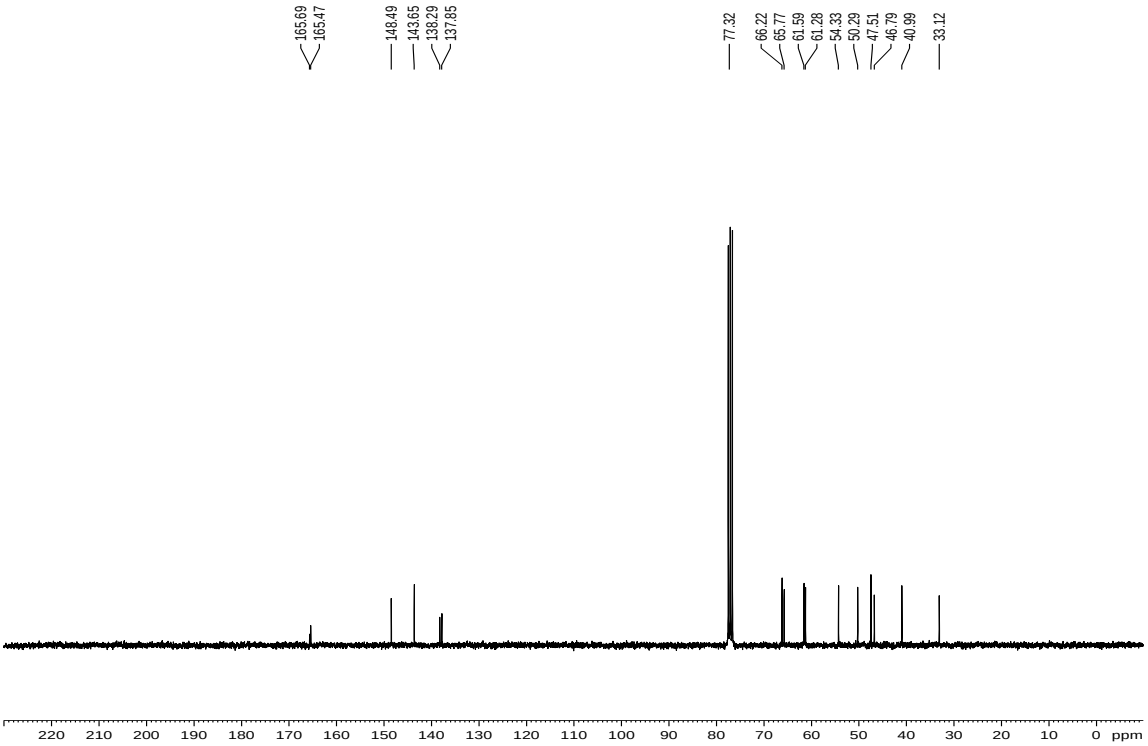

^{1}H and ^{13}C NMR spectra for compound **71**

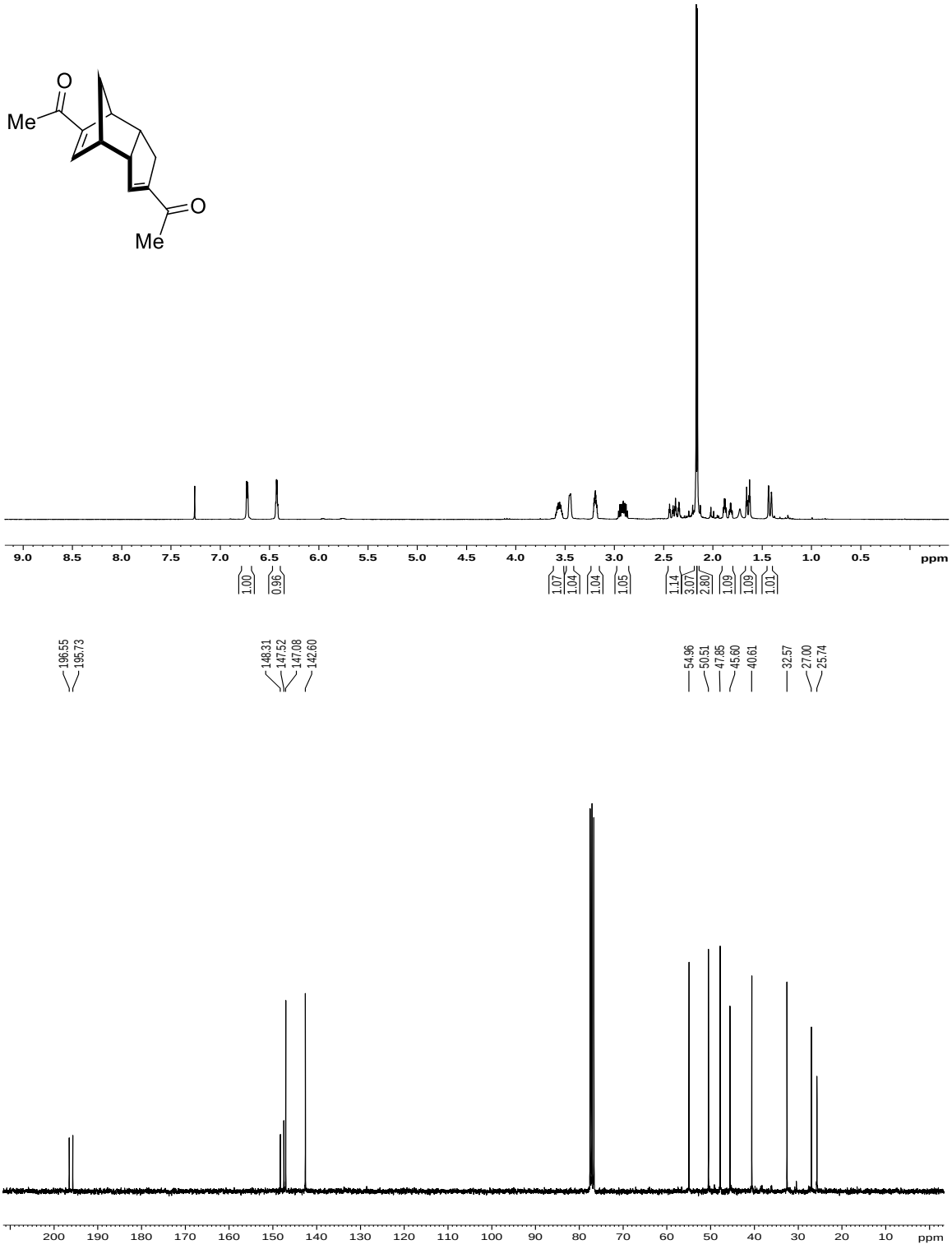

^{1}H and ^{13}C NMR spectra for compound **73**

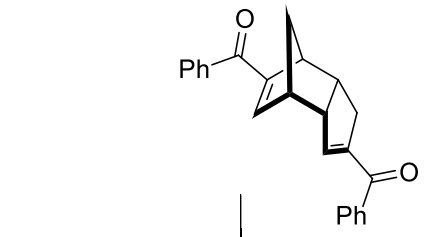

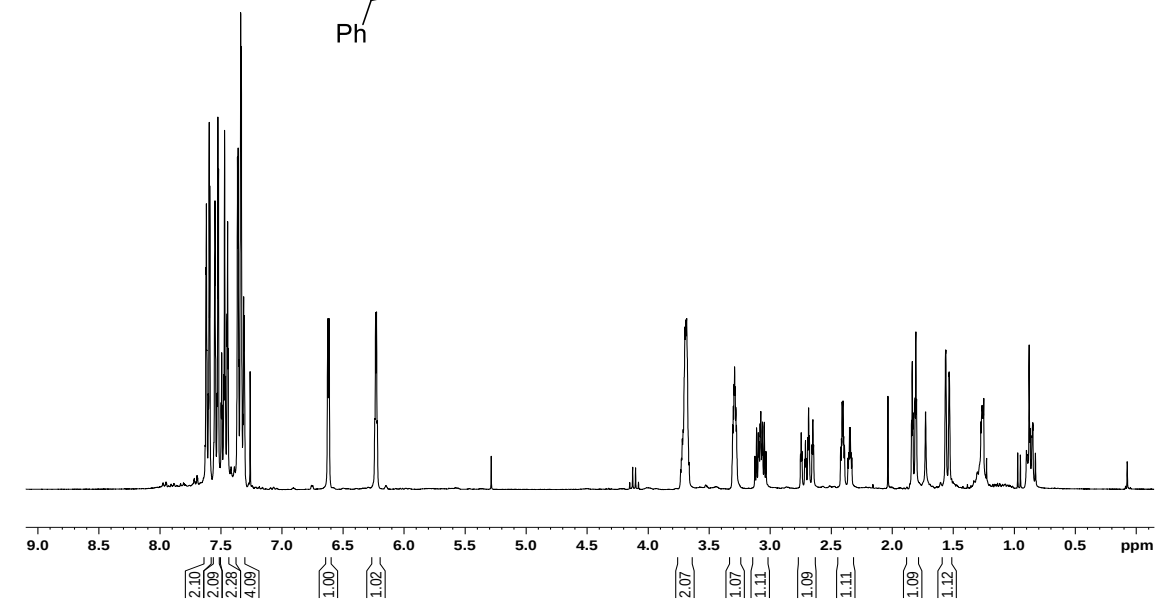

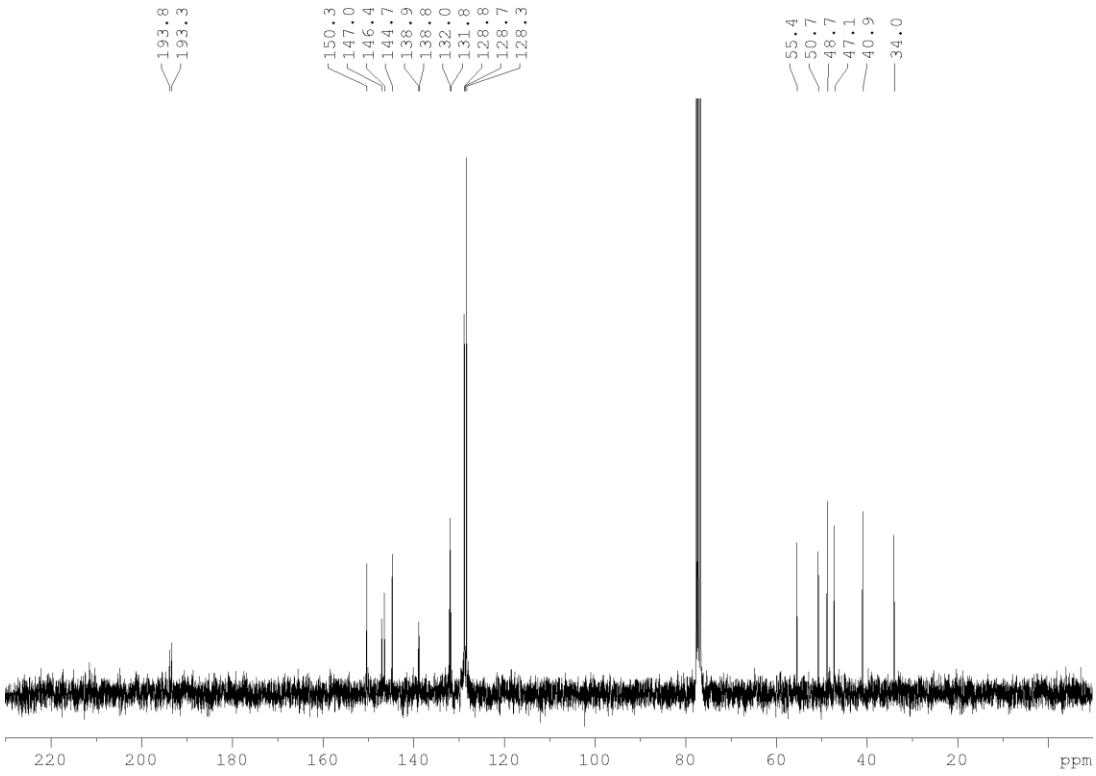

^{1}H and ^{13}C NMR spectra for compound **83**

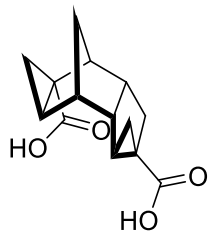

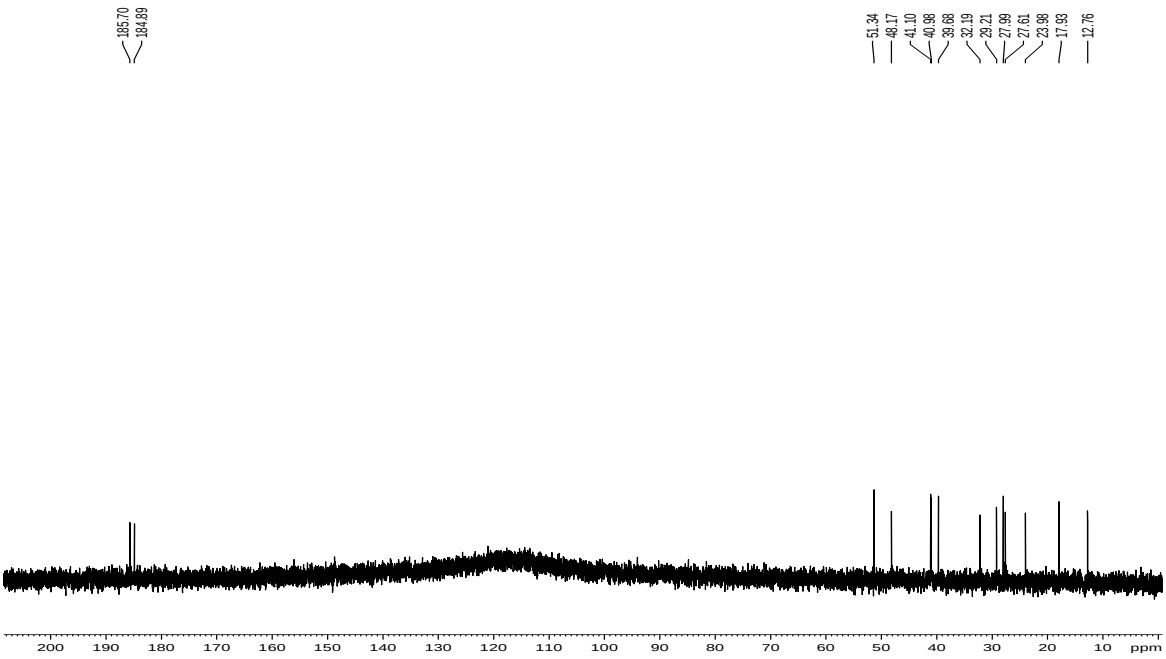

^{1}H and ^{13}C NMR spectra for compound **85**

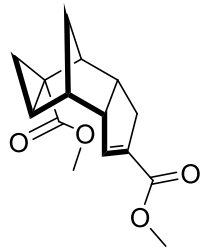

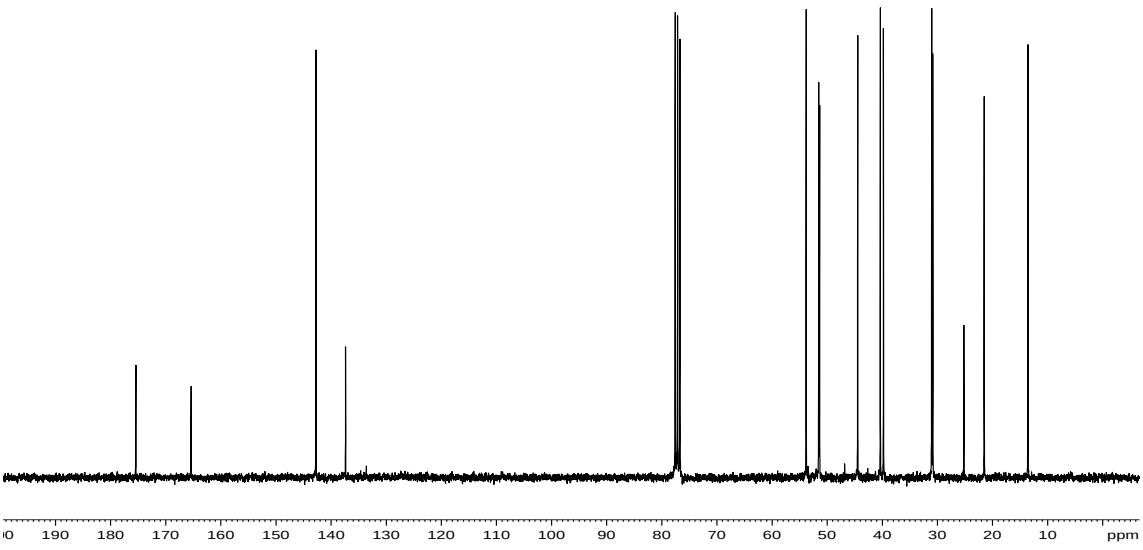

^{1}H and ^{13}C NMR spectra for compound **86**

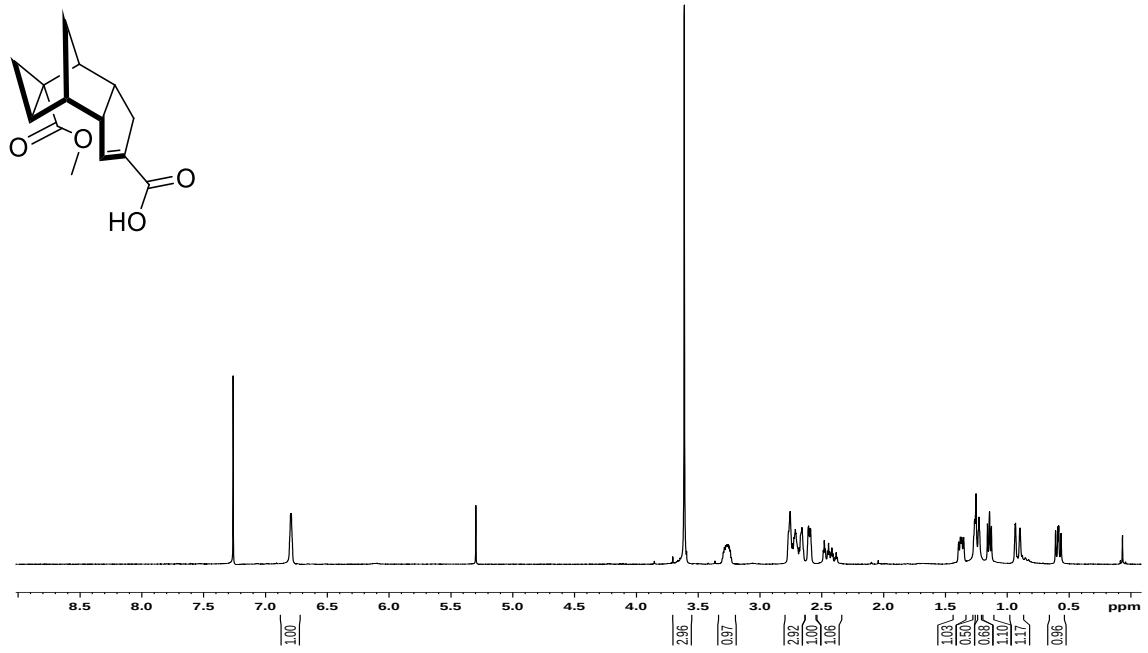

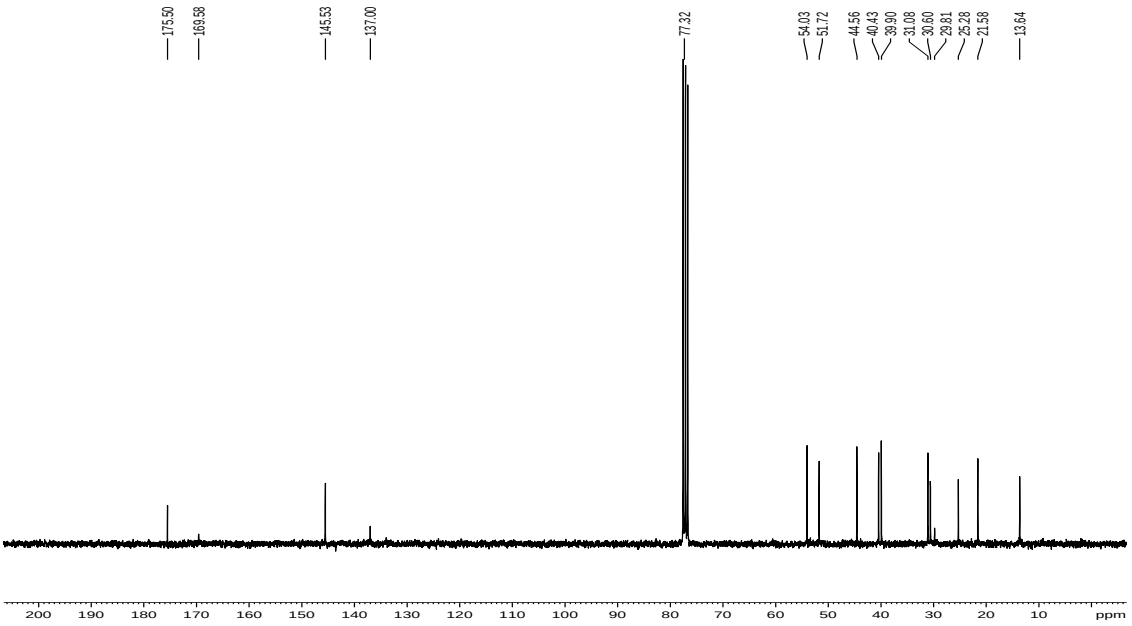

^{1}H and ^{13}C NMR spectra for compound **88**

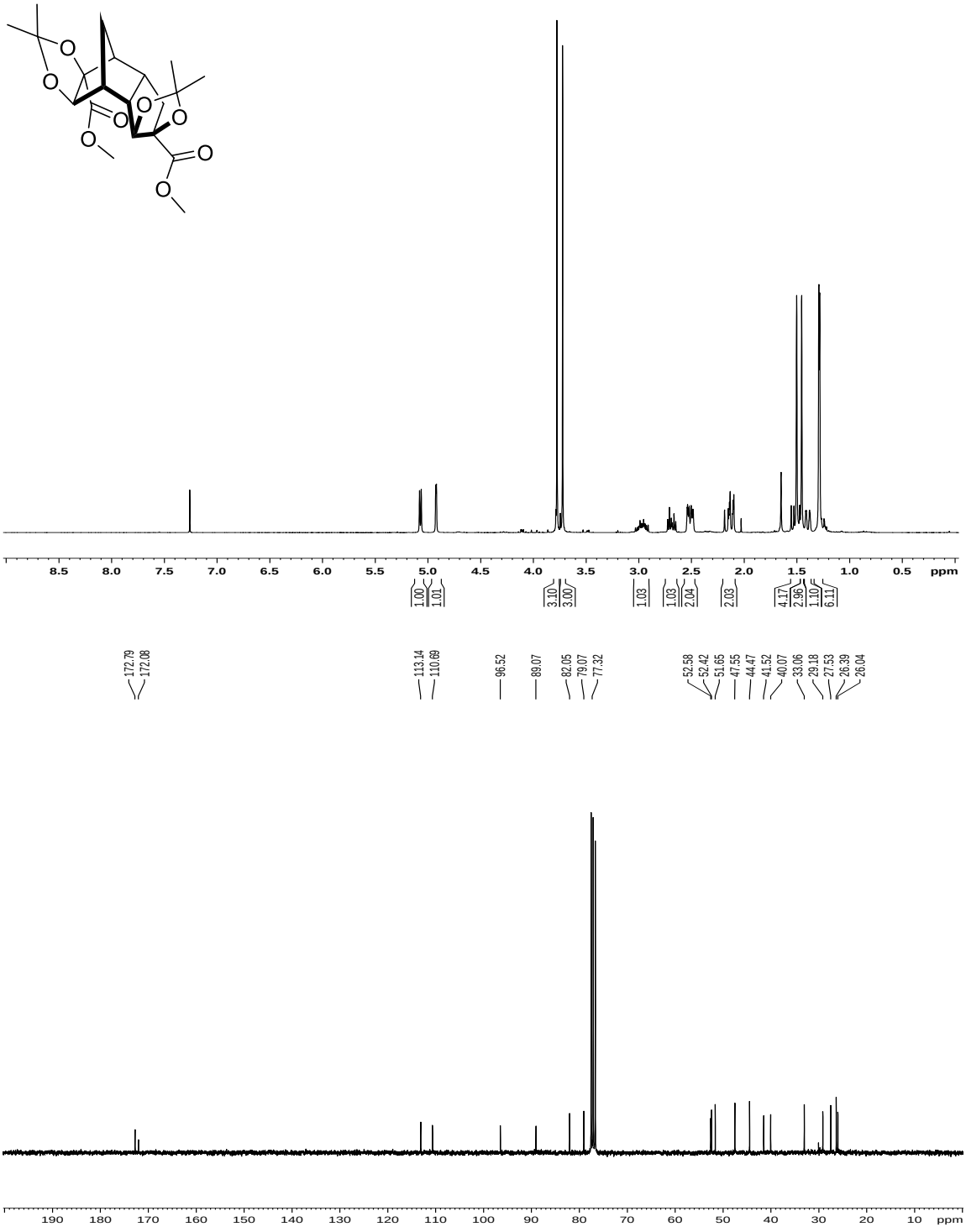

^{1}H and ^{13}C NMR spectra for compound **89**

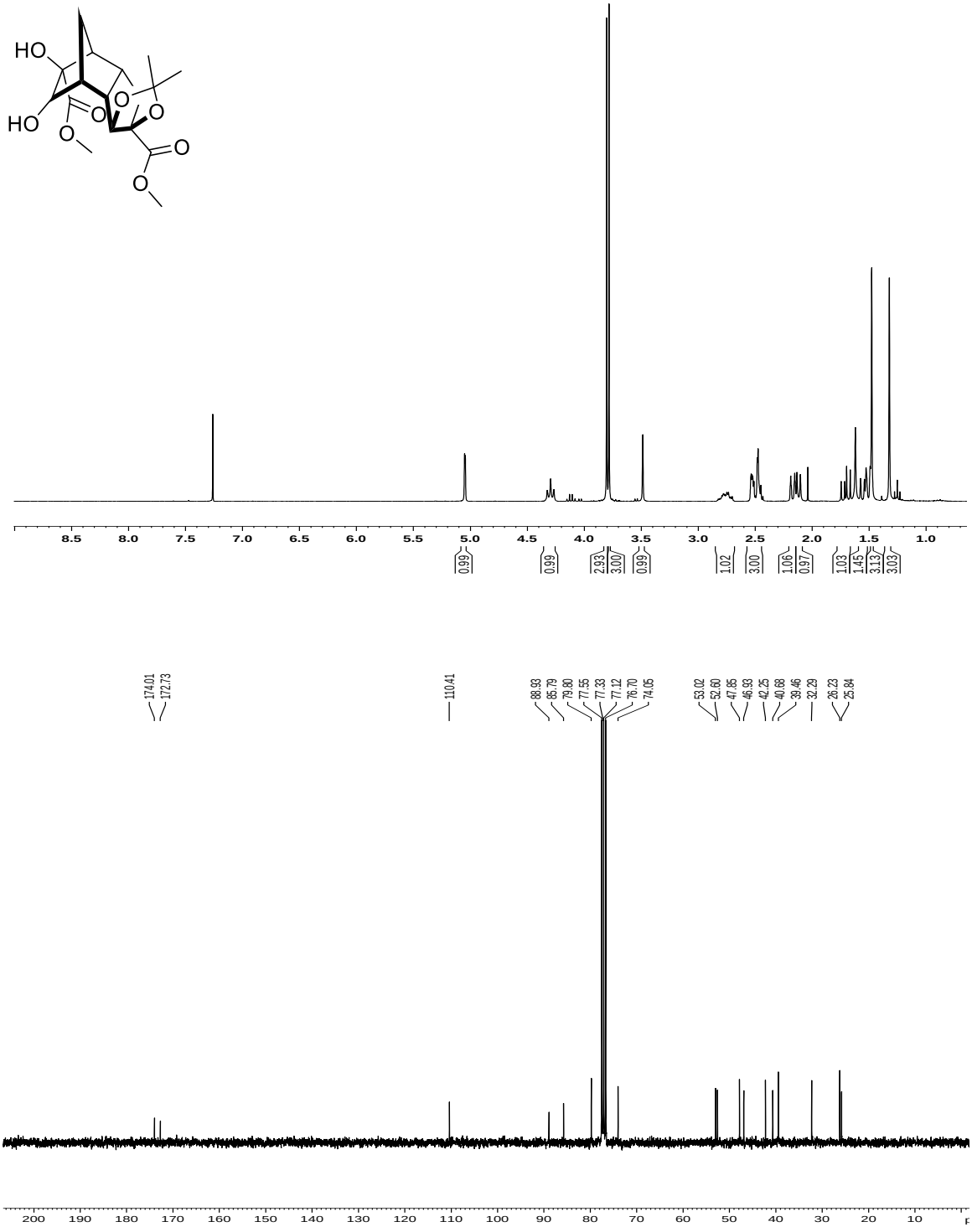

^{1}H and ^{13}C NMR spectra for compound **90**

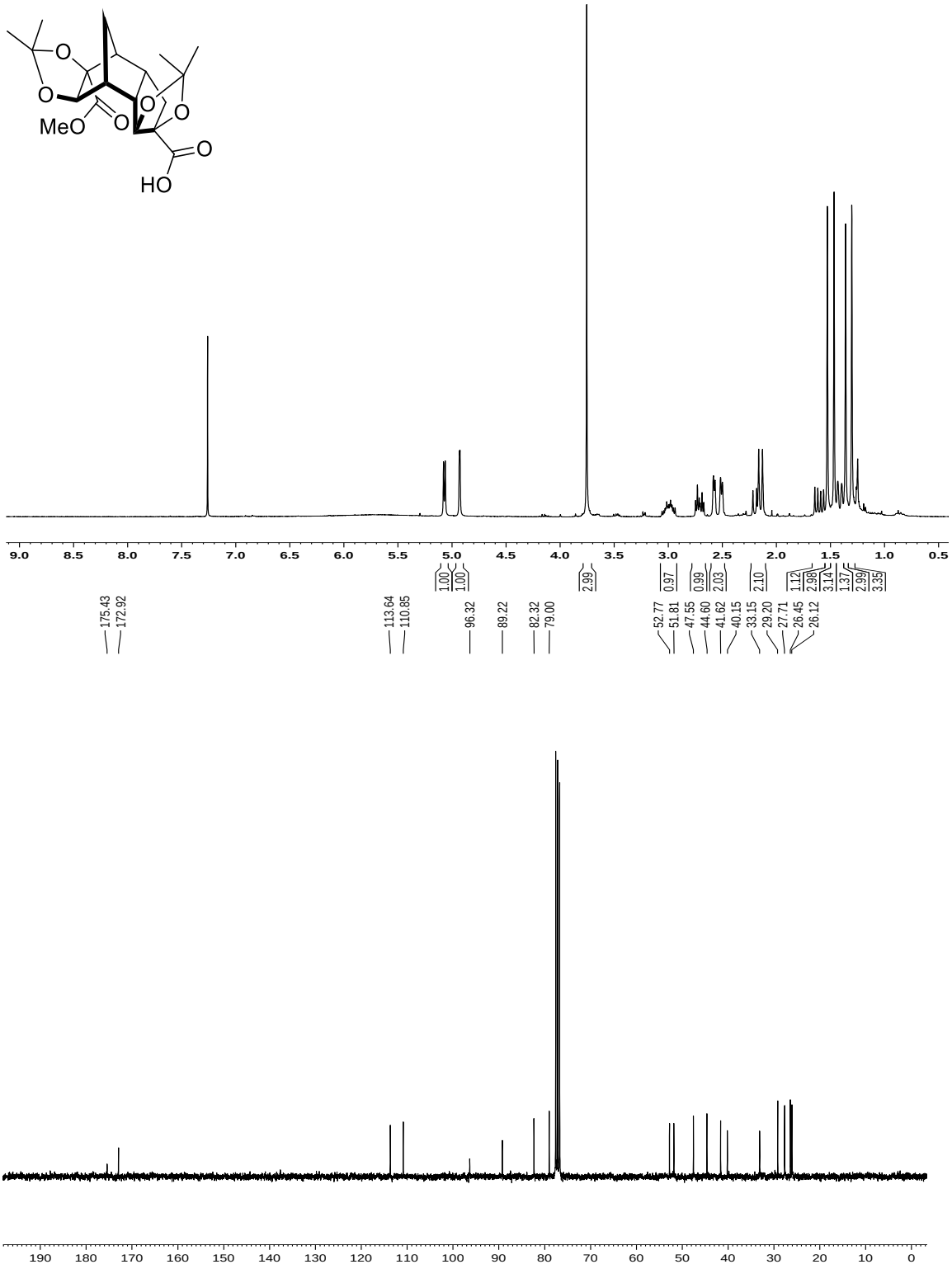

^{1}H and ^{13}C NMR spectra for compound **91**

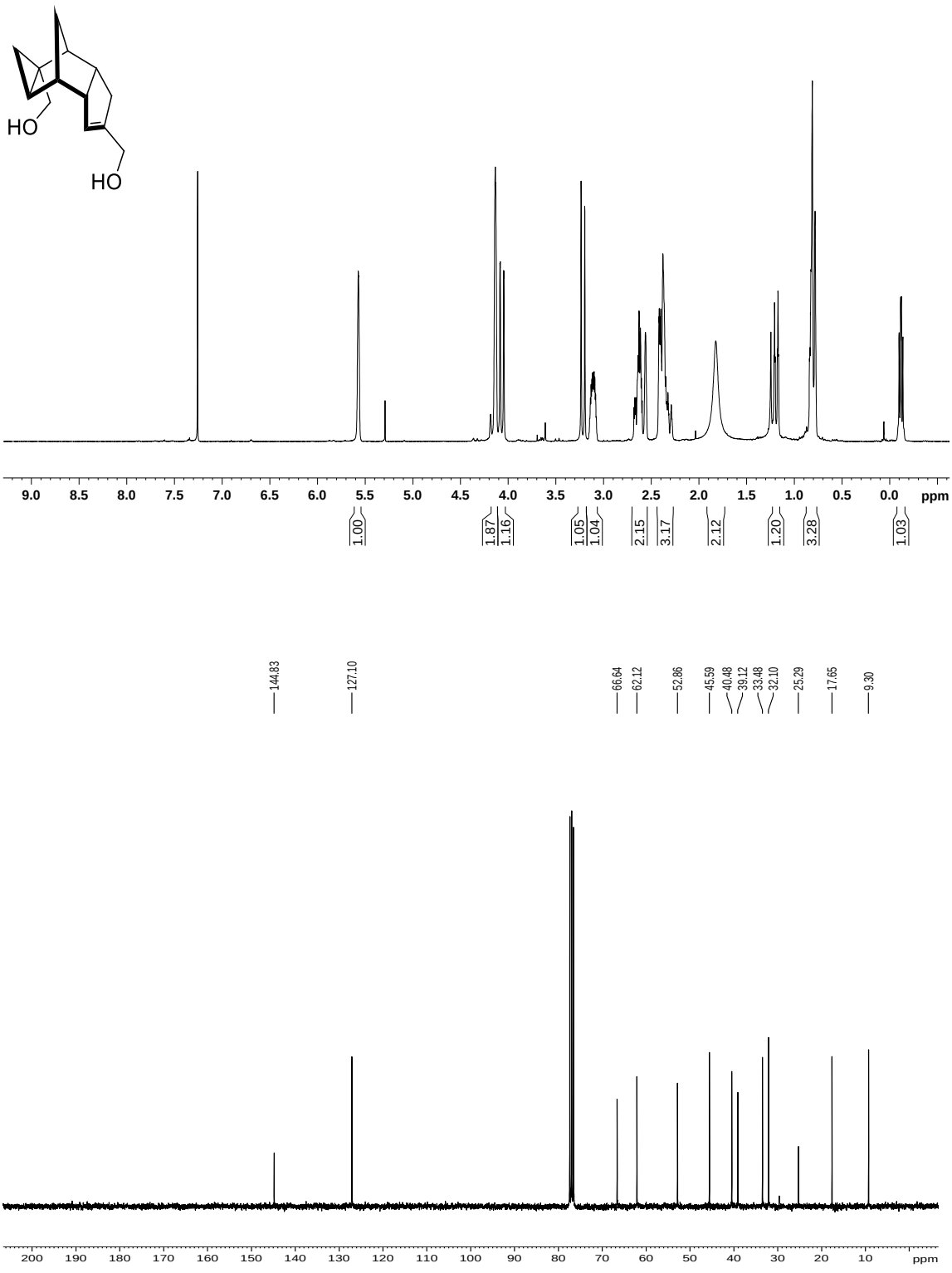

^{1}H and ^{13}C NMR spectra for compound **92**

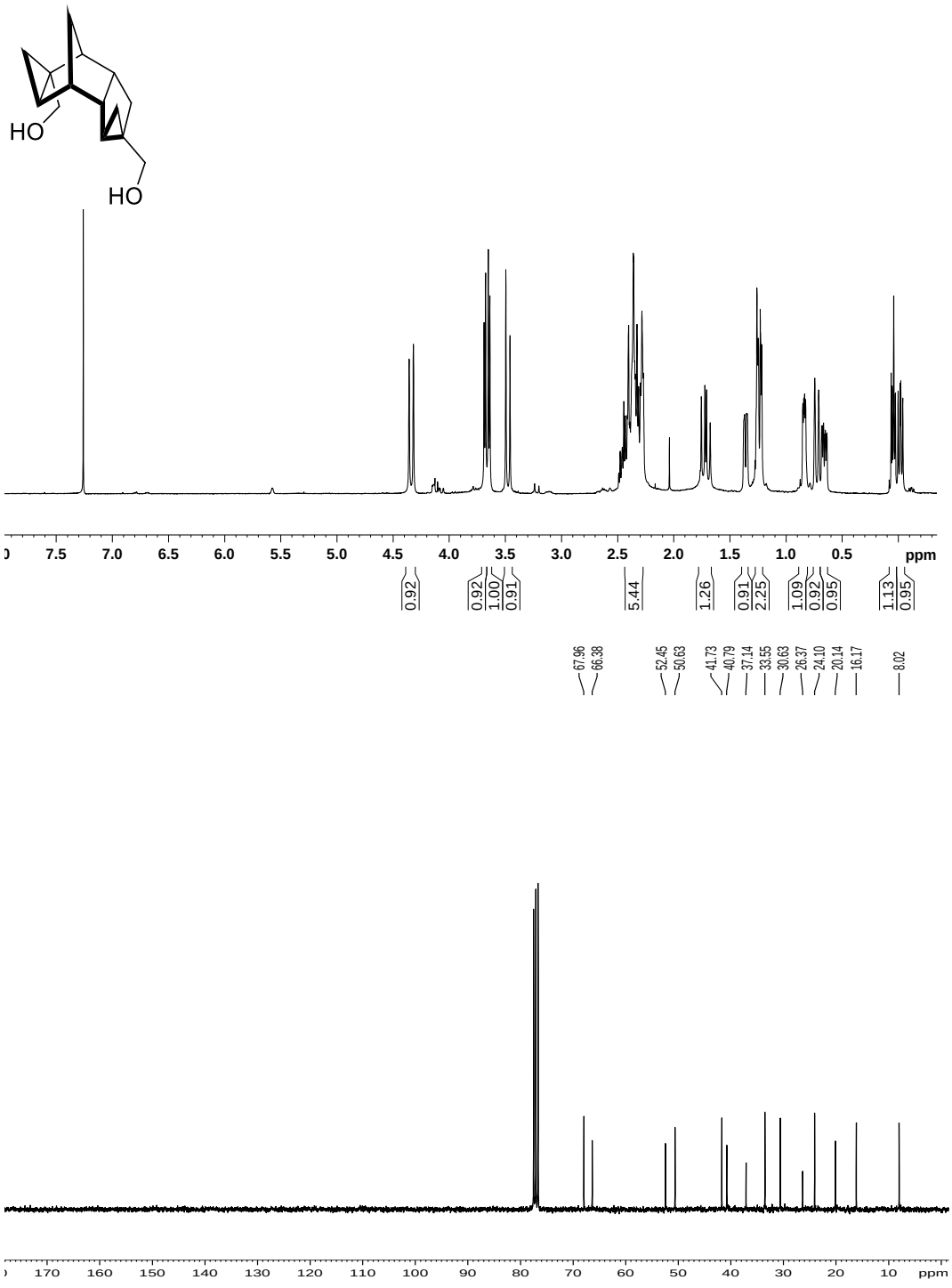

^{1}H and ^{13}C NMR spectra for compound **93**

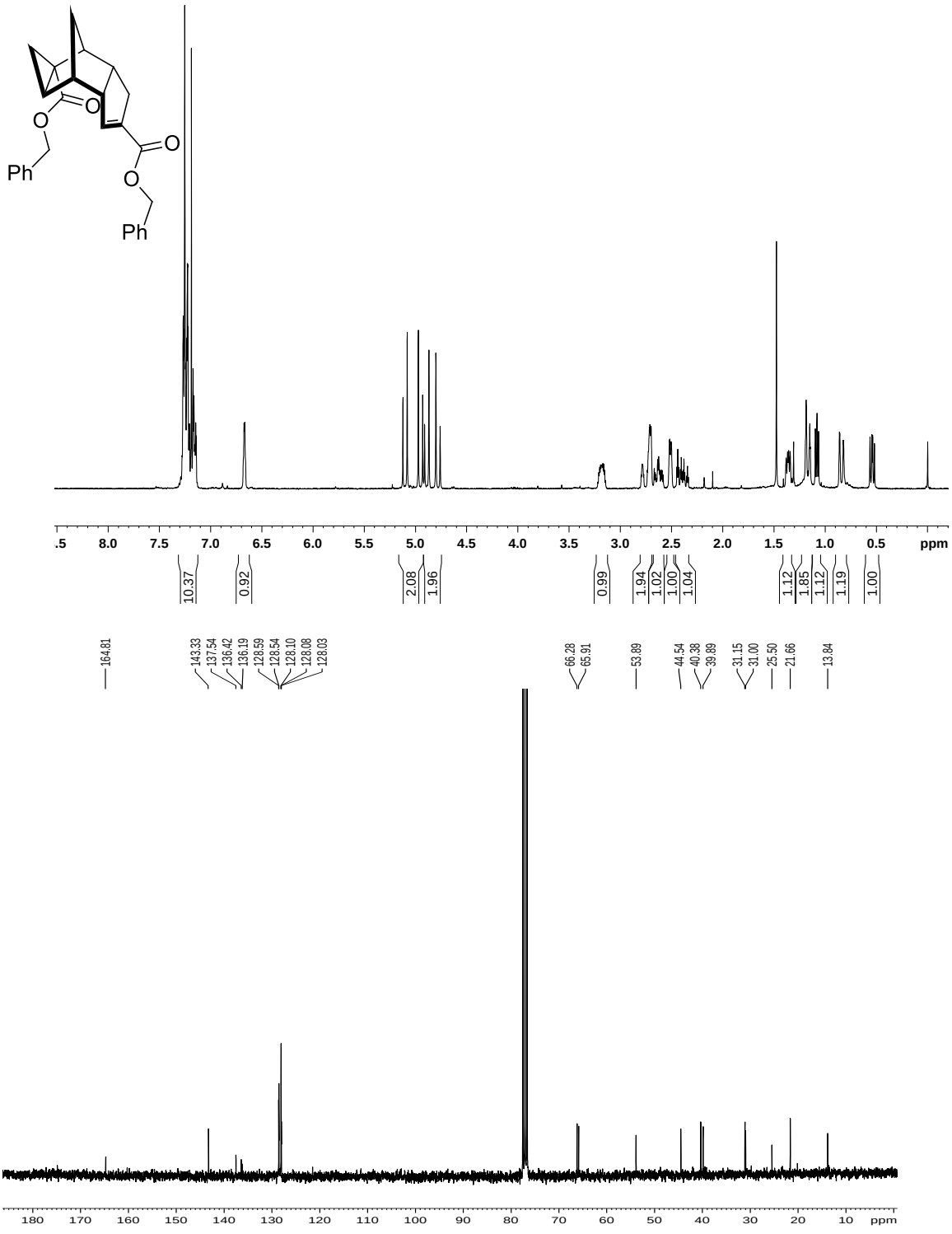

^{1}H and ^{13}C NMR spectra for compound **94**

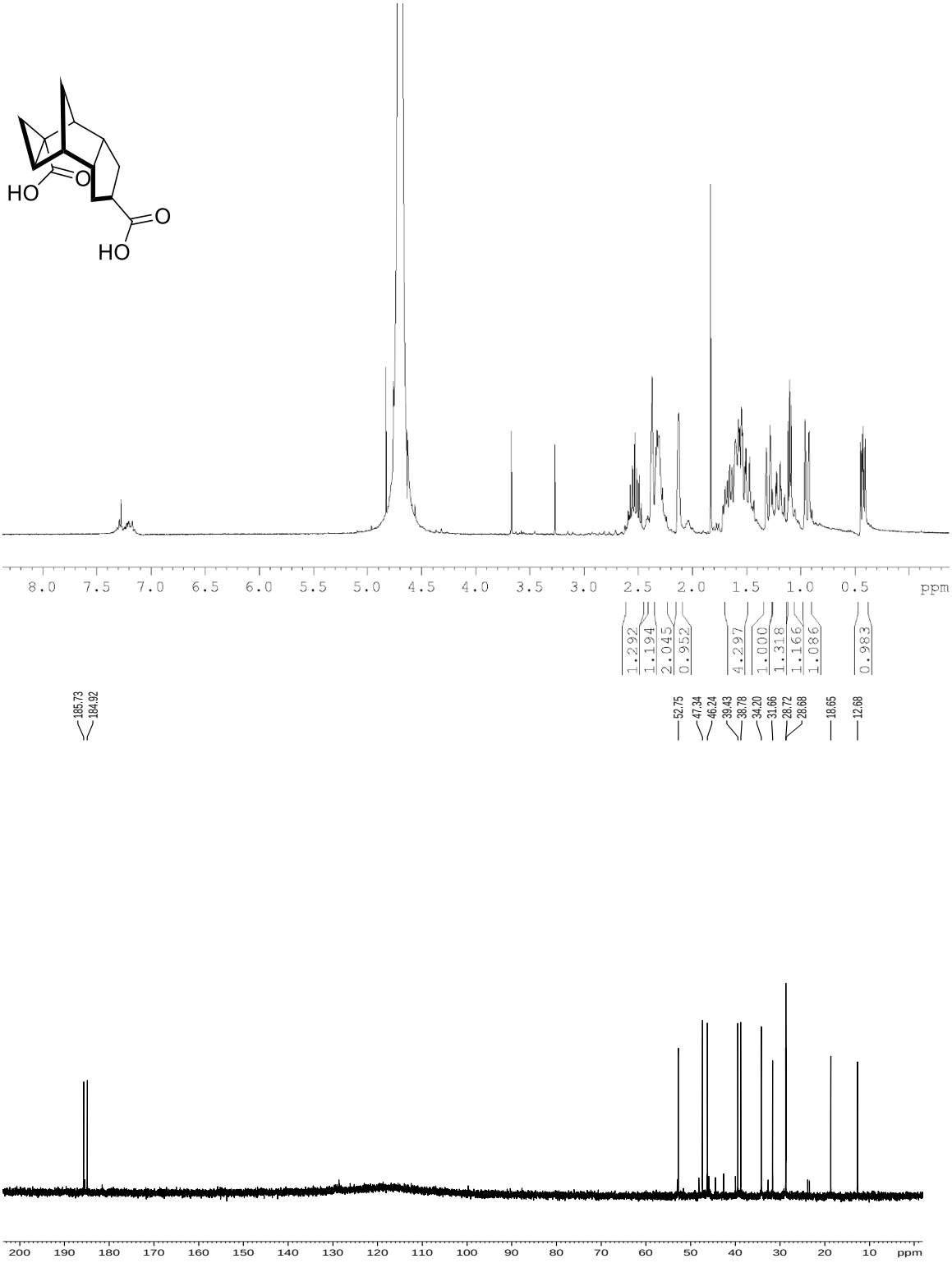

^{1}H and ^{13}C NMR spectra for compound **98**

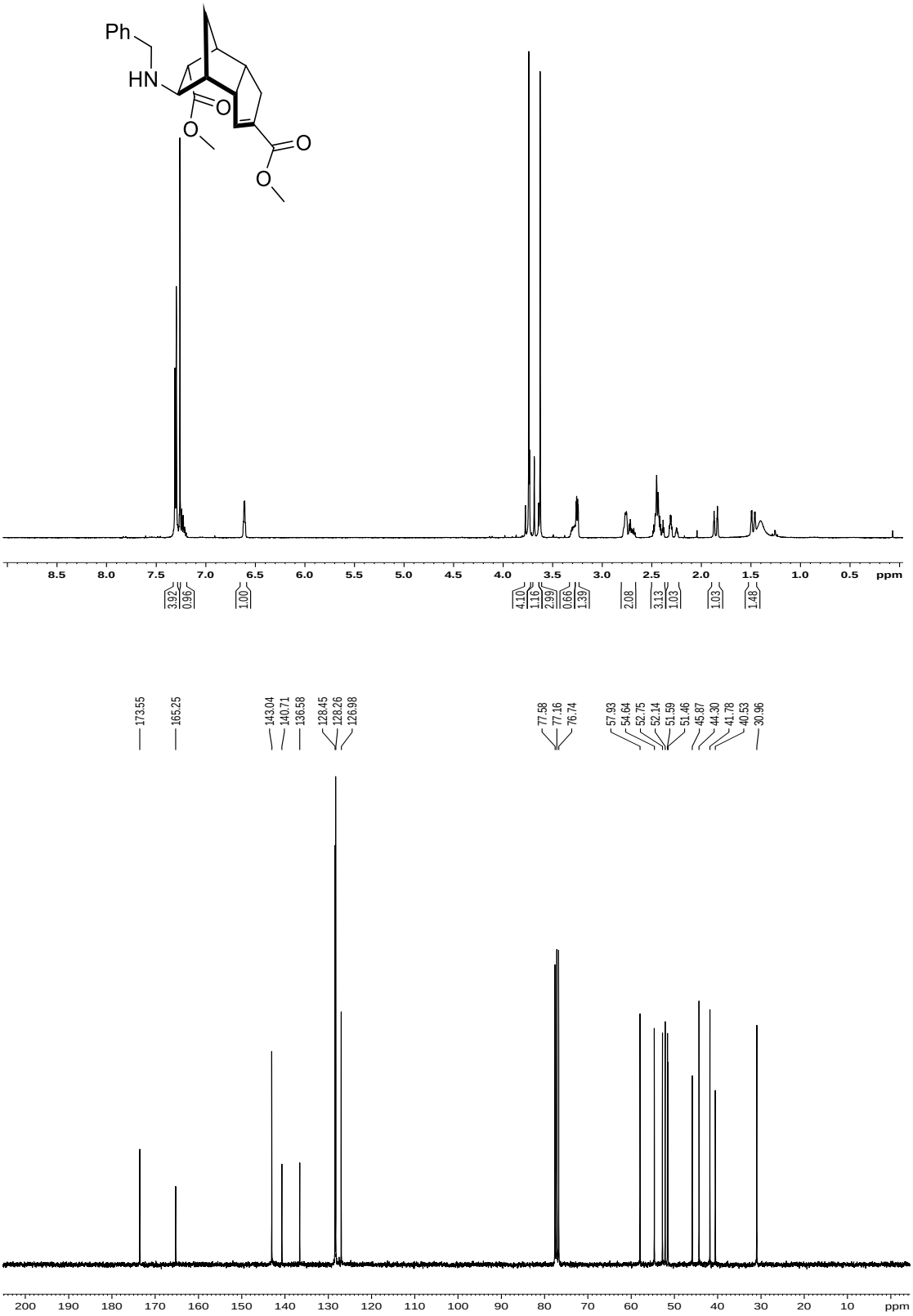

^{1}H and ^{13}C NMR spectra for compound **99**

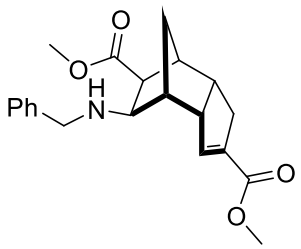

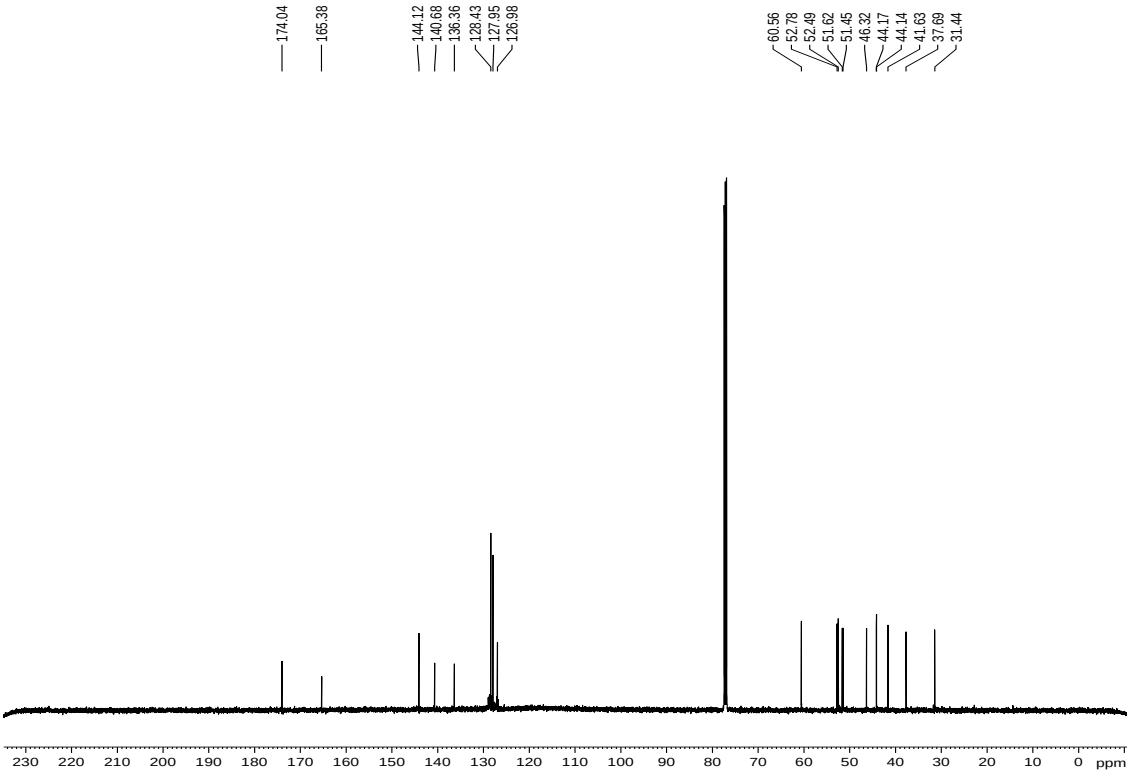

^{1}H and ^{13}C NMR spectra for compound **100**

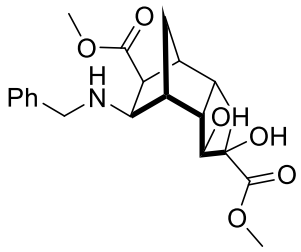

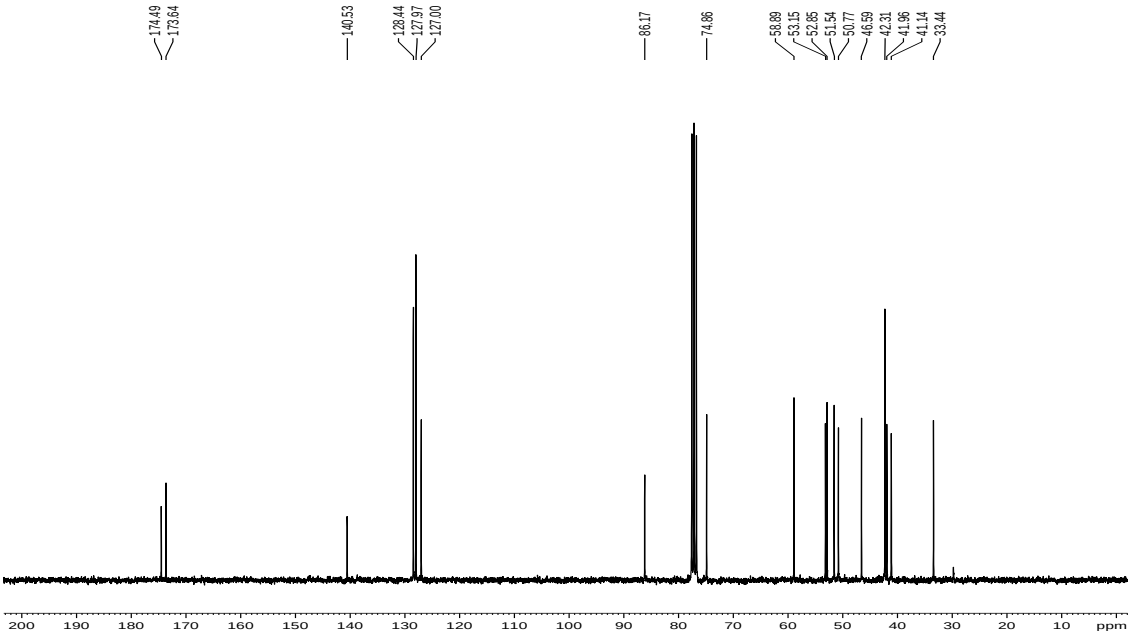

^{1}H and ^{13}C NMR spectra for mixture of **61** and **116**

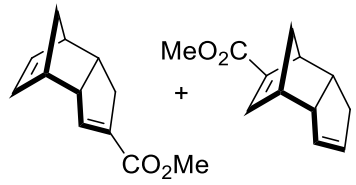

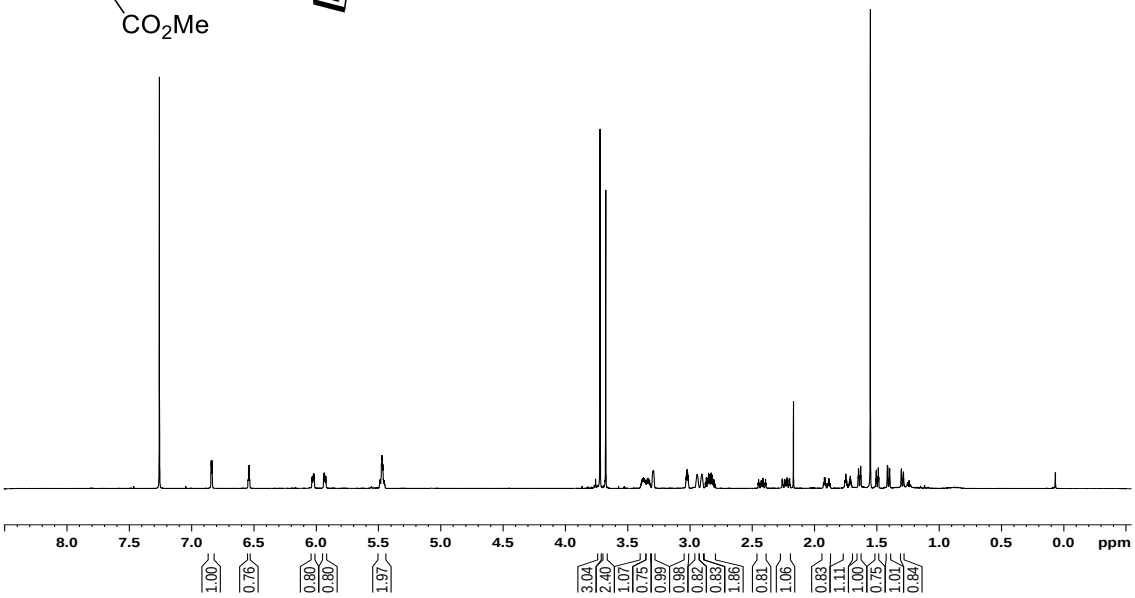

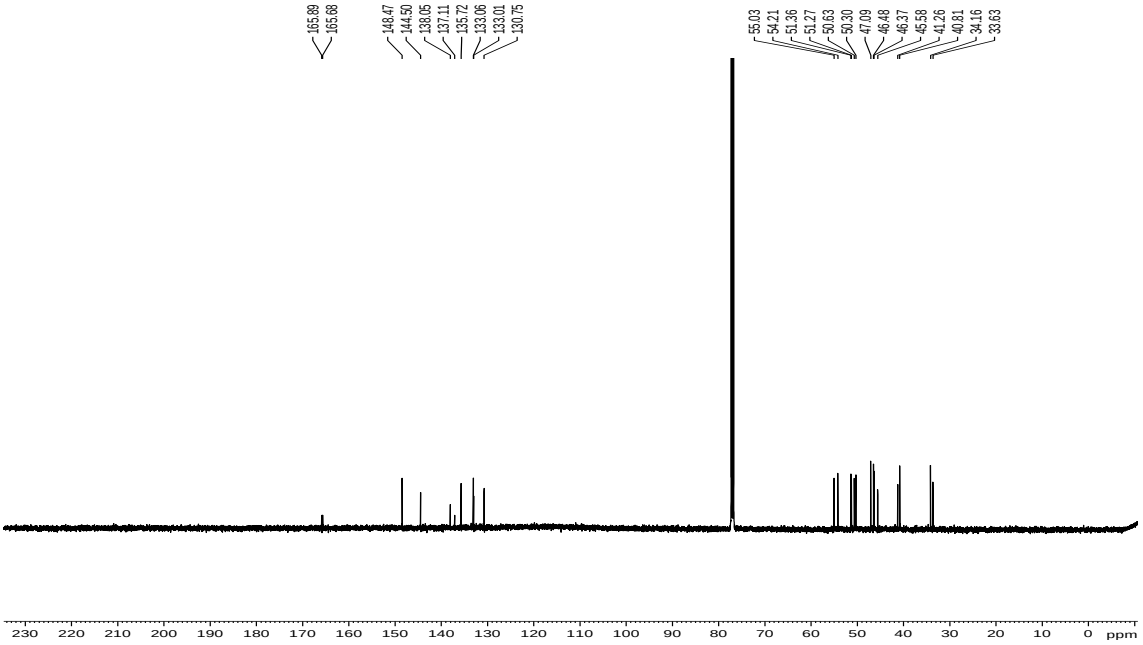

^{1}H NMR Spectrum for **109Ba** in $CDCl_3$

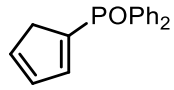

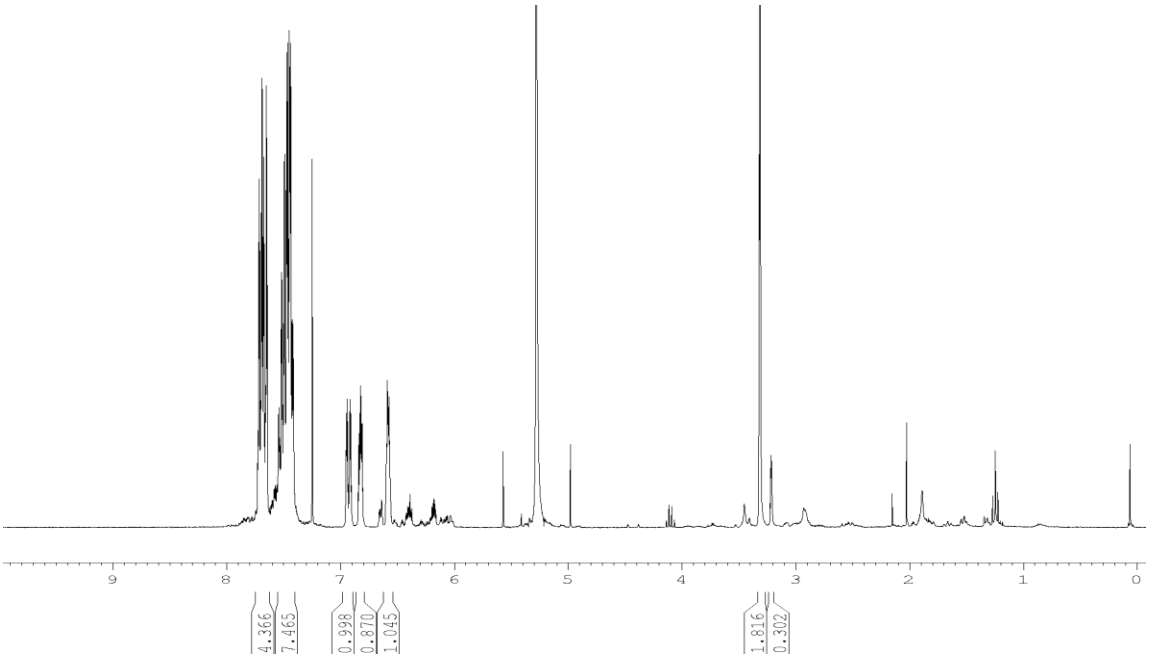

^{31}P NMR Spectrum for **109Ba** in $CDCl_3$

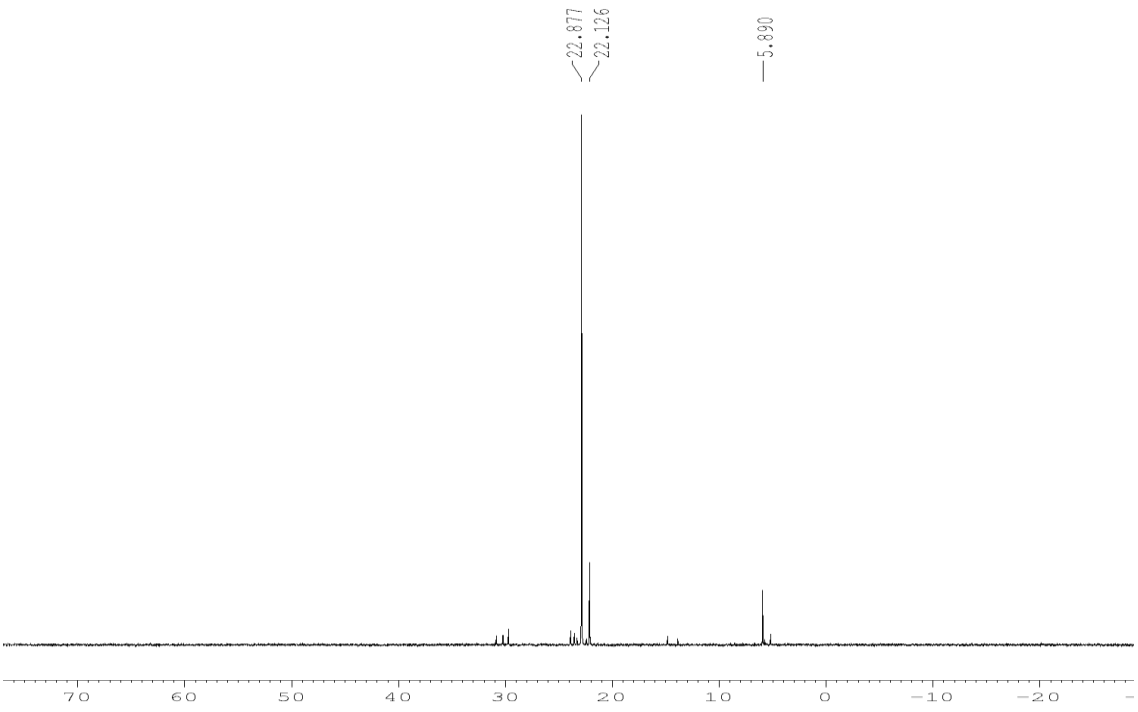

P-HMBC Spectrum for **109Ba** in $CDCl_3$

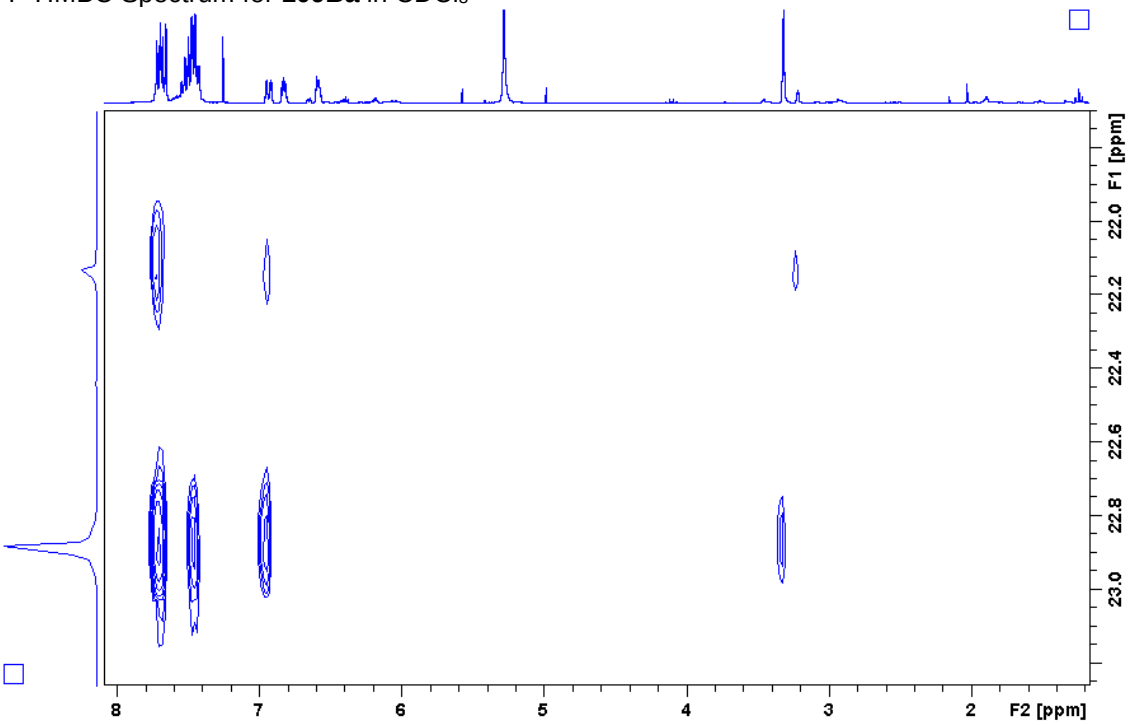

^{1}H and ^{13}C NMR spectra for compound **110a**

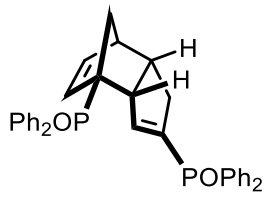

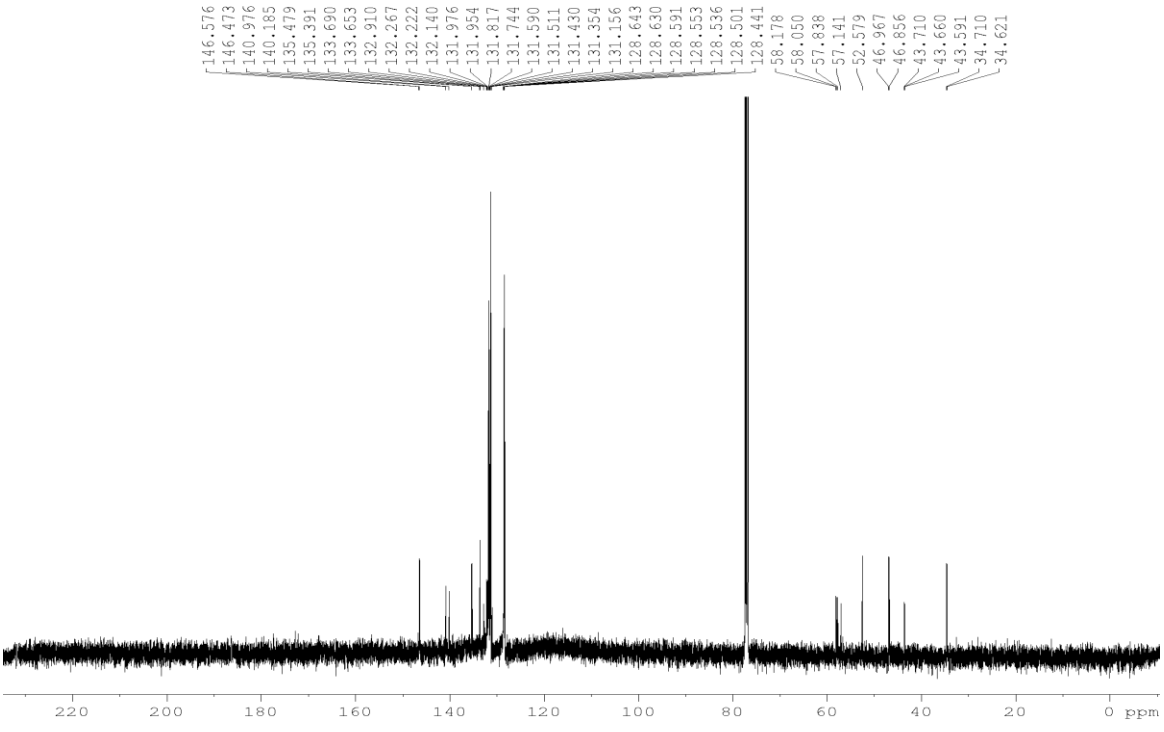

DEPT135 Spectrum for **110a** in $CDCl_3$

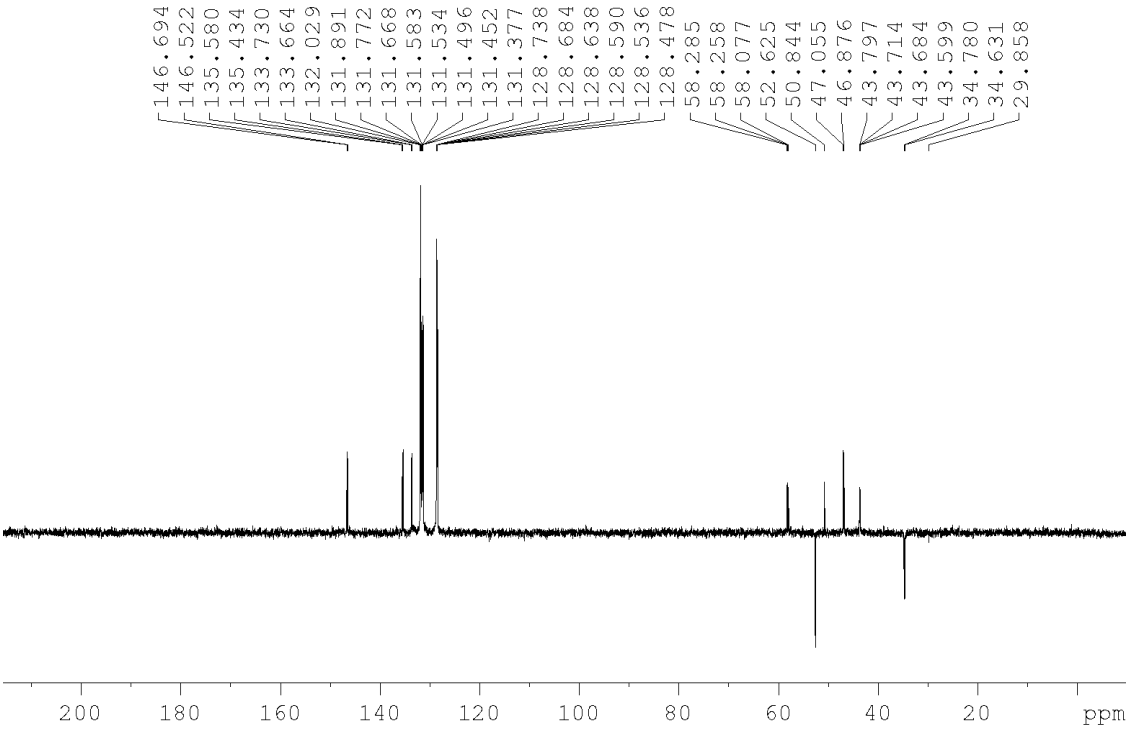

^{31}P NMR Spectrum for **110a** in $CDCl_3$

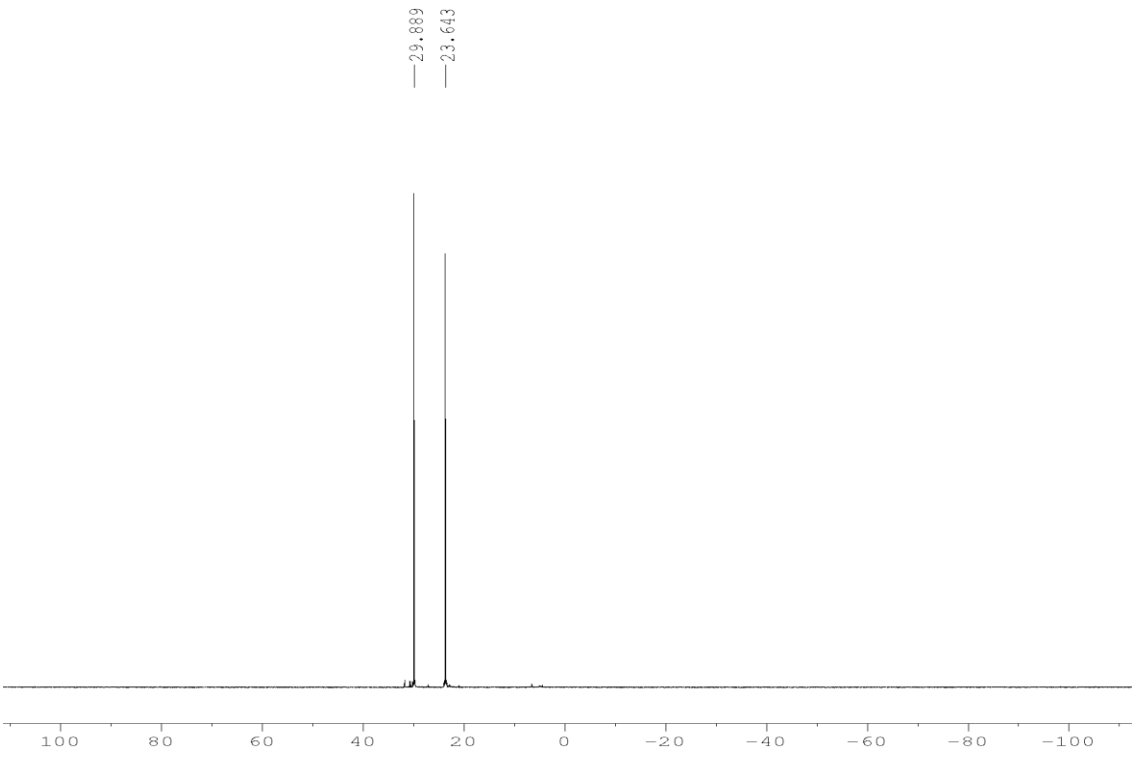

P-HMBC Spectrum for **110a** in $CDCl_3$

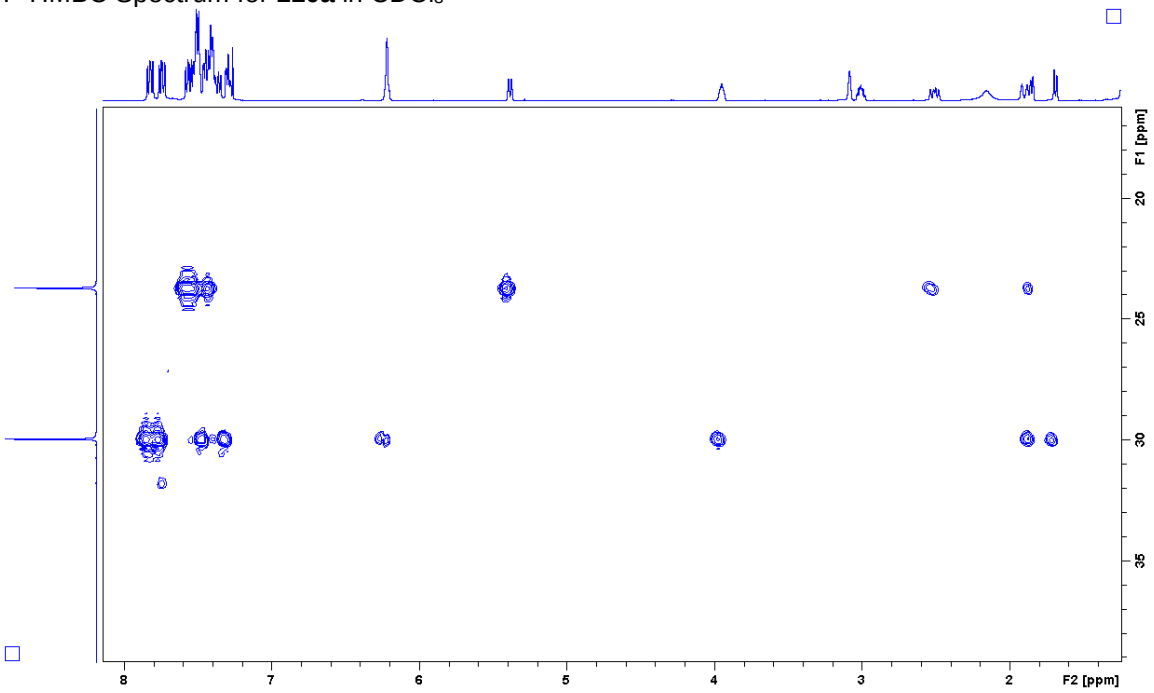

1D-NOE Spectrum for **110a**, with irradiation at 3.98 ppm

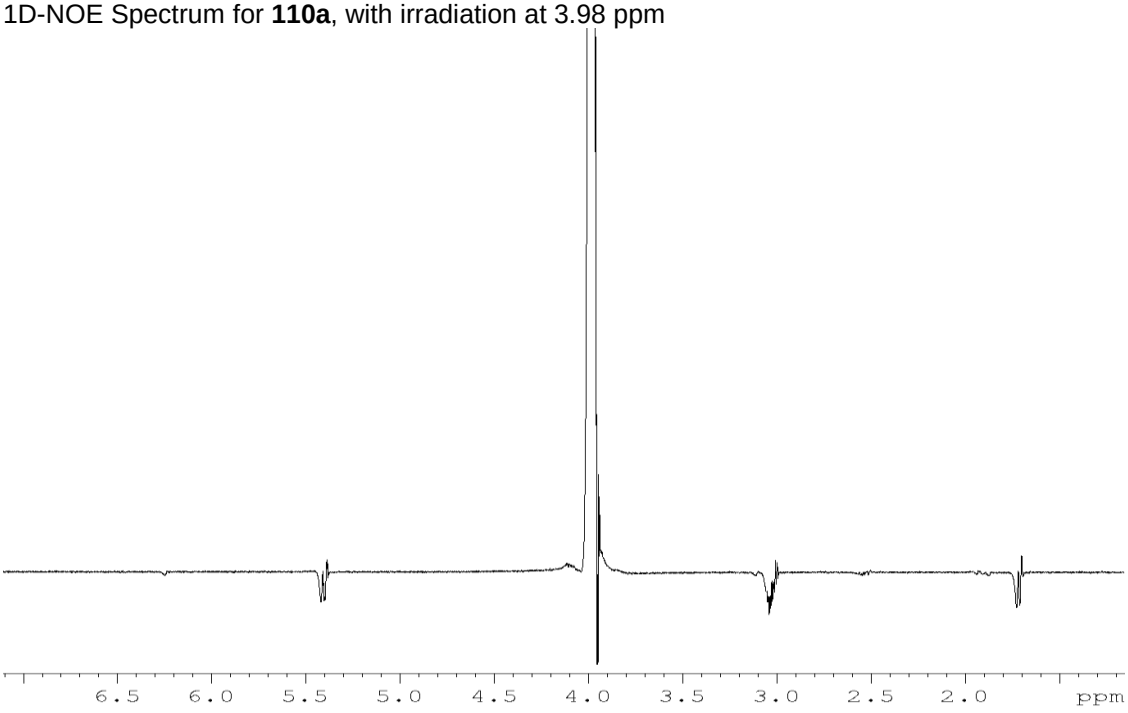

1D-NOE Spectrum for **110a**, with irradiation at 1.60 ppm

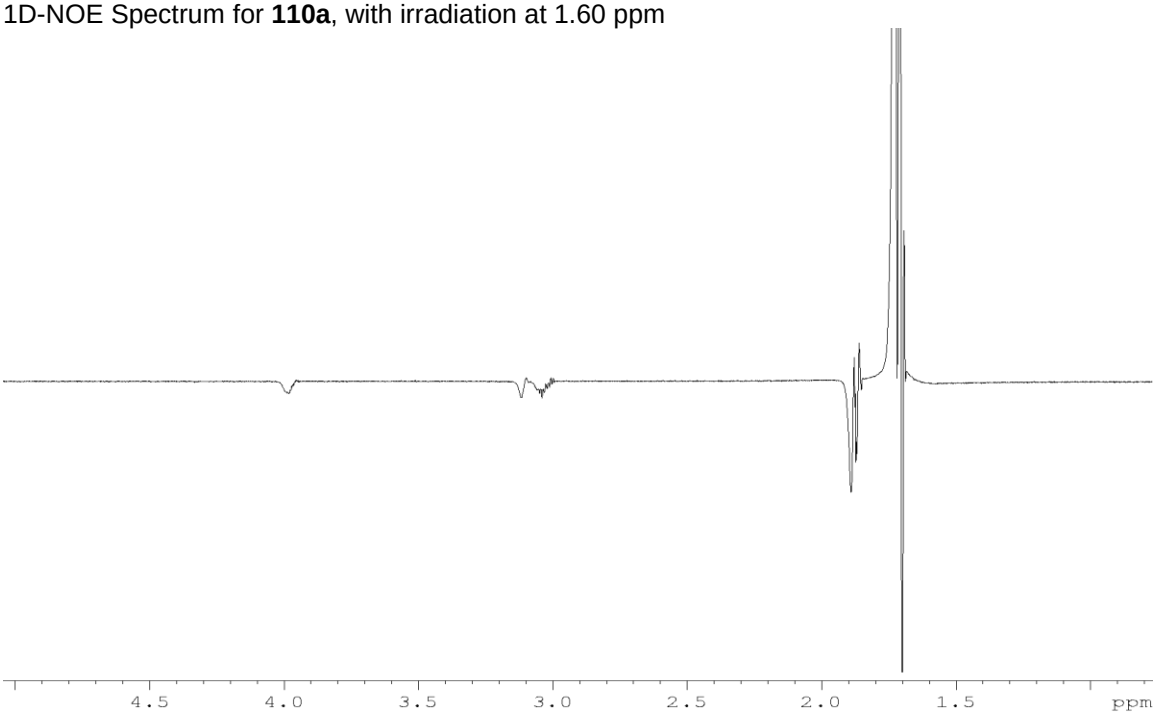

COSY Spectrum for **110a** in $CDCl_3$

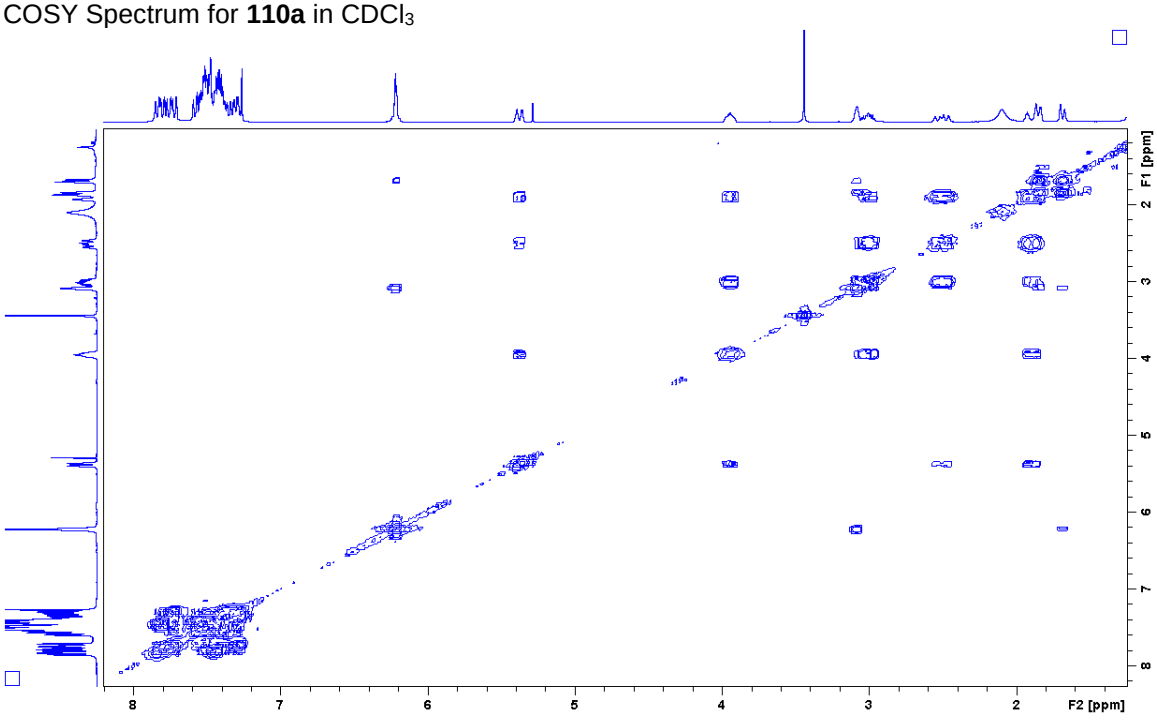

HMQC Spectrum for **110a** in $CDCl_3$

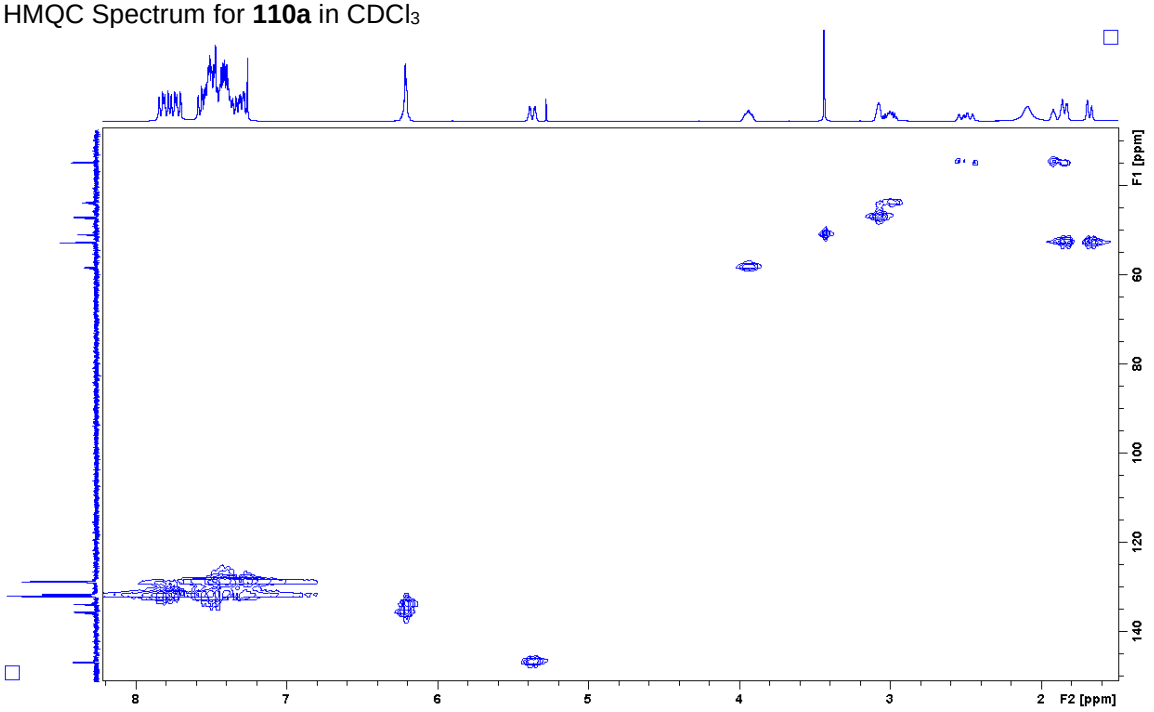

^{1}H NMR Spectrum for **110b** in MeOD

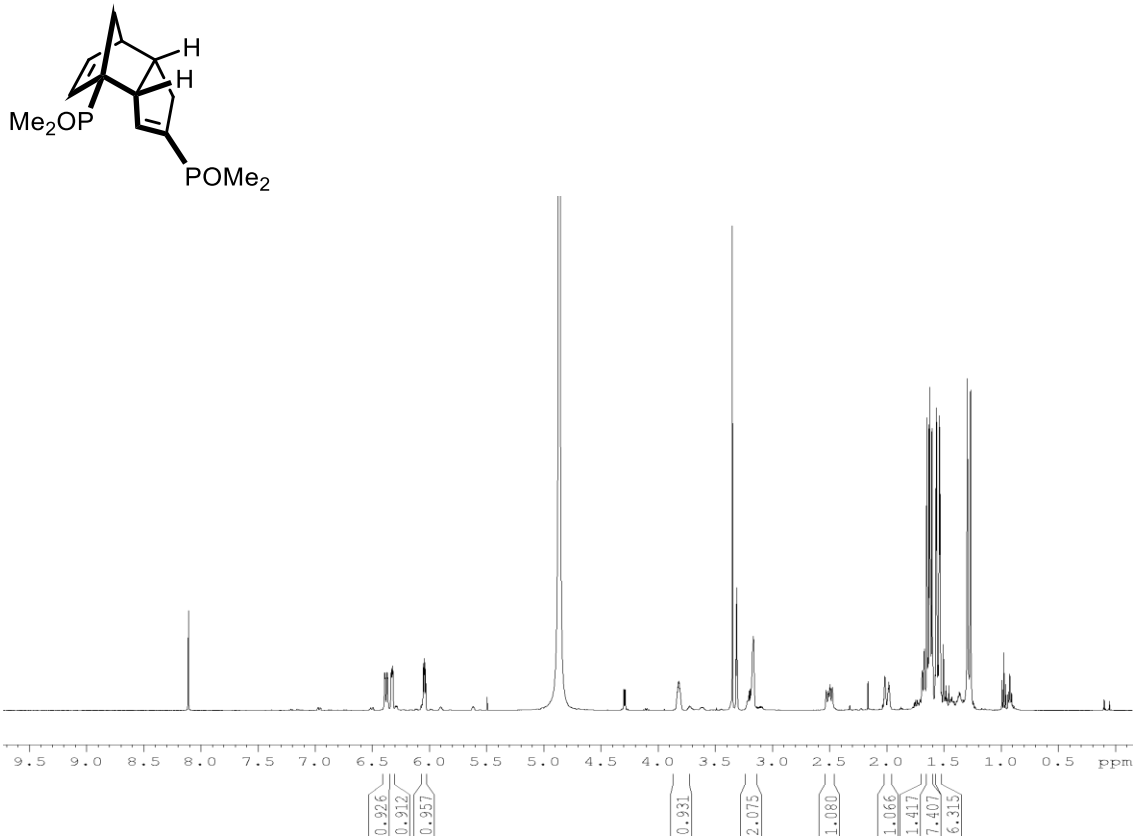

^{13}C NMR Spectrum for **110b** in MeOD

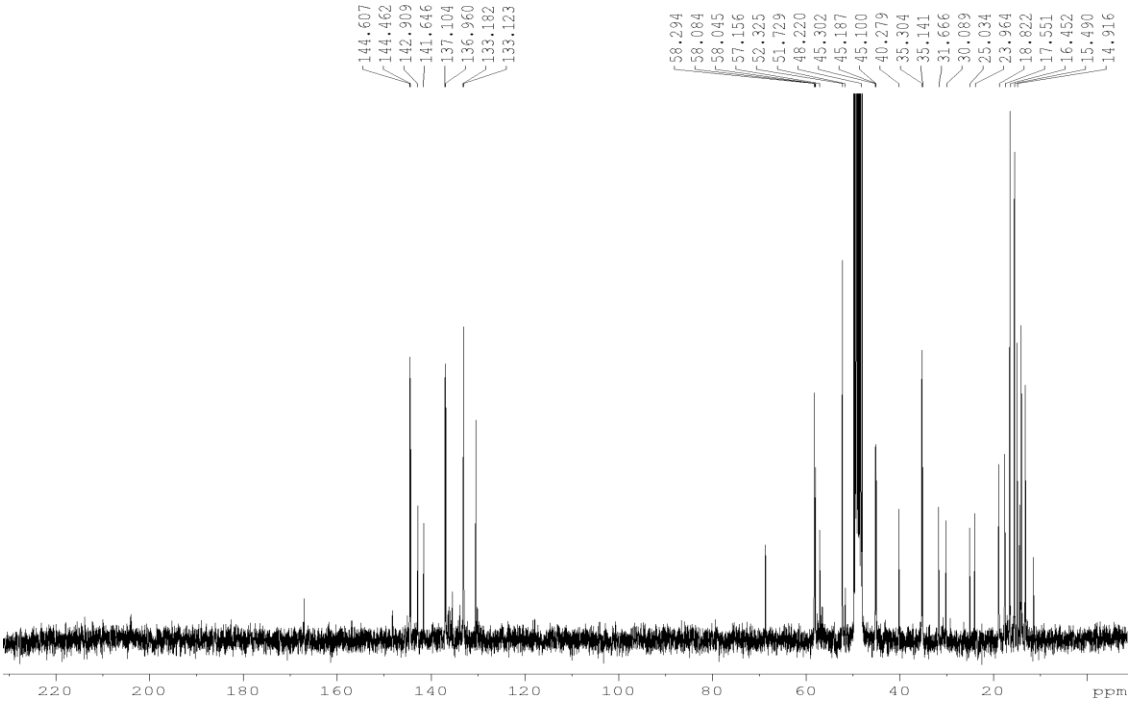

DEPT135 Spectrum for **110b** in MeOD

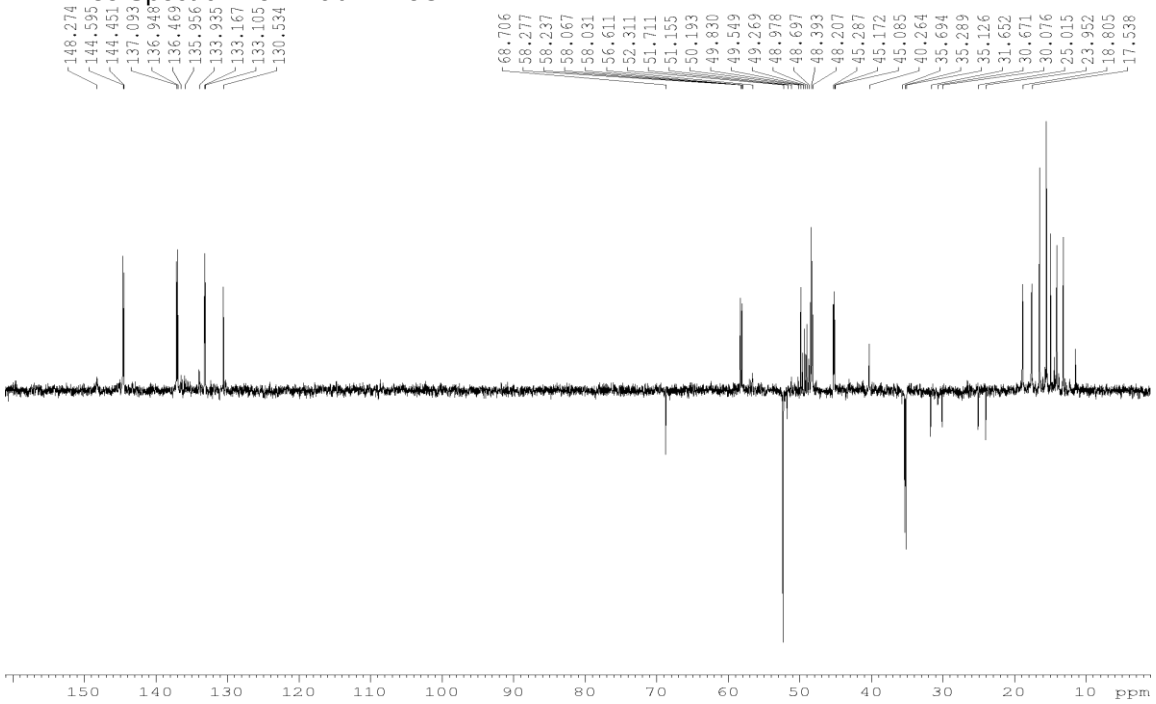

^{31}P NMR Spectrum for **110b** in MeOD

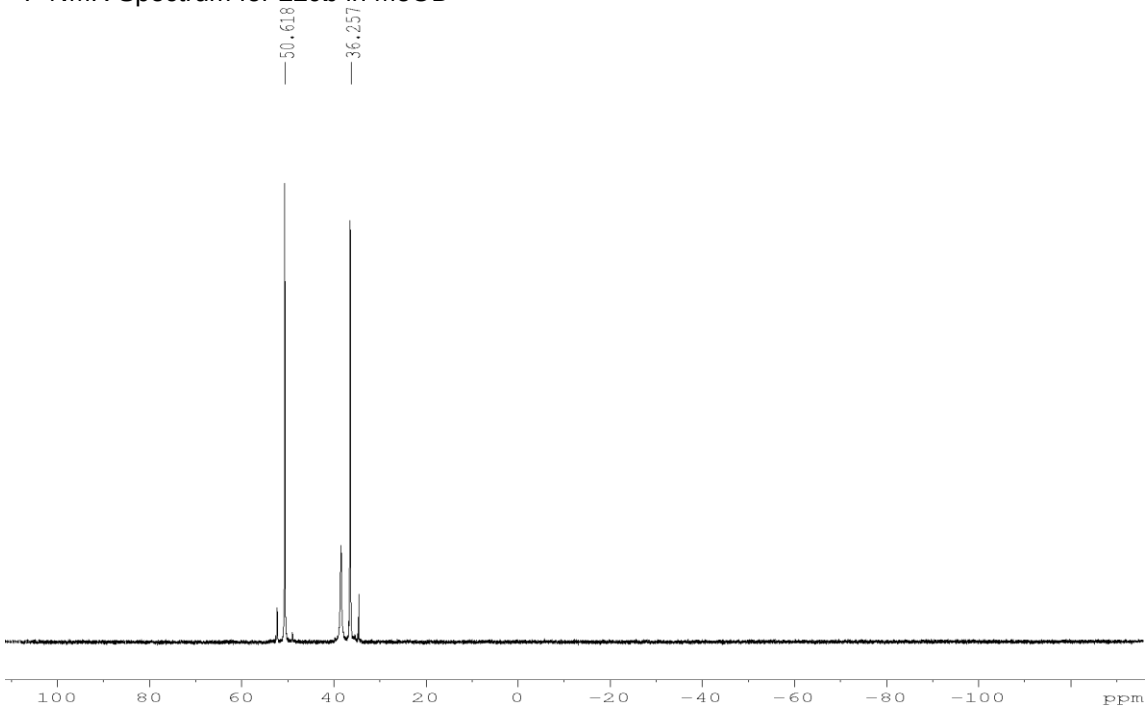

COSY Spectrum for **110b** in MeOD

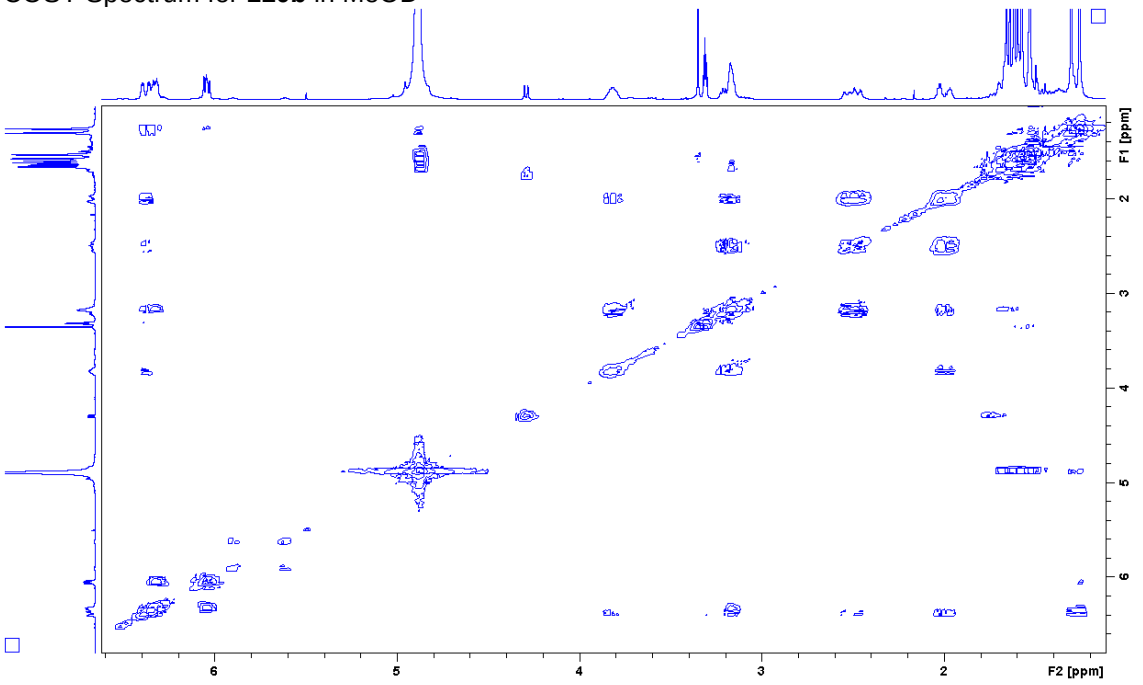

HMQC Spectrum for **110b** in MeOD

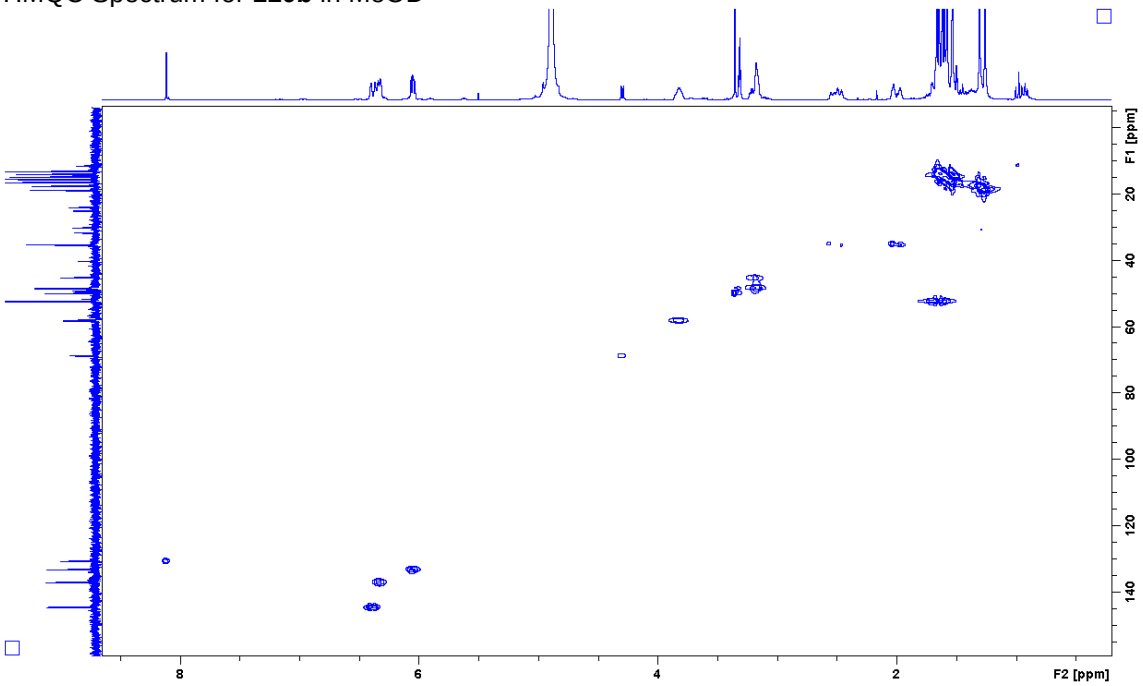

P-HMBC Spectrum for **110b** in MeOD

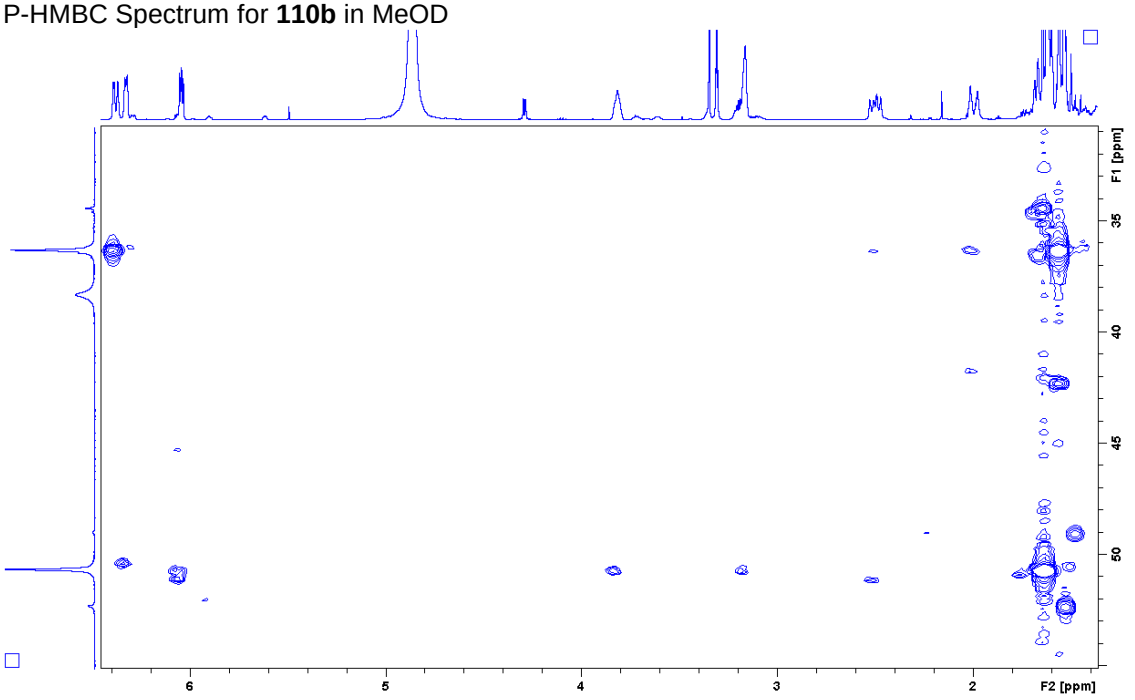

1D-TOCSY Spectrum **110b**, with irradiation at 6.31-6.42 ppm

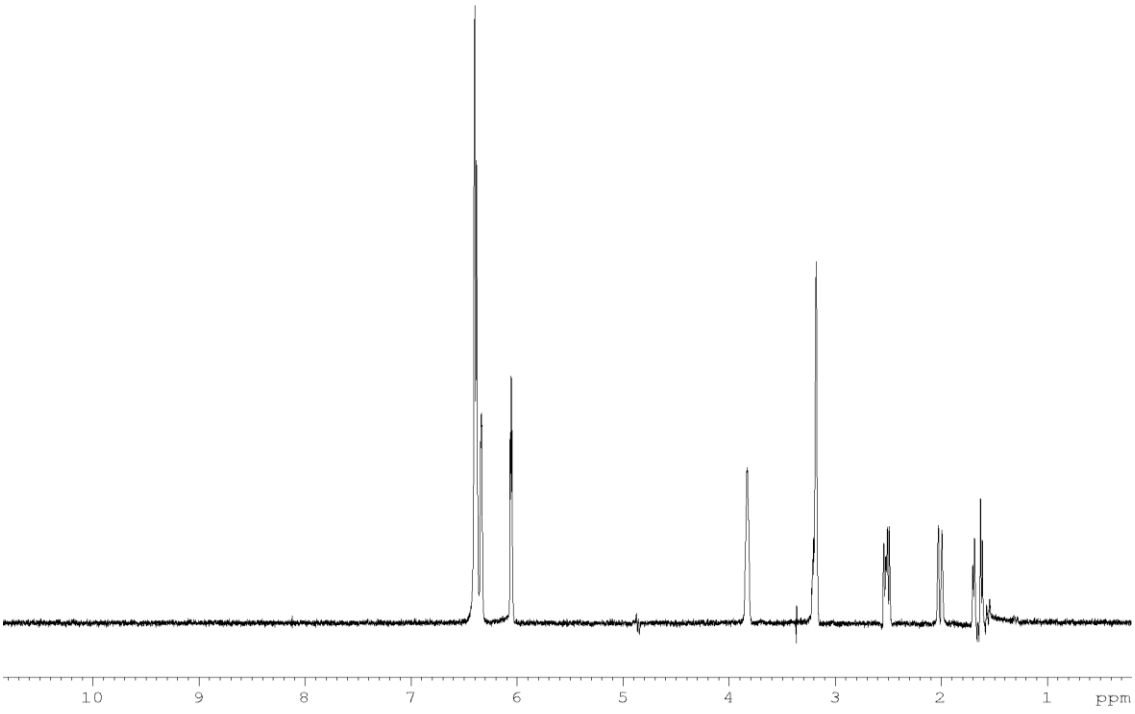

1D-NOE Spectrum **110b**, with irradiation at 3.85 ppm

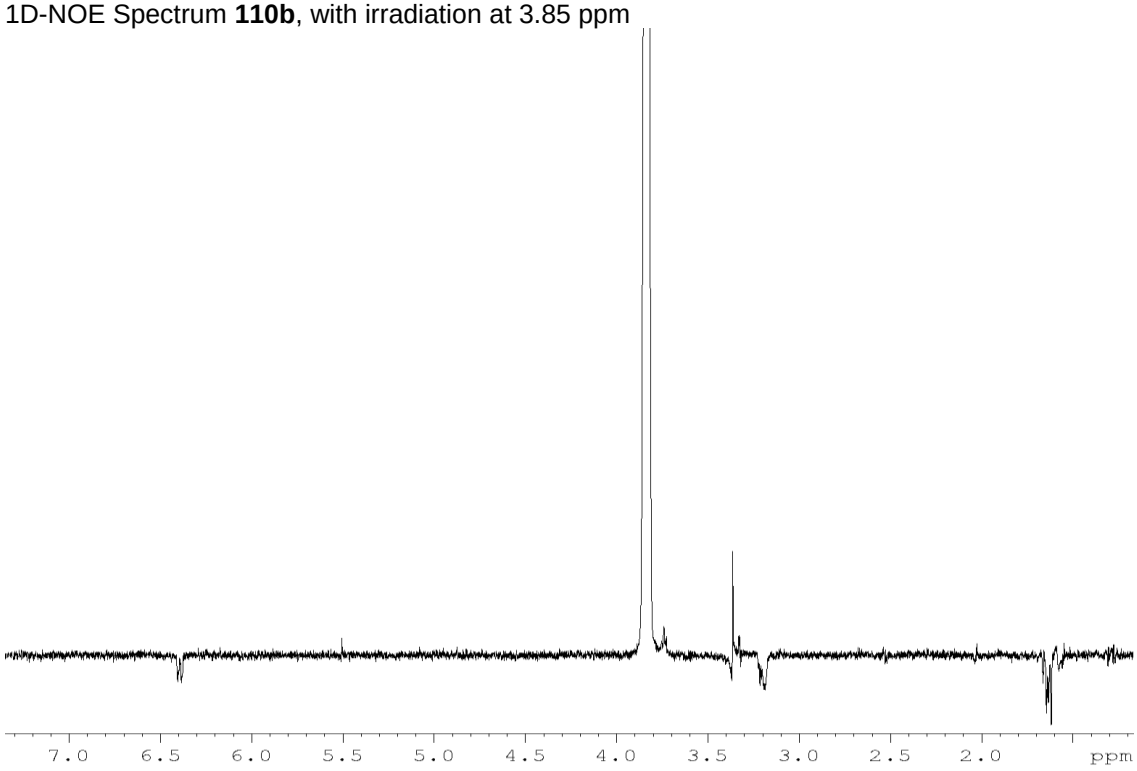

^{1}H NMR Spectrum for compound **116** with solvent contaminant (recovered ether supernatant from the synthesis of polymer **124**)

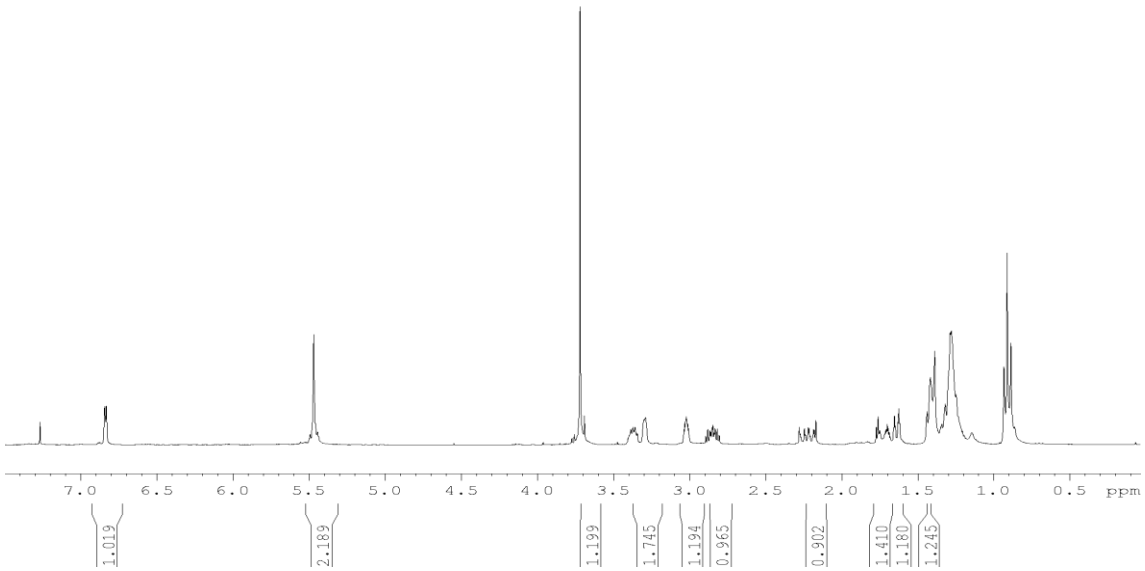

^{1}H NMR Spectrum for compound **61** with contaminants (obtained from an additional conjugate addition reaction between the mixture of **61** and **116** and benzylamine)

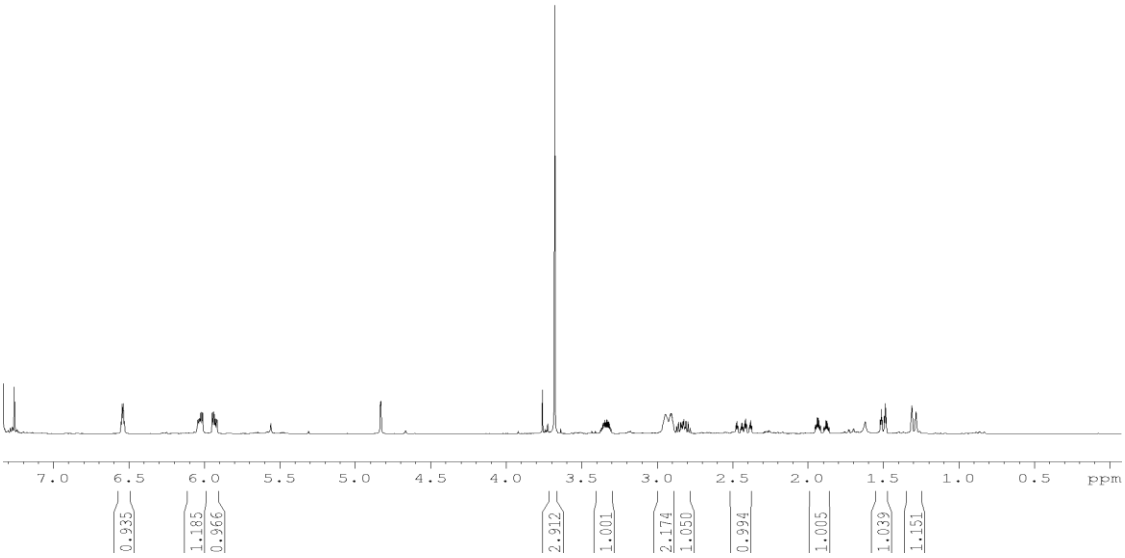

^{1}H NMR Spectrum for compound **124**

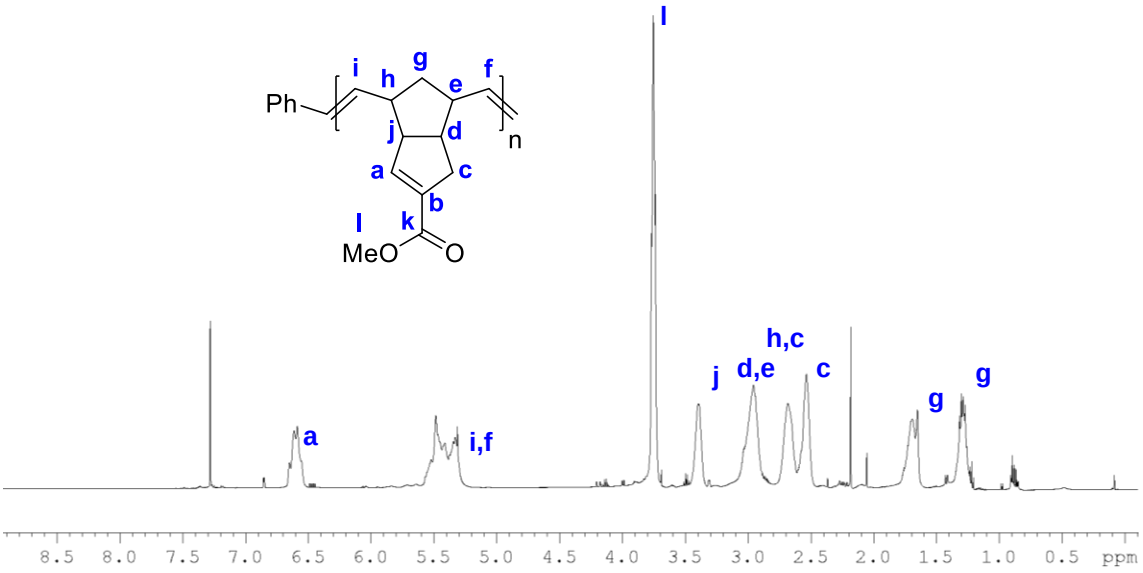

^{13}C NMR Spectrum for compound **124**

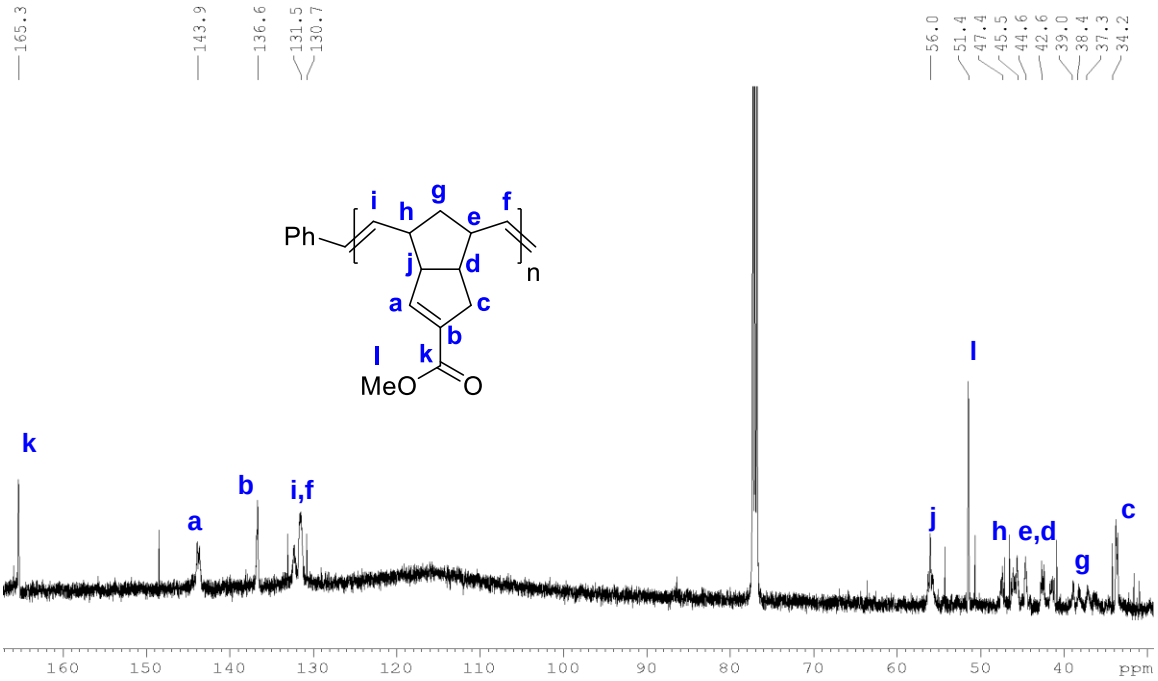

HSQC Spectrum for compound **124**

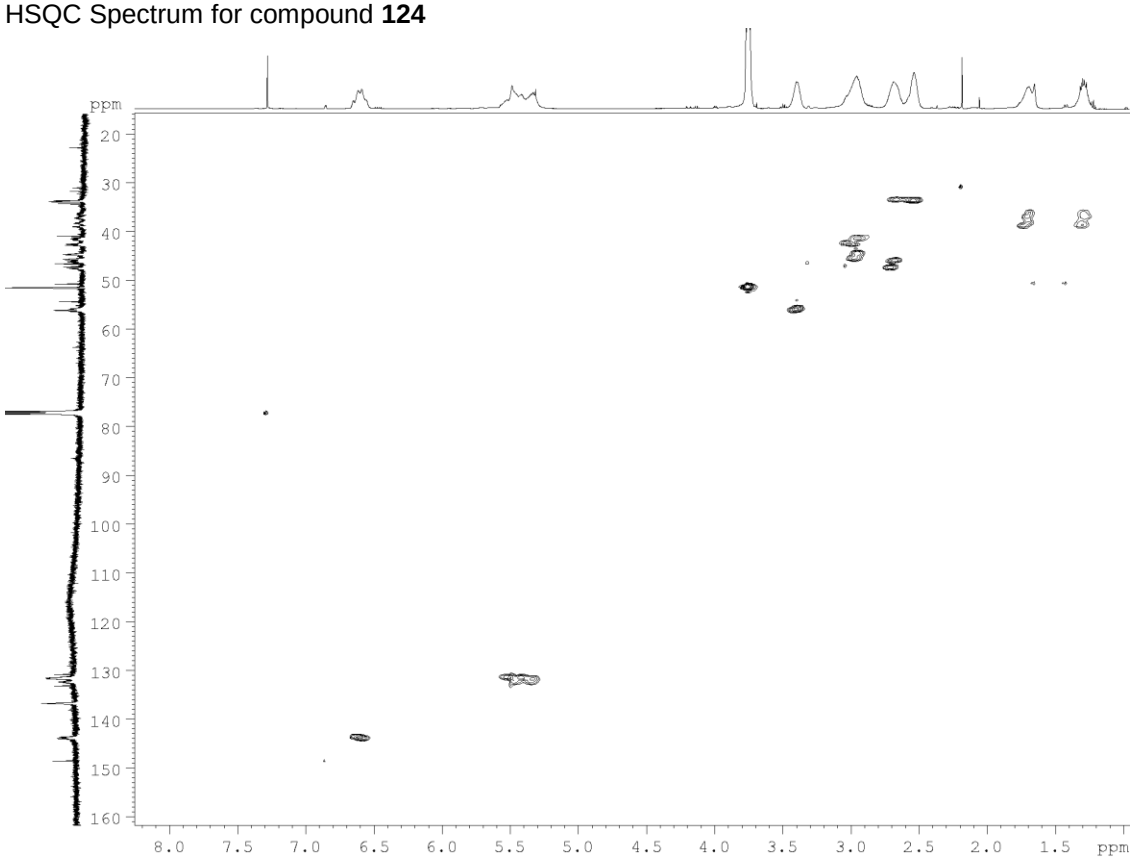

COSY Spectrum for compound **124**

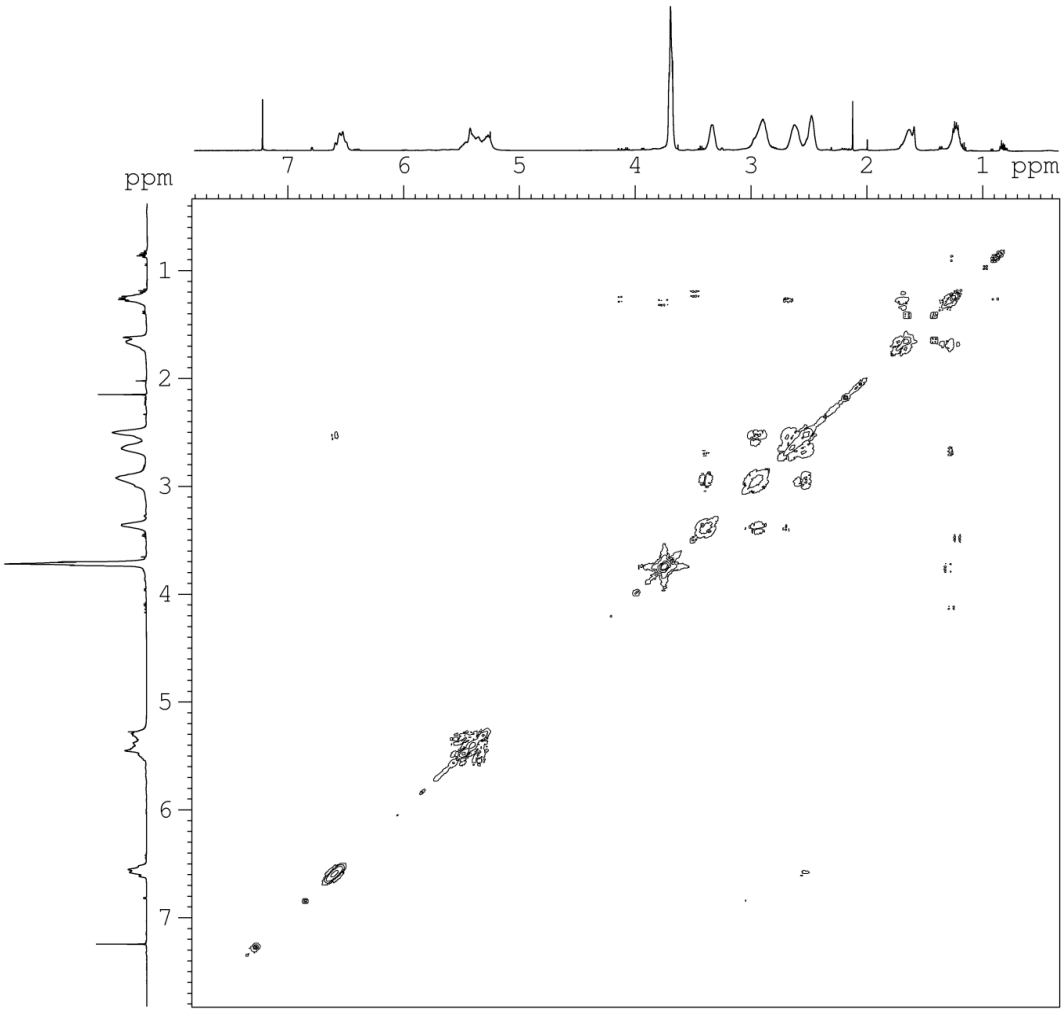

Estimated Molecular weight of **124** by ^{1}HNMR Spectrum in CD_2Cl_2

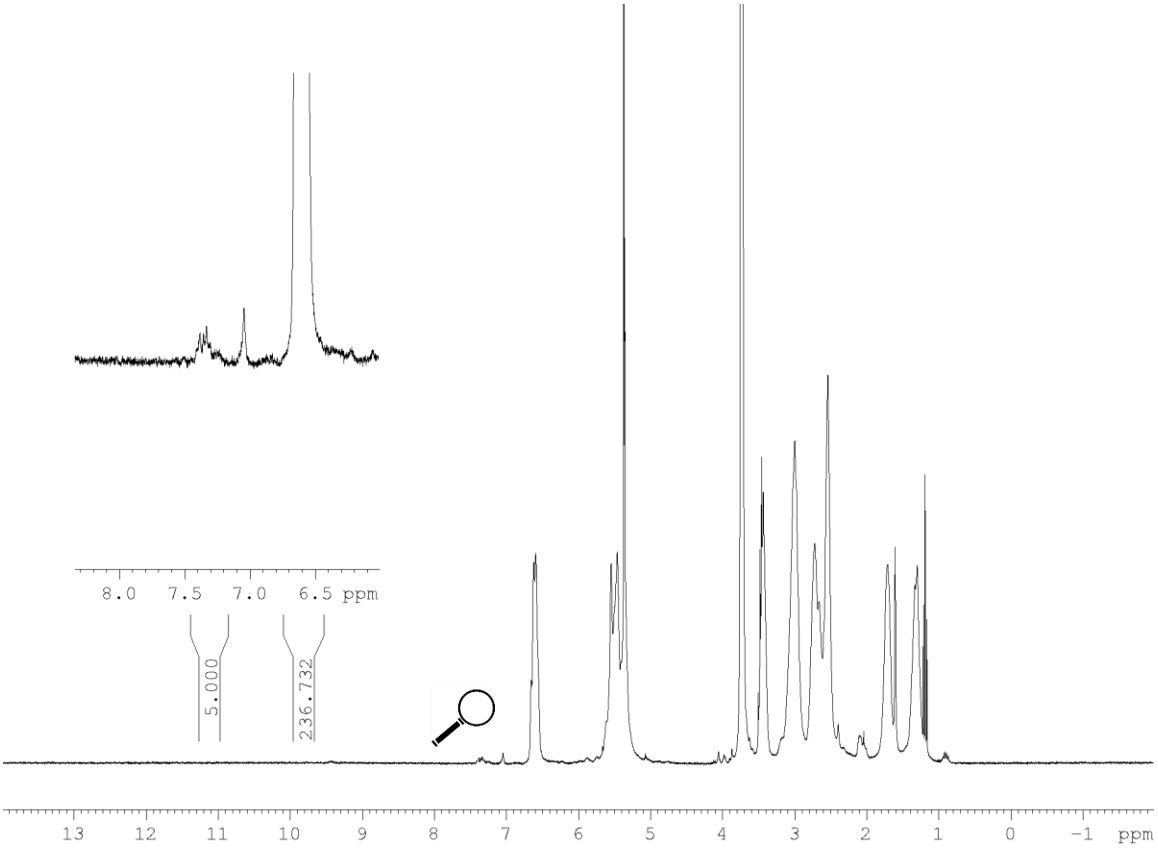

^{1}H NMR spectrum for the salt of (–)-Thiele's acid with brucine in 8.3:1 C_6D_6:$CDCl_3$

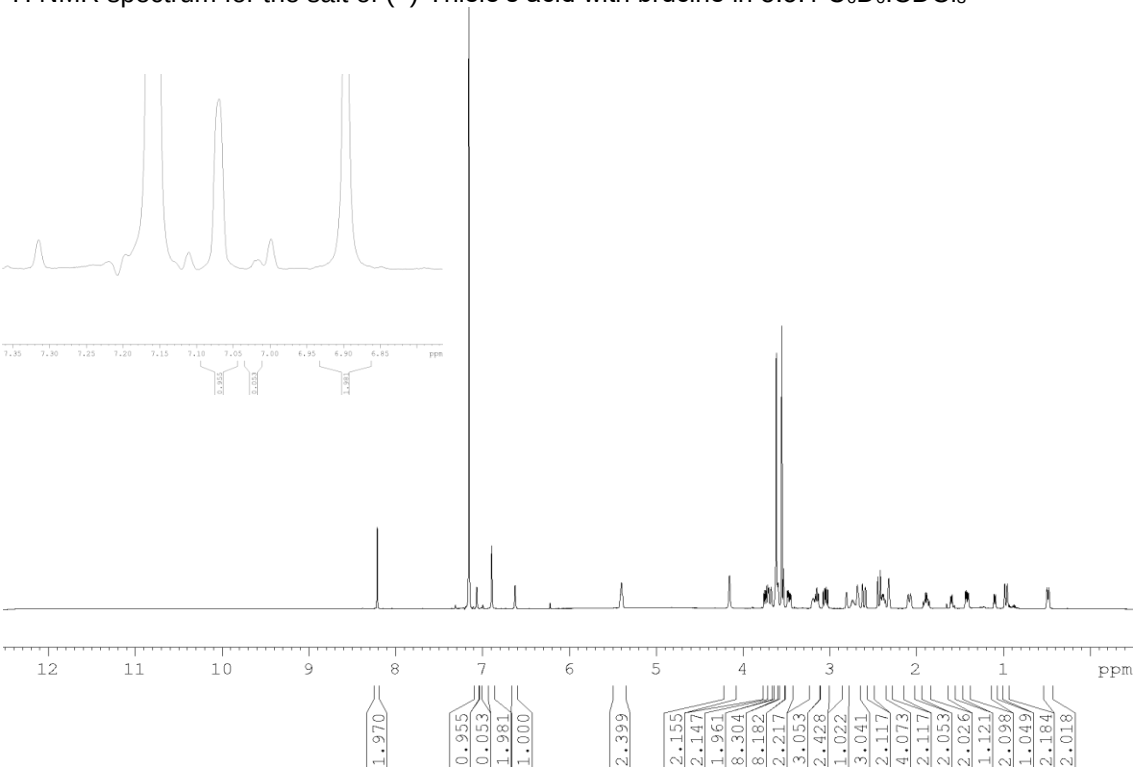

^{13}C NMR spectrum for the salt of (–)-Thiele's acid with brucine in 8.3:1 C_6D_6:$CDCl_3$

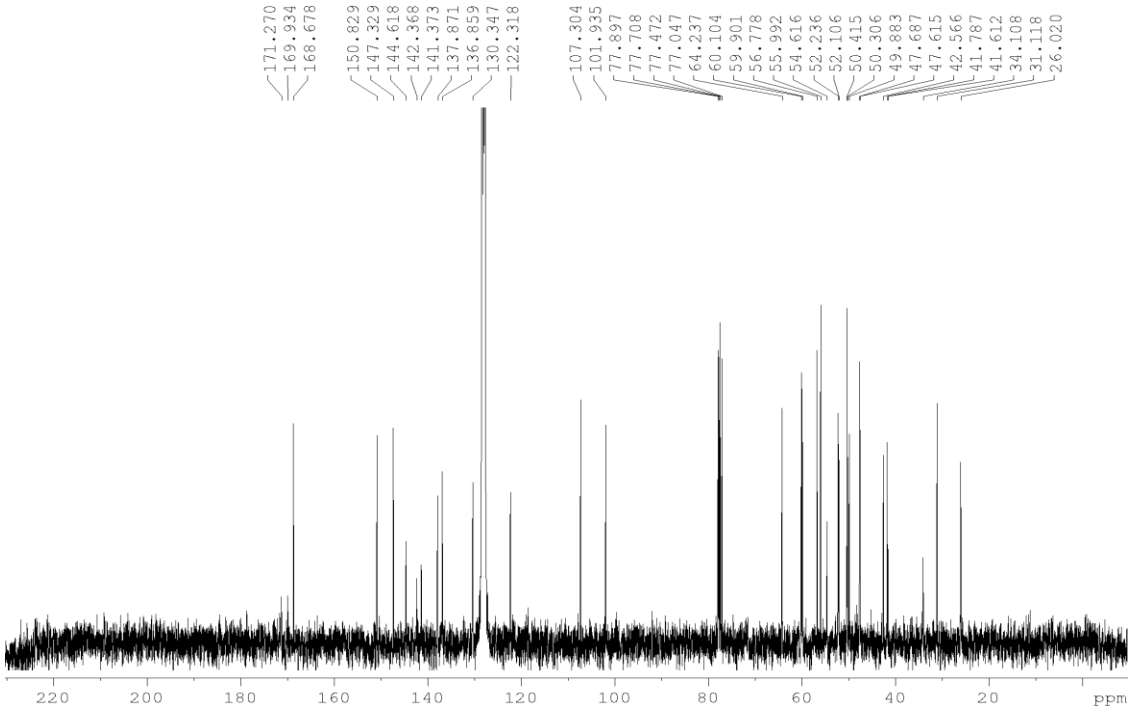

^{1}H and ^{13}C NMR spectra for compound **153a**

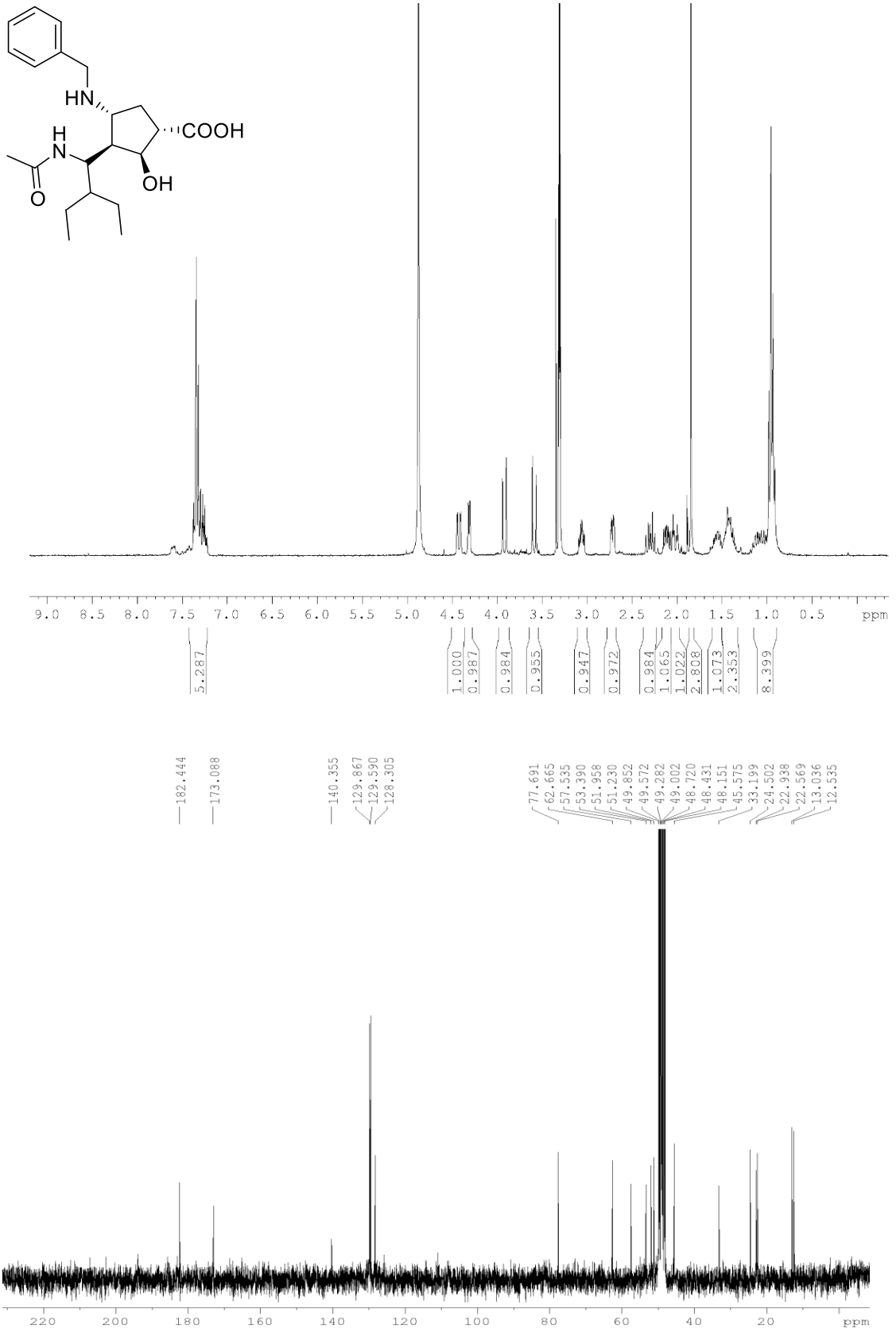

LS-MS trace of **153a** based on the mass of 377

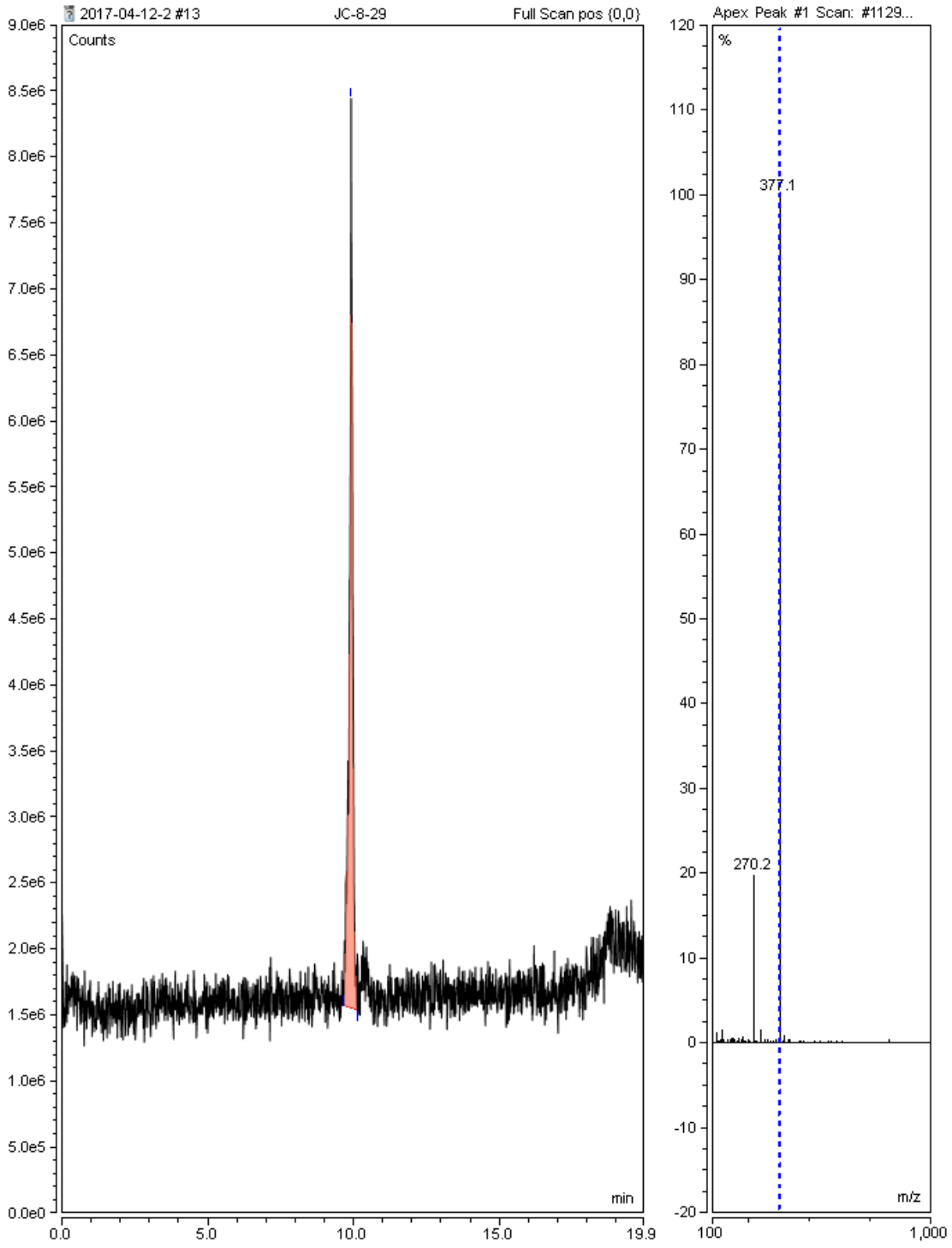

^{1}H and ^{13}C NMR spectra for compound **153b**

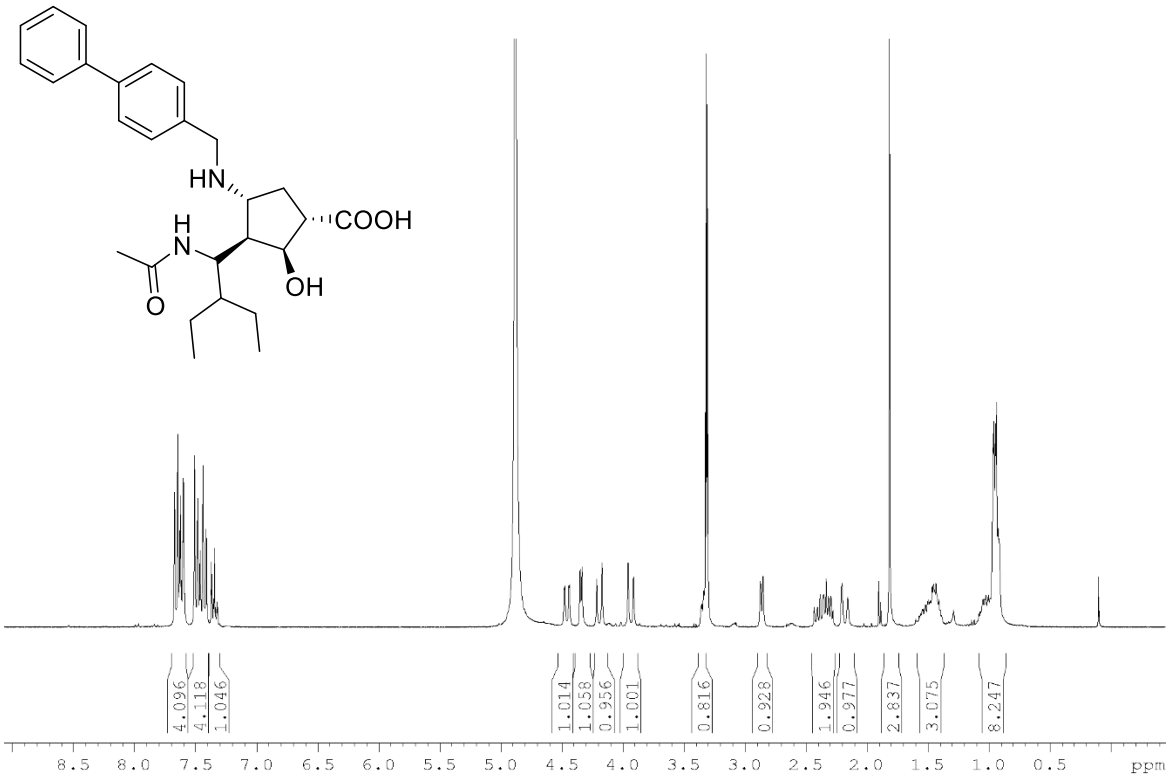

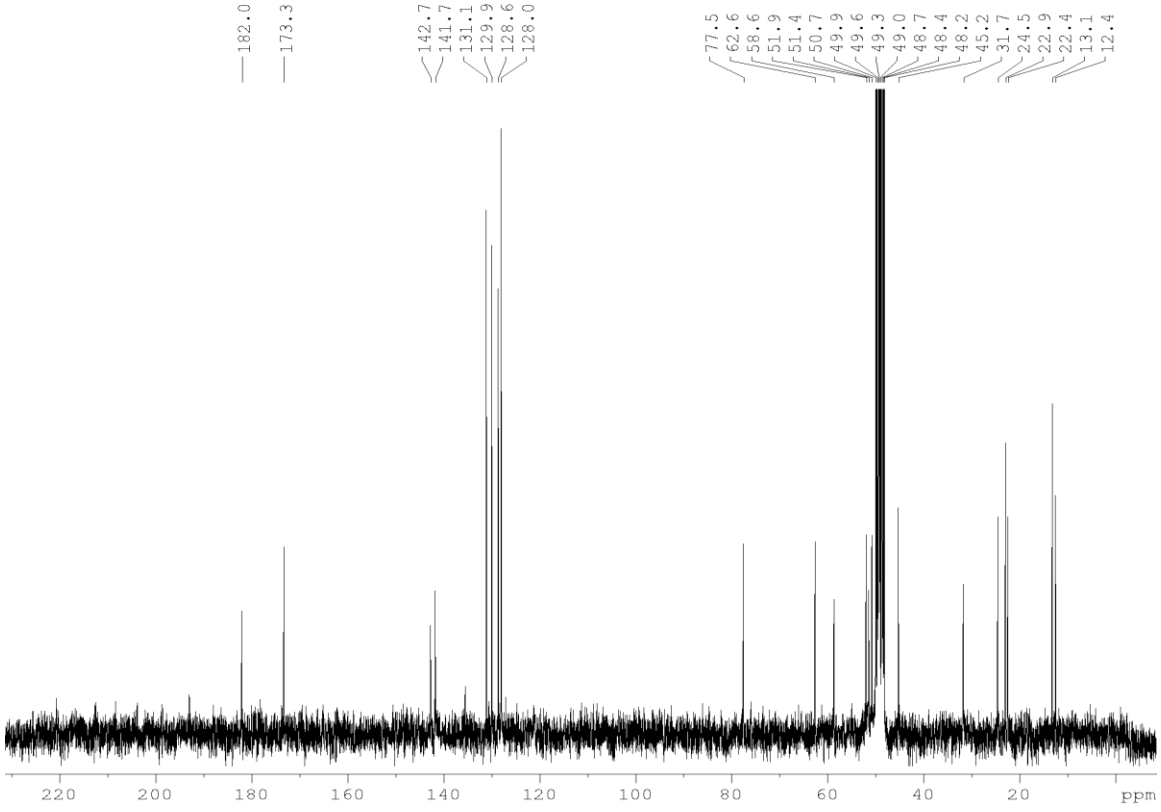

LS-MS UV (254 nm) trace of **153b**

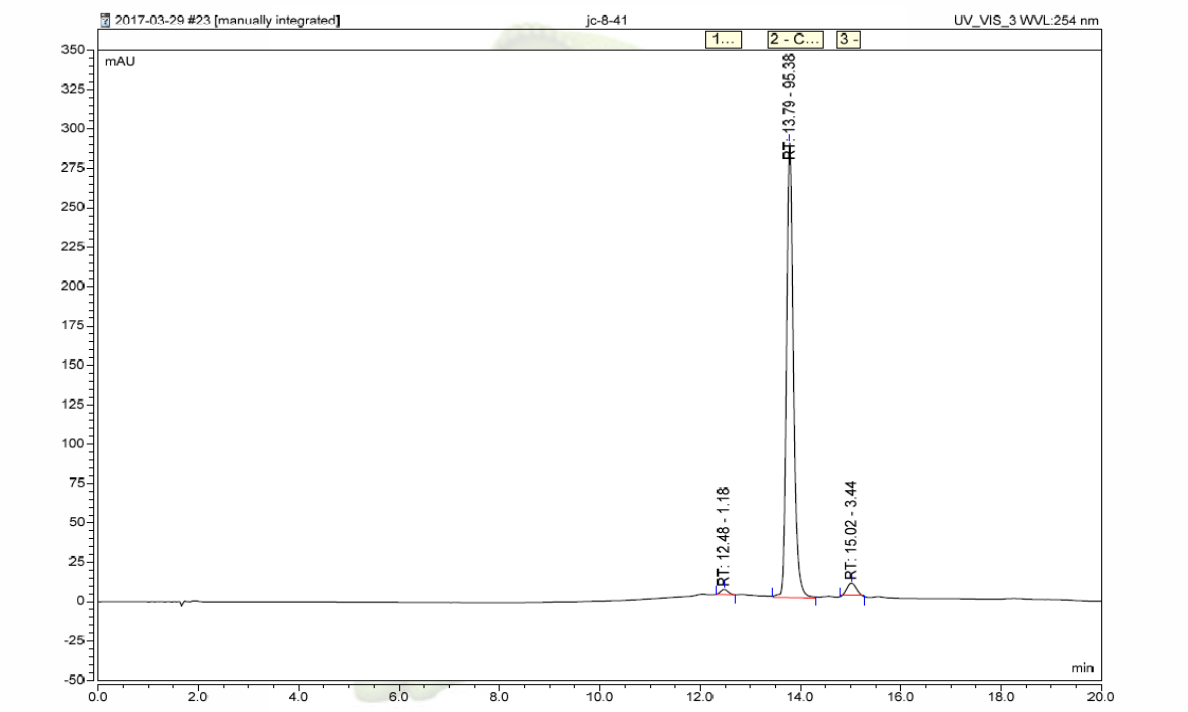

^{1}H and ^{13}C NMR spectra for compound **153c**

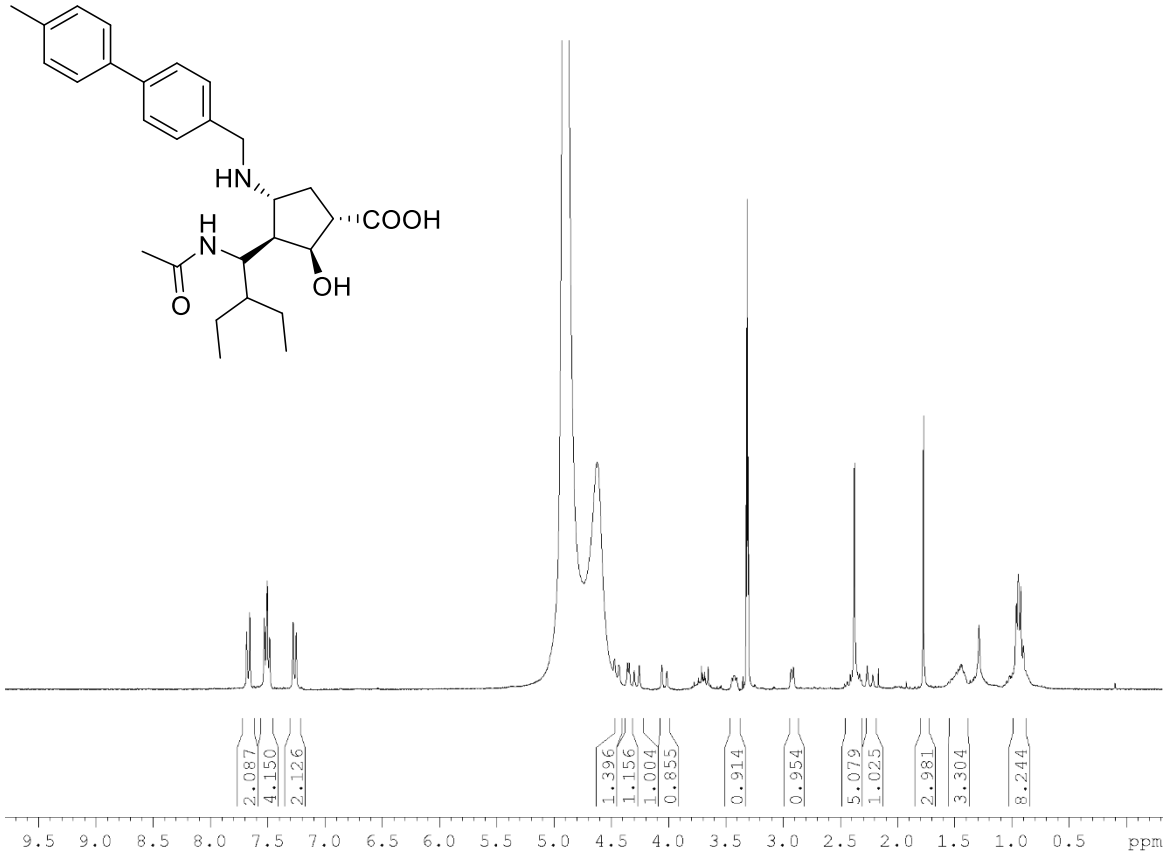

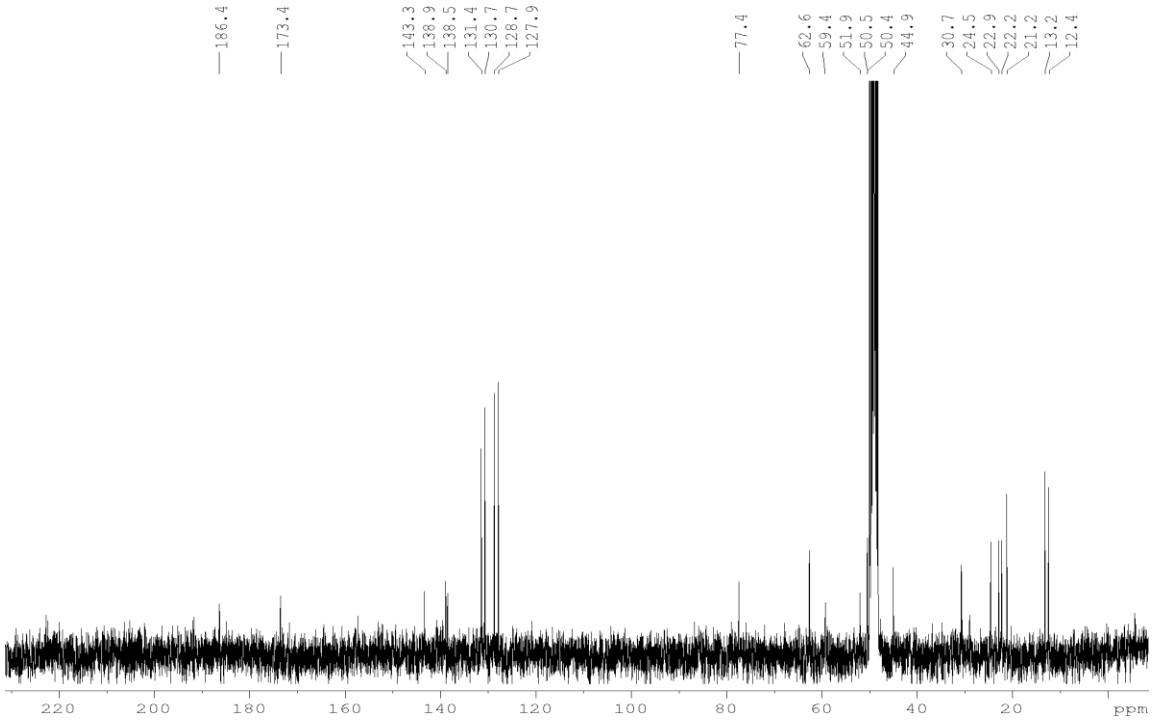

LS-MS UV (254 nm) trace of **153c**

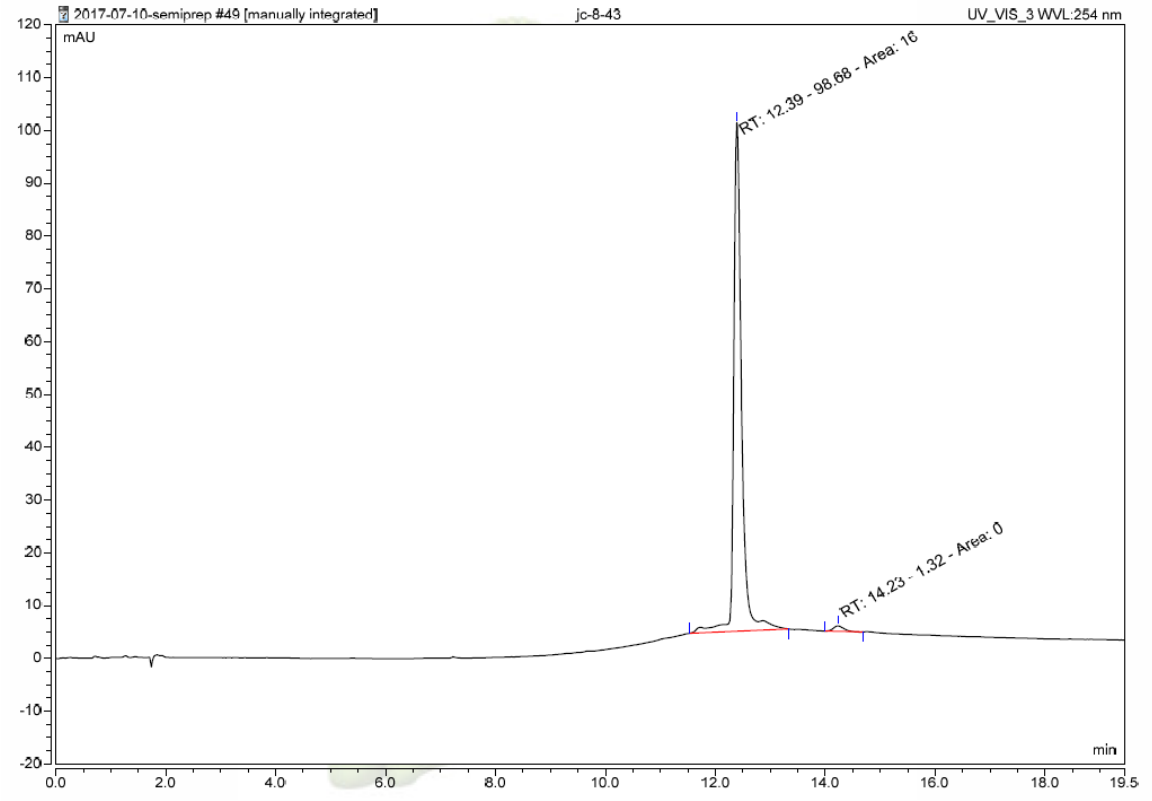

^{1}H and ^{13}C NMR spectra for compound **153d**

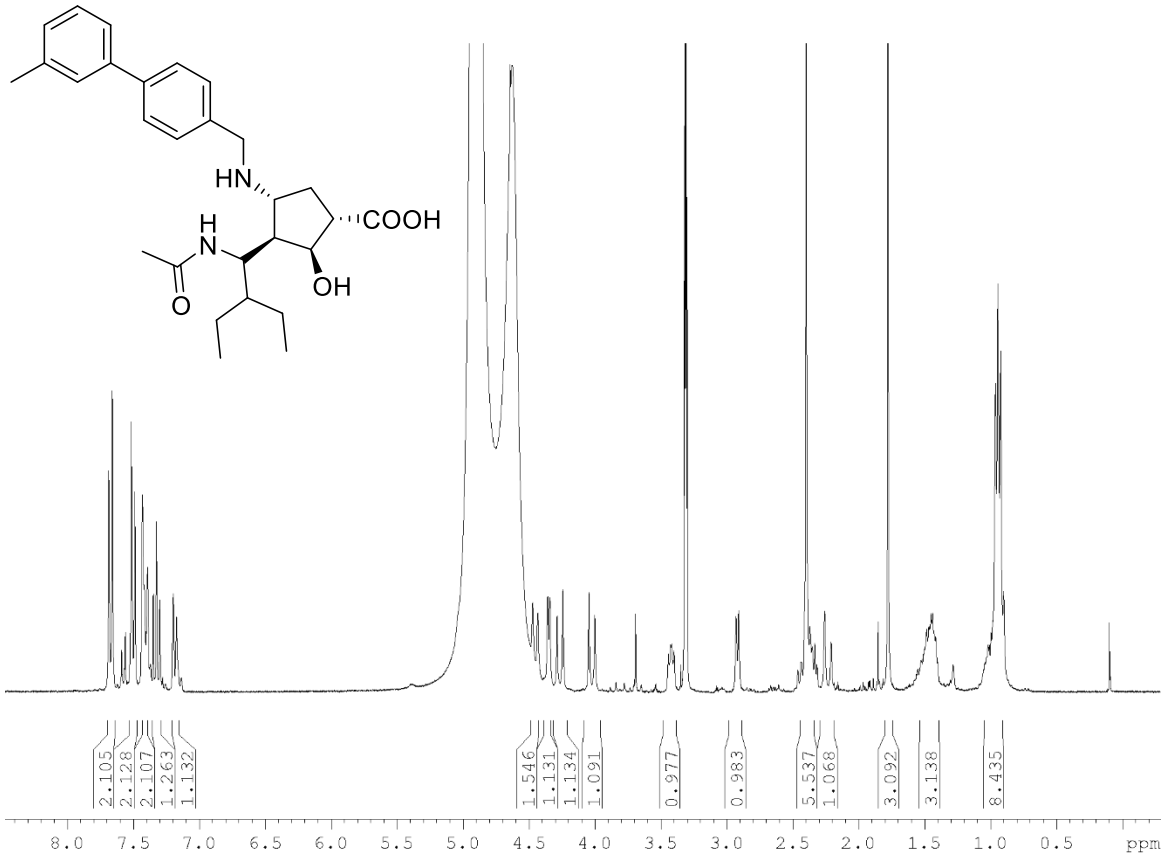

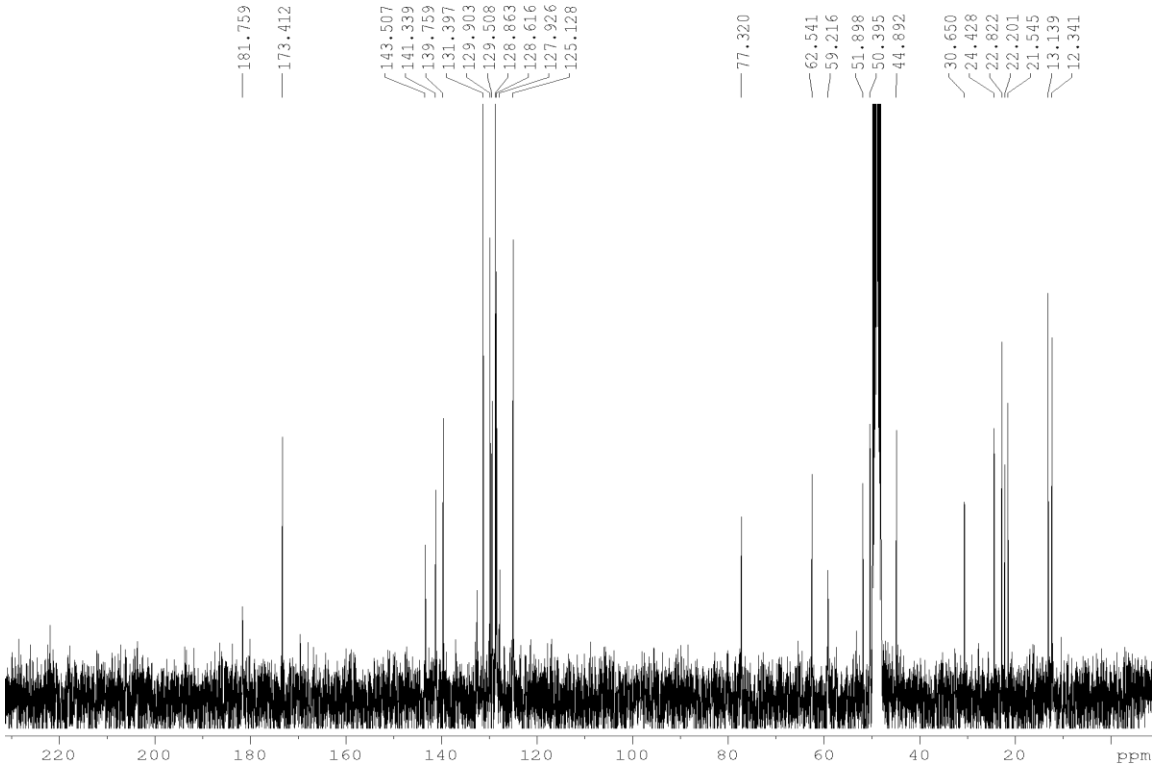

^{1}H and ^{13}C NMR spectra for compound **153e**

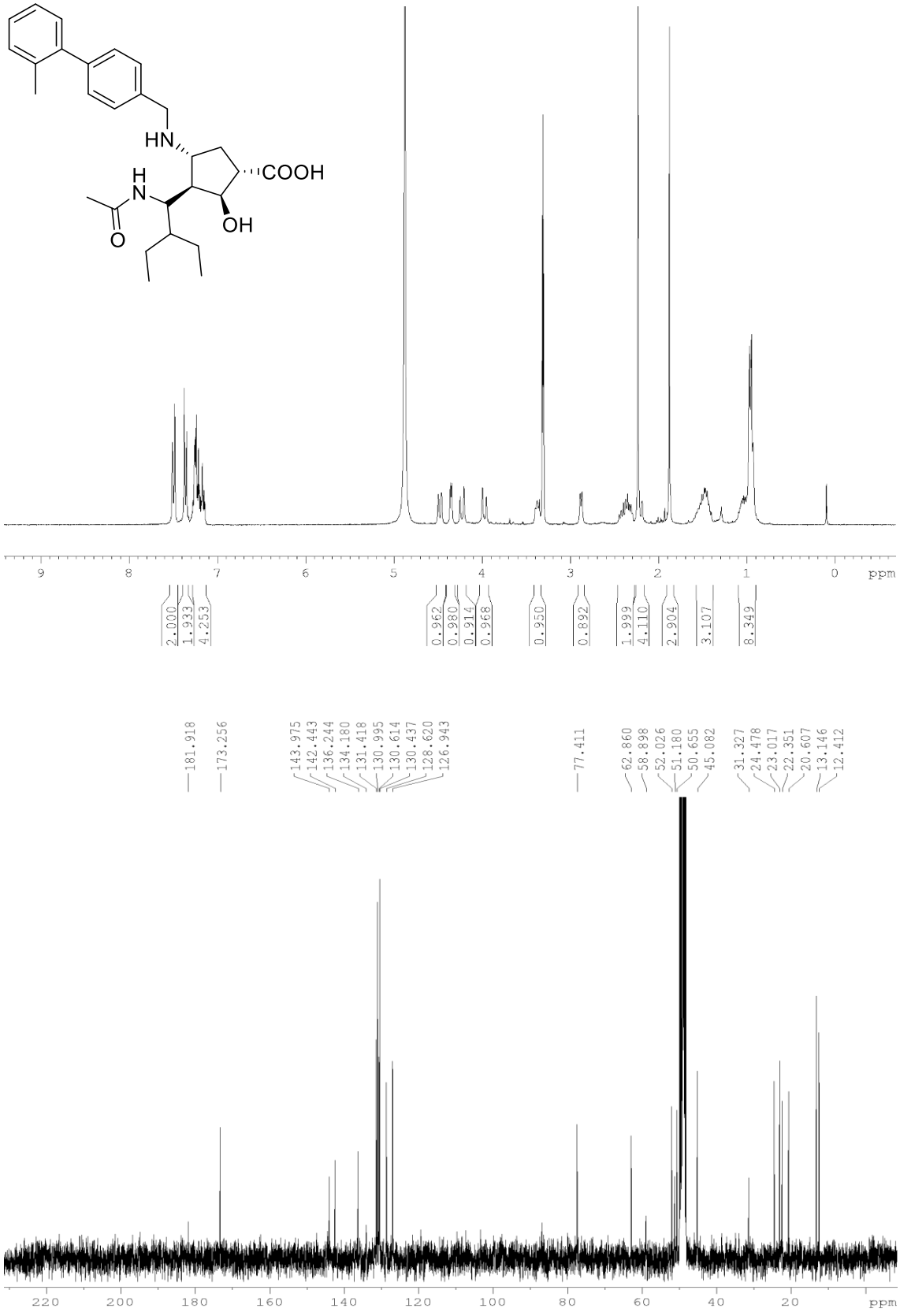

LS-MS UV (254 nm) trace of **153e**

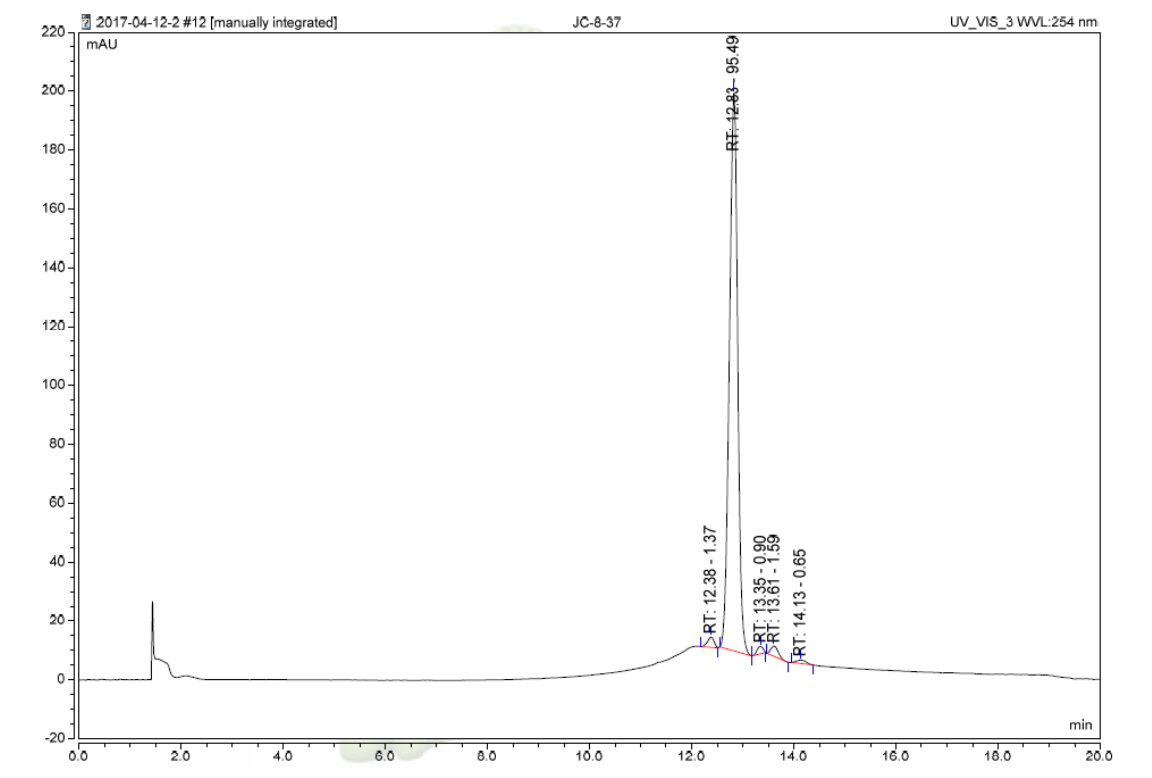

^{1}H and ^{13}C NMR spectra for compound **153f**

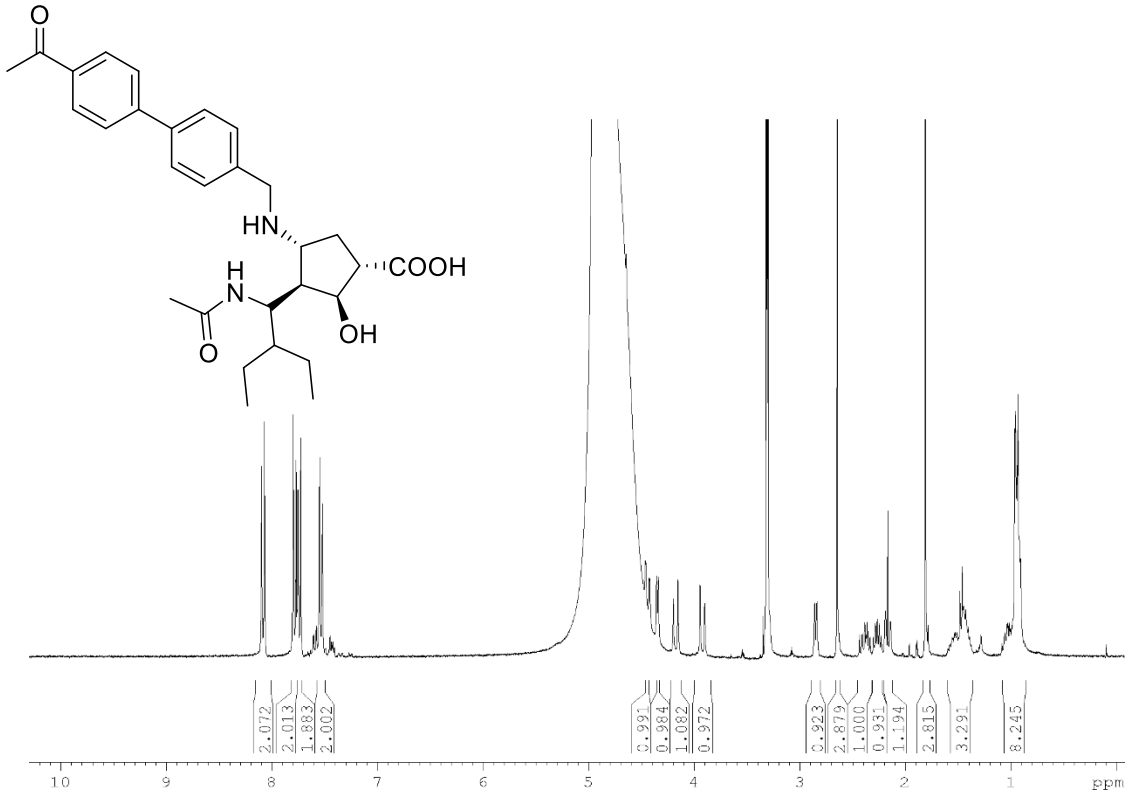

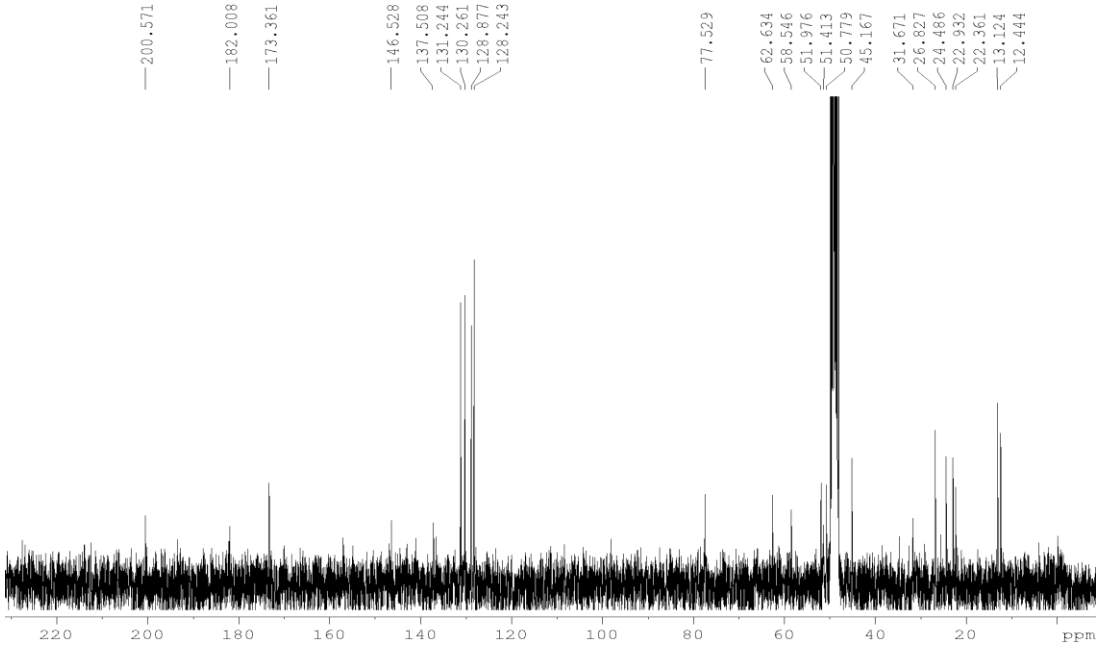

LS-MS UV (290 nm) trace of **153f**

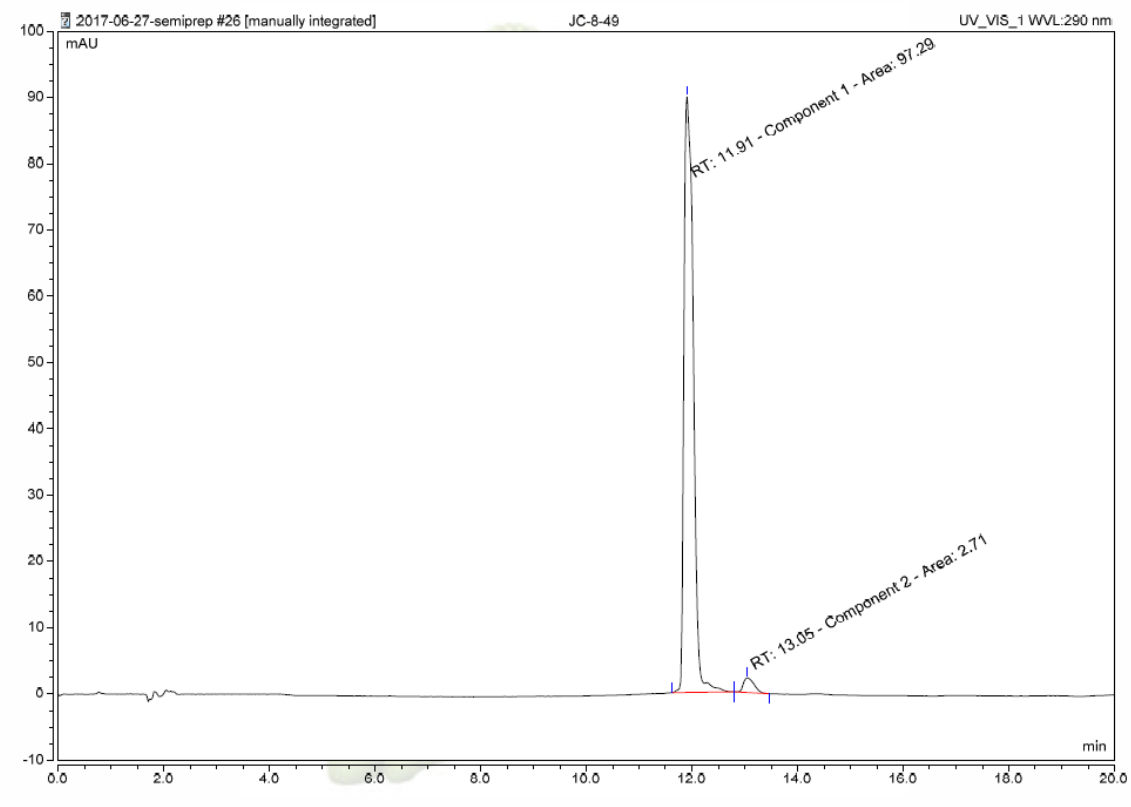

^{1}H and ^{13}C NMR spectra for compound **153h**

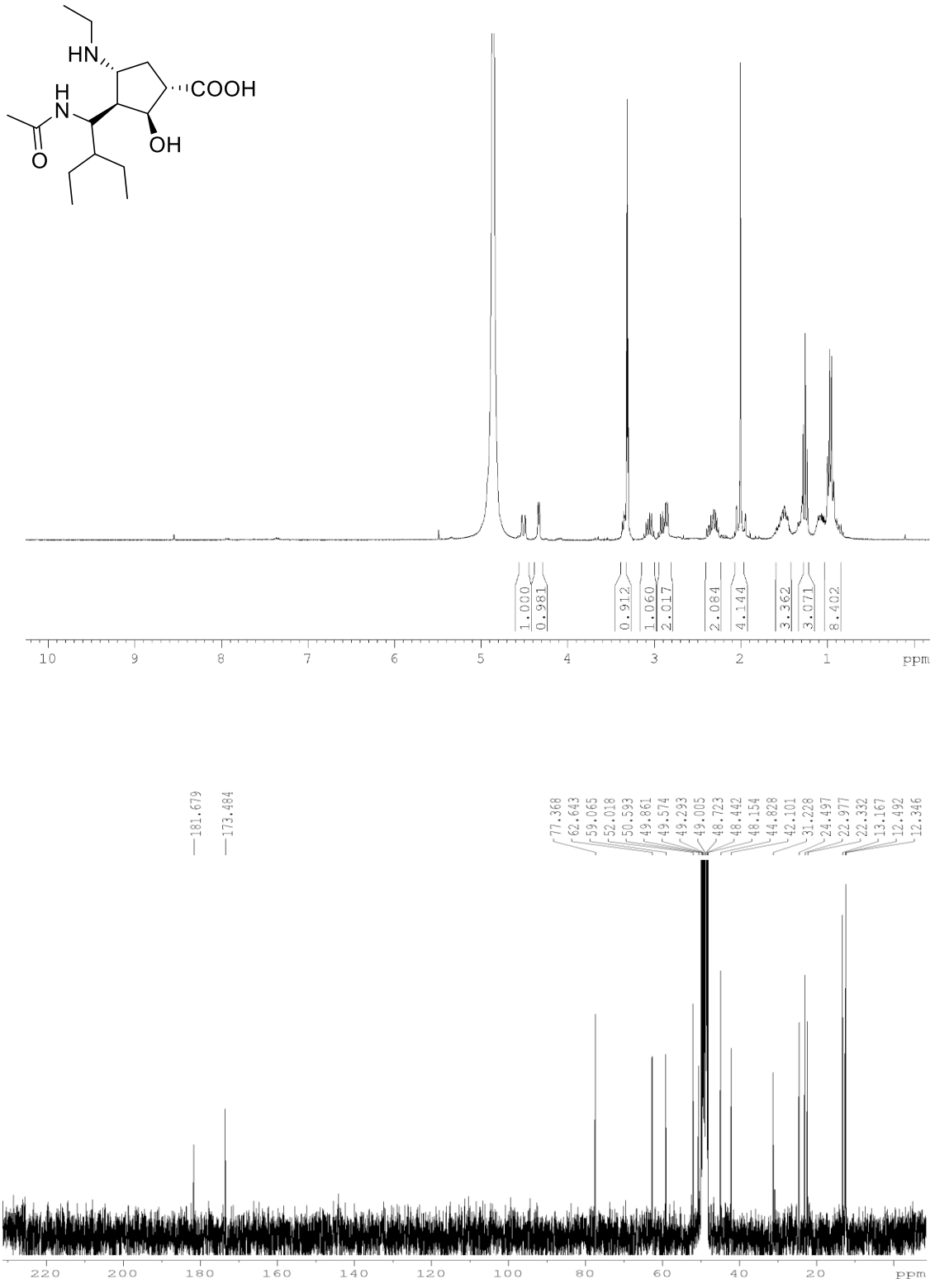

LS-MS trace of **153h** based on the mass of 315

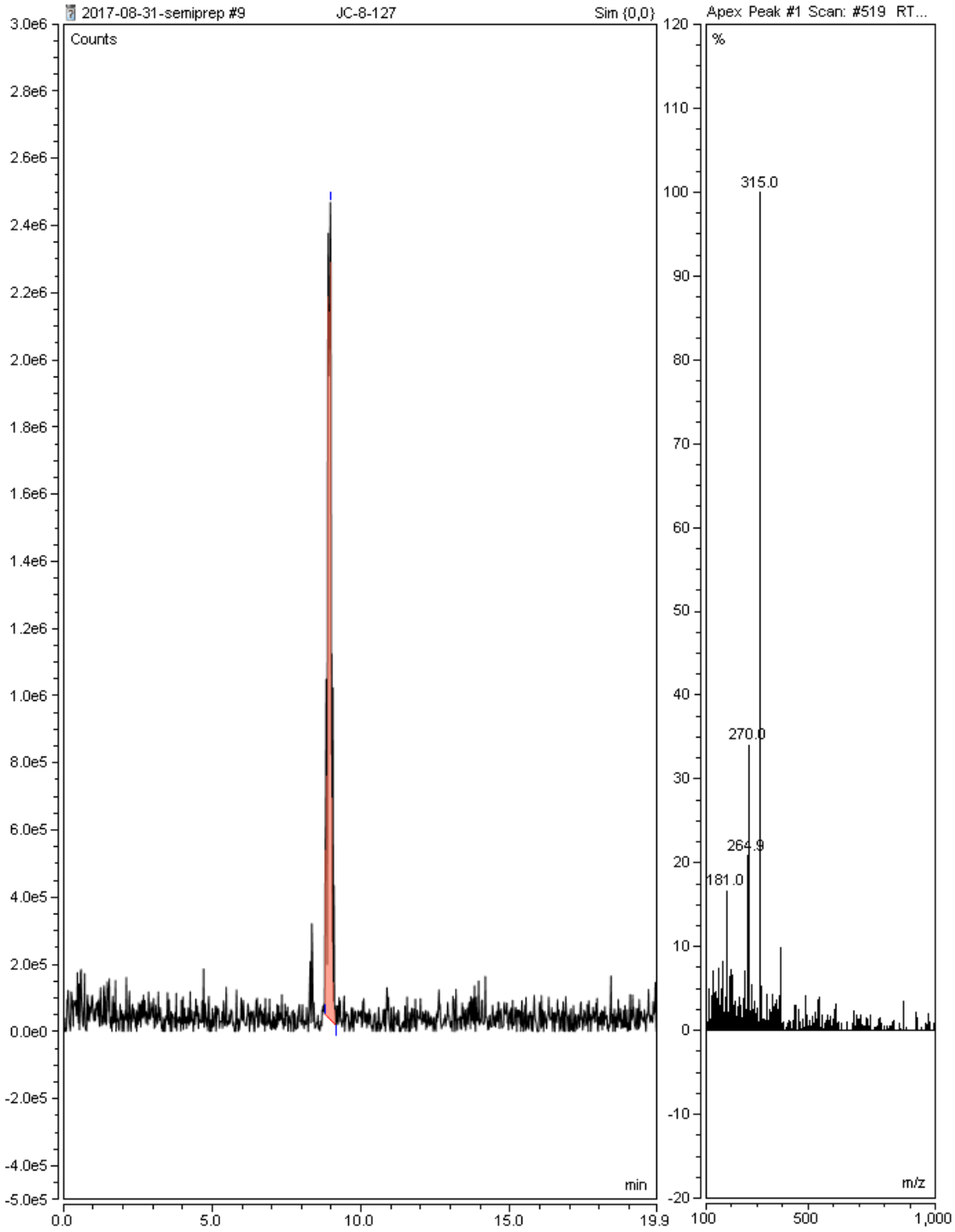

^{1}H and ^{13}C NMR spectra for compound **153i**

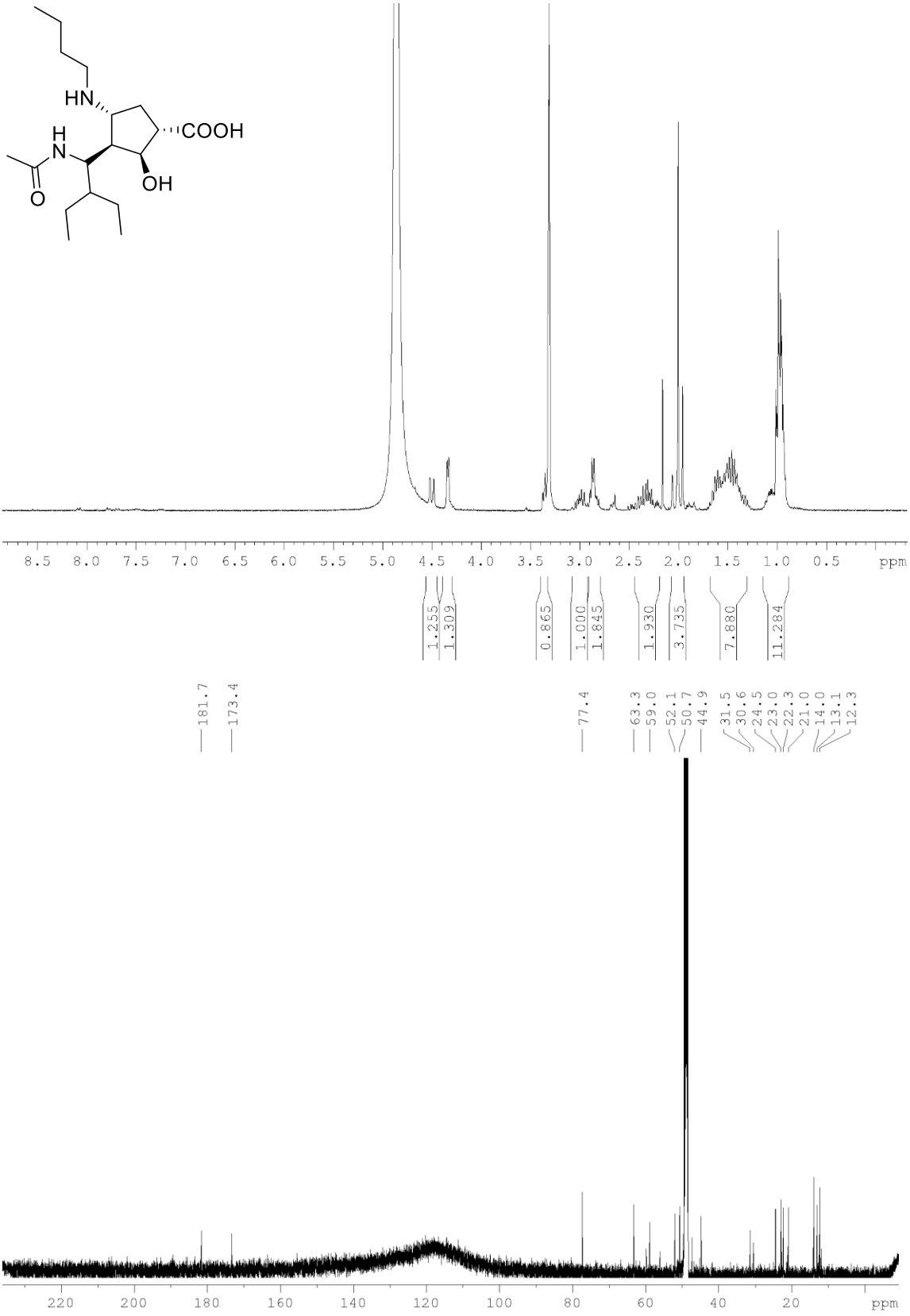

^{1}H and ^{13}C NMR spectra for compound **153j**

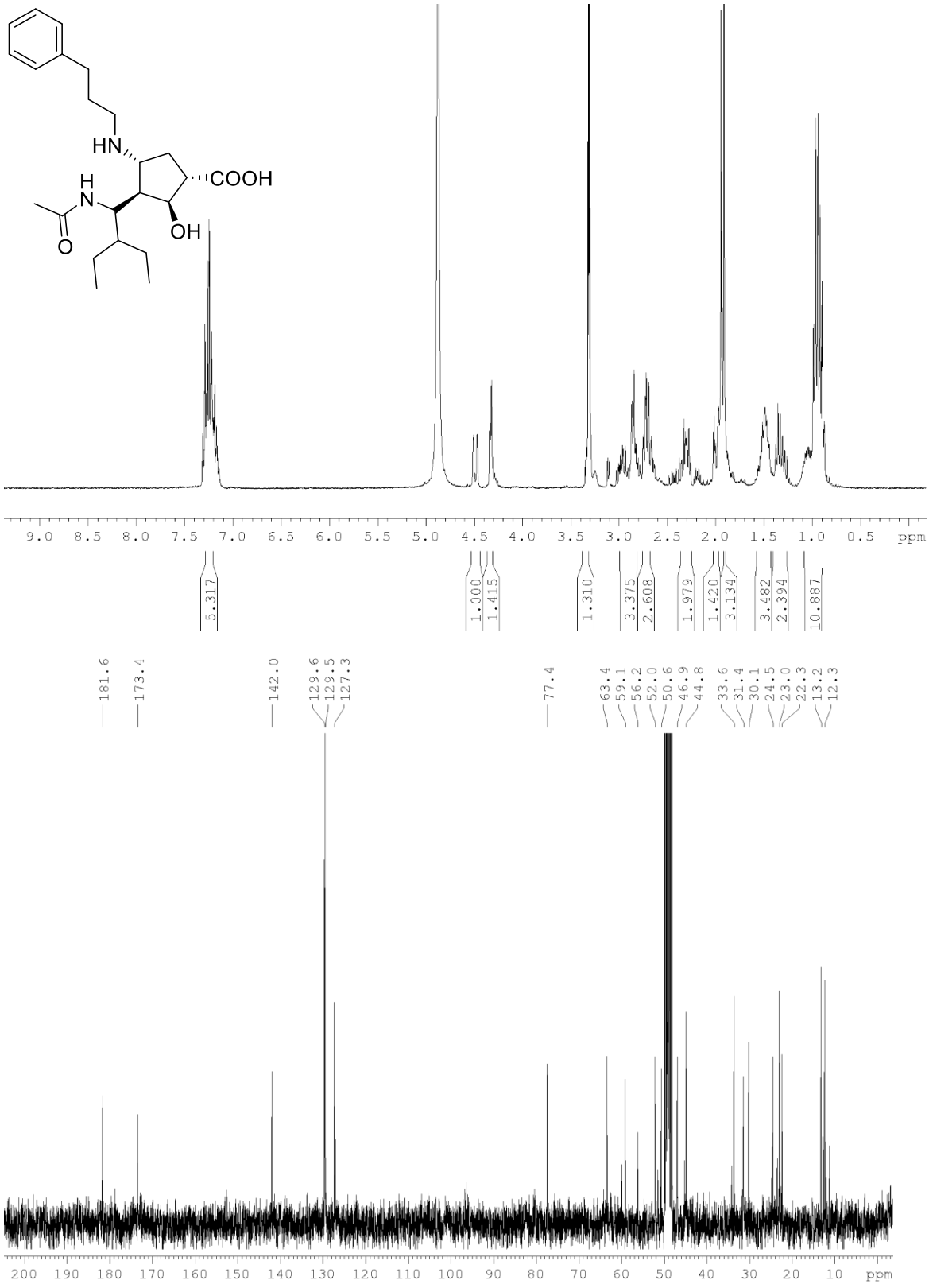

^{1}H and ^{13}C NMR spectra for compound **153k**

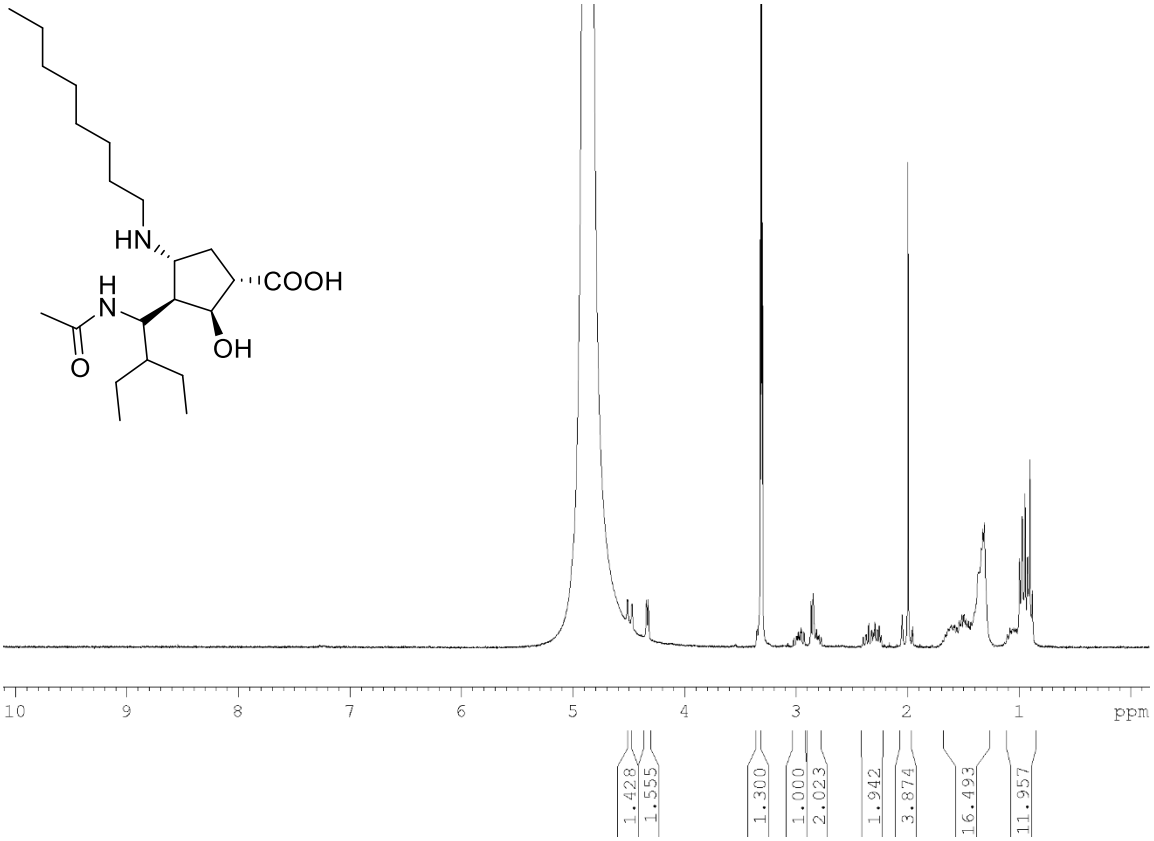

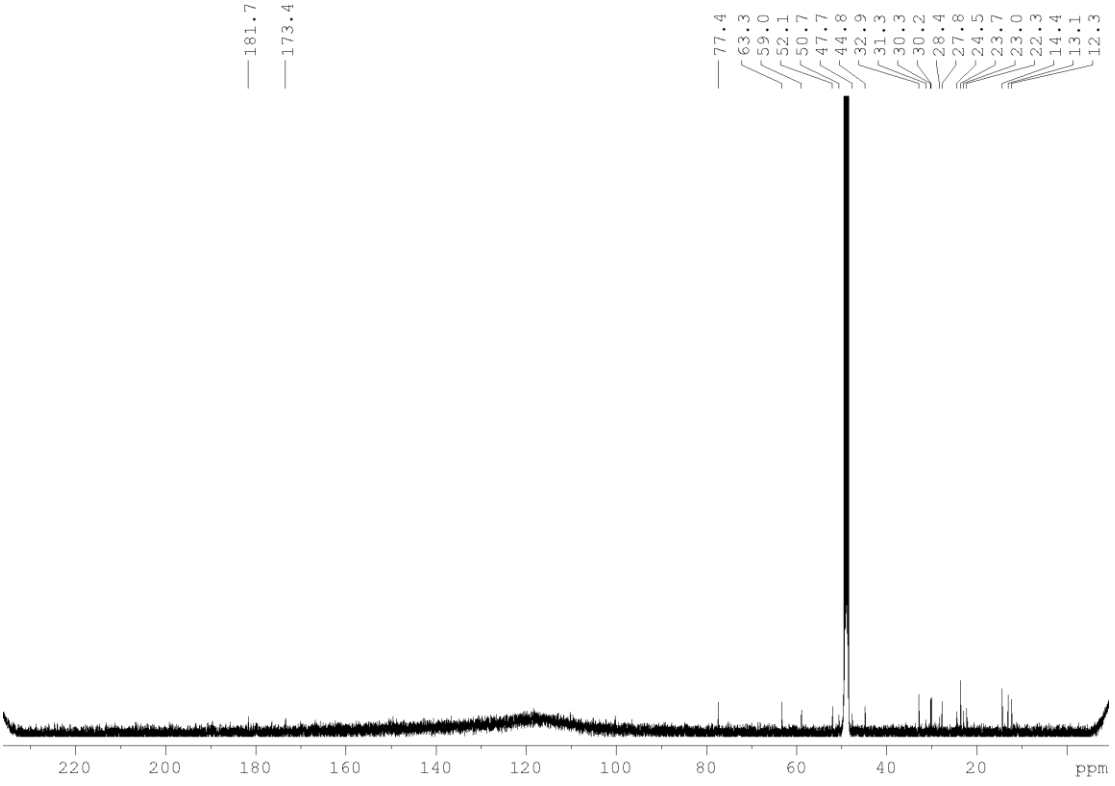

LS-MS trace of **153k** based on the mass of 399

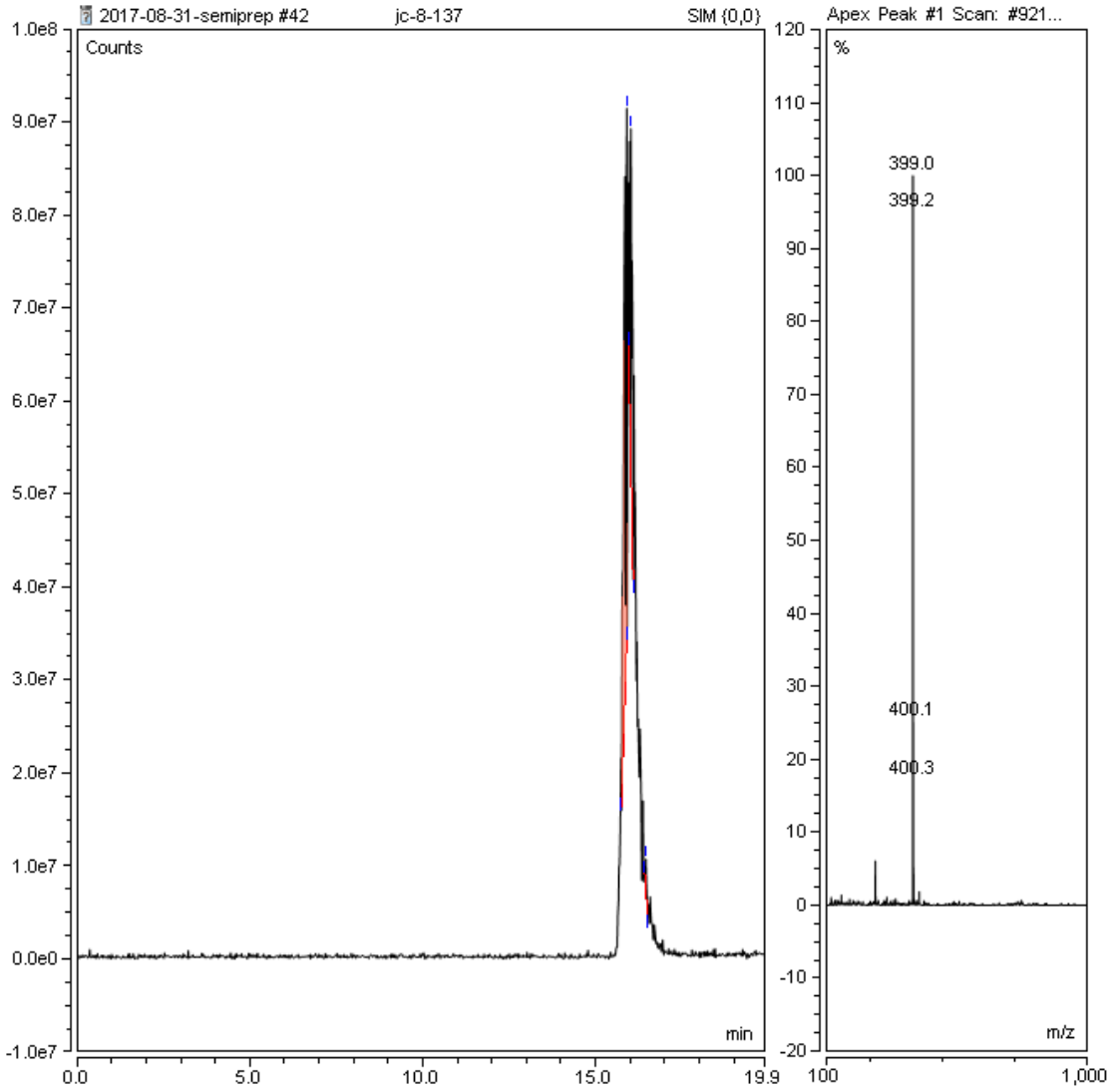

^{1}H and ^{13}C NMR spectra for compound **153l**

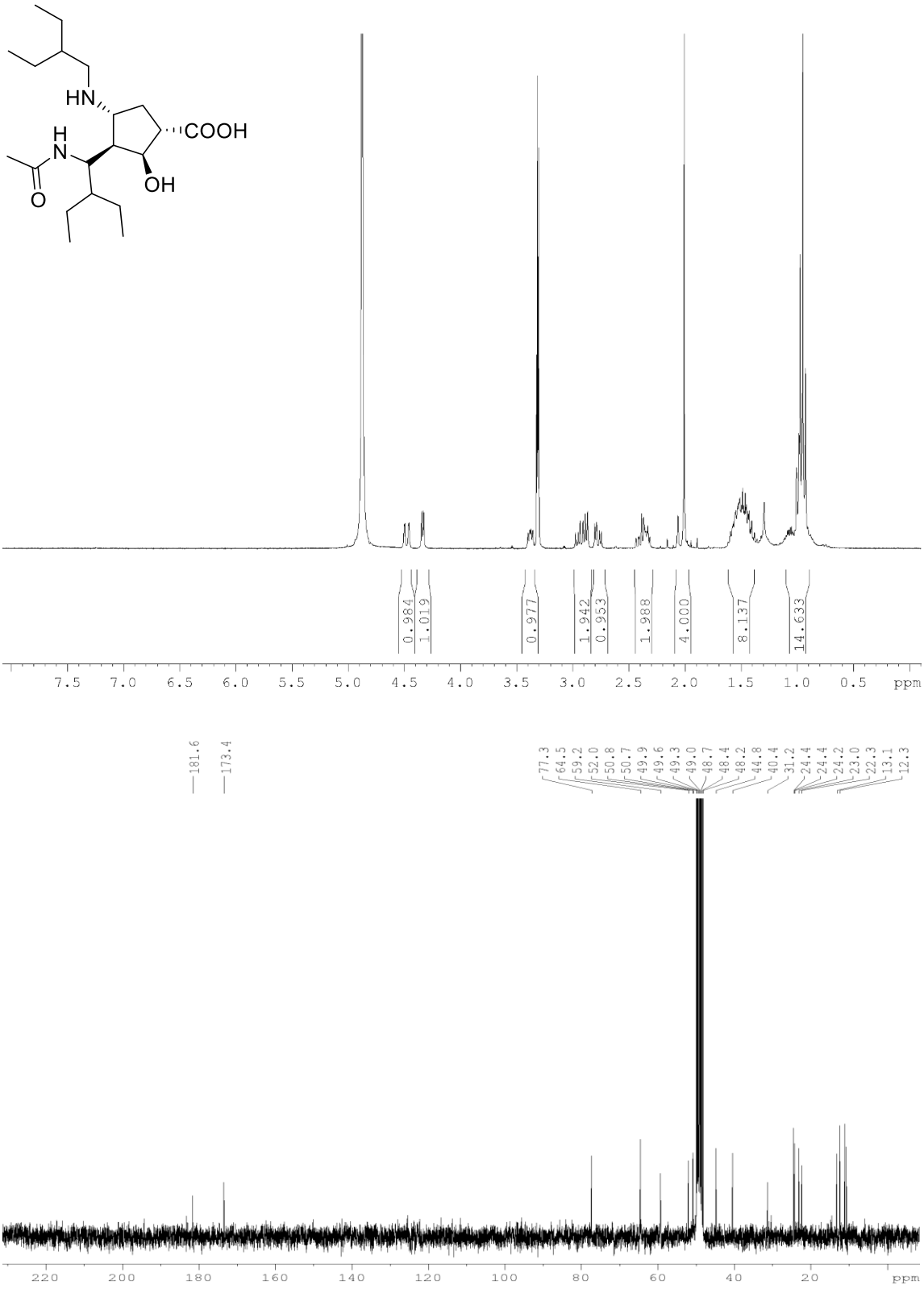

LS-MS trace of **153l** based on the mass of 371

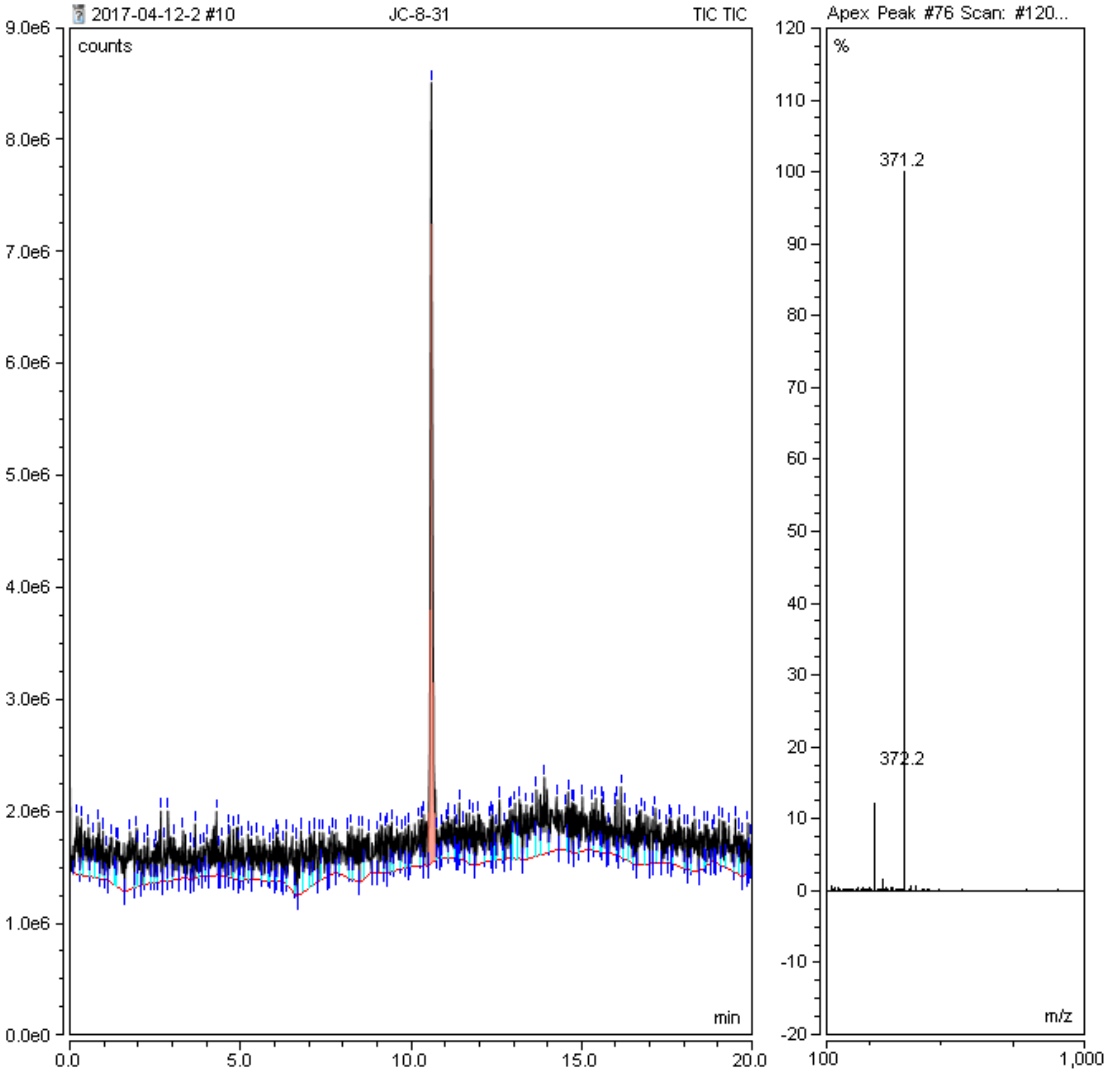

^{1}H and ^{13}C NMR spectra for compound **153m**

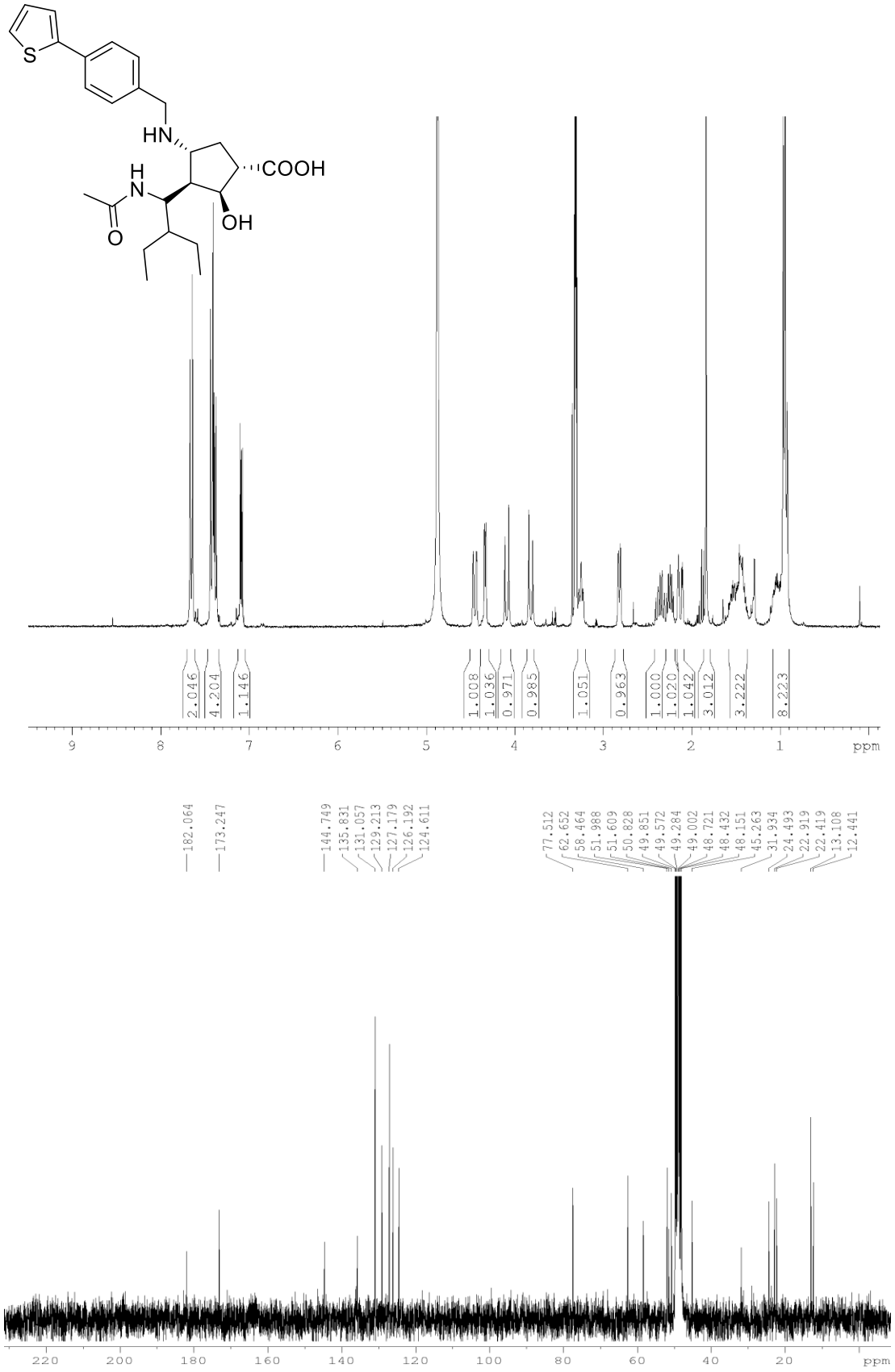

LS-MS UV (290 nm) trace of **153m**